A redox-active splice variant of NADPH oxidase 4 as a potential regulator of cardiomyocyte proliferation in the adult heart

Savage, Natalie Louise

Awarding institution:
King's College London

A redox-active splice variant of NADPH oxidase 4 as a potential regulator of cardiomyocyte proliferation in the adult heart

Natalie Louise Savage

Submitted for the Degree of Doctor of Philosophy

June 2019

Supervisors

Professor Ajay M Shah & Dr Els Henckaerts

School of Cardiovascular Medicine & Sciences

British Heart Foundation Centre of Research Excellence

Faculty of Life Sciences & Medicine

King's College London

“Remember to look up at the stars and not down at your feet. Try to make sense of what you see and wonder about what makes the Universe exist. Be curious. And however difficult life may seem, there is always something you can do and succeed at. It matters that you don’t just give up.”

- *Professor Stephen Hawking*

Abstract

Background – The NADPH oxidases (Noxs) are a family of reactive oxygen species (ROS)-generating enzymes with crucial roles in the regulation of redox signalling pathways, which have been implicated in several physiological processes including cellular differentiation, proliferation, and survival. Since the heart has the highest oxygen consumption among body organs, redox-mediated signalling is central to both cardiac function as well as pathophysiology. Nox4 is expressed in cardiomyocytes and has been shown to mediate distinct adaptive phenotypes in the heart in response to chronic disease stress. We previously identified that a splice variant of Nox4, Nox4D, is nuclear-localised, capable of ROS production, and is associated with increased proliferation of neonatal cardiac myocytes. The aim of this project was to investigate the effects of Nox4D in adult cardiomyocytes in vivo.

Methods and Results – We generated mice with inducible cardiomyocyte-specific overexpression of Nox4D (Ind-csNox4D). After tamoxifen induction in adult mice, Ind-csNox4D showed a 10-fold increase in Nox4D protein levels in the heart compared to controls, whilst echocardiography revealed similar cardiac structure and function. No changes were found in baseline cardiomyocyte cell cycling or redox signalling as assessed by EdU nucleotide analog incorporation and the expression of cell cycle genes and pathways. The impact of Ind-csNox4D on the response to myocardial infarction (MI) induced by permanent left anterior descending coronary artery (LAD) ligation was next determined. At 4 weeks post-MI, Ind-csNox4D mice demonstrated region-specific improvements in contractile function, but no differences were found in global left ventricular (LV) function and volumes compared to control mice. This was consistent with a partial protective response in Ind-csNox4D hearts during postinfarction remodelling, but there were no differences in the gene expression of markers of the cell cycle versus control hearts in either the infarct border zone or remote zone. However, using a model of cultured adult cardiomyocytes stimulated to induce dedifferentiation, we found that Nox4D overexpression is associated with increased cell cycle progression compared to control cells.

Conclusions – In vitro overexpression of Nox4D increases proliferation of neonatal cardiomyocytes but this is unchanged in adult hearts. Induction of cardiomyocyte-specific overexpression of Nox4D in adult mice is well tolerated, capable of mediating a regionalised reparative and functional response in the setting of post-MI remodelling but insufficient to fully rescue recovery. Further research is needed to understand whether the proliferative effects of Nox4D in vitro may be realised in the adult heart.

Acknowledgements

I would first like to thank my primary supervisor Professor Ajay Shah, for the opportunity to undertake my PhD in his laboratory group, for all his guidance and support throughout the project, and for his ability to always make sense of data. I have particularly enjoyed gaining from his vast knowledge on cardiovascular sciences and medicine. Lastly, I wish to thank him for encouraging me to share my work at scientific meetings and events, as these have been some of the most invaluable and rewarding times of my PhD experience. I also thank Dr Narayana Anilkumar for his supervision and sharing his lab expertise with me, and Dr Els Henckaerts for her guidance and for the opportunity to work in her laboratory.

My hugest thanks go to the British Heart Foundation. This charity and their fundraisers never cease to amaze me, and have always provided motivation during the tougher times to remind me why we do this research. Of course, I could not have completed my project if it were not for all my great colleagues and friends in the group. I would like to especially thank Richard Thompson for his amazing support, Matteo Beretta for always so kindly donating his time and being able to help with practically anything, Norman Catibog for his brilliant ultrasound expertise, and Greta Sawyer and Helena Zhang for their fantastic surgical skills. Special thanks go to Daniel Martin for sharing his technical wisdom, Ioannis Smyrnias for helping me tackle adult cardiomyocyte isolations, and Monica Stollery for her endless help and support. Extended thanks also go to Anna Zoccarato, Celio Santos, Daniel Bromage, Daniel Brayson, Stephen Grey, Daniel Richards, Izaj Rahman and George Chennell. Last but not least, thank you to Giulia Emanuelli, for being my partner in crime and sharing this experience with me right from the start.

I cannot thank my family and friends closest to me enough for their support and encouragement, for I have put them through this process as well. Thank you to my Mum, for being gifted in her ability to always uplift me, believe in me, motivate me, help me to see the positives, make me smile and for teaching me to aim high. Thank you also to my Dad, for always supporting me and making me laugh. A very special thank you to Simon, who I was able to meet because of our PhDs. Thank you for always being there during the lab times and the trips for tea and chocolate, and thank you especially for your amazing support and for looking out for me during these recent months. Lastly, I would also like to thank Dwaine and Prof Baxter, for igniting my passion for cardiovascular research in the first place and for encouraging me to pursue a PhD.

Declaration

I declare that I am the sole author of this PhD thesis and it contains my own work, except where indicated.

Natalie Savage

Table of contents

Abstract **3**

Acknowledgements **4**

Declaration **5**

Table of contents **6**

Table of figures **11**

Table of tables **15**

Abbreviations **16**

Chapter 1 General introduction **19**

1.1 The impact of cardiomyocyte loss 20

1.1.1 Heart development and growth 20

1.1.2 Acute myocardial infarction 20

1.2 Potential for mammalian cardiomyocyte proliferation as a basis for cardiac regeneration 21

1.2.1 Sources of cardiomyocytes and strategies for repair 21

1.2.2 The mammalian cell cycle 22

1.2.3 Endogenous heart regeneration in lower vertebrates and neonatal mice in response to injury 25

1.2.4 The regulation of postnatal cardiomyocyte cell cycle withdrawal 27

1.2.5 Evidence for cardiomyocyte turnover in the adult heart 28

1.3 Mechanisms stimulating cardiomyocyte renewal 30

1.3.1 Genetic manipulation of cell cycle regulators 30

1.3.2 MicroRNAs 31

1.3.3 Signal transduction pathways 32

1.3.4 Redox control of proliferation 35

1.4 Cardiac redox signalling 37

1.4.1 The signalling functions of reactive oxygen species 37

1.4.2 The main sources of ROS in cardiomyocytes 38

1.5 The NADPH oxidase family of enzymes 38

1.5.1 Nox structure and function 38

1.5.2 Identification of novel Nox4 splice variants 40
1.5.3 Nox4D is a nuclear-localised, redox-active splice variant of Nox4 42
1.6 Hypothesis 44
1.7 Objectives 44
Chapter 2 Materials and methods 45
2.1 Animals 46
2.2 Generation of genetically-modified mice 46
2.2.1 Nox4D transgenesis strategy and breeding 46
2.2.2 Determination of genotype 47
2.3 Induction of Nox4D overexpression 49
2.4 Surgical induction of myocardial infarction 50
2.4.1 Permanent coronary artery ligation 50
2.4.2 Cardiac troponin I sampling 24 hours post-surgery 51
2.5 Echocardiography 51
2.6 EdU labelling 52
2.7 Cardiac tissue harvest 53
2.8 Adult cardiomyocyte isolations 54
2.8.1 Surgical procedure 55
2.8.2 Heart dissociation 55
2.8.3 Cardiomyocyte purification and culture 56
2.8.4 Cardiomyocyte viability assays 57
2.8.5 Adult cardiomyocyte dedifferentiation 57
2.9 qPCR analysis of gene expression 58
2.9.1 RNA extraction 58
2.9.2 Reverse transcription 59
2.9.3 Quantitative PCR 59
2.9.4 qPCR primer design 60
2.10 Western blotting 62
2.10.1 Protein extraction 62
2.10.2 Protein content determination 62

2.10.3 Immunoblotting 63
2.11 Cell and tissue staining 65
2.11.1 Cryosections 65
2.11.2 Immunostaining 65
2.11.3 EdU detection 66
2.11.4 Wheat germ agglutinin and isolectin B4 67
2.11.5 TUNEL staining 67
2.11.6 Picrosirius red 68
2.11.7 Microscopy 68
2.12 Cardiac troponin I ELISA 69
2.13 ROS detection by HPLC 70
2.14 H9c2 cell culture 70
2.15 siRNA-mediated Nox4D knockdown in H9c2 cells 71
2.16 Recombinant adeno-associated virus production 71
2.16.1 shRNA and plasmid production 71
2.16.2 AAV9 vector production 72
2.17 Statistical analysis 73
Chapter 3 Baseline characterisation of the inducible cardiomyocyte-specific Nox4D transgenic mouse model 74
3.1 Introduction 75
3.1.1 Initial characterisation of Nox4D 75
3.1.2 Nox4D is a potential regulator of cardiomyocyte proliferation 76
3.2 Aims 79
3.3 Summary of methods 80
3.4 Results 81
3.4.1 Induction of Nox4D overexpression in cardiomyocytes of adult Ind-csNox4D mice 81
3.4.2 Induction of cardiomyocyte-specific Nox4D overexpression in vivo does not affect basal cardiac function, structure or morphology 86
3.4.3 Cardiac-specific Nox4D overexpression does not affect basal cell proliferation in adult mice 88

3.4.4 Cardiac-specific Nox4D overexpression does not affect redox signalling pathways or transcriptional profiles associated with cell cycle modulation 90

3.4.5 Under baseline conditions, induction of cardiac-specific Nox4D overexpression does not provide an immediate proliferative window 93

3.5 Discussion 96

3.5.1 Generation of an inducible cardiomyocyte-specific transgenic mouse model with Nox4D overexpression 96

3.5.2 Impact of cardiomyocyte-targeted overexpression of Nox4D on cell cycle modulation in the adult heart 97

Chapter 4 The impact of inducible cardiomyocyte-specific Nox4D overexpression on recovery after myocardial infarction 101

4.1 Introduction 102

4.1.1 The pathophysiology of permanent coronary artery ligation 102

4.1.2 Assessment of myocardial infarct size 103

4.1.3 Postinfarction left ventricular adverse remodelling 104

4.2 Aims 108

4.3 Summary of methods 109

4.4 Results 110

4.4.1 Induction of cardiomyocyte-targeted Nox4D overexpression elicits a differential temporal functional response post-myocardial infarction 110

4.4.2 The localised protective effects of cardiac-specific Nox4D overexpression are insufficient to fully limit postinfarction remodelling processes 126

4.4.3 Cardiac-specific Nox4D overexpression does not enhance proliferative capacity in the infarct border or remote zones 135

4.5 Discussion 146

4.5.1 Verification of the permanent LAD ligation model 146

4.5.2 Cardiac-specific Nox4D transgenic mice show a transient improvement in functional response after myocardial infarction 146

4.5.3 Inducible cardiomyocyte-specific Nox4D overexpression confers a partial reparative response during postinfarction remodelling 147

4.5.4 Cardiomyocyte-targeted Nox4D overexpression does not elicit regenerative recovery in response to myocardial infarction 149

Chapter 5 The manipulation of Nox4D in an in vitro model of adult cardiomyocyte dedifferentiation..... 156

5.1 Introduction..... 157

5.1.1 Dedifferentiation of cardiomyocytes in vivo and in vitro..... 157

5.1.2 Regulation of cardiomyocyte dedifferentiation by oncostatin M..... 158

5.1.3 Partial dedifferentiation of cardiomyocytes may promote proliferative potential..... 159

5.2 Aims..... 161

5.3 Summary of methods..... 162

5.4 Results..... 163

5.4.1 Development of splice variant-targeted Nox4D knockdown..... 163

5.4.2 Establishment of model of cultured isolated adult mouse cardiomyocytes 167

5.4.3 Nox4D overexpression is associated with modulation of cell cycle progression of dedifferentiated adult mouse cardiomyocytes..... 170

5.5 Discussion..... 178

5.5.1 Targeted siRNA mediates Nox4D knockdown..... 178

5.5.2 Isolated adult cardiomyocytes adapt to maintain viability in culture..... 179

5.5.3 The role of Nox4D in the proliferation of dedifferentiated adult cardiomyocytes in vitro..... 180

Chapter 6 General discussion..... 183

6.1 Summary of findings..... 184

6.2 Physiological impact of inducible Nox4D overexpression in the adult mammalian heart..... 186

6.2.1 Nox4D is linked to cardiomyocyte proliferation in a context-dependent manner..... 186

6.2.2 Induction of Nox4D in the adult heart may regulate redox-dependent prosurvival signalling pathways after ischaemic injury..... 191

6.3 Translational implications..... 194

6.4 Limitations and future work..... 195

6.5 Conclusions..... 199

References..... 200

Table of figures

Figure 1.1. Regulation of the mammalian cell cycle. 23
Figure 1.2. Cardiomyocyte cell cycling fate in the adult mammalian heart. 29
Figure 1.3. Pathways controlling cardiomyocyte proliferation. 36
Figure 1.4. NADPH oxidase structure and molecular organisation. 39
Figure 1.5. Exon structure of Nox4D splice variant. 41
Figure 2.1. Generation of the Nox4D transgenic mouse line. 46
Figure 2.2. Breeding strategy for generation of inducible cardiomyocyte-specific Nox4D transgenic mice. 47
Figure 2.3. Analysis of genotype. 49
Figure 2.4. Experimental protocol for initial validation of tamoxifen induction. 49
Figure 2.5. 4-Week myocardial infarction study protocol. 51
Figure 2.6. Experimental protocol for assessment of EdU incorporation in the absence of injury. 53
Figure 2.7. 2-Week myocardial infarction study protocol for assessment of EdU incorporation. 53
Figure 2.8. Nox4D overexpression in csNox4D hearts. 54
Figure 2.9. Optimisation of EdU labelling and validation of detection in vitro. 58
Figure 2.10. Experimental protocol for induction of dedifferentiation in cultured adult cardiomyocytes and assessment of proliferation. 58
Figure 2.11. Optimisation of EdU detection and immunostaining. 67
Figure 2.12. Representative cTnI standard curve 70
Figure 3.1. Overexpression of Nox4D increases proliferation of neonatal cardiac myocytes. 77
Figure 3.2. Induction of Nox4D overexpression in the adult heart. 81
Figure 3.3. Induction of Nox4D overexpression in the adult heart is splice variant-specific. 82
Figure 3.4. Localisation of Nox4D after induction of overexpression in the adult heart. 83
Figure 3.5. Optimisation of immunostaining of Nox4D localisation in isolated adult cardiomyocytes. 84
Figure 3.6. Final optimisation of immunostaining of Nox4D localisation in isolated adult cardiomyocytes. 85
Figure 3.7. Cardiac structure and function are unchanged in inducible cardiomyocyte-specific Nox4D (Ind-csNox4D) transgenic mice. 87
Figure 3.8. Inducible cardiomyocyte-specific Nox4D overexpression does not affect cardiac morphology. 88

Figure 3.9. Cardiomyocyte-specific Nox4D overexpression induced in adult mice does not promote cardiomyocyte proliferation in the absence of injury. 89
Figure 3.10. Cardiac-specific Nox4D overexpression does not enhance signalling of proliferative redox-sensitive pathway Akt..... 91
Figure 3.11. Nox4D overexpression in the adult heart does not affect gene expression profiles associated with dedifferentiation or cell cycle modulation..... 92
Figure 3.12. Induction of Nox4D in the adult heart is not associated with an immediate window for cardiomyocyte proliferation..... 94
Figure 3.13. Nox4D overexpression in the adult heart does not affect transcript expression of markers of dedifferentiation or cell cycle modulation immediately after induction..... 95
Figure 4.1. Systolic function is unchanged in Inducible cardiomyocyte-specific Nox4D animals prior to myocardial infarction. 111
Figure 4.2. Cardiac troponin I release 24 hours post-myocardial infarction estimates similar myocardial injury in Inducible cardiomyocyte-specific Nox4D mice. ... 112
Figure 4.3. Analysis of cardiac contractility by Vevo Strain Software..... 113
Figure 4.4. Cardiomyocyte-specific Nox4D overexpression in adult mice demonstrates functional improvement 2 weeks after myocardial infarction. 114
Figure 4.5. Induction of cardiomyocyte-specific Nox4D overexpression limits deterioration in global longitudinal strain 2 weeks after myocardial infarction. 115
Figure 4.6. Segmental strain analysis of regional cardiac contractility by Vevo Strain Software..... 116
Figure 4.7. Inducible cardiomyocyte-specific Nox4D mice show similar strain rates in specific left ventricular segments 2 weeks after myocardial infarction. 118
Figure 4.8. Cardiac-specific Nox4D overexpression does not sustain improvement in volume-dependent functional parameters 4 weeks after myocardial infarction. 120
Figure 4.9. Induction of cardiomyocyte-specific Nox4D overexpression does not prevent deterioration in global longitudinal strain 4 weeks after myocardial infarction. 121
Figure 4.10. Inducible cardiomyocyte-specific Nox4D mice show regional improvement in strain rate 4 weeks after myocardial infarction. 123
Figure 4.11. Inducible cardiomyocyte-specific Nox4D mice subjected to sham myocardial infarction show no change in cardiac structure and function 4 weeks after surgery. 125
Figure 4.12. Cardiomyocyte-targeted Nox4D overexpression induced in adult mice does not protect against myocardial infarction-induced changes in cardiac morphology. 126

Figure 4.13. Cardiac-specific Nox4D overexpression does not prevent increased transcript expression of markers of hypertrophy 4 weeks after myocardial infarction. 127
Figure 4.14. Cardiomyocyte-specific Nox4D overexpression induced in adult mice results in reduced fibrosis coverage 4 weeks after ischaemic injury. 129
Figure 4.15. Inducible cardiomyocyte-specific Nox4D mice show equivalent cardiac hypertrophy 4 weeks after myocardial infarction. 131
Figure 4.16. Inducible cardiomyocyte-specific Nox4D mice show equivalent cardiac capillary density 4 weeks after myocardial infarction. 132
Figure 4.17. Inducible cardiomyocyte-specific Nox4D mice show trend for reduced cardiomyocyte apoptosis 4 weeks after myocardial infarction. 134
Figure 4.18. Cardiomyocyte-specific Nox4D overexpression induced in adult mice does not promote cardiomyocyte cell cycle activity in the infarct border or remote zone. 136
Figure 4.19. Cardiomyocyte-specific Nox4D overexpression induced in adult mice does not promote cardiomyocyte proliferation in the infarct border or remote zone. 138
Figure 4.20. Nox4D overexpression in the adult heart does not affect transcript expression of markers of proliferation 4 weeks after myocardial infarction. ... 140
Figure 4.21. Nox4D overexpression in the adult heart does not affect transcript expression of markers of dedifferentiation 4 weeks after myocardial infarction. 141
Figure 4.22. Cardiac-specific Nox4D overexpression does not significantly affect transcript expression of markers of angiogenesis 4 weeks after myocardial infarction. 142
Figure 4.23. Cardiac-specific Nox4D overexpression does not affect transcript expression of Nrf2 target genes 4 weeks after myocardial infarction. 143
Figure 4.24. Cardiomyocyte-specific Nox4D overexpression induced in adult mice does not promote cardiomyocyte proliferation in the infarct border or remote zone 2 weeks after myocardial infarction. 145
Figure 4.25. Incremental dosage of tamoxifen appears to be associated with a trend for greater reactive oxygen species generation. 152
Figure 4.26. Incremental dosage of tamoxifen appears to be associated with a trend for greater cardiomyocyte DNA damage. 154
Figure 5.1. Optimisation of siRNA-mediated Nox4D knockdown in vitro. 164
Figure 5.2. Targeted siRNA mediates Nox4D knockdown. 165
Figure 5.3. Targeted siRNA mediates Nox4D knockdown at protein level. 166
Figure 5.4. Isolation of rod-shaped cardiomyocytes from the adult mouse heart. 167

Figure 5.5. Isolated adult mouse cardiomyocytes have organised sarcomeric structures. 168
Figure 5.6. Isolated adult cardiomyocytes remain viable after three days in culture. . 169
Figure 5.7. Oncostatin M induces dedifferentiation of adult mouse cardiomyocytes. . 171
Figure 5.8. Cell size is unchanged in dedifferentiated Nox4D-overexpressing cardiomyocytes. 172
Figure 5.9. Nox4D overexpression increases DNA synthesis in dedifferentiated cardiomyocytes. 174
Figure 5.10. Nox4D overexpression promotes cell cycling in dedifferentiated cardiomyocytes. 176
Figure 5.11. Nox4D overexpression is associated with enhanced proliferation in dedifferentiated cardiomyocytes. 177
Figure 6.1. Redox regulation of stress response signalling cascades in the heart. 193

Table of tables

Table 1. Primers required per reaction for determination of genotype. 48
Table 2. Buffer recipes for adult cardiomyocyte isolation. 56
Table 3. Buffer and media recipes for adult cardiomyocyte purification and culture. ... 57
Table 4. Mouse qPCR primer sequences. 61
Table 5. Primer sequences used for Nox4D knockdown in vitro..... 61
Table 6. Lysis buffers used for protein extraction in cells and tissue. 62
Table 7. Primary and secondary antibodies used for immunoblotting..... 64
Table 8. Primary and secondary antibodies used for immunostaining. 66

Abbreviations

7-AAD	7-aminoactinomycin D
AAR	Area-at-risk
AAV9	Adeno-associated virus serotype 9
Angpt2	Angiopoietin 2
ANP	Atrial natriuretic peptide
ATP	Adenosine triphosphate
AV	Adenovirus
BNP	Brain natriuretic peptide
BrdU	5-bromo-2'-deoxyuridine
BSA	Bovine serum albumin
BZ	Border zone
Cdk	Cyclin-dependent kinases
CDKI	Cyclin-dependent kinase inhibitor
CHD	Coronary heart disease
CIP	Cdk-interacting protein
CPC	Cardiac progenitor cell
csNox4D	Cardiomyocyte-specific Nox4D (constitutive)
cTnI	Cardiac troponin I
CVD	Cardiovascular disease
DDR	DNA damage response
DHE	Dihydroethidium
DNA	Deoxyribonucleic acid
ECM	Extracellular matrix
EDTA	Ethylenediaminetetraacetic acid
EdU	5-ethynyl-2'-deoxyuridine
ERK1/2	Extracellular signal-regulated kinase 1/2
ESC	Embryonic stem cell
FAD	Flavin adenine dinucleotide
FBS	Foetal bovine serum
FGF	Fibroblast growth factor
Gclc	Glutamate-cysteine ligase catalytic subunit
GLS	Global longitudinal strain
GSK-3β	Glycogen synthase kinase-3β
Gsta2	Glutathione S-transferase, alpha 2
H_2O_2	Hydrogen peroxide
HDACs	Class II histone deacetylases

Hif1α	Hypoxia-inducible factor 1 alpha
HPLC	High performance liquid chromatography
IGF1	Insulin-like growth factor 1
Ind-csNox4D	Inducible cardiomyocyte-specific Nox4D
INK4	Inhibitor of Cdk4
iPSC	Induced pluripotent stem cell
IVS, d	Interventricular diastolic septum thickness
KIP	Kinase inhibitor protein
LAD	Left anterior descending coronary artery
LV	Left ventricle
LVEDV	Left ventricular end-diastolic volume
LVESV	Left ventricular end-systolic volume
MAPK	Mitogen-activated protein kinase
MCM	MerCreMer
MI	Myocardial infarction
miRNA	MicroRNA
Mlc2v	Ventricular myosin light chain 2
MPS1	Monopolar spindle protein 1
mRNA	Messenger RNA
Myh6	Myosin heavy chain 6
Myh7	Myosin heavy chain 7
NADPH	Nicotinamide adenine dinucleotide phosphate
NOS	Nitric oxide synthase
Nox2	NADPH oxidase 2
Nox4	NADPH oxidase 4
Nox4D	NADPH oxidase 4D
NRG1	Neuregulin 1
NRVMs	Neonatal rat ventricular myocytes
$O_2^{\bullet-}$	Superoxide
OSM	Oncostatin M
PAGE	Polyacrylamide gel electrophoresis
PBS	Phosphate buffered saline
pHH3	Phospho-histone H3
PI3K	Phosphoinositide 3-kinase
PKA	Protein kinase A
PKG	Protein kinase G
PLAX	Parasternal long axis
PP	Protein phosphatase

PSAX	Parasternal short axis
PTEN	Phosphatase and tensin homolog
PTP	Protein tyrosine phosphatase
RNA	Ribonucleic acid
ROS	Reactive oxygen species
RTK	Receptor tyrosine kinase
RZ	Remote zone
SDS	Sodium dodecyl sulphate
SOD	Superoxide dismutase
ssTNI	Slow skeletal troponin I
TBS	Tris buffered saline
Tg	Transgenic
TGF-β	Transforming growth factor-β
Vegfa	Vascular endothelial growth factor A
VSMC	Vascular smooth muscle cell
WT	Wild type
αMHC	α-Myosin heavy chain

Chapter 1 General introduction

1.1 The impact of cardiomyocyte loss

1.1.1 Heart development and growth

The heart is essential for vertebrate life. As one of the first organs to function, the heart supports blood circulation through the maintenance of continuous and rhythmic contractility.[1,2] Cardiac morphogenesis progresses along a highly conserved developmental pathway, involving formation as a single tube, which then loops and expands to form the chambers.[3] All vertebrates possess a closed and multi-chambered heart comprising 2 to 4 chambers, and therefore show marked variations in final structure between species and classes.[1,4] The adult mammalian heart is composed of 2 atria and 2 ventricles,[5] the key component of which, as shared with most hearts, is the thickened, vascularised and innervated muscular wall.[1] This muscular wall – the myocardium – is responsible for pump function and is enveloped by a thin endothelial cell layer in contact with the blood flow – the endocardium – and an outer mesothelial cell layer – the epicardium.[6] The basic contractile unit of the myocardium is the cardiomyocyte.[7] Though not necessarily the most abundant cell type of the adult mammalian heart; cardiomyocytes occupy 70 – 85% of the volume whilst only constituting 30 – 40% of the cellular population.[8,9] During early development, mammalian heart growth is primarily shaped by cardiomyocyte division, however shortly after birth this ability is mostly lost, and growth becomes determined by physiological hypertrophy. This extensive transition to “terminal” differentiation has generated great interest, as identification of the extrinsic and intrinsic mechanisms that may modulate this proliferative switch is strongly linked to regeneration.[10–12]

1.1.2 Acute myocardial infarction

Several forms of heart disease are characterised by the loss of functional cardiac tissue.[13] Coronary heart disease (CHD) is the most common type of cardiovascular disease (CVD), and remains the leading cause of death worldwide.[14] CHD usually develops over time with increasing age, and is fuelled by concurrent health conditions including diabetes, hypertension and obesity in addition to habitual stressors such as smoking.[15] The major pathological manifestation of CHD is acute myocardial infarction (MI), which usually arises due to the thrombotic occlusion of a coronary artery secondary to rupture of a vulnerable atherosclerotic plaque.[16,17] The human left ventricle has 2 – 4 billion cardiomyocytes, and a single myocardial infarction event can result in the loss of 1 billion of these within hours.[18] This massive depletion of cardiomyocytes is irreversible, and so represents the primary obstacle to complete functional recovery. The most cited basis for this is the limited regenerative ability of the adult mammalian heart to replenish significant numbers of cardiomyocytes.[10] As a consequence, the heart instead undergoes a series of progressive adverse remodelling processes characterised by the

formation of a non-contractile fibrotic scar and compensatory alterations of remote cardiac tissue, which ultimately culminate in the development of heart failure.[11,19]

Despite major advancements in the acute management of MI with revascularisation by primary percutaneous coronary intervention, pharmacological therapies that aim to prevent or delay the progression of heart failure are limited.[20,21] Current clinical guidelines recommend a number of drug treatments post-MI that target the mechanical characteristics of the cardiovascular system, including inhibitors of the renin-angiotensin system and the sympathetic nervous system.[22,23] The implementation of these strategies over the last 30 years has contributed significantly to the improvements seen in early and long-term survival after MI.[24,25] According to the British Heart Foundation, there are over 200,000 hospital admissions in the UK each year due to MI, and 70% of these cases are now survived.[14] However, improved survival has led to the growth of an ageing population and increased incidence of postinfarction heart failure. Epidemiological studies have suggested that this increase has even paralleled the decrease in mortality after MI, meaning that heart failure has become a global health and economic burden.[17,24,25]

As such, currently used therapies are intrinsically non-curative as they remain focussed on myocardial salvage rather than replacement, and therefore fail to address the underlying issue of cardiomyocyte loss. This clearly underscores the clinical need for novel and targeted treatments that stimulate regenerative repair following MI, a concept that represents a key goal for cardiovascular research.[19,21,23]

1.2 Potential for mammalian cardiomyocyte proliferation as a basis for cardiac regeneration

1.2.1 Sources of cardiomyocytes and strategies for repair

The concept of myocardial regenerative therapy is based on the premise that the replacement of cardiomyocytes in the injured heart would address the fundamental issue of cardiomyocyte death through the concomitant restoration of cardiac structure and rescue of cardiac function.[26] For the development of such an intervention, it is important to consider the potential sources from which new cardiomyocytes may be derived. Current myocytes replacement strategies fall into 4 general categories: (i) reactivation of proliferation by induction of cell cycle re-entry in pre-existing cardiomyocytes;[27] (ii) mobilisation of an endogenous cardiomyogenic cardiac progenitor cell (CPC) pool;[28] (iii) exogenous delivery of cardiomyogenic progenitor cells or their cardiomyocyte derivatives originating from pluripotent stem cells (embryonic stem cells [ESCs] or induced pluripotent stem cells [iPSCs]) or adult progenitor cells,[29] which may be bioengineered

as a patch;[30] and (iv) direct reprogramming, or transdifferentiation, of non-cardiomyocytes (such as fibroblasts) to a cardiomyocyte fate.[31]

Although lineage-tracing studies have found insufficient evidence to support a significant contributory role of resident stem cell populations in myocardial repair,[32,33] the last 15 years have seen considerable effort into the development of stem cell-based therapies for cardiac regeneration.[18,34] Studies in animal models and clinical trials in humans have demonstrated that direct transplantation of differentiated myocytes or myogenic stem cells has been associated with, at most, modest improvement in cardiac function.[35,36] The progress of these transplanted stem cell populations as cell replacement therapies has been limited by concerns over transient survival and poor retention in the heart, cell maturation, arrhythmogenesis, immunogenicity, and the need for large-scale production.[10] Furthermore, the mechanistic basis of any functional improvement following stem cell engraftment remains unclear, and may be attributable to paracrine effects.[37] Direct reprogramming of non-myocytes offers a cell-free approach, but requires further development due to the low efficiency of reprogramming vectors.[38]

Based on the limited success of stem cell approaches, the focus of regenerative strategies has shifted to the stimulation of endogenous cardiomyocyte proliferation. Induction of cardiac renewal through the promotion of cardiomyocyte cell cycle activity in the surviving myocardium after injury is a particularly interesting strategy, as this appears to be the major source of new cardiomyocytes in animal models of regeneration.[39,40] This method does not require stimulation of cellular differentiation and maturation, is likely able to generate new cardiomyocytes with excellent electromechanical and vascular integration within the myocardium, and therefore constitutes an attractive and the most direct approach for regenerating the heart.[41,42]

1.2.2 The mammalian cell cycle

In order to understand how adult mammalian cardiomyocytes may be manipulated to enhance their proliferative capacity, it is necessary to consider the molecular signals that regulate cell cycle progression.

The cell cycle in mammalian cells is a tightly regulated process that revolves around 2 main alternating sequences, namely interphase, during which a cell typically spends most of its lifetime, and division, in which the genome is halved to yield 2 identical daughter cells. These sequences are driven by an ordered series of molecular events, which comprise 5 distinct phases: 3 Gap phases – G0, G1, and G2, and S-phase (synthesis), and M-phase (mitosis and cytokinesis). Interphase collectively refers to G0, G1, S, and G2, i.e. all phases between mitoses. Cells in G0 are considered to have ceased proliferation, either due to a lack of mitogenic or the presence of antimitogenic

signals, and are considered to be in a state of quiescence. Upon stimulation, cells enter the G1 phase of the cell cycle, increase in size, and undergo ribonucleic acid (RNA) synthesis and protein synthesis. During late G1, a checkpoint control mechanism (restriction point) serves to regulate commitment to the cycle and permits preparation for chromosomal replication by doubling of the deoxyribonucleic acid (DNA) content in S-phase. The second gap period (G2) proceeds after S-phase, during which cells continue to grow and synthesise protein and RNA, and prepare for M-phase following the G2/M checkpoint.[43,44]

The end of G2 marks the onset of mitosis, a complex and highly regulated process, which is further divided into several stages sequentially known as prophase, prometaphase, metaphase, anaphase, and telophase. These events describe the alignment of condensed chromosomes in the centre of the cell and separation of sister chromatids to opposite poles of the mitotic spindle to allow the equal division of DNA and cellular components.[45] This is accompanied by fragmentation and reformation of the nuclear envelope, and is facilitated by another important checkpoint known as the spindle checkpoint.[45,46] The checkpoints of the cell cycle are therefore essential control mechanisms that monitor the transition between various phases by assessment of the integrity of replication and division to selectively permit cell cycle progression (Figure 1.1).[44,47]

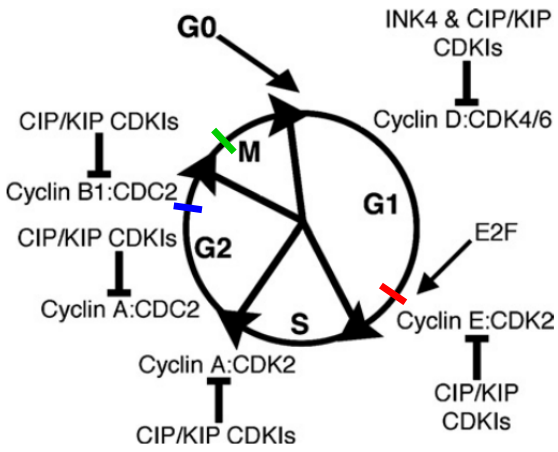

Figure 1.1. Regulation of the mammalian cell cycle. Each round of cell division requires passage through Gap 1 (G1), S-phase (synthesis), Gap 2 (G2), and M-phase (mitosis and cytokinesis). Quiescent cells remain in Gap 0 (G0). Integrity is assessed at the 3 main checkpoints: the restriction point (red), at the G1/S transition; the G2/M checkpoint (blue); and the spindle checkpoint (green), at the metaphase to anaphase transition. Cell cycle progression is controlled by positive regulators (cyclin:Cdk complexes), which are negatively regulated by INK4 and CIP/KIP CDKI family members. E2F transcription factors function at the restriction point, leading to activation of genes required for DNA synthesis. Cdk, cyclin-dependent kinase; CDKI,

cyclin-dependent kinase inhibitor; CIP, Cdk-interacting protein; INK4, inhibitor of Cdk4; KIP, kinase inhibitor protein. Adapted from Bicknell et al, 2007.[43]

Orderly progression through each sequential phase of the cell cycle is dependent on the controlled expression of various cell cycle molecules – the positive regulators (cyclins and cyclin-dependent kinases [Cdks]) and the negative regulators (Cdk inhibitors [CDKIs]), which are in turn regulated by phosphorylation and dephosphorylation events. Cyclins (regulatory subunits) specifically interact with Cdks (catalytic kinase subunits) to form distinct active complexes that phosphorylate a number of substrates to drive the cell cycle from one phase to the next.[43,44] The cyclins can be functionally grouped into the G1 cyclins (cyclins D and E), the S phase cyclins (cyclins A and E), and the mitotic cyclins (cyclins A and B).[47] Most cyclins therefore show dramatic fluctuation in their messenger RNA (mRNA) and protein expression levels throughout the cell cycle as a consequence of changes in their transcription and ubiquitin-mediated degradation. The Cdks are a family of serine-threonine protein kinases that, on their own, possess no detectable kinase activity but require the sequential activation by their specific cyclin partner(s), and therefore play an essential regulatory role once complexed through the integration of signals from extracellular mitogenic molecules such as growth factors.[43,44]

Growth factors can stimulate a number of signalling pathways, of which the Ras-dependent mitogen-activated protein kinase (MAPK) pathway plays a major role in induction of G1 entry. The D-type cyclins (cyclins D1, D2, and D3) accumulate in response to mitogenic stimulation and bind to Cdk4 or Cdk6 in early G1.[43,48] Cyclin D:Cdk4/6 complexes then initiate progression through G1 by phosphorylation of members of the retinoblastoma (Rb) family of pocket proteins, allowing the release of E2F transcription factors, which promotes cell cycle progression through the G1/S-phase transition by transcriptional activation of cyclins A and E and target genes required for DNA synthesis. Cyclins E and A form complexes with Cdk2 and are important for transition through the restriction point and progression through S-phase, respectively. The cyclin A:cell division cycle 2 (Cdc2, also known as Cdk1) complex forms in and promotes progression through G2, then cyclin B1:CDC2 promotes G2/M transition and progression through M-phase, degradation of which is required to enable exit from mitosis and cytokinesis.[43,44]

The expression of the Cdks remains relatively constant throughout the phases of the cell cycle, and so their activity is negatively modulated by association with various CDKIs.[44] The CDKIs are categorised into 2 structurally distinct families – the inhibitor of Cdk4 (INK4) family and the broader specificity CIP/KIP (Cdk-interacting protein/kinase inhibitor protein) family.[49] The INK4 CDKIs comprise p14, p15, p16, p18, and p19, which target cyclin D:Cdk4/6 complexes, and are therefore involved in G1-phase control, whilst the

CIP/KIP CDKIs include p21, p27, and p57, and can inhibit all Cdks.[43,44] Members of the 2 CDKI classes show differential mechanisms of Cdk inhibition; the INK4 members indirectly block cyclin binding and complex formation by causing allosteric changes in the Cdk binding site, whereas the CIP/KIP members bind to and inhibit the catalytic kinase activity of the entire cyclin:Cdk complex.[44] Although the degradation of cyclins via the ubiquitin-proteasome pathway is an important regulatory mechanism for cyclin:Cdk activity, the CDKIs function as another form of control during checkpoint regulation and in the modulation of cell cycle progression throughout.[47] Their expression is therefore increased in response to antiproliferative signals such as contact inhibition,[50] senescence,[51] and extracellular antimitogenic factors such as transforming growth factor-β (TGF-β).[52]

1.2.3 Endogenous heart regeneration in lower vertebrates and neonatal mice in response to injury

Discoveries of animals that can naturally regenerate their hearts after injury have provided great insight into the innate regulation and extrinsic environmental stimuli of cardiomyocyte proliferation.[21] It is now clear that, in contrast to the limited regenerative ability of adult mammalian hearts, certain teleost fish and urodele amphibians possess a robust capacity for cardiac regeneration throughout life.[13] Although there is a long history of research into the regeneration of urodele amphibian hearts, the zebrafish has emerged as possibly the most developed model system for adult heart regeneration in light of its high amenability to genetic manipulation.[10,18]

Zebrafish hearts can regenerate with limited or no scarring in a variety of severe injury models.[10] This was first demonstrated in 2002 by surgical resection of approximately 20% of the apical myocardium, after which the wound is initially sealed by a fibrin-rich clot, which is not replaced by collagen but rather the gradual restoration of vascularised cardiac muscle, resulting in complete regeneration of the ventricle within 60 days.[53] This mode of recovery has also been reproduced in cryoinjury of approximately 20% of the ventricular wall,[54] genetic ablation of up to 60% of the myocardial cardiomyocyte population through inducible expression of cardiomyocyte-specific diphtheria toxin A,[55] and hypoxia-reoxygenation injury.[56]

Such robust models of zebrafish heart regeneration have provided the ideal basis to directly assess the cellular source(s) of renewed myocardium through the use of tamoxifen-inducible, Cre-based genetic fate-mapping tools that irreversibly label cardiomyocytes with a fluorescent reporter protein prior to injury. Once activated, the reporter protein is expressed in all cardiomyocytes and their progeny, and is thus indicative of the source of newly generated cardiomyocytes.[57] Such lineage tracing

experiments have conclusively shown that almost all new cardiomyocytes post-injury are labelled, and are therefore derived from pre-existing cardiomyocytes that are capable of entering the cell cycle and dividing.[39,58] The mechanisms underlying proliferation of the pre-existing cardiomyocyte pool are considered to involve the reactivation of endogenous mitogenic pathways that guide embryonic heart development, including neuregulin 1 (NRG1)[59] and Notch signalling,[60] with upregulation of cell cycle regulators such as Mps1 (monopolar spindle protein 1 – a mitotic checkpoint kinase).[53] Studies have also shown that this response involves the redeployment of embryonic or juvenile developmental gene programs, since most regenerating myocytes show activation of regulatory sequences of the transcription factor GATA4, an important gene during heart development known to regulate cardiomyocyte differentiation and survival.[58,61,62] This is consistent with increased transcript expression of other transcription factor genes synonymous with early development, including GATA5 and Hand2.[63] Interestingly, these findings coincided with observations that regenerating zebrafish cardiomyocytes acquire a less organised, dissociated sarcomeric structure with transient uncoupling of electrical conductance before cell division, then undergo a maturation process and reintegrate into the myocardium.[39,55,58] These features are consistent with a reversion of maturity, and collectively describe cardiomyocyte dedifferentiation. Thus, it is now accepted that pre-existing, differentiated adult cardiomyocytes reduce their contractile state by dedifferentiating to a more embryonic phenotype in order to facilitate cell division in the regenerating heart.[1,11]

Although previously considered exclusive to zebrafish, other teleost fish and some urodele amphibians, it was later learnt in 2011 that the 1-day-old neonatal mouse heart is also capable of regenerating after surgical resection of approximately 15% of the cardiac apex. This regenerative response was characterised by cardiomyocyte proliferation with minimal residual scarring and hypertrophy, and normalisation of cardiac systolic function within 2 months of surgery.[40] This has also been demonstrated in other models of injury, including MI[64], in which a robust angiogenic response was also reported, and cryoinjury (partial regeneration).[65] Reminiscent to that in zebrafish, lineage tracing and histological analysis revealed that the dominant cellular source of regenerated cardiomyocytes in the neonatal mouse heart is global proliferation of the resident cardiomyocyte pool, accompanied by evidence of sarcomere disassembly,[40,64,65] and has also been show to require GATA4.[66]

However, in contrast to the zebrafish heart whose regenerative capacity is retained throughout adulthood, the ability of the neonatal murine heart to regenerate after injury is lost by postnatal day 7 (P7).[40,67] This is considered to coincide with the stage at which rodent cardiomyocytes lose their proliferative potential,[68] and so the transient

regenerative response is likely to harness the early developmental growth pathways.[11] Indeed, the neonatal regenerative ability has even been argued to decline sharply within 48 hours of birth as a result of differentially expressed transcripts encoding for extracellular matrix (ECM) components and cytoskeletal constituents, thus highlighting the regenerative influence of the local microenvironment rather than autonomous cellular proliferative mechanisms.[69] Nevertheless, the discovery of regeneration in the neonatal mouse heart suggests that this mode of repair is not evolutionarily lost by mammals, and so it is paramount that factors are identified that may extend this response into adulthood.[21]

1.2.4 The regulation of postnatal cardiomyocyte cell cycle withdrawal

Cardiomyocyte cell cycle arrest in postnatal life is accompanied by the uncoupling of DNA synthesis and mitosis from cytokinesis.[12] This characteristic switch in cardiomyocyte growth potential from a proliferative to a hypertrophic phenotype occurs at different stages of development in different species.[43] In rodents, most cardiomyocytes exit the cell cycle within the first week of birth and become multinucleated and polyploid,[70] whereas in humans this occurs in early adulthood, with most cardiomyocytes remaining mononucleated throughout life.[9] The molecular basis for this transition is defined by the changing expressions of cell cycle regulatory components, where positive regulators of cell cycle progression – certain cyclins, Cdks, and the major E2F transcription factors – are significantly downregulated in adult cardiomyocytes,[71] whereas key repressors of cell cycle progression such as p21Cip1 and p27Kip1 become highly expressed.[72] These changes underpinning postnatal arrest may in turn be critically regulated by the transcription factor Meis1, deletion of which has been shown to extend the postnatal proliferative window in mouse cardiomyocytes.[73] Microarray analysis has also revealed a regulatory role for microRNAs (miRNAs) in mitotic arrest through the identification of the miR-15 family, known to target a number of cell cycle genes, as a highly upregulated miRNA subset in the postnatal mouse heart.[74]

It remains unclear whether the signals that modulate cardiomyocyte exit from the cell cycle are intrinsic or extracellular.[12] Correlative evidence suggests that multinucleation and polyploidisation create barriers to cytokinesis and therefore myocardial regeneration.[75,76] In support of this inverse correlation between myocardial ploidy and regenerative capacity, a recent study has shown that approximately 99% of cardiomyocytes in the highly regenerative adult zebrafish heart are mononuclear and diploid. In addition, experimental polyploidisation of zebrafish cardiomyocytes was indeed sufficient to impair their proliferative capacity and ability to recover after apical resection such that scar formation was consistently observed.[77]

Both the zebrafish and mammalian foetal heart reside in relatively hypoxic environments. In contrast, oxygen tension rapidly rises soon after birth and drastically changes the oxygenation state of cardiomyocytes. Consequently, this is considered to predispose to the generation of reactive oxygen species (ROS) through the embryonic-to-postnatal switch from glycolysis to utilisation of oxygen-dependent mitochondrial oxidative phosphorylation as a major energy source.[78] Although this confers a significant energy advantage, the postnatal increase in ROS levels in cardiomyocytes has been linked to mitochondrial-dependent oxidative stress and cell cycle arrest via activation of the DNA damage response (DDR) pathway.[79] Furthermore, in comparison with the low-pressure, 2-chambered zebrafish heart, mammalian hearts are structurally more complex, possess a greater fibroblast constituency, and are subjected to greater mechanical stretch as a result of increased blood pressure. The highly organised architecture of mature sarcomere proteins may even physically hinder cytokinesis. As such, the large-scale, organ-wide cardiomyocyte dedifferentiation and concomitant electric uncoupling required for proliferation, as seen in the zebrafish heart, may not be compatible with mammalian heart function or survival.[11,12]

These hallmark metabolic and mechanical features of adult mammalian cardiomyocytes likely share considerable overlap in the modulation of cell cycle withdrawal, since the increased metabolic efficiency required to cope with increased workload might collectively represent an evolutionary trade-off at the expense of the ability to proliferate.[78]

1.2.5 Evidence for cardiomyocyte turnover in the adult heart

The adult mammalian heart has traditionally been viewed as a postmitotic, terminally differentiated organ limited to a single mechanism of growth by cardiomyocyte enlargement.[80] With the development of significant technological advancements, this classical paradigm has been actively challenged and modified to accept the emerging consensus that whilst hypertrophy remains the dominant mechanism of growth, the adult heart retains some capacity for cardiomyocyte renewal, although very limited.[81,82]

Labelled thymidine and thymidine analogs are stably incorporated into the genome during S-phase and have been widely used to measure cell cycle events.[81] Using tritiated thymidine labelling assays, studies in the late 1990s were able to map cardiomyocyte DNA synthesis and cell cycle dynamics after birth in mice and showed a very modest but detectable level in adulthood, although the outcome of these cells with regard to polyploidisation, karyokinesis, and cytokinesis remained unclear (Figure 1.2).[68,83,84]

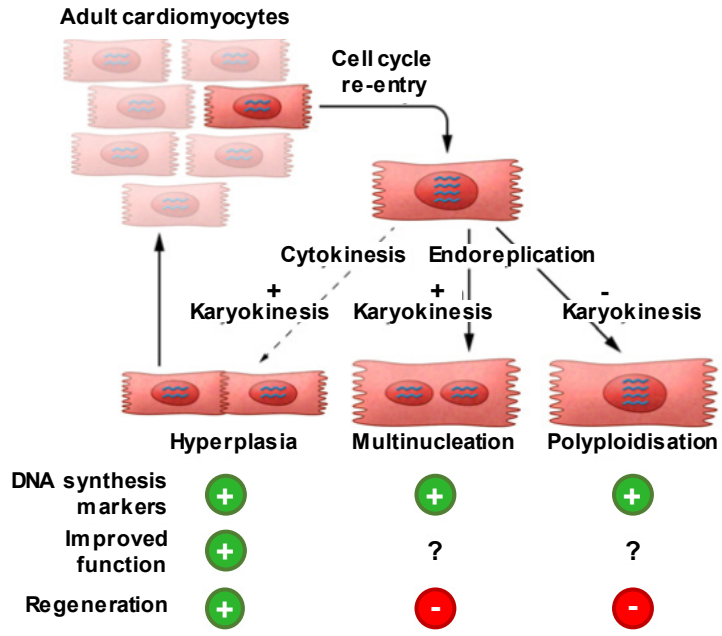

Figure 1.2. Cardiomyocyte cell cycling fate in the adult mammalian heart. In the adult mammalian heart, most cardiomyocytes remain quiescent and are not progressing through the cell cycle. Rare events of cardiomyocytes that do re-enter the cell cycle may be classified as those that complete the cell cycle phases by undergoing mitosis followed by karyokinesis and cytokinesis, or more commonly, those that are non-proliferative. The latter cell cycle events of endoreplication describe an increase in DNA content with or without karyokinesis to produce multinucleate and polyploid cells, respectively, and pose a challenge for investigation of proliferation. Only cardiomyocyte cell cycles that result in hyperplasia may contribute to regeneration. Adapted from Karra and Poss, 2017.[85]

To resolve this issue, a more direct assessment of cardiomyocyte cell cycling in the adult mouse heart was undertaken using multi-isotope imaging mass spectrometry combined with genetic fate mapping for detection of the non-radioactive thymidine analog ^{15}N-thymidine.[86] This was able to demonstrate that cardiomyocytes are renewed from pre-existing cardiomyocytes in young adult mice at an annual rate of 0.76% under normal homeostatic conditions, and at declined rates in aged mice. Importantly, cardiomyocyte exchange was augmented after permanent myocardial infarction in the border zone region, suggesting activation of endogenous proliferative pathways secondary to injury.[86]

Further evidence gained from the adult mouse heart identified the potential for a small subset of cardiomyocytes to possess greater propensity to proliferate. Lineage tracing by hypoxia fate mapping was able to selectively label hypoxic cardiomyocytes through fusion of the oxygen-dependent degradation domain of hypoxia-inducible factor 1 alpha (Hif1α) to a tamoxifen-inducible Cre recombinase.[87] Identification of this rare population of myocytes and their progenies revealed the contribution, though not exclusive, of hypoxia signalling to new cardiomyocyte formation in the adult heart (projected at approximately 0.3 – 1% per year). This was linked to reduced oxidative damage and

greater retention of characteristics resembling neonatal cardiomyocytes such as smaller size and mononucleation (as discussed in the regulation of postnatal cardiomyocyte cell cycle withdrawal in *1.2.4*). It remains unclear whether this model describes a persistent subpopulation of myocytes or an oscillating state between hypoxia and normoxia.[87]

The dramatic increase in atmospheric ^{14}C as a result of post-war nuclear weapon tests enabled the investigation of cardiomyocyte turnover in humans using the radiocarbon dating technique in conjunction with stereological and flow cytometric analysis. These techniques were able to assess the pulse labelling of cardiomyocyte DNA in order to establish the age of cardiac cells.[9,88] The measurements from human cardiac tissue revealed a low but continuous cardiomyocyte renewal level that falls with age, corresponding to a replacement rate of approximately 1% per year at the age of 20, declining to lower than 0.5% in elderly individuals. In the approach to the adult renewal rate in the second decade of life, DNA content was found to increase per cardiomyocyte nucleus, indicating a switch to polyploidisation. These data support a continuous turnover of the cardiomyocyte population in which cell birth is counterbalanced by cell death, thus maintaining the cardiomyocyte number established after the perinatal period constant throughout life.[9,88]

Overall, collective analysis of these major studies and others by a consensus statement has established that in the healthy, uninjured adult mouse and human heart, the total number of cardiomyocytes remains essentially stable, and annual rates of turnover are currently estimated at 0.5 – 2% in both species.[82]

1.3 Mechanisms stimulating cardiomyocyte renewal

Regardless of the absolute level of intrinsic proliferative capacity retained by the adult mammalian heart, it is clear that heart failure frequently persists after significant myocardial injury. This means that, in the absence of intervention, this degree of cell turnover is evidently insufficient to compensate for the loss of up to 1 billion cardiomyocytes following a major ischaemic event. Although the underlying mechanisms for cardiomyocyte regeneration remain highly debated, a number of therapeutic strategies have been investigated in an attempt to counteract the initial cardiomyocyte loss by augmentation of cell cycle re-entry in the surviving cardiomyocyte population.[26,89]

1.3.1 Genetic manipulation of cell cycle regulators

Multiple attempts have been made to stimulate cardiomyocyte proliferation by overexpression of various cell cycle components. Cyclin A2 was one of the first cell cycle targets to demonstrate enhanced progression through the cell cycle in mature cardiomyocytes.[23] Transgenic overexpression of cyclin A2, which is important during S-phase and G2 progression, has been reported to stimulate cardiomyocyte proliferation,[90]

and mediate functional benefit associated with increased DNA synthesis and mitotic indices after ischaemic injury in mice.[91] Subsequent studies have also shown that adenoviral-mediated delivery of cyclin A2 in a porcine model of myocardial ischaemia was associated with improved recovery and induction of cytokinesis of pre-existing cardiomyocytes in addition to preservation of sarcomeric structure in newly generated cells.[92]

Overexpression of the early G1 D-type cyclins in transgenic mice has been sufficient to stimulate DNA synthesis in adult myocardium under basal conditions, but was associated with differential effects on recovery following injury. Mice overexpressing cyclins D1 or D3 showed a reduction in the level of cardiomyocyte synthesis following injury, whilst overexpression of cyclin D2 showed sustained DNA synthesis, leading to regenerative growth and infarct regression.[93,94] However, there have been concerns that the demonstration of DNA synthesis in these studies has been inadequately accompanied by evidence of cytokinesis, and therefore may not be reflective of true proliferation.[12]

More recently, adenoviral-mediated overexpression of a combination of 4 cell cycle regulators (Cdk1, Cdk4, cyclin B1, and cyclin D1) was shown to efficiently induce cardiomyocyte cell cycle activation in the adult mouse heart with significant improvement in cardiac function after myocardial infarction.[95] Importantly, this study was able to rigorously assess cell division events in vivo by utilisation of the Cre-recombinase-dependent mosaic analysis with double markers (MADM) lineage tracing system in order to genetically label cardiomyocytes demonstrative of cytokinesis, and therefore able to attribute the improved functional response to cardiomyocyte regeneration.[95]

1.3.2 MicroRNAs

MiRNAs represent a class of small, non-coding RNAs that negatively modulate gene expression either through the repression of protein translation or the promotion of mRNA degradation. A single miRNA can target hundreds of different mRNAs, whilst a single mRNA may be interfered with by multiple miRNAs.[12] Given their capacity to suppress large collections of mRNAs encoding for proteins involved in common signalling pathways, miRNAs are now recognised as central regulators of cardiac development and disease.[96]

As some miRNAs have been implicated in the postnatal cardiomyocyte cell cycle exit (as discussed in *1.2.4)*, it was reasoned that others could stimulate the reverse. This was addressed by a high-throughput screening assay using a genome-wide, human miRNA library, resulting in the identification of 40 miRNAs with the capacity to stimulate cell cycle activity as evidenced by DNA replication and cytokinesis of cultured mouse and rat neonatal cardiomyocytes.[97] The most effective hits of this initial selection, namely miR-

199a and miR-590, were also able to demonstrate evidence of cell cycle re-entry and division in cultured adult cardiomyocytes. The downstream targets of miR-199a and miR-590, including the calcium signalling regulator Homer1 and the homeodomain protein Hopx, were all identified as inhibitors of cardiomyocyte proliferation. When administered by exogenous delivery to the adult mouse myocardium, these miRNAs selectively stimulated cardiomyocyte proliferation and markedly improved recovery of cardiac functional parameters with reduced fibrotic scarring following infarctive injury.[97,98] Furthermore, this has very recently been strengthened by evidence in large mammals, in which adeno-associated viral delivery of miR-199a was able to demonstrate marked improvement in both global and regional contractility after MI in pigs, mediated by endogenous cardiomyocyte proliferation and dedifferentiation. However, persistent and uncontrolled expression of the miRNA resulted in sudden arrhythmic death and myocardial infiltration of the proliferating cells, demonstrating the clinical potential of this strategy but reinforcing the importance of tight dosage control.[99]

Another group of miRNAs implicated in cardiomyocyte proliferation is the miR-17-92 cluster. Originally identified as a human oncogene, the miR-17-92 cluster has demonstrated its importance in cardiomyocyte cell cycle re-entry through gain- and loss-of-function studies in which cardiomyocyte-specific deletion of this cluster resulted in cardiac hypoplasia, whilst its transgenic overexpression induced cardiomyocyte proliferation in embryonic, postnatal, and adult hearts; that latter of which was sufficient to enhance cardiac function after myocardial infarction.[100] Interestingly, these effects were shown to be mediated via regulation of the tumour suppressor phosphatase and tensin homolog (PTEN) – an important endogenous inhibitor of the phosphoinositide 3-kinase (PI3K) signalling pathway.[100]

1.3.3 Signal transduction pathways

Since the adult heart is composed of a heterogeneous cellular population, multiple cell types, including fibroblasts, endothelial, and smooth muscle cells, are likely to contribute to the regulation of cardiomyocyte biology through the release of diffusible molecules.[12] The identification of potential ligands and their receptors that play a role in cardiomyocyte proliferative and regenerative signalling has been an important target for research.[101]

The Notch signalling pathway activates a set of genes encoding transcriptional activators that regulate genes involved in heart growth and patterning, and is thus a key pathway in cardiac development. Notch signalling is mediated via cell transactivation, in which a ligand-expressing cell transactivates a neighbouring cell, which positively propagates further signalling by upregulation of ligand and receptor expression in signalling and receiving cells, respectively.[102] As discussed in section *1.2.3*, the importance of Notch signalling in cardiac regeneration has been demonstrated in the adult zebrafish heart,

which involves the re-engagement of a number of developmental signalling pathways.[60,89] Notch pathway activation has also been shown to sustain cardiomyocyte proliferation at birth in the mammalian heart.[103,104] Despite these findings, reactivation of this pathway in the adult mouse heart has proved ineffective in inducing cardiac regeneration after myocardial infarction, as a result of blunted efficacy due to the presence of permanent epigenetic repressive marks at Notch-responsive promoters.[105]

Likewise, NRG1 signalling is also essential during cardiac development, acting as a key mitogen via the ERBB2 and ERBB4 receptor tyrosine kinases of the epidermal growth factor receptor family.[106,107] NRG1 signalling is also required for zebrafish heart regeneration, and its overexpression induces cardiomyocyte proliferation even in the absence of injury.[59] Multiple downstream effectors of NRG1/ERBB signalling in cardiac models have been identified, including Akt and MAPK/extracellular signal-regulated kinase 1/2 (ERK1/2).[101] In adult differentiated rat cardiomyocytes, NRG1 has been shown to stimulate DNA synthesis and cytokinesis facilitated by sarcomeric disassembly through the activation of ERBB4 signalling.[75] When administered in vivo, recombinant NRG1 is associated with enhanced cardiomyocyte proliferation and functional recovery after myocardial infarction in adult mice,[75] although the regenerative effects of this pathway in the adult heart have been contested (Figure 1.3).[108] Furthermore, the signalling molecule p38 MAPK is a negative cell cycle regulator and its activity is therefore inversely correlated with cardiac growth during development. As such, inhibition of p38 has been shown to initiate dedifferentiation and proliferation of adult cardiomyocytes in vitro,[109] and, when coupled with FGF1, p38 inhibition in vivo has demonstrated the ability to promote cardiomyocyte proliferation and enhance functional parameters post-MI in adult rats.[110] However, it is important to note that even though these mitogens are associated with some degree of adult cardiomyocyte proliferation, their efficiency to stimulate cell cycle re-entry is considered to be low, and appears to be restricted to the mononucleated subset of cardiomyocytes in rodent models.[89] As with Notch signalling, cardiac regeneration in the adult mammalian heart may not necessarily recapitulate the events of development, meaning that adult cardiomyocytes may not be permissive to cell cycle re-entry in response to the same developmental signals.[12,89]

The Hippo pathway is an evolutionarily conserved pathway that has emerged as a major regulator of cell proliferation, growth, and organ size.[111] Its core signalling components in mammals include the mammalian STE20-like protein kinases 1 and 2 (Mst1 and Mst2), the scaffolding protein Salvador (Salv), the large tumour suppressor homolog 1 and 2 (Lats1 and Lats2) protein kinases, the terminal effector Yes-associated protein (Yap) and transcriptional co-activator with PDZ-binding motif (Taz). Activation of this signalling cascade leads to phosphorylation of Yap and Taz, resulting in their exclusion from the

nucleus and consequent disrupts their association with DNA binding transcription factors that normally drive cellular growth. Hippo signalling therefore acts to control heart size during cardiac development by limiting cardiomyocyte proliferation.[111] Consistent with this, the levels of phosphorylated Yap in the heart have been found to increase in mice after P7 compared to hearts at P2.[112]

The key components of the Hippo pathway have been studied for their effects on proliferation in mature cardiomyocytes. Hearts with postnatal cardiomyocyte-specific knockout of the gene encoding Salv have shown evidence of regenerated myocardium with reduced scar size after apical resection at P8, indicative of prolongation of the postnatal proliferative window. In addition, induction of Hippo deficiency in 2 genetic models by cardiac-specific knockout of Salv and both Lats1 and Lats2 was sufficient to mediate cardiomyocyte cell cycle re-entry and cytokinesis in unstressed adult mice, and confer regenerative protection from infarctive injury with normalisation of cardiac function within 3 weeks.[112] Deletion of cardiomyocyte Salv in the adult mouse heart has also been shown to induce a reparative genetic response with increased cardiomyocyte renewal, scar border vascularity, reduced fibrosis, and recovery of function even when deleted in established ischaemic heart failure 3 weeks after myocardial infarction.[113] Furthermore, the transgenic and viral-mediated overexpression of the downstream component Yap in the adult heart has similarly been shown to promote cardiomyocyte proliferation and elicit therapeutic benefit in models of cardiac injury.[114,115]

These results clearly support the regulatory role for the Hippo pathway in cardiomyocyte proliferation not only during development but also during postnatal and adult life. Previous evidence suggests that this pathway may also be subject to modulation by ligand-receptor binding (Figure 1.3).[116] The induction of Yap-mediated proliferation has been shown to de-repress the genes activated by the Wnt/β-catenin pathway,[117] involving the activation of insulin-like growth factor 1 (IGF1) receptor signalling, phosphorylation of Akt and inactivation of glycogen synthase kinase-3β (GSK-3β), leading to the stabilisation of β-catenin.[115,118] Interestingly, investigation of the link between the Hippo pathway and the PI3K-Akt pathway identified Pik3cb – an isoform encoding the PI3K catalytic subunit – as a crucial direct target and effector of Yap, and further demonstrated that overexpression of Pik3cb in adult mice after MI was able to promote cardiomyocyte cell cycle activity and survival.[119]

Implicated as a central signal transduction cascade in proliferation, the PI3K-Akt pathway plays an important role in cardiac viability and growth.[120] The downstream effector, Akt, is a serine-threonine kinase that has been implicated in the inhibition of CDKIs and opposition of cell cycle arrest.[121] Studies in which mice were genetically modified to overexpress a nuclear-targeted, constitutively active Akt revealed superior

cardiomyocyte survival,[122] and a greater number of cardiomyocytes in the adult heart in the absence of hypertrophy, but smaller in volume with enhanced contractility.[123] This model has also been associated with prolongation of the postnatal proliferative window 3 weeks after birth.[124]

1.3.4 Redox control of proliferation

The intracellular activity of ROS has emerged as a an additional potential regulator of cardiomyocyte proliferation.[101] As discussed in section *1.2.4*, there has been research to suggest that ROS contribute a negative regulatory role to the cardiomyocyte cell cycle, particularly emphasised during the postnatal hyperplastic-to-hypertrophic transition.[79] In support of this, the impact of increased oxygenation state in adult mammals has recently been further demonstrated by gradual exposure of mice to severe systemic hypoxaemia. This was shown to decrease ROS production and oxidative DNA damage, and reactivate cardiomyocyte mitosis sufficiently to enable a robust regenerative response with decreased myocardial scarring and improvement in left ventricular systolic function 1 week after infarctive injury.[125] Moreover, the ROS that are produced during the postnatal transition have additionally been shown to activate the Hippo pathway through modulation of Mst1 and Mst2.[126] Conversely, a study that aimed to investigate the downstream factors that promote renewal in a heart regeneration mouse model of Hippo deficiency identified the homeodomain transcription factor Pitx2 as being upregulated in the border zone of infarcted hearts. Genomic analyses revealed a primary role for Pitx2 in promoting ROS scavengers to mediate protection from oxidative damage, which was also found to involve Nrf2 as a regulator of the antioxidant response.[127]

Nevertheless, the influences of hypoxia and ROS generation on cardiomyocyte proliferation remain somewhat unclear. ROS scavenging in the context of postnatal cardiomyocyte cell cycle arrest was only found to postpone, not impede this transition,[79] strongly suggestive that other intrinsic or extrinsic mechanisms are involved. Interestingly, the reactive species hydrogen peroxide (H_2O_2) has actually been proposed as a positive factor in zebrafish heart regeneration, since scavenging of this molecule by transgenic catalase overexpression was shown to impair regenerative recovery.[128] Treatment with low-level H_2O_2 has also been shown to enhance the proliferation of murine neonatal cardiomyocytes and embryonic stem cell-derived cardiomyocytes in vitro, involving downregulation of p27Kip1 and nuclear translocation of cyclin D1.[129] Additionally, transgenic mice with excess myocardial H_2O_2 generation have been reported to demonstrate larger, hyperplastic hearts with a prolonged postnatal cardiomyocyte cycling period.[130] It is therefore evident that the modulation of cellular effects by ROS are crucially determined by the level and context in which they are released, and could be dependent on the differentiation between the functions of ROS

within redox-mediated signalling pathways as opposed to the concept of oxidative stress.[131]

As such, it has become increasingly recognised that the proliferation of cardiomyocytes and other cell types is under the control of redox-regulated signalling pathways. Redox sensing of cell cycle regulation has been shown to involve targets such as reactive cysteine thiols present in cell cycle regulator molecules.[132] Intracellular-generated ROS has also been shown to target mitogenic signalling cascades such as MAPK/ERK1/2 and Akt,[130,132] which may in part be mediated by inactivation of protein tyrosine phosphatases (PTPs) (Figure 1.3).[133] It is thus of significant interest to understand the mechanisms that link intracellular ROS to increased cardiomyocyte proliferation by elucidation of the precise source, site of generation, and redox targets of the reactive species involved.

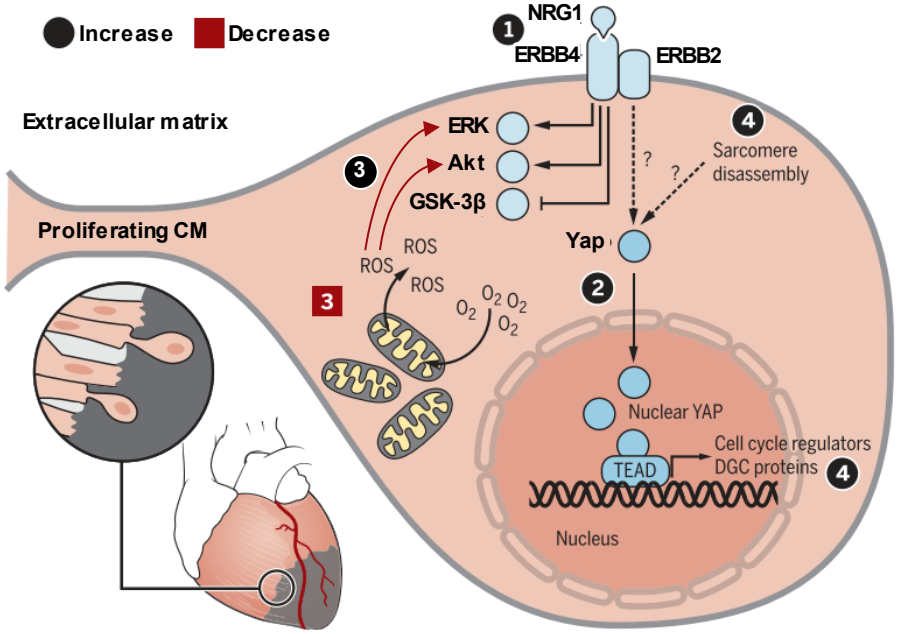

Figure 1.3. Pathways controlling cardiomyocyte proliferation. Pathways that initiate cardiomyocyte proliferation may be targeted for cardiac regeneration. (1) Several ligands have been identified that promote proliferation in models of regeneration, including neuregulin 1 (NRG1), which activates multiple downstream effector pathways through ERBB signalling in adult mononuclear cardiomyocytes. (2) Inhibition of upstream inhibitory Hippo kinases promotes nuclear entry of unphosphorylated Yes-associated protein (Yap), leading to transcriptional activation of factors that drive cellular growth. (3) Increased oxygenation and mitochondrial reactive oxygen species (ROS) formation after birth contribute to cardiomyocyte cell cycle arrest, but localised ROS also promote proliferation via redox modification of sensor proteins that are centrally involved in cell cycle regulation. (4) Cardiomyocyte proliferation requires cellular dedifferentiation by sarcomeric disassembly, which may be inhibited by the dystrophin glycoprotein complex (DGC)-mediated inhibition of Yap nuclear localisation. ERK, extracellular

signal-regulated kinase; GSK-3β, glycogen synthase kinase-3β; TEAD, TEA domain family members. Adapted from Tzahor and Poss, 2017.[134]

1.4 Cardiac redox signalling

1.4.1 The signalling functions of reactive oxygen species

ROS have traditionally been viewed as by-products of mitochondrial oxidative metabolism with a primary role in causing macromolecular damage. Mitochondrial ROS are known to cause cellular toxicity by promoting damage of lipids, protein, or DNA, resulting in cell cycle arrest, apoptosis, or cellular senescence.[78] As such, it has been considered that a pathologically high level of oxidant species in cells may underlie the development of many cardiovascular diseases, including atherosclerosis, hypertension, and heart failure, through exposure to oxidative stress.[131,135] However, antioxidant strategies have failed to show efficacy in ameliorating disease progression, and so this concept has neglected the paradoxical wider roles of ROS in the maintenance of redox balance. ROS therefore also serve important biological functions through modulation of a variety of physiological processes by redox signalling reactions.[131]

As opposed to the broad and non-specific range of oxidations that might occur in stressed tissues, redox signalling refers to the specific, usually reversible, oxidative and reductive reactions that result in the targeted post-translational modification of biomolecules involved in cellular signalling pathways.[131,136] Such molecular targets are protein sensors that respond to variations in local redox state by a change in conformation, interactions, stability, and activity, and therefore serve as signal transducers. These proteins include receptors, ion transporters, enzymes (notably kinases and phosphatases), transcription factors, and cytoskeletal filaments, the most susceptible targets of which are likely cysteine residue thiols.[131] The major reactive species involved in redox signalling are the superoxide anion ($O_2^{\bullet -}$), the product of a one-electron reduction of oxygen, and the more stable nonradical H_2O_2 to which it dismutates, either spontaneously or catalysed by superoxide dismutases (SOD). H_2O_2 is relatively stable in vivo, but may be decomposed by catalase or oxidising enzymes such as peroxidase. It is also lipid-soluble, and can diffuse freely across cellular membranes.[131,137]

In the heart, redox signalling plays a key role in the regulation of physiological processes (e.g. cellular differentiation, proliferation, survival), adaptation to stress, and pathophysiological processes (e.g. adverse ventricular remodelling). The signalling outcomes of ROS are crucially influenced by factors including the precise species released and half-life, cellular localisation, local concentration, and subcellular antioxidant pools. In addition to the ROS-decomposing enzymes stated above, the local

antioxidant environment is also determined by the ROS scavengers glutathione, which can reduce a diverse range of oxidised proteins, and thioredoxin, which may have more specific reductive functions.[131,138]

1.4.2 The main sources of ROS in cardiomyocytes

The predominant ROS sources in the heart include the mitochondria, metabolic enzymes, uncoupled nitric oxide synthases (NOSs), and the specialised enzymes of ROS generation – the nicotinamide adenine dinucleotide phosphate (NADPH) oxidases, also known as Noxs.[131,138]

Mitochondria can generate ROS at different stages during the reduction of O_2 to H_2O in the electron transport chain (ETC) due to electron leakage.[138] The steady-state levels of ROS produced here depend on the rates of production at different sites in the ETC as well as the activity of antioxidants present in the matrix and cytosol. Mitochondrial ROS may be particularly detrimental in the setting of mitochondrial dysfunction secondary to ischaemia-reperfusion injury.[139] Metabolic pathways also contribute to the production of ROS during several oxidase-mediated biosynthetic reactions; in many cases the ROS are consumed, but oxidases that utilise O_2 as the terminal electron acceptor generate $O_2^{\bullet-}$ or H_2O_2.[131] Among these, xanthine oxidase and monoamine oxidases have been implicated in the pathology of heart failure.[140,141] In addition, cardiomyocytes constitutively express certain NOS enzymes, which switch from NO to $O_2^{\bullet-}$ when they become uncoupled due to cofactor depletion.[142] This is triggered by excessive mitochondrial ROS and so acts as an amplifying mechanism. Lastly, in contrast to the above described sources of ROS, which unlikely contribute a substantial role to regulated redox signalling, the Nox family enzymes catalyse the generation of ROS as their primary function, and so represent crucial regulators of redox-mediated signal transduction pathways.[131]

1.5 The NADPH oxidase family of enzymes

1.5.1 Nox structure and function

The Noxs have no known biosynthetic or catabolic function but specifically serve as a dedicated source of ROS, and have emerged as the major cellular contributors of signalling ROS involved in redox pathways.[143] Noxs use NADPH as an electron donor for the reduction of O_2 to $O_2^{\bullet-}$ and H_2O_2 via electron transfer to flavin and heme moieties (Figure 1.4).[131,138] They are a family of multisubunit transmembrane enzymes comprising 7 known isoforms: Nox1 – Nox5 and dual oxidases Duox1 and Duox2, each with a distinct catalytic subunit responsible for oxidase activity, and with varying properties according to requirements for additional accessory subunits, predominant oxidative species produced, and intracellular compartments in which they are found.[143] The Noxs

are particularly suited for their role in redox signalling because their activity and expression may be modulated by diverse agonists and conditions of stress, which, in combination with their precise localisation, allows for the tightly regulated and spatially confined production of low-level ROS in the vicinity of target proteins.[131,138]

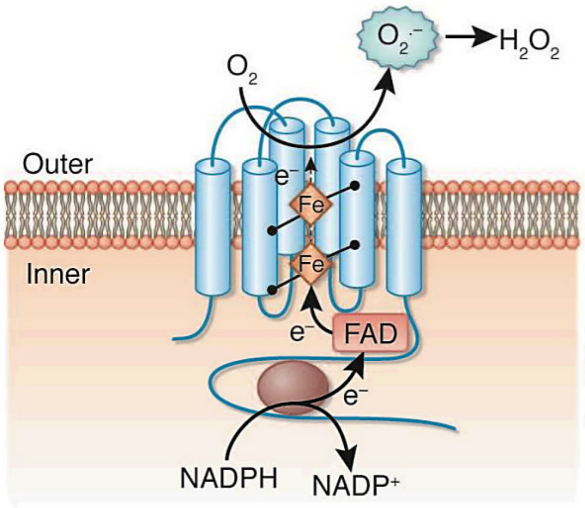

Figure 1.4. NADPH oxidase structure and molecular organisation. All Nox enzymes contain an amino-terminal hydrophobic domain that is predicted to form a catalytic core of 6 transmembrane-spanning α-helices. This region contains conserved histidine residues, which provide binding sites for 2 haem (Fe) groups. The carboxy-terminal portion folds into an independent cytoplasmic domain that contains binding sites for the co-enzymes flavin adenine dinucleotide (FAD) and nicotinamide adenine dinucleotide phosphate (NADPH). Nox1, Nox3, and Nox4 are nearly identical in size and structure to Nox2, whilst Nox5 contains an additional amino-terminal calcium-binding domain. Nox enzymes catalyse the NADPH-dependent reduction of oxygen (O_2) via transfer of 2 electrons from NADPH to FAD, forming the reduced flavin FADH, which are transported across the membrane by the haem electron carriers to form superoxide ($O_2^{\bullet-}$) and hydrogen peroxide (H_2O_2).[136] Adapted from Barnes and Gorin, 2011.[144]

The Nox complexes are differentially expressed between tissues. The first discovered member of the Nox family, Nox2, also known as gp91phox, is most highly expressed in phagocytes where it is responsible for phagocytic respiratory burst. The isoforms Nox1, Nox2, Nox4, and Nox5 are expressed in the cardiovascular system, and among these, Nox2 and Nox4 are expressed in cardiomyocytes.[143] Both isoforms exist as a heterodimeric flavocytochrome bound to a smaller $p22^{phox}$ subunit, but otherwise display significant differences in activation, function, and localisation.[131] Nox2 is localised at the sarcolemma (plasma membrane of cardiomyocytes) and t-tubules and is acutely activated by agonists such as angiotensin II, endothelin-1, cytokines, growth factors, and mechanical forces. These induce a complex process involving post-translational modifications in cytosolic regulatory subunits ($p47^{phox}$, $p67^{phox}$, $p40^{phox}$, Rac1), which

promote their association with Nox2-p22^{phox} to form the fully activated enzyme and initiate $O_2^{\bullet -}$ production. By contrast, Nox4 is found in the sarcoplasmic reticulum (endoplasmic reticulum of cardiomyocytes) and possibly mitochondria, and seems to predominantly generate H_2O_2. Nox4 does not require acute activation but is constitutively active with no obligatory requirement for additional subunits other than p22^{phox}. It is thus primarily regulated by changes in abundance induced by stimuli including hypoxia, endoplasmic reticulum stress, and pressure overload.[131,138]

Current evidence from experimental animal studies suggests that under normal physiological conditions, the Nox proteins and their redox products contribute to the maintenance of cardiovascular homeostasis by participation in processes such as calcium regulation and vascular tone. Nox-regulated redox signalling may also potentiate diverse pathways involved in tissue repair including proliferation.[145] Conversely, it is also established that their dysregulation may promote certain pathological conditions.[143] Nox2 has been closely linked to inflammation as its activation has been shown to mediate the release of pro-inflammatory cytokines,[146] as well as trigger monocyte adhesion, which is critically implicated in atherosclerotic lesion formation.[147] In the heart, Nox2 has also been shown to detrimentally participate in adverse cardiac remodelling and contractile dysfunction after injury, as Nox2-null mice demonstrate reduced hypertrophy and fibrosis and improved ventricular function 4 weeks post-MI.[148] However, Nox-dependent ROS generation is also vital for signalling pathways that protect against myocardial injury. Cardiomyocyte Nox4 has been shown confer protection against pressure overload-induced hypertrophy and remodelling via distinct pro-angiogenic effects on myocardial capillarisation.[149,150] The cardioprotective effects of Nox4 have been additionally demonstrated in the context of acute cardiac injury through enhancement of the integrated stress response,[151] and in haemodynamic overload via direct upregulation of Nrf2.[152]

The magnitude of difference in the response of these cardiac Nox isoforms to injury highlights the selectivity that would be necessary for therapeutic targeting.[143] Furthermore, it is intriguing that alternative isoforms of Nox4 have additionally been discovered, with potential for variations in subcellular localisation and therefore key functional differences in redox-regulated cell signalling.[153]

1.5.2 Identification of novel Nox4 splice variants

The existence of 4 splice variants of Nox4 – termed Nox4B, C, D and E – was originally reported in both the human lung A549 cell line and lung tissues by Goyal et al in 2005 during analysis of Nox4 expression.[153] Western blot analysis of a specific antibody targeted to Nox4 demonstrated the presence of several bands between the 20-70 kDa range; results which were mirrored in parallel with the presence of several smaller bands

at the mRNA expression level, sequencing of which revealed the isolation of Nox4 splice variant products.[153]

The differential splicing and structural organisation of the isoforms were characterised according to the exon structures and alignment of the corresponding amino acid sequences, which showed key differences in the expression of the Nox4 structural and functional domains. Similar to Nox4, the isoforms Nox4B and C were predicted to associate with the endoplasmic reticulum, but were found to possess dominant negative characteristics for ROS generation, which was structurally consistent with the critical deletion of the first NADPH binding site, and all FADH and NADPH binding sites, respectively. In contrast, the other variants Nox4D and E were found to lack the hydrophobic transmembrane domains, suggesting these as non-membrane-associated isoforms. Interestingly, whilst Nox4E, which additionally lacks the first NADPH binding domain, exhibited no change in ROS concentration, Nox4D generated ROS at a comparable rate to full-length Nox4.[153]

In comparison to the full-length structure of Nox4, Nox4D skips exons 3 – 11 to generate a truncated protein (Figure 1.5). However, NADPH oxidase activity is preserved due to retained possession of the FADH and NADPH binding domains necessary for ROS production.[153] The capacity of Nox4D to maintain such enzymatic activity in spite of its critical structural deletion proved particularly interesting in light of the conserved histidine residues of the classical Nox transmembrane domain that are considered essential to facilitate electron transfer through haem binding (Figure 1.4).[136] This finding therefore questioned the necessity of these residues, although it was not addressed whether the function of Nox4D is dependent on additional partner subunits such as $p22^{phox}$.[153]

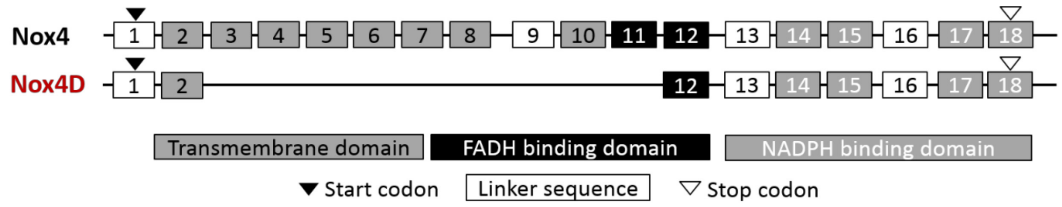

Figure 1.5. Exon structure of Nox4D splice variant. Nox4D is a truncated protein generated by splicing of exons 3 – 11 of Nox4. Nox4D lacks the characteristic Nox transmembrane domain but retains the binding sites for the co-enzymes flavin adenine dinucleotide (FADH) and nicotinamide adenine dinucleotide phosphate (NADPH), suggesting it is a non-membrane-associated isoform capable of reactive oxygen species (ROS) generation. Adapted from Goyal et al, 2005.[153]

1.5.3 Nox4D is a nuclear-localised, redox-active splice variant of Nox4

Further work on the characterisation of Nox4D was carried out in vitro by the Shah laboratory.[154] This work uncovered a prominent localisation of Nox4D to the nucleus of multiple cardiovascular cell types, including neonatal cardiomyocytes, fibroblasts, and vascular smooth muscle cells (VSMCs), with a granular distribution within the nuclear matrix and focal staining corresponding to the nucleolus. This pattern of distribution was consistent with Western blotting of the membrane- and nuclear-fractionated VSMCs, the latter of which contained the more dominant band and major isoform found in this fraction, and was confirmed as 28 kDa Nox4D.[154]

Consistent with the initial characterisation in lung cells,[153] Nox4D was further demonstrated to be functionally active in terms of ROS generation. Catalase-inhibitable, NADPH-dependent H_2O_2 production by Nox4D was proven comparable to Nox4 using models of overexpression.[154] Importantly, Nox4D was also demonstrated to exhibit electron transfer activity, which is supported by previous evidence that the Nox4 carboxy-terminal dehydrogenase domain, which is preserved in Nox4D, is capable of constitutive electron transfer activity. This represents an important discriminating feature since the equivalent regions of Nox1, Nox2, and Nox5 are associated with negligible constitutive electron transfer activity.[155] Since the amino-terminal transmembrane portion of the full-length Nox complexes functions to facilitate electron transfer across the membrane to generate ROS on the opposite side of the membrane, the constitutive activity of Nox4D together with its lack of transmembrane domain collectively suggest that this splice variant may specifically serve to generate intracellular ROS in cytosolic compartments. Although the transcriptional mechanisms that regulate Nox4 splicing are unknown, the nuclear localisation of ROS release may have several important implications for the post-translational modification of site-specific protein sensors by manipulation of downstream effectors within the nucleus.[154] Indeed, Nox4D-generated ROS was also shown to mediate nuclear-localised redox signalling through increased activation of ERK1/2, previously reported as a redox target of the Nox family enzymes,[143] and downstream transcription factor Elk-1. Such effects could be mediated directly or indirectly via oxidative inactivation of nuclear phosphatases.[154]

In summary, Nox4D represents a functionally active, nuclear-localised splice variant of Nox4, with the capacity to constitutively generate NADPH-dependent ROS and modulate redox signalling pathways. These initial data highlighted the potential for Nox4D to play important roles in the transduction of nuclear-localised signalling pathways.[154] Subsequent work by the Shah laboratory provided preliminary data to support the specific involvement of this Nox4 isoform in cardiomyocyte proliferation. This was realised after Nox4D-overexpressing neonatal cardiomyocytes showed characteristic

changes in cell size and number, accompanied by increased expression of proliferation markers and redox activation of signal transduction pathways involved in cell cycle modulation (discussed in more detail in *3.1.2*). Given the extensive implication of redox-mediated signal transduction pathways in the regulation of cardiomyocyte proliferation, it is essential to establish the sources of ROS that are crucially involved so that these may be therapeutically targeted. As such, it was of great interest to determine the effects of targeted Nox4D in the adult mammalian heart.

1.6 Hypothesis

An increase in cardiomyocyte Nox4D expression levels in the adult heart can increase cardiomyocyte cell number by enhancing the capacity for cell cycle re-entry and improve cardiac functional recovery following myocardial infarctive injury.

1.7 Objectives

(i) Investigate the effects of Nox4D in the adult mammalian heart in vivo by generation of a transgenic model of inducible cardiac-specific Nox4D overexpression and characterisation of baseline phenotype;

(ii) Investigate the effects of inducible Nox4D overexpression in the pathological setting of myocardial infarction;

(iii) Investigate the role of Nox4D in proliferation ex vivo using a cell culture model of isolated adult mouse cardiomyocytes.

Chapter 2 Materials and methods

2.1 Animals

Nox4D STOP-flox transgenic (Nox4D Tg) mice were generated by Taconic Biosciences. α-myosin heavy chain-MerCreMer (αMHC-MCM) and ventricular myosin light chain 2-Cre (Mlc2v-Cre) mice were originally obtained from The Jackson Laboratory. All mice were bred on a C57BL/6J genetic background and maintained in the institutional animal house, with free access to food and water and exposure to 12 hourly cycles of light per day. C57BL/6J strains are weakly regenerative.[156]

All experimental procedures involving animals were conducted in healthy age- and gender-matched mice. Animals were cared for and used in accordance with governmental guidance as directed by the Animals (Scientific Procedures) Act 1986 (Home Office, UK). Experiments were locally approved by the institutional Animal Welfare and Ethical Review Body at King's College London.

2.2 Generation of genetically-modified mice

2.2.1 Nox4D transgenesis strategy and breeding

The Nox4D Tg mouse line was originally generated by targeted cloning of the mouse Nox4D splice variant transgene to the Rosa26 locus, driven by the CAGGS promoter, which is composed of sequences from the chicken β-actin and human cytomegalovirus immediate early promoters, and can be expressed ubiquitously.[157] This was designed in conjunction with a STOP-flox strategy, so that expression of the Nox4D transgene is silenced with a STOP sequence – a bacterial chloramphenicol acetyltransferase gene (CAT)[158] – before the initial codon of Nox4D. Expression of the transgene is then dependent on the tissue-specific, Cre-mediated excision of the LoxP sequences that flank the STOP cassette (Figure 2.1).

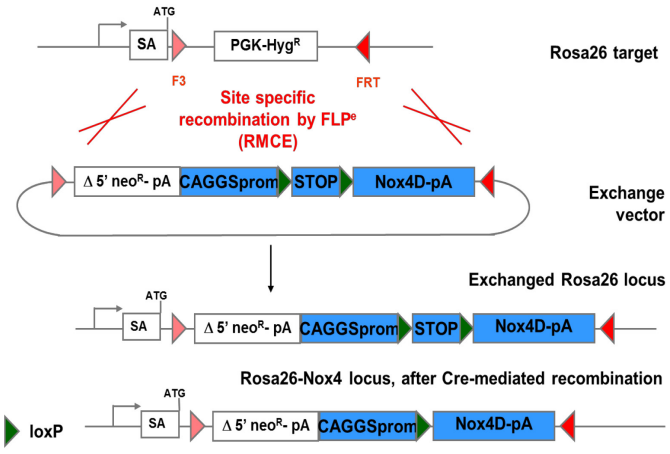

Figure 2.1. Generation of the Nox4D transgenic mouse line. The Nox4D transgene is targeted to the Rosa26 locus, driven by a human cytomegalovirus immediate early enhancer/chicken β-

actin (CAGGS) promoter, and silenced by a STOP sequence. Nox4D transgene silencing is relieved by Cre-Lox recombination. From Taconic Biosciences.

The Nox4D colony was maintained by crossing heterozygous Nox4D Tg females with C57BL/6J or heterozygous Nox4D Tg males to generate both heterozygous and homozygous offspring. The inducible cardiomyocyte-specific Nox4D (Ind-csNox4DInd-csNox4D) Tg mouse model was then generated by crossing heterozygous or homozygous Nox4D females with heterozygous αMHC-MCM males, in which the ligand-binding domain of a mutated murine oestrogen receptor (Mer) is fused to each end of Cre recombinase and expressed under the cardiac muscle-specific αMHC promoter.[159] Upon binding to tamoxifen, the MCM double fusion protein translocates from the cytoplasm to the nucleus and mediates recombination of the LoxP sites, thus allowing temporal regulation of targeted gene expression (Figure 2.2).[157] The constitutive cardiomyocyte-specific Nox4D (csNox4D) Tg mouse model was generated by crossing heterozygous or homozygous Nox4D females with heterozygous Mlc2v-Cre males, in which Cre recombinase expression is directed in cardiac ventricular muscle, starting at approximately embryonic day 8 (E8).[160] Littermates from the respective Ind-csNox4D and csNox4D breeding pairs with positive Nox4D transgene expression but negative Cre expression were designated wild type (WT) controls. The offspring from all breeding pairs were obtained at the expected Mendelian ratios, and no significant morbidity or mortality was observed. Assistance with the maintenance of all colonies was kindly provided by Mr Richard Thompson.

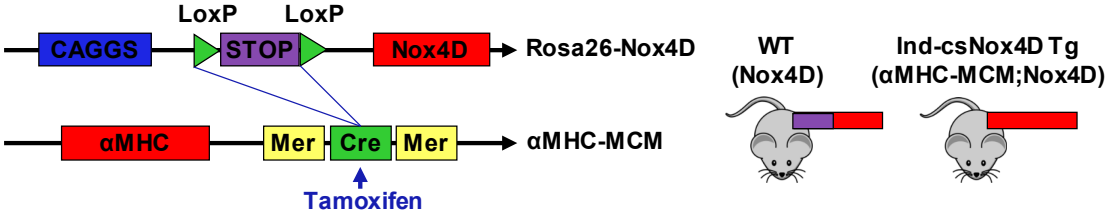

Figure 2.2. Breeding strategy for generation of inducible cardiomyocyte-specific Nox4D transgenic mice. Animals with inducible cardiomyocyte-specific Nox4D (Ind-csNox4D) overexpression were generating by crossbreeding Nox4D transgenic female mice with α-myosin heavy chain-MerCreMer (αMHC-MCM) male mice to enable tamoxifen-inducible excision of the LoxP-flanked STOP cassette. Offspring with the STOP-floxed Nox4D allele only were used as wild type (WT) animals.

2.2.2 Determination of genotype

Nox4D, αMHC-MCM, Mlc2v-Cre, Ind-csNox4D, and csNox4D mice were lightly anaesthetised in a chamber with 2.5% isoflurane in 97.5% oxygen at 1 L/minute, then tissue samples were collected for genotyping by ear punch biopsy.

Samples were incubated with 300 µL sodium hydroxide (NaOH) 50 mM at 95ºC for 30 minutes, then neutralised with 50 µL Tris hydrochloride (Tris-HCl, pH 8.0) 1 M for a further 30 minutes to extract the DNA. Reaction mastermixes were prepared containing 12.5µL REDTaq® ReadyMix™ PCR reaction mix (Sigma), 2 µL forward and reverse primer mix 10 µM, 2 µL DNA, and 8.5 µL nuclease-free water. Nox4D, Rosa, Cre, and control primers were designed by the respective animal suppliers (Table 1).

Table 1. Primers required per reaction for determination of genotype. Ctrl, control.

Mouse Line	Reaction	Primers (5' – 3')	Amplicon
Nox4D	**1**	Nox4D F - CTGTACCTCAGTCAAACAGATGG Nox4D R - CTTAAGCTAGCTCAGCTAACG	263 bp
		Ctrl F - GAGACTCTGGCTACTCATCC Ctrl R - CCTTCAGCAAGAGCTGGGGAC	~500 bp
	2	Rosa F - CATGTCTTTAATCTACCTCGATGG Rosa R - CTCTTCCCTCGTGATCTGCAACTCC	299 bp
		Ctrl F - GAGACTCTGGCTACTCATCC Ctrl R - CCTTCAGCAAGAGCTGGGGAC	~500 bp
αMHC-MCM Mlc2v-Cre	**1**	Cre F - TGCCAGGATCAGGGTTAAAG Cre R - CCCGGCAAAACAGGTAGTTA	264 bp
		Ctrl F - GAGACTCTGGCTACTCATCC Ctrl R - CCTTCAGCAAGAGCTGGGGAC	~500 bp
Ind-csNox4D csNox4D	**1**	Nox4D F - CTGTACCTCAGTCAAACAGATGG Nox4D R - CTTAAGCTAGCTCAGCTAACG	263 bp
		Ctrl F - GAGACTCTGGCTACTCATCC Ctrl R - CCTTCAGCAAGAGCTGGGGAC	~500 bp
	2	Cre F - TGCCAGGATCAGGGTTAAAG Cre R - CCCGGCAAAACAGGTAGTTA	264 bp
		Ctrl F - GAGACTCTGGCTACTCATCC Ctrl R - CCTTCAGCAAGAGCTGGGGAC	~500 bp

Genomic DNA was amplified by polymerase chain reaction (PCR) in a thermal cycler (AB Applied Biosystems) under the following cycling parameters: initial denaturation at 95ºC for 5 minutes, then 35 cycles of a separate denaturation step at 95ºC for 30 seconds, an annealing step at 60ºC for 30 seconds, and an extension step at 72ºC for 1 minute, followed by a final extension at 72ºC for 10 minutes. PCR products were electrophoresed on a 1.5% agarose gel (in Tris-acetate buffer containing Tris-acetate 40 mM, ethylenediaminetetraacetic acid [EDTA] 1 mM, pH 8.3) containing Nancy-520 (Sigma) 0.05 µL/mL as a nucleic acid stain in Tris-acetate as running buffer at 120V for 20 – 30 minutes, then imaged under ultraviolet light. Genotypes were determined according to the presence of the relative bands (Figure 2.3).

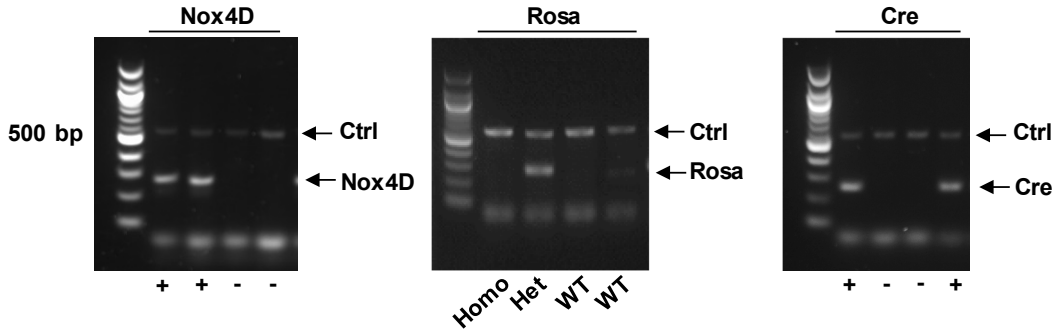

Figure 2.3. Analysis of genotype. Nox4D positivity (left) indicates that at least one allele possesses the sequence. Heterozygous Nox4D transgenic animals are indicated by the presence of a Nox4D band plus a Rosa band (middle), meaning the Rosa band is still present, whereas Nox4D positivity in the absence of Rosa is representative of a homozygous animal. Rosa positivity in the absence of Nox4D is equal to a wild type (WT) animal. αMHC-MerCreMer or Mlc2v-Cre positivity (right) in conjunction with Nox4D positivity is indicative of an Ind-csNox4D or csNox4D transgenic animal, respectively. Ctrl, control.

2.3 Induction of Nox4D overexpression

As performed previously in the Shah laboratory,[150] to induce the nuclear translocation of MerCreMer and overexpression of Nox4D in cardiomyocytes of adult Ind-csNox4D mice, mice were injected intraperitoneally at 8 weeks of age with tamoxifen (Sigma) at 20 mg/kg body weight once per day for 5 consecutive days. Littermate WT control mice received the same dosage in parallel. Tamoxifen injection was prepared by initial reconstitution at 1 in 10 parts of ethanol whilst heating at 37ºC for 30 minutes, then final dilution in peanut oil (Sigma) to approximately 5 mg/mL (containing <5% ethanol).

The use of this induction protocol was initially validated in male and female WT and Ind-csNox4D mice as part of the baseline characterisation studies by serial functional monitoring and analysis of Nox4D protein expression 3 weeks after tamoxifen administration (Figure 2.4). For the tamoxifen dose response experiment, male and female adult Ind-csNox4D mice were injected as above but randomised to receive 5 mg/kg, 10 mg/kg, 15 mg/kg, or 20 mg/kg body weight, then harvested after 2 weeks.

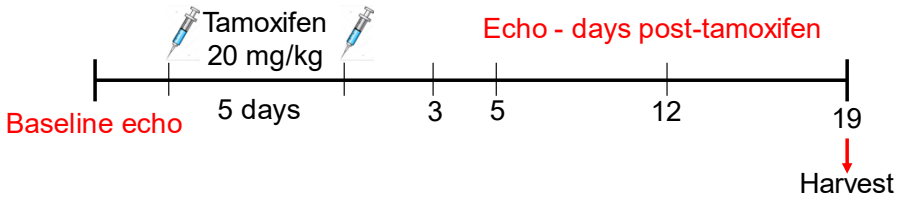

Figure 2.4. Experimental protocol for initial validation of tamoxifen induction. Adult WT and Ind-csNox4D mice received daily intraperitoneal tamoxifen injections for 5 days, and were monitored by echocardiography before and after until cardiac tissues were harvested for analysis of induction of Nox4D overexpression.

2.4 Surgical induction of myocardial infarction

2.4.1 Permanent coronary artery ligation

MI was induced in female adult mice at 10 – 12 weeks of age by permanent ligation of the left anterior descending coronary artery (LAD). Female mice were used exclusively as standard procedure in the laboratory group due to previous experience of frequent myocardial rupture and poorer survival rates when performed in male mice. After tamoxifen induction, cohorts of Ind-csNox4D and WT mice were randomly assigned to receive MI or sham surgeries, which were performed in parallel (Figure 2.5).

Mice were anaesthetised by intraperitoneal injection of ketamine (75 mg/kg body weight) and medetomidine (1 mg/kg body weight) and warmed until asleep. Mice were then administered analgesia with 0.3 µg buprenorphine by intramuscular injection and 50 µg flunixin by subcutaneous injection. Fur was removed from the surgical area using an electric razor and lubricant gel was applied to both eyes. The trachea was intubated and 100% oxygen at 1-1.5 L/minute was provided via mechanical ventilation. Mice were then secured in the supine position on a heating pad at 37ºC, and the chest area was disinfected with iodine followed by chlorhexidine. The correct depth of anaesthesia was confirmed by no response from the interdigital pedal reflex. An oblique transversal skin incision was made over the left thorax, and the muscle layers were separated by blunt dissection and retracted.

A thoracotomy was then performed through the 4th intercostal space, the muscle layer was penetrated and retracted to expose the heart. The pericardium was gently pulled apart to visualise the anterior wall and an 8-0 nylon suture was passed underneath the LAD coronary artery, 1 – 2 mm below the edge of the left atrium. The LAD was then ligated, and successful induction of ischaemia was confirmed by blanching of the myocardium below the ligation. The chest cavity was closed with a 5-0 suture, the muscle layers and skin were sutured, and the anaesthesia was reversed by intraperitoneal injection of atipamezole. Mice were extubated upon signs of recovery, transferred to a new cage and kept warm in an incubator for 4 hours. Sham-operated animals were subjected to the same surgical procedures except the 8-0 nylon suture was passed underneath the LAD but was not tied. Tracheal intubation and LAD ligation and sham surgical procedures were kindly performed by experienced microsurgeons in the laboratory group; Dr Helena Zhang and Dr Greta Sawyer, respectively.

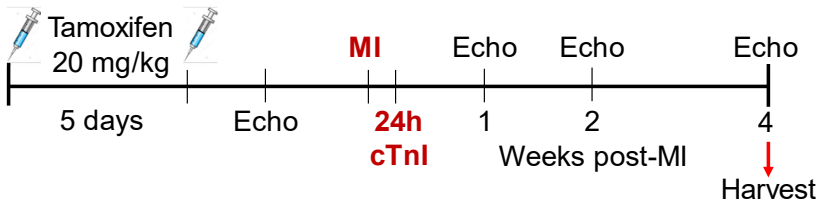

Figure 2.5. 4-Week myocardial infarction study protocol. Female WT and Ind-csNox4D transgenic mice were injected at 8 weeks of age with tamoxifen at 20 mg/kg body weight once a day for 5 days, then subjected to myocardial infarction (MI) or sham surgery at 10 – 12 weeks of age and harvested after 4 weeks. Plasma cardiac troponin I (cTnI) was measured 24 hours post-surgery for quantification of cardiac injury, and cardiac function was measured before and after surgery by echocardiography.

2.4.2 Cardiac troponin I sampling 24 hours post-surgery

At 24 hours post-surgery, mice were bled via the jugular vein for sampling of plasma cardiac troponin I (cTnI) as a quantitative biomarker for myocardial injury. Mice were anaesthetised in a chamber with 4% isoflurane in 100% oxygen at 1 L/minute, fur was removed from the surgical area using an electric razor and lubricant gel was applied to both eyes. Mice were then transferred to a heating pad at 37ºC, secured in the supine position and maintained using a nose cone at 2% isoflurane. Analgesia was administered with 50 µg flunixin by subcutaneous injection and the surgical area was disinfected with iodine followed by chlorhexidine. The jugular vein was accessed by right-sided neck dissection. A heparinised, 29-gauge insulin needle (BD Micro-Fine™ Plus) was slightly curved and inserted through the overlying pectoral muscle to avoid bleeding on withdrawal. The vein was punctured and approximately 100 µL blood was withdrawn. This surgical procedure for plasma sampling was kindly performed by Dr Helena Zhang and Dr Greta Sawyer.

Whole blood samples were transferred to microcentrifuge tubes and stored at 4ºC. The plasma was separated by centrifugation at 1,500 g at 4ºC, and the resulting supernatant was immediately transferred to a clean microcentrifuge tube with a Pasteur pipette, then stored at -80ºC until quantification.

2.5 Echocardiography

Echocardiography was performed at baseline, and prior to and after surgery. Mice were anaesthetised in a chamber with 4% isoflurane in 97.5% oxygen at 1 L/minute, then transferred to the imaging stage, secured in the supine position and maintained using a nose cone at 1.25 – 1.5% isoflurane. Fur was removed from the chest using a topical depilatory cream and thoroughly cleaned with water. Heart rate, respiration rate, and electrocardiograms were continuously monitored by attachment of limbs to the gel-coated electrodes. Body temperature was monitored rectally and maintained between

36ºC and 37ºC, using a heating lamp if required. Heart rate was maintained above 400 beats per minute (bpm) by control of body temperature and adjustment of isoflurane anaesthesia. Each mouse was permitted to acclimatise for a minimum of 5 minutes prior to collection of data.

After stabilisation of parameters, ultrasound transmission gel was applied to the chest and mice were imaged within a heart rate range of 400 – 500 bpm with a handheld 40-MHz linear probe, using either a Vevo® 2100 or a Vevo® 3100 Imaging System (Visualsonics). The probe was positioned to obtain parasternal long axis (PLAX) and parasternal short axis (PSAX) views in motion-mode (M-mode) and brightness-mode (B-mode) for measurement of systolic function and left ventricular (LV) dimensions. All echo images were kindly acquired by experienced cardiac sonographer in the laboratory group; Mr Norman Catibog.

Echo images were analysed using Vevo® LAB ultrasound analysis software (Visualsonics). For the baseline characterisation of LV structure and function before and after tamoxifen induction, basic LV parameters were measured by LV trace of end-diastole and end-systole over 2 cardiac cycles in B-mode images in PLAX view. Interventricular diastolic septum thickness was measured over 2 cardiac cycles in PLAX M-mode. For animals subjected to MI or sham surgery, the Vevo® Strain package was used for advanced assessment of traditional LV parameters as well as global and regional myocardial dysfunction by deformation analysis. Images were analysed in B-mode PLAX by careful LV tracing of the endocardial and epicardial borders over 2 cardiac cycles, starting in end-diastole, for determination of volume-dependent parameters and global longitudinal strain (GLS) (Figure 4.3). This mode of analysis relies on speckle tracking algorithms that harness the high spatial and temporal resolution of high frequency ultrasound.[161] Further strain analysis was carried out using the quantitative Segmental Synchronicity Page within Vevo® Strain, which divides the anterior and posterior regions of the LV into 3 different segments each (Figure 4.6). This was used to detect regional differences in myocardial contractile function by analysis of longitudinal and radial strain rate in each LV segment. All echo data were analysed in a blinded manner by identification of each animal by unique number only.

2.6 EdU labelling

5-ethynyl-2'-deoxyuridine (EdU), a thymidine nucleoside analog, was used to label cycling cells in vivo by incorporation in DNA. EdU (Thermo Scientific) was administered by intraperitoneal injection at 50 mg/kg body weight. EdU injection was prepared by reconstitution in PBS to 10 mg/mL, and heated at 37ºC for 30 minutes. Adult WT and

Ind-csNox4D mice were administered 2 doses of EdU during basal characterisation, once on the last day of tamoxifen induction, repeated after 3 days (Figure 2.6).

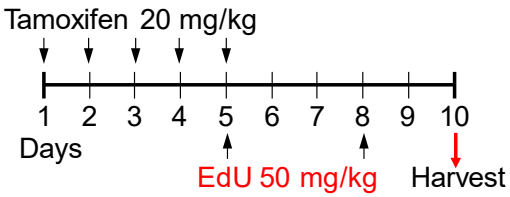

Figure 2.6. Experimental protocol for assessment of EdU incorporation in the absence of injury. Male and female WT and Ind-csNox4D transgenic mice were injected at 8 weeks of age with tamoxifen on days 1 – 5, then EdU on days 5 and 8 followed by cardiac harvest on day 10.

Adult WT and Ind-csNox4D mice were also injected with EdU post-MI or -sham, commencing 24 hours after surgery and repeated every 4 days thereafter until tissues were harvested at 2 weeks (Figure 2.7).

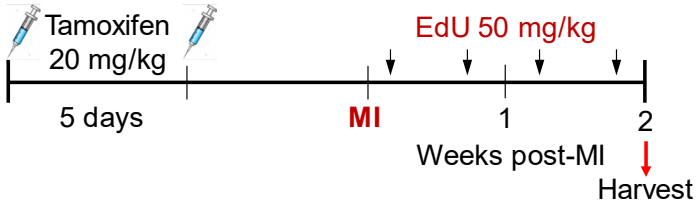

Figure 2.7. 2-Week myocardial infarction study protocol for assessment of EdU incorporation. Female WT and Ind-csNox4D transgenic mice were injected with tamoxifen for 5 days at 8 weeks of age, then subjected to myocardial infarction (MI) or sham surgery at 10 – 12 weeks of age and harvested after 2 weeks. EdU was injected 24 hours post-surgery and every 4 days thereafter.

2.7 Cardiac tissue harvest

Animals were weighed, then anaesthetised in a chamber with 4% isoflurane in 97.5% oxygen at 1 L/minute and transferred to the supine position and maintained using a nose cone at 3% isoflurane. A lateral incision was made below the diaphragm, the chest cavity was opened, and the ribs were retracted to expose the heart. The LV was injected with 200 µL 5% potassium chloride (KCl) in phosphate buffered saline (PBS) to induce diastolic arrest. The heart was excised and washed twice in 0.9% saline solution to remove blood, then dried. Excess tissue was removed, heart weight was recorded, and the heart was dissected using a 22 surgical scalpel blade according to experiment.

For the baseline characterisation studies, hearts were transversely sectioned into the base, mid, and apex regions for RNA extraction, frozen tissue sections, and protein extraction, respectively. The base and apex samples were snap frozen in liquid nitrogen and stored in liquid nitrogen. The mid segment was mounted on cork embedded in

optimal cutting temperature (OCT) medium and stored at -80ºC. Hearts subjected to MI and sham surgeries were allocated to harvest for RNA extraction or frozen tissue sections. For RNA, the heart was transversely cut just above the ligature and at the apex. Samples were then cut according to MI region: infarct zone, border zone (defined as a 2 mm area encircling the dense fibrotic scar area of pathologic infarction[162]), and the non-infarcted remote zone, and snap frozen as described above. The mid segment, containing all 3 MI regions, was cut above the ligature and embedded in OCT as described above. Similar anatomic regions were dissected from sham-operated hearts. For the tamoxifen dose response studies, the mid region was cut for frozen tissue sections as above, and the apex was cut for high performance liquid chromatography (HPLC), snap frozen and stored at -80ºC.

2.8 Adult cardiomyocyte isolations

Adult cardiomyocytes were isolated by a Langendorff-free method as recently described.[163] Adult WT and csNox4D mice at 10 – 12 weeks of age were used for cardiomyocyte culture experiments. As discussed in section *2.2.1*, cardiomyocyte-targeted Nox4D is constitutively expressed in the csNox4D Tg mouse model, commencing during embryonic development. This model was used here in preference to the Ind-csNox4D model to avoid the additional step of tamoxifen induction. The level of Nox4D overexpressed in csNox4D mice is demonstrated in Figure 2.8. For optimisation of assessment of Nox4D localisation in the Ind-csNox4D Tg model, adult cardiomyocytes were isolated from WT and Ind-csNox4D mice 2 weeks after tamoxifen induction.

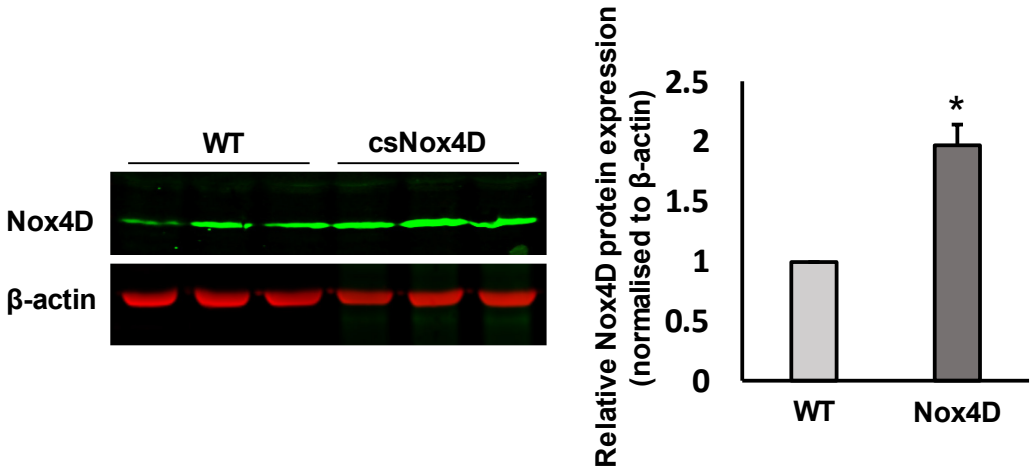

Figure 2.8. Nox4D overexpression in csNox4D hearts. Representative immunoblot (left) and relative quantification (right) of Nox4D protein expression in hearts of adult WT and csNox4D transgenic mice. csNox4D hearts show a 2-fold increase in Nox4D protein level compared to control mice. n = 5 per group. Data represent mean ± SEM. *P<0.05 by unpaired two-tailed t-test. Work by Dr Narayana Anilkumar, unpublished.

2.8.1 Surgical procedure

Animals anaesthetised in a chamber with 4% isoflurane in 97.5% oxygen at 1 L/minute and transferred to the supine position and maintained using a nose cone at 3% isoflurane. Full anaesthesia was confirmed by reduced respiration rate and no response from the interdigital pedal reflex. The mouse chest was disinfected with 70% ethanol. A lateral incision was made below the diaphragm, the chest cavity was opened, and the ribs were retracted to expose the heart. The descending aorta and inferior vena cava were cut, and 7 mL EDTA buffer (Table 2) was injected into the base of the right ventricle (RV) over 1 minute to cease contractions and clear the heart of blood. The ascending aorta was then clamped, and the heart was removed and transferred to the first petri dish containing 10 mL EDTA buffer.

2.8.2 Heart dissociation

The heart was digested ex vivo by sequential perfusion with several buffers by injection through the LV wall, 2 or 3 mm above the apical point. Application of the aortic clamp ensures myocardial perfusion by forcing passage of the buffers through the coronary circulation. All buffers were manually perfused via sterile 27-gauge needles (a list of buffers is shown in Table 2). The heart was submerged in the first dish, and injected with 10 mL EDTA over 6 minutes. The heart was then transferred to the second dish containing perfusion buffer, and 3 mL perfusion buffer was injected over 2 minutes via the same entry site created by the first injection. The heart was transferred to the third dish containing collagenase buffer (collagenase, Worthington Biochemicals; protease XIV, Sigma), and the LV was further injected through the same point with 40 mL collagenase buffer over approximately 20 minutes. Enzymatic digestion steps were performed at 37ºC by prewarming collagenase buffer. Digestion was confirmed by a pale appearance and loss of shape and rigidity, the clamp was then removed and the heart was transferred to the last dish containing fresh collagenase buffer. The tissue was dissociated by gentle separation and trituration, then enzymatic activity was inhibited by addition of 5 mL stop buffer to the cell-tissue suspension. The suspension was further triturated, and cellular yield was estimated by brightfield microscopy.

Table 2. Buffer recipes for adult cardiomyocyte isolation.

Buffer	Constituents
EDTA	NaCl 130 mM, KCl 5mM, NaH_2PO_4 0.5 mM, HEPES 10 mM, glucose 10 mM, BDM 10 mM, taurine 10mM, EDTA 5 mM In ultrapure H_2O, pH 7.8, sterile filtered
Perfusion	NaCl 130 mM, KCl 5mM, NaH_2PO_4 0.5 mM, HEPES 10 mM, glucose 10 mM, BDM 10 mM, taurine 10mM, $MgCl_2$ 1 mM In ultrapure H_2O, pH 7.8, sterile filtered
Collagenase	Collagenase type 2 0.5 mg/mL, collagenase type 4 0.5 mg/mL, protease XIV 0.05 mg/mL In perfusion buffer, pH 7.8, sterile filtered
Stop	FBS 5% In perfusion buffer

2.8.3 Cardiomyocyte purification and culture

The cell suspension was passed through a 100 µm filter and washed with a further 5mL stop buffer. Rod-shaped, viable cardiomyocytes were purified by 4 sequential rounds of gravity settling – an initial 20-minute settling period followed by 3 incremental calcium reintroduction buffers (Table 3) for 10 minutes each to gradually restore calcium concentration to physiological levels. The supernatant, containing non-viable myocytes, non-myocytes, and debris, was removed from each round to produce a cell pellet highly enriched for cardiomyocytes.

Pre-coated glass tissue culture surfaces (Nunc™ Lab-Tek™ Chamber Slide system, 8-well, Thermo Scientific) with laminin (Sigma) at 25 µg/mL in PBS were aspirated and washed once with PBS. The total cardiomyocyte yield per heart was resuspended in 2 mL prewarmed culture medium and 2 mL plating medium (Table 3), then seeded over 16 wells, evenly distributed and supplemented with a further 150 µL plating medium per well. Cells were placed in a humidified culture incubator at 37ºC/5% carbon dioxide/95% air and allowed to adhere for 1 hour. After 1 hour, wells were carefully washed individually, and re-incubated in 300 µL culture medium containing 2% heat-inactivated foetal bovine serum (FBS). Medium was replaced every 48 hours thereafter. Cardiomyocytes isolated from WT and Ind-csNox4D mice were fixed (as described in *2.8.5*) after plating for Nox4D immunostaining.

Table 3. Buffer and media recipes for adult cardiomyocyte purification and culture.

Medium/buffer	Constituents
Calcium reintroduction buffer	For total volume of 20 mL per buffer: Buffer 1: perfusion buffer 15 mL, culture medium 5 mL Buffer 2: perfusion buffer 10 mL, culture medium 10 mL Buffer 3: perfusion buffer 5 mL, culture medium 15 mL
Plating medium	FBS 5%, BDM 10 mM, 1x L-glutamine-penicillin-streptomycin solution (Sigma) In Medium 199 (M2154 [Sigma]), sterile filtered
Culture medium	FBS 2%, BSA 0.1%, insulin-transferrin-selenium 1x (Sigma), BDM 10 mM, chemically defined lipid concentrate 1x (Thermo Scientific), 1x L-glutamine-penicillin-streptomycin solution In Medium 199 (M2154), sterile filtered (BDM removed after first 48 hours of culture)

2.8.4 Cardiomyocyte viability assays

Following isolation, cell viability was assessed after 72 hours in culture by dye exclusion tests with trypan blue and 7-aminoactinomycin D (7-AAD). Trypan blue (Sigma) was added directly to the media and stained for 5 minutes at room temperature at a final concentration of 0.04%. To reduce background, trypan blue was further diluted with PBS to 0.01% and cells were imaged by brightfield microscopy.

In parallel, half the culture media was removed and 20 µL 7-AAD solution was added per well (containing 0.5 µL 7-AAD and 0.4 µL Hoechst [Thermo Scientific] in PBS), then incubated at room temperature in the dark for 15 minutes. Confocal stitched images were obtained with a 20x objective using an inverted spinning disc microscope (Nikon Eclipse Ti-E).

2.8.5 Adult cardiomyocyte dedifferentiation

Isolated adult cardiomyocytes were allowed to recover in culture medium for the first 48 hours, after which 2,3-butanedione monoxime (BDM) was removed from the medium. The concentration of mouse oncostatin M (OSM [Sigma]) to be used for the induction of cardiomyocyte dedifferentiation was first optimised by exposure to OSM at 20, 50, and 100 ng/mL for 8 days. The lowest effective concentration of OSM (50 ng/mL) was selected as the optimum concentration for further experiments. For assessment of proliferation events by EdU incorporation, the concentration of EdU to be used was optimised and the detection was validated in the H9c2 rat cardiomyoblast cell line. Cultured H9c2 cells were incubated with EdU overnight at 5, 10, and 20 µM, then detected using the Click-iT™ EdU imaging kit (Invitrogen), as described in *2.11.3*. This

identified 10 μM as the optimum concentration of EdU and was selected for use in cardiomyocyte cultures (Figure 2.9).

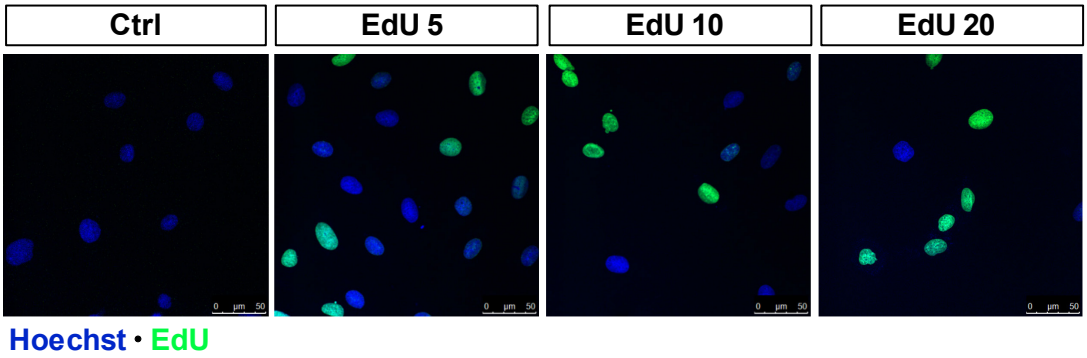

Figure 2.9. Optimisation of EdU labelling and validation of detection in vitro. Representative images of fluorescence staining for 5-ethynyl-2'-deoxyuridine (EdU) (green) incorporation, labelling cells that have synthesised DNA, with Hoechst (blue) as a nuclear marker in H9c2 cells after overnight culture with EdU at 5, 10, and 20 μM. Scale bars: 50 μm. n = 1.

Cardiomyocytes were then incubated with OSM 50 ng/mL for 6 days followed by treatment with mouse fibroblast growth factor 2 (FGF2 [Cell Signaling Technology]) 100 ng/mL for the final 2 days. Cardiomyocytes were also treated with OSM only for 8 days, and without OSM but with FGF2 from day 6 to 8. Untreated cardiomyocytes were maintained in culture medium throughout the protocol. All experimental conditions were cultured with EdU 10 μM from day 6 to day 8. Cells were fixed on day 8 by removal of the media and incubation with 200 μL 4% paraformaldehyde (PFA [Thermo Scientific) in PBS at room temperature for 15 minutes, then washed twice with PBS (Figure 2.10).

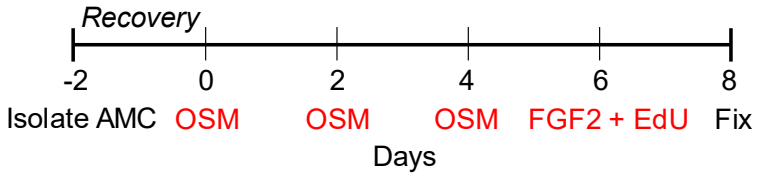

Figure 2.10. Experimental protocol for induction of dedifferentiation in cultured adult cardiomyocytes and assessment of proliferation. Adult cardiomyocytes were isolated from WT and csNox4D mice and recovered for 2 days in culture. Oncostatin M (OSM) 50 ng/mL was commenced on day 0 and medium (containing 2% foetal bovine serum) was replaced every 48 hours. FGF2 100 ng/mL treatments and EdU 10 μM were added on day 6 for the final incubation period, and cells were fixed on day 8.

2.9 qPCR analysis of gene expression

2.9.1 RNA extraction

H9c2 cells were lysed in 350 μL lysis buffer RLT (containing β-mercaptoethanol) and centrifuged through a QIAshredder™ spin column (Qiagen) for 2 minutes at 13,000 g.

RNA was extracted using the RNeasy® Mini Kit according to the manufacturer's instructions (Qiagen) and eluted in nuclease-free water. Cardiac tissue samples (10 – 20 mg) were lysed in 500 µL lysis buffer LBA (containing 1-thioglycerol) (Promega) and homogenised using FastPrep® lysing matrix D beads (MP Biomedicals) in a Precellys® 24 tissue homogeniser (Bertin Instruments) at 2 x 20 seconds at 6000 rpm. RNA was extracted using the ReliaPrep™ RNA Tissue Miniprep System according to the manufacturer's instructions (Promega) and eluted in nuclease-free water. The concentration and purity of all RNA samples were quantified using a NanoDrop® ND-1000 spectrophotometer (Labtech International). RNA extracts were stored at -80ºC.

2.9.2 Reverse transcription

Complementary DNA (cDNA) was synthesised by reverse transcription of the single-stranded RNA template. Samples were prepared by dilution of 1 µg RNA to 13 µL with nuclease-free water, to which 1 µL oligo-dT_{18} primers 1 µg/µL and 1 µL dNTPs 10 mM (Promega) were then added. Samples were initially heated at 70ºC for 3 minutes to disrupt any secondary structures, then cooled to 4ºC. This was followed by addition of 4 µL 5x reverse transcriptase buffer (Promega), 0.5 µL RNase inhibitor (Promega), and 0.5 µL reverse transcriptase enzyme (Moloney murine leukaemia virus [Promega]) to 20 µL final reaction volume. Equivalent samples were prepared as negative controls, containing all reaction components except reverse transcriptase, to enable identification of genomic DNA contamination. All samples were then heated in a thermal cycler (AB Applied Biosystems) at 42ºC for 90 minutes, then 70ºC for 10 minutes. The resulting cDNA was diluted to 10 ng/µL with nuclease-free water and stored at -20ºC.

2.9.3 Quantitative PCR

Quantitative PCR (qPCR) was used to determine the relative mRNA expression of genes of interest through fluorescence detection. This methodology was employed using a non-specific fluorescent dye (SYBR® Green), which intercalates with double-stranded DNA to emits a fluorescent signal that increases proportionally to the amount of double-stranded DNA that is amplified within each PCR cycle.

Each qPCR reaction was prepared with 2 µL cDNA template, 2 µL primer mix 3 µM, 10 µL 2x qPCRBIO SyGreen Mix Hi-ROX (PCR Biosystems), and 6 µL nuclease-free water to 20 µL final reaction volume. qPCR was performed by a StepOnePlus™ Real-Time PCR machine (Applied Biosystems). Samples were initially denatured at 95ºC for 10 minutes, then amplified for 40 cycles of: denaturation (95ºC for 15 seconds) and annealing and extension (60ºC for 30 seconds). Samples were then heated at 95ºC for 15 seconds, 60ºC for 1 minute, then re-heated to 95ºC in 0.3ºC increments for 15 seconds for melt curve analysis of primer specificity.

For the Nox4D knockdown experiments in H9c2 cells, qPCR reaction conditions were optimised for the detection of Nox4D. The 2 primer sets with greatest specificity were selected from the original series and trialled at reduced concentration in conjunction with increased cDNA template volume. This identified 2 μM and 4 μL as the optimum primer concentration and template volume, respectively, for the detection of Nox4D knockdown.

mRNA expression was calculated relative to housekeeper control gene (GAPDH or β-actin) using the cycle threshold (C_t) value as determined by the amplification plot for each gene. The C_t value represents the cycle number at which the emitted fluorescence reaches the fixed signal threshold and is thus indicative of the relative abundance of the target sequence between samples. Relative mRNA expression was determined using the $\Delta\Delta C_t$ method.[164] Normalised expression was further normalised as a fold-change relative to the respective control group within each experiment.

2.9.4 qPCR primer design

Gene-specific primers were designed using the NCBI primer design tool against set criteria, including target amplicon size of 70 – 200 base pairs, spanning of exon-exon boundaries, and an optimal melting temperature of 60ºC (Table 4). For the Nox4D knockdown optimisation studies in H9c2 cells, a series of 5 primers sets were designed for the forward sequence to target exon 1 or 2, and the reverse sequence to target the exon 2/12 junction specific to Nox4D (Table 5). Primer specificity was evaluated by the ability to demonstrate a single melting peak and further assessed by detection of a single PCR product after gel electrophoresis (as described in *2.2.2*).

Table 4. Mouse qPCR primer sequences.

Gene	Forward primer (5' – 3')	Reverse primer (5' – 3')
Angpt2	AGTCAGGACTCACCACCAGT	TCCATGTCACAGTAGGCCTTG
ANP	CGTCTTGGCCTTTTGGCTTC	GGTGGTCTAGCAGGTTCTTGAAA
Aurkb	CGGGAGAAGAAGAGCCGTTT	ATGTTGGGATGTTTCAGGTGC
β-actin	CGTGAAAAGATGACCCAGATCA	TGGTACGACCAGAGGCATA
BNP	CTTCGGTCTCAAGGCAGCA	TACAACAACTTCAGTGCGTTACA
Cdk2	CACTCATGAGGTGGTGACCC	GGTGCTGGGTACACACTAGG
Cdk4	GGCCCTCAAGAGTGTGAGAG	AGACATCCATCAGCCGTACA
ckit	CGTTCCTCGCCTCCAAGAAT	AATCTTTGTGATCCGCCCGT
Cyclin A2	TGGCTTTTAATGCAGCTGTCTCTT	AGACATATCCATAGCATGTGGTGA
Cyclin D1	GCCATCCATGCGGAAAATCG	GGAAGACCTCCTCGCAC
Cyclin E1	GGCGAGGATGAGAGCAGTTC	AGTCCTGTGCCAAGTAGAACG
Dab2	CAGCCTTGAGGCTTCGGG	GGGCAGGTCTCAAAAGGACA
GAPDH	GGGTTCCTATAAATACGGACTGC	CCATTTTGTCTACGGGACGA
GATA4	AAACGGAAGCCCAAGAACCT	TGGCATTGCTGGAGTTACCG
Gclc	GTTATGGCTTTGAGTGCTGCAT	ATCACTCCCCAGCGACAATC
Gsta2	GCTTGATGCCAGCCTTCTG	GGCTGCTGATTCTGCTCTTGA
Myh6	AACCTGTCCAAGTTCCGCA	ATTCCTCGTCGTGCATCTTCTTG
Myh7	CCTTACTTGCTACCCTCAGGTGG	GTAAGCCCAGGCCTGTAGAAG
Nox4	CCGGACAGTCCTGGCTTATC	TGCTTTTATCCAACAATCTTCT
Nox4D	ACAACCAAGGGCCAGAATAC	TCGTTCTGTCCAGTCTCCTAC
p21Cip1	CAGCAGAATAAAAGGTGCCACA	GACAACGGCACACTTTGCTC
p27Kip1	GTTTCAGACGGTTCCCCGAA	CTTAATTCGGAGCTGTTTACGTC
Runx1	ACGATGGCTTCAGACAGCATT	CTCATCTTGCCGGGGCTC
ssTNI	AGCTCCACGAGGACTAAACT	CCTCTCAACTTCCGGCATGG
Vegfa	GCAGCGACAAGGCAGACTAT	AACCTCCTCAAACCGTTGGC

Table 5. Primer sequences used for Nox4D knockdown in vitro.

Gene	Set	Forward primer (5' – 3')	Reverse primer (5' – 3')
Nox4D	**1**	CACCTCTGTCTGCTTGTTTGG	TTGCTTTGGTTTCAGTAGGACAGC
	2	GCTGTCCCTAAATGTCCTGC	TGCTTTGGTTTCAGTAGGACA
	3	ACCTTCCTGCTGTACAACCA	TGCTTTGGTTTCAGTAGGACAG
	4	ACCTTCCTGCTGTACAACCA	TTGGTTTCAGTAGGACAGCC
	5	ACCTTCCTGCTGTACAACCA	GGTTTCAGTAGGACAGCCCAAC
β-actin		CGTGAAAAGATGACCCAGATCA	TGGTACGACCAGAGGCATA
Nox4		CCGGACAGTCCTGGCTTATC	TGCTTTTATCCAACAATCTTCT

2.10 Western blotting

2.10.1 Protein extraction

H9c2 cells were lysed in triplicates per 6-well culture plate in a total of 250 µL lysis buffer (Table 6). If necessary, lysates were sonicated briefly for 5 seconds to further disrupt cellular membranes, then centrifuged for 5 minutes at 13,000 g at 4 ºC. The supernatant was collected into a clean microcentrifuge tube and stored at -80ºC. Cardiac tissue samples (10 – 20 mg) were lysed in lysis buffer (Table 6) at 25 µL/mg tissue, and homogenised as described in *2.9.1*. Tissue lysates were transferred to clean microcentrifuge tubes and stored at -80ºC.

Table 6. Lysis buffers used for protein extraction in cells and tissue.

Lysis buffer	Constituents
Cells	NaCl 150 mM, Tris base 50mM, SDS 0.1%, Nonidet P-40 1% In ultrapure H_2O, pH 8.0 Protease inhibitor mixture (Sigma) added at 1:200 before use
Tissue	NaCl 150 mM, Tris base 25 mM, EDTA 5 mM, EGTA 2 mM, Nonidet P-40 0.5% In ultrapure H_2O, pH 7.4 Protease and phosphatase inhibitor mixtures (Sigma) added at 1:100 before use

2.10.2 Protein content determination

The bicinchoninic acid (BCA) assay (Pierce™ BCA Protein Assay Kit [Thermo Scientific]) was used for the colorimetric detection and quantification of total protein. This assay relies on the reduction of copper ions by protein and chelation of reduced copper ions with BCA to form a purple-coloured complex. Protein content was determined against the reference protein bovine serum albumin (BSA) according to the manufacturer's instructions. Briefly, a BSA standard curve was prepared by serial dilution of the 2 mg/mL stock solution with the same lysis buffer used to prepare the samples, to produce a working range of 0 – 1000 µg/mL. Samples were first diluted at 1:5 (cells) or 1:10 (tissue) with respective lysis buffer, then pipetted along with the standards in 25 µL duplicates into a 96-well plate (Thermo Scientific). 200 µL BCA working reagent (containing 50 parts reagent A to 1 part reagent B) was then added to each well and mixed thoroughly. The plate was incubated for 30 minutes at 37ºC, and the absorbance was read at 562 nm on a plate reader (GENios pro, Tecan).

Protein concentrations were quantified against the BSA standard curve, then samples were prepared at 1 µg/µL by dilution in 5x sample buffer (containing 0.5 M DTT, 0.02%

bromophenol blue, 30% glycerol, 10% SDS in 250 mM Tris base, pH 6.8), then 1x sample buffer to final volume, sonicated for 5 seconds and stored at -80ºC.

2.10.3 Immunoblotting

Proteins were separated according to their molecular weight by sodium dodecyl sulphate polyacrylamide gel electrophoresis (SDS-PAGE) using a Bio-Rad system. 10% separating gels were cast (containing 3.3 mL 30% acrylamide/bis-acrylamide, 2.5 mL Tris HCl 1.5 M pH 8.8, 4 mL distilled water, 100 µL 10% SDS, 85 µL 10% ammonium persulphate, 20 µL TEMED) and layered with stacking gel (containing 650 µL 30% acrylamide/bis-acrylamide, Tris HCl 0.5 M pH 6.8, 3.05 mL distilled water, 50 µL 10% SDS, 25 µL 10% ammonium persulphate, 10 µL TEMED). Protein samples were loaded at 20 µg per well and electrophoresed at 120V for 80 minutes in running buffer (containing Tris base 25 mM, glycine 192 mM, 0.5% SDS). Proteins were transferred onto nitrocellulose membranes at 65V for 60 minutes in transfer buffer (containing Tris base 25 mM, glycine 192 mM, 20% methanol).

Membranes were stained with Ponceau S solution (Sigma) to confirm efficient protein transfer, then blocked with 5% non-fat milk (in tris buffered saline containing 0.1% Tween-20; TBS-T) for 60 minutes, then probed overnight with primary antibody (Table 7) at 4ºC under agitation. Membranes were washed 3 times for 15 minutes in TBS-T then incubated with secondary antibody (Table 7) for 1 hour at room temperature under agitation. Membranes were washed again 3 times for 15 minutes in TBS-T then once for 10 minutes in TBS, and developed by direct near-infrared fluorescence using an Odyssey® CLx imaging system (LI-COR® Biosciences). Membranes were then re-exposed to loading control primary antibody (GAPDH, α-tubulin, or total protein of phosphorylated target).

Relative protein levels were determined by quantification of blots using Image Studio™ software. The signal of the target protein was normalised to the signal of the respective loading control, then further normalised as a fold-change relative to the respective control group within each experiment.

Table 7. Primary and secondary antibodies used for immunoblotting.

Antibody	Concentration	Diluent	Manufacturer
Primary			
Nox4	Overexpression: 1:2,000; knockdown: 1:1,000	Milk 5% (in TBS-T)	Prepared in-house
Phospho-Akt (Ser473)	1:1,000		Cell Signalling Technology
p27 Kip1			
Akt (pan)			
GAPDH	1:4,000		Sigma
α-tubulin	1:10,000		Sigma
Secondary			
Donkey anti-rabbit, conjugated to IRDye®800CW or IRDye®680RD	1:10,000	Milk 5% (in TBS-T)	LI-COR® Biosciences
Donkey anti-mouse, conjugated to IRDye®800CW or IRDye®680RD			

2.11 Cell and tissue staining

2.11.1 Cryosections

Frozen tissue sections were prepared using a cryostat (CryoStar™ NX70 [Thermo Scientific]). Transverse sections were cut at 10 µm thickness and 3 sections were mounted per glass microscope slide (Superfrost Plus™ [Thermo Scientific]). Slides were air-dried for 30 minutes then stored at -80ºC. Prior to tissue staining, cryosections were thawed at room temperature for 30 minutes then fixed with 4% PFA in PBS for 15 minutes.

2.11.2 Immunostaining

Fixed cryosections and fixed cultured adult cardiomyocytes were washed twice with 3% BSA in PBS, permeabilised with 0.5% Triton™ X-100 in PBS (Sigma) for 20 minutes, then washed twice with 3% BSA. Slides were incubated with blocking buffer (containing 3% BSA and 1% goat serum [Sigma] in PBS) for 20 minutes, then incubated with primary antibody diluted in blocking buffer for 60 minutes in a humidified chamber at room temperature (a list of antibodies and dilutions is provided in Table 8). Slides were washed 3 times with 3% BSA then incubated with the corresponding rabbit or mouse fluorescent-conjugated secondary antibody (Invitrogen) diluted at 1:200 in blocking buffer for 60 minutes at room temperature. Slides were washed again 3 times with 3% BSA, then nuclei were stained with Hoechst diluted 1:2000 in PBS for 30 minutes. Slides were washed twice with PBS, then mounted with Mowiol® mounting medium or DAPI mounting medium (Vectashield® [Vector Laboratories]), if nuclei not stained with Hoechst, and covered with glass coverslips. Negative controls were incubated with secondary antibody only to detect background fluorescence.

For the optimisation of immunostaining for Nox4D localisation, initial attempts were made in tissue staining by prolongation of permeabilisation time to 60 minutes, and extension of Nox4 primary antibody incubation time to overnight at a range of concentrations. This was further optimised in isolated adult WT and Ind-csNox4D cardiomyocytes, in which an additional step was taken after permeabilisation to quench autofluorescence by incubation with freshly prepared sodium borohydride (Sigma) 1 mg/mL in PBS for 10 minutes. Finally, Nox4 immunostaining in isolated cardiomyocytes was optimised by enhancement of antibody concentration and binding. The blocking buffer was modified (3% BSA, 1% goat serum, plus 0.1% Triton™ X-100 in PBS), the blocking period was extended to 40 minutes, Nox4 antibody dilution was increased to 1:100, and the incubation period was extended to 2 hours.

Table 8. Primary and secondary antibodies used for immunostaining.

Antibody	Dilution	Diluent	Manufacturer
Primary			
Ki67	Cells 1:200 Tissue 1:100	Blocking buffer (BSA 3%, goat serum 1% in PBS)	Novus Biologicals
Phospho-histone H3 (pHH3) (serine 10)	1:200		Cell Signalling Technology
α-Smooth muscle actin			Abcam
Sarcomeric α-actinin			Sigma-Aldrich
γ-H2AX (serine 139)			Cell Signalling Technology
Nox4	1:100	Blocking buffer (BSA 3%, goat serum 1%, Triton™ x-100 0.1% in PBS)	Prepared in-house
Secondary			
Goat anti-rabbit Alexa Fluor 488	1:200	Blocking buffer (BSA 3%, goat serum 1% in PBS)	Invitrogen
Goat anti-mouse Alexa Fluor 546			
Goat anti-mouse Alexa Fluor 488			

2.11.3 EdU detection

EdU staining was performed using the Click-iT™ Alexa Fluor 488 EdU imaging kit according to the manufacturer's instructions. Detection of EdU incorporation is based on a click reaction, which is a copper-catalysed covalent reaction between an azide (Alexa Fluor dye) and an alkyne (EdU). Fixed cryosections and fixed cultured adult cardiomyocytes subjected to dedifferentiation were washed twice with 3% BSA in PBS, permeabilised with 0.5% Triton™ X-100 in PBS for 20 minutes, then washed twice with 3% BSA. Optimisation of EdU staining in conjunction with sarcomeric α-actinin staining revealed that primary antibody binding was only visualised when performed before EdU (Figure 2.11). Therefore, primary and secondary antibody incubations were done after permeabilisation. Slides were then incubated with the Click-iT™ reaction cocktail (containing Click-iT™ reaction buffer, copper sulphate, Alexa Fluor 488 azide, and reaction buffer additive) for 30 minutes at room temperature, protected from light. The reaction cocktail was then removed, slides were washed once with 3% BSA in PBS, nuclei were stained and slides were mounted as described in *2.11.2*.

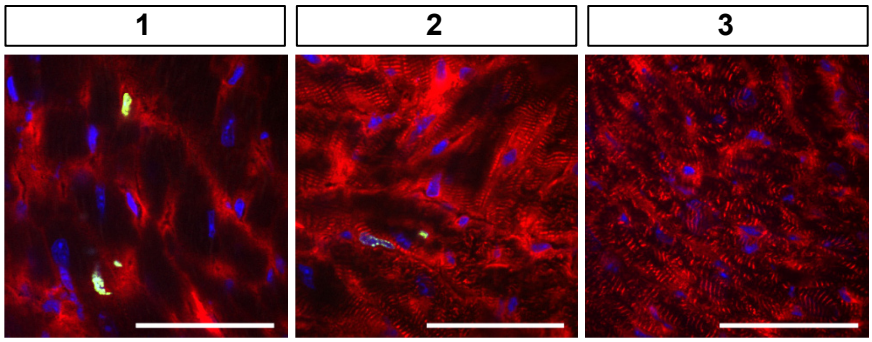

Figure 2.11. Optimisation of EdU detection and immunostaining. Representative images of immunofluorescence staining of EdU (green) incorporation, labelling cells that have synthesised DNA, with α-actinin (red) as a cardiomyocyte marker and Hoechst (blue) as a nuclear marker on cardiac cryosections. Optimisation of experimental conditions was carried out to resolve poor sarcomeric α-actinin staining: (1) 30-minute fixation and permeabilisation then EdU detection before immunostaining; (2) immunostaining before EdU detection; (3) Immunostaining only. Method (2) was compatible with visualisation of α-actinin staining. Scale bars: 50 μm.

2.11.4 Wheat germ agglutinin and isolectin B4

Wheat germ agglutinin (WGA) is a lectin that preferentially binds to residues of N-acetylglucosamine and sialic acid, which are common structures to many membrane glycoproteins. Isolectin B4 (IB4) is also a lectin, the B subunit of which is selective for terminal α-galactosyl residues and is a useful marker for endothelial cells.[165]

Fixed cryosections were washed 3 times with Hanks' Balanced Salt Solution (HBSS, 14175 [Gibco™]), then blocked with 3% BSA, 1% goat serum in PBS for 15 minutes. Tissues were washed 3 times with HBSS and incubated with biotinylated IB4 (Vector Laboratories) 1:50 in HBSS in a humidified chamber for 60 minutes at room temperature. Sections were washed 3 times with HBSS then incubated with fluorescein Avidin D 1:200 and rhodamine-labelled WGA 1:250 (Vector Laboratories) in HBSS for 60 minutes as above. Sections were washed again 3 times with HBSS then permeabilised with 0.1% Triton™ X-100 in PBS for 10 minutes. Slides were washed 3 times with PBS and nuclei were stained with Hoechst 1:2000 in PBS for 10 minutes. Washing was repeated with PBS and slides were mounted with Mowiol® mounting medium.

2.11.5 TUNEL staining

Apoptotic DNA fragmentation was detected enzymatically in situ by terminal deoxynucleotidyl transferase dUTP nick end labelling (TUNEL).[166] This was performed using the ApopTag® In Situ Apoptosis Detection Kit (Merck), which is based on the TUNEL assay, according to the manufacturer's instructions. Fixed tissue sections were washed 3 times with PBS, permeabilised with 0.5% Triton™ X-100 in PBS for 20 minutes, then washed twice with PBS. Sections were incubated in equilibration buffer for

10 minutes, then incubated with working strength TdT enzyme (containing 70% reaction buffer and 30% TdT enzyme) in a humidified chamber for 60 minutes. The reaction was stopped by washing 3 times with working strength stop/wash buffer, then washed 3 times with PBS. Sections were incubated with working strength anti-digoxigenin-rhodamine conjugate (containing 53% blocking solution and 47% anti-digoxigenin conjugate antibody) in a humidified chamber for 30 minutes, protected from light. Sections were washed 4 times in PBS, then blocked and co-stained with α-actinin as described in *2.11.2*. Positive controls were incubated with DNase I (Promega) 1:100 in DTT 0.1 mM for 10 minutes, washed 5 times with distilled water and followed with equilibration buffer.

2.11.6 Picrosirius red

Picrosirius red is a strong histological stain which associates along collagen fibres through acidic sulfonic groups that strongly interact with basic groups in collagen molecules, and is therefore used for the assessment of fibrillar collagen networks.[167]

Slides were immersed in xylene for 5 minutes, then rehydrated through a decreasing ethanol gradient at 100%, 70%, 50%, 25% then distilled water (dH_2O) for 1 minute each. Slides were washed in PBS for 5 minutes then fixed with 4% PFA in PBS for 5 minutes, and washed 3 times with dH_2O. Sections were then incubated with 0.2% phosphomolybdic acid in dH_2O (Sigma) for 30 seconds, and washed twice with dH_2O. Slides were transferred to incubation with 0.1% picrosirius red solution (containing 0.1% Sirius red [Fluka] in 1.3% saturated picric acid [Fluka]) for 1 hour. Slides were washed in 3 changes of acidified water (10% acetic acid in dH_2O) for 10 seconds each, then incubated in saturated picric acid for 15 minutes. Tissues were rinsed 3 times with dH_2O, then dehydrated through the same ethanol series as above but in reverse, for 1 minute each. Tissues were cleared in xylene for 5 minutes, and slides were mounted with DPX mountant (Sigma) and covered with coverslips.

2.11.7 Microscopy

Fluorescent images were captured with a Leica laser scanning confocal microscope (TCS-SP5) (Ind-csNox4D baseline studies) or an inverted spinning disc confocal microscope (Nikon Eclipse Ti-E) (Ind-csNox4D MI studies and isolated cardiomyocytes). All quantifications of control and experimental groups were analysed in parallel in a blinded manner with identical settings.

For each genotype, 3 sections were imaged per heart, in which the whole LV was analysed in sham-operated and basal mice, and the infarct border and remote zones were analysed in MI mice. Using 40x or 60x oil immersion objectives, cardiomyocytes were carefully identified by positive sarcomeric α-actinin staining and Z-stack imaging to show overlap with positive nuclear staining. Positive cardiomyocytes were quantified by

positive Ki67, pHH3, EdU, γ-H2AX, and TUNEL staining in α-actinin-positive cells using NIS-Elements software. Z-stacks were imaged over a 15-µm range at a 0.3-µm step size, and deconvolved using NIS-Elements software. Sections stained with WGA and IB4 were imaged using a 20x objective, and the cross-sectional area of cardiomyocytes with centrally located nuclei (minimum 200 per heart) and capillary density per area were analysed using the General Analysis module in NIS-Elements. Large images of isolated cardiomyocytes subjected to dedifferentiation were obtained by stitching, with the same fixed field dimensions and position per well. Positive cardiomyocytes were quantified manually relative to total cardiomyocyte number, and cell area was determined using ImageJ software.

Picrosirius red slides were imaged by brightfield and polarised light using a Leica DM2000 LED microscope, and fibrosis was quantified relative to the area of the whole cross-section according to colour threshold using ImageJ software.

2.12 Cardiac troponin I ELISA

The concentration of cTnI in mouse plasma was quantified using the High Sensitivity Mouse Cardiac Troponin-I ELISA Kit (Life Diagnostics). This kit utilises an enzyme-linked immunosorbent assay (ELISA), which uses 2 different affinity purified antibodies that recognise an epitope on mouse cTnI. The first is immobilised in the solid phase and the second is conjugated to horseradish peroxidase (HRP), so that cTnI becomes sandwiched between both antibodies, the concentration of which may be detected by colorimetry upon addition of an HRP substrate.

A standard curve was prepared by serial dilution of the reconstituted cTnI stock solution with standard diluent to produce a working range of 0 – 10 ng/mL. Plasma samples were prepared by 4-fold dilution of 30 µL with plasma diluent and further dilution to 200 µL with standard diluent. All standards and samples were pipetted in 100 µL duplicates into a microtiter plate, then mixed and incubated on an orbital shaker at 150 rpm at room temperature for 60 minutes. The microtiter wells were emptied and washed 6 times using the 1x wash solution at 400 µL per well. Residual droplets were removed, 100 µL HRP substrate (TMB Reagent) was added to each well and incubated on an orbital shaker as above for 20 minutes. The enzyme reaction and colour development were stopped by adding 100 µL Stop Solution to each well. The plate was mixed and the absorbance was read at 450 nm on a plate reader (Elx800, BioTek).

The corresponding cTnI plasma concentrations were quantified against the cTnI standard curve using a single-site, total and non-specific binding model (GraphPad Prism).

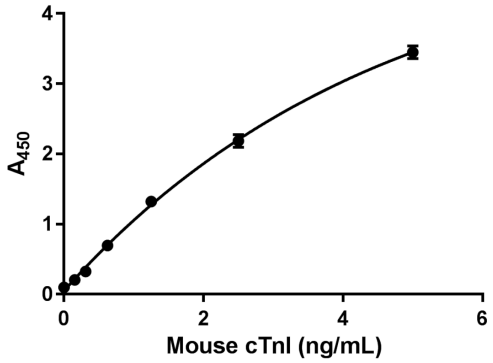

Figure 2.12. Representative cTnI standard curve. Plasma cardiac troponin I (cTnI) was quantified against the standard curve, in which the concentration of cTnI is proportional to the absorbance at 450 nm. Plasma concentration was quantified using a single-site, total and non-specific binding model.

2.13 ROS detection by HPLC

ROS detection in Ind-csNox4D hearts treated with a tamoxifen dose response was carried out using dihydroethidium-HPLC (DHE-HPLC), kindly performed by Dr Celio XC Santos. Briefly, cardiac tissues were incubated with 500 µL DHE 100 µM (Molecular Probes) (in PBS, containing 100 µM DTPA [Sigma]) at 37ºC for 30 minutes, protected from light. Buffer was removed and tissues were washed with PBS. Organic extraction was performed by addition of 500 µL HPLC grade acetonitrile. Samples were sonicated briefly and centrifuged at 13,000 g for 10 minutes at 4ºC. The supernatants were collected and dried using a speed vacuum (Savant SpeedVac [Thermo Scientific]). The resulting solid powders were dissolved in 100 µL PBS-DTPA then analysed by HPLC and quantified as previously described.[168,169] HPLC peak values were normalised to tissue weight.

2.14 H9c2 cell culture

H9c2 cells were cultured in a humidified incubator at 37ºC/5% carbon dioxide/95% air in Dulbecco's modified Eagle's medium (DMEM, D5671 [Sigma]), supplemented with 10% heat-inactivated FBS and 1x L-glutamine-penicillin-streptomycin solution. Cells were passaged and medium was changed every 4 days at a 1:5 ratio. Cells were cryopreserved in DMEM containing 40% FBS and 10% dimethyl sulfoxide at -20ºC overnight, then transferred to liquid nitrogen for long-term storage.

2.15 siRNA-mediated Nox4D knockdown in H9c2 cells

Due to the difficulties associated with splice variant-specific targeting, the development of efficient small interfering (siRNA)-mediated knockdown of Nox4D required a series of optimisation steps to enhance both selectivity and detection (discussed in more detail in section *5.3.1*). To enable discrimination from full-length Nox4, the choice for design of siRNA and primer sequences is limited to the short sequence spanning the exon 2/12 junction that is created by splicing of exons 3 – 11.

Custom-designed siRNA directed against rat and mouse Nox4D (sequence 5' – 3': ATGTTGGGC/TGTCCTACTGAA, where / denotes the exon 2/12 junction), and a control sequence (5' – 3': AATTCTCCGAACGTGTCACGT) were designed using the GeneAssist™ Custom siRNA Builder (Thermo Scientific). Commercially available, pre-validated siRNA targeted to exon 3 of Nox4 (Ambion) was used as a positive control for the transfection protocol. Transfections were performed using the transfection reagent Lipofectamine™ RNAiMAX (Thermo Scientific), according to the manufacturer's instructions. Briefly, H9c2 cells were seeded in 6-well culture plates to establish 60 – 80% confluency at the time of transfection. Transfection reagent and siRNA were diluted separately in Opti-MEM™ Reduced Serum Medium (Gibco™), then mixed at a 1:1 ratio and incubated for 5 minutes. The medium was replaced with 750 µL serum-free DMEM, and 250 µL siRNA-lipid complex (containing 5 µL transfection reagent) was added per well. Additional control cells were incubated with Opti-MEM™ only (untreated) or Opti-MEM™ plus transfection reagent. After 4 hours, the medium was supplemented with 5% FBS and cells were incubated for a further 72 hours, then harvested for mRNA and protein analysis for assessment of knockdown efficiency. All siControl and siNox4 were transfected at 10nM. siNox4D was initially transfected at 10 nM, which was later confirmed as the most optimal concentration after transfection of 2.5 nM – 20 nM.

2.16 Recombinant adeno-associated virus production

2.16.1 shRNA and plasmid production

The corresponding short hairpin RNA (shRNA) sequence to the siNox4D sequence was designed and synthesised, and the shRNA oligo was cloned into an AAV construct containing the U6 promoter and GFP sequence, flanked by AAV2 inverted terminal repeats (pAAV-GFP-U6-shNox4D). A control plasmid was also made with a pre-validated scrambled shRNA sequence (pAAV-GFP-U6-shScramble). The shRNA synthesis and plasmid cloning techniques were performed externally by Vector Biolabs.

2.16.2 AAV9 vector production

Adenovirus-free recombinant adeno-associated virus serotype 9 (rAAV9) was produced by transient transfection in 293T cells. 293T cells were triple transfected at 70 – 80% confluency with the AAV2 ITR-containing plasmid carrying the shNox4D or shScramble expression cassette (AAV cis-plasmids), a separate construct expressing in trans the AAV2 Rep and AAV9 Cap genes, and a third plasmid providing the adenovirus helper factors (HGTI) in a 1:1:3 plasmid ratio using 1 mg/mL polyethyleneimine MAX (Polysciences, Inc).

Cells were harvested 72 hours post transfection and centrifuged at 2,500 g for 10 minutes at 4ºC. The cell pellets were resuspended in 10mL lysis buffer each (containing Tris HCl 50 mM, NaCl 150 mM, $MgCl_2$ 2 mM, pH 8.0) and lysed by 3 freeze-thaw cycles (-80ºC/37ºC), vortexing for 30 seconds between each cycle. Lysates were treated with benzonase 50 U/mL (Sigma) and incubated for 30 minutes at 37ºC, then cleared by centrifugation at 2,500 g for 30 minutes at 4ºC to remove cell debris. The supernatants obtained post-harvest were mixed with 31.3g ammonium salts per 100 mL collected media, incubated on ice for 30 minutes, then centrifuged at 8,300 g for 30 minutes. The pellets were resuspended with the cleared lysates and purified by an iodixanol gradient. The gradient was built in ultracentrifuge tubes (Beckman Instruments) by layering the lysate over iodixanol (OptiPrep™ Density Gradient Medium [Sigma]) in increasing order (15%, 25%, 40%, and 60%). The tubes were placed in a TH641 rotor and centrifuged (Sorvall Discovery 90SE) at 200,000 g for 3 hours at 18ºC with the brake off. The AAV9 vectors were extracted between the 60 – 40% fractions with a 19-gauge needle, diluted in PBS and concentrated to 1 mL final volume in a Vivaspin 20 (100 kDa cut-off [Sartorius]) and filter sterilised.

The capsid protein content and vector purity were assessed by visualisation of the capsid proteins VP1, VP2, and VP3 by SYPRO® Ruby Protein Gel Stain (Thermo Scientific) after SDS-PAGE. The genome titres of the concentrated vectors were determined using alkaline agarose gel electrophoresis. Alkaline gels were run at 20V overnight at 4ºC with 0.05 M NaOH as running buffer, stained with nucleic acid stain 4x GelRed® in NaCl 0.1 M (Biotium) for 2 hours, then imaged under ultraviolet light and quantified against the 1kb HyperLadder™ (Bioline).

2.17 Statistical analysis

All data sets were graphically and statistically analysed using GraphPad Prism software. All data is expressed as mean ± standard error of the mean (SEM) unless stated otherwise. Levels of significance are defined as: *P < 0.05, **P < 0.01, ***P < 0.001, ****P < 0.0001.

Samples for animal studies were randomly selected and assigned to the experimental groups, and analysed in a blinded fashion with regard to genotype during outcome assessment, where possible. No animals were excluded from analyses. The minimum sample sizes required to detect statistical significance between groups were estimated at $\alpha = 0.05$ and Power ($1 - \beta$ error probability) = 0.8.

A normal distribution was assumed for all values in each data set, and so parametric tests were used for all statistical analyses. Analyses between 2 experimental groups were performed using an unpaired two-tailed t-test. A one-way analysis of variance (ANOVA) was used to compare the mean differences between 3 or more independent experimental groups against 1 variable, and a two-way ANOVA was used to compare the mean differences between experimental groups against 2 independent variables. All ANOVA analyses were completed with a Bonferroni's multiple comparisons post-hoc test for comparison of individual groups. Linear regression was used to determine the relationship between a dependent an independent variable, and to assess the difference in slope and y-intercept between the regression lines of 2 experimental groups, shown with the 95% confidence intervals.

Chapter 3 Baseline characterisation of the inducible cardiomyocyte-specific Nox4D transgenic mouse model

3.1 Introduction

Although classically viewed as key drivers of oxidative stress, it is now widely recognised that ROS paradoxically also play important roles as reactive biomolecules in intracellular signalling cascades. In the heart, this is essential for the regulation of several pathophysiological processes including survival and stress response pathways, cellular differentiation and proliferation.[131,139]

The Nox family are a crucial enzymatic source of regulated ROS production within defined subcellular compartments and are therefore critically involved in redox signalling.[170,171] The Nox enzymes Nox1 – Nox5 are expressed in the cardiovascular system,[143] of which Nox2 and Nox4 are expressed in cardiomyocytes.[170,172] The myocardial expression level of Nox4 has been shown to rise in situations of cardiac stress, and studies published by our laboratory and others have found that this Nox isoform exerts several protective effects in the heart against adverse remodelling.[149–152,173–177] Although such extensive research has enhanced our understanding of the role of Nox4, it is likely that the complexities regarding the precise mechanisms of Nox4-mediated redox signalling pathways in the heart are yet to be fully understood.[172] Moreover, it is of interest that different Nox4 isoforms are likely to be present in specific subcellular compartments,[143] with potential implications for differences in functions in ROS-related cell signalling.[153] However, the prevalence and functional roles of such variants remain to be explored.

3.1.1 Initial characterisation of Nox4D

As described in *1.5.2*, the identification of 4 novel splice variants of Nox4 was originally reported in 2005. Compared to the other Nox4 splice variants, Nox4D represented the most intriguing as this 28-kDa isoform was found to be fully functional in terms of ROS generation due to retention of the FADH and NADPH binding domains, despite lacking most of the classical Nox transmembrane domain (Figure 1.5). The lack of this domain is a result of splicing at exons 3 – 11 of Nox4, suggesting that Nox4D may localise in non-membrane associated compartments.[153]

Despite such a critical difference in structure in comparison to full-length Nox4, it was found that Nox4D is capable of NADPH oxidase activity and therefore distinct redox-mediated effects due to compartmentalised ROS generation.[153] Additional work in our laboratory further characterised the functional role of Nox4D, highlighting the potential for this splice variant to exert (patho)physiological effects by redox-modulation of nuclear-based signalling pathways.[154]

3.1.2 Nox4D is a potential regulator of cardiomyocyte proliferation

We became interested in a potential role for Nox4D in cell cycle modulation during gain-of-function experiments in neonatal rat cardiomyocytes. Isolated neonatal rat ventricular myocytes (NRVMs) were infected with recombinant adenovirus expressing either Nox4D (Ad.Nox4D) or β-galactosidase control (Ad.β-gal), then cultured for a further 48 hours. Splice variant-specific overexpression of the 28-kDa isoform was primarily associated with strong focal intranuclear immunostaining, whereas the nuclear expression of endogenous Nox4D was significantly lower in myocytes infected with Ad.β-gal (Figure 3.1A). Interestingly, Nox4D-overexpressing neonatal cardiomyocytes showed changes in cell number and cell size characteristic of a greater rate of proliferation (Figure 3.1B and C). This led to further investigation for molecular readouts of cell proliferation, and later observed that such changes were accompanied by increased expression of markers of proliferation including Ki67 (Figure 3.1D), 5-bromo-2'-deoxyuridine (BrdU) incorporation (Figure 3.1E) and 3H-leucine incorporation (Figure 3.1F) as well as consistent phosphorylation of Akt in comparison to Ad.β-gal control cells (Figure 3.1G).

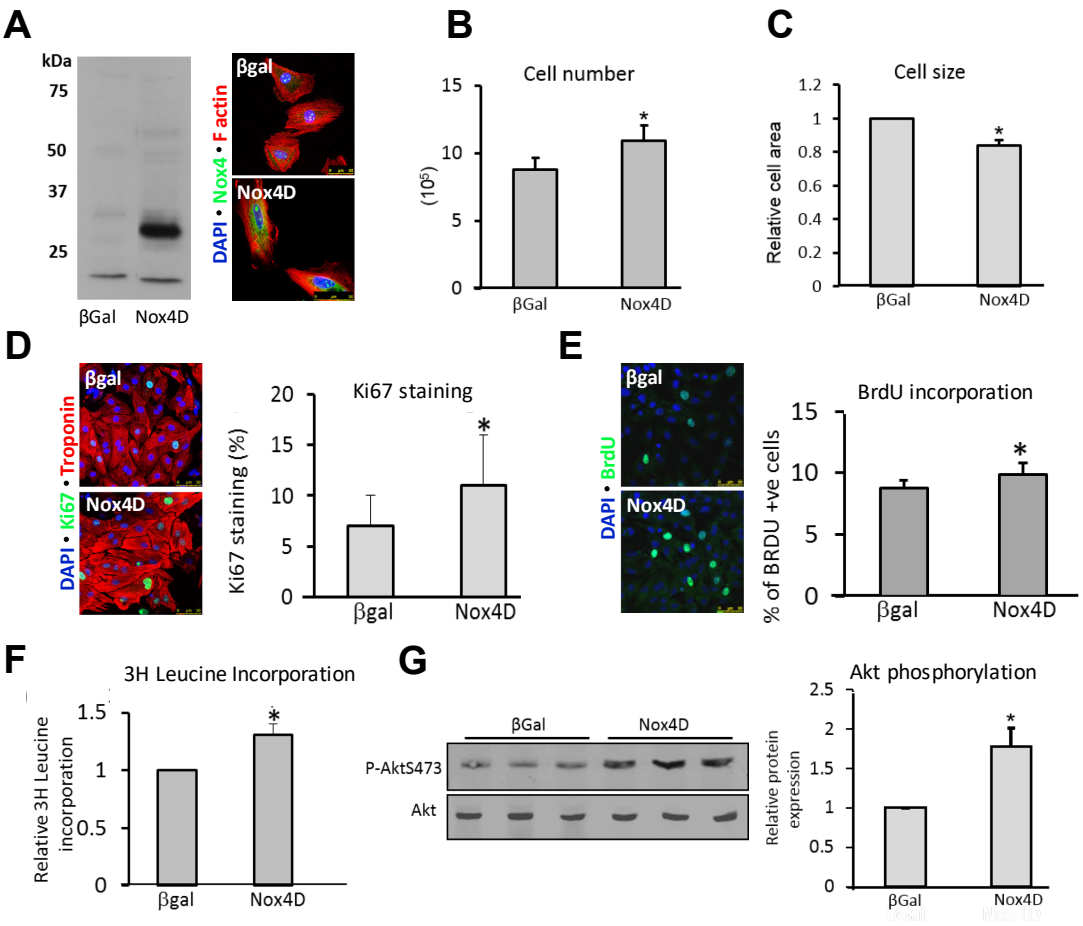

Figure 3.1. Overexpression of Nox4D increases proliferation of neonatal cardiac myocytes. Isolated neonatal rat cardiac myocytes were infected with adenovirus expressing Nox4D (Ad.Nox4D) or β-galactosidase control (Ad.β-gal) and cultured for 48 hours. (A) Western blot (left) and immunofluorescence (right) show overexpression and nuclear localisation of the 28-kDa splice variant. Nox4D-overexpressing myocytes show greater cell number (B) and smaller cell size (C) relative to Ad.β-gal control. Immunofluorescence staining also shows increased expression of the cell cycle marker Ki67 (D) and increased DNA synthesis by 5-bromo-2'-deoxyuridine (BrDu) incorporation (E), in conjunction with increased protein synthesis by 3H-leucine incorporation (F). (G) Western blot (left) and relative quantification (right) reveals Nox4D overexpression is associated with enhanced phosphorylation of the redox-sensitive kinase Akt, which has proliferative activity. Scale bars in (A), (D) and (E): 50 μm. n = 3 per group. Data represent mean ± SEM. *P<0.05 by unpaired two-tailed t-test. Work by Dr Narayana Anilkumar, unpublished.

Collectively, these findings provided initial evidence that overexpression of Nox4D is able to enhance the proliferation of neonatal cardiomyocytes in vitro. Smaller cell size has previously been reported as a characteristic of proliferating neonatal cardiomyocytes,[87] and together with greater cell number, is suggestive of enhanced cell cycling. Positive Ki67 immunostaining is a marker for progression through the cell cycle as this detects cells that are actively in G1, S, G2 or M-phase[81,178] More specifically, incorporation of the labelled thymidine analogue BrdU directly measures de novo DNA synthesis and is therefore a readout for detection of S-phase synthesis in the cell cycle.[81] Similarly, incorporation of the labelled amino acid 3H-leucine is indicative of protein biosynthesis, which is essential for cell growth and translational control of the cell cycle. The active phases of the cell cycle during which most protein synthesis occurs are the gap phases G1 and G2, thus 3H-leucine incorporation functions as an additional readout of cell cycle progression.[179,180]

Given that these changes occurred in conjunction with enhanced phosphorylation of Akt, it would appear that Nox4D overexpression increases neonatal cardiomyocyte proliferation in a redox-mediated, Akt-dependent manner. The PI3K-Akt pathway is known to be centrally involved in the regulation of cardiomyocyte proliferation and survival,[119,181,182] and is also susceptible to ROS-driven redox modulation.[183] Based on this, we reasoned that Nox4D may represent a novel redox regulator of cardiomyocyte cell cycle progression.

As discussed in *1.2.4*, adult mammalian cardiomyocytes possess a very limited regenerative capacity.[78] Any intrinsic proliferative activity remains insufficient to achieve complete functional recovery following disease characterised by cardiomyocyte loss, and so the prospect that cardiomyocyte proliferation could be induced by appropriate therapeutic manipulation represents a major unmet clinical need.[26,184] Thus, this formed the rationale for the present work as we wanted to investigate the potential of Nox4D to promote cardiomyocyte proliferation in the adult mammalian heart.

3.2 Aims

The aims of this chapter were to generate and characterise a novel transgenic model of cardiac-targeted Nox4D overexpression, specifically with a view to investigate the effects of manipulation of Nox4D levels on cardiomyocyte cell cycle activity in the adult mammalian murine heart.

3.3 Summary of methods

Ind-csNox4D Tg mice were generated by crossing female Nox4D Tg mice with male αMHC-MCM mice, as described in 2.2. For baseline characterisation of the Ind-csNox4D phenotype, cardiomyocyte-specific overexpression of Nox4D was selectively induced in male and female adult Ind-csNox4D mice by administration of tamoxifen at 20 mg/kg body weight once per day for 5 consecutive days. WT littermate controls were treated in parallel (section 2.3).

Experiments were performed according to 2 protocols. During the initial protocol (Figure 2.4), cardiac structure and function were serially monitored by echocardiography (section 2.5), and cardiac tissues were harvested at 3 weeks following tamoxifen induction (section 2.7). The efficiency of the tamoxifen protocol to induce overexpression of Nox4D was evaluated by Western blotting (section 2.10). The subcellular localisation of endogenous and overexpressed Nox4D was initially assessed by immunohistochemistry with Nox4 antibody in cardiac cryosections (sections *2.11.1* & *2.11.2*), but due to unsatisfactory results with the use of this antibody in tissue sections, this required further optimisation ex vivo in adult cardiomyocytes isolated from WT and Ind-csNox4D mice 2 weeks after tamoxifen induction (sections 2.8 & *2.11.2*). The potential for cardiac-specific Nox4D overexpression to target redox signalling pathways and promote cardiomyocyte cell cycle re-entry was investigated by Western blotting and immunohistochemistry, respectively. This was also investigated transcriptionally by qPCR screening for gene expression profiles associated with cell cycle modulation (section 2.9).

To capture a potential immediate window of cardiomyocyte proliferation secondary to induction of Nox4D overexpression, a second cohort of Ind-csNox4D and WT animals were administered EdU and harvested 5 days following completion of tamoxifen induction (Figure 2.6). EdU incorporation, as a marker of S-phase activity, was measured in cardiac cryosections by fluorescent detection of EdU in conjunction with immunohistochemistry (sections *2.11.2* & *2.11.3*). These tissues were also analysed by qPCR using the same panel of markers as above.

3.4 Results

3.4.1 Induction of Nox4D overexpression in cardiomyocytes of adult Ind-csNox4D mice

To explore the role of Nox4D in the adult heart, Ind-csNox4D Tg (αMHC-MCM;Nox4D) mice were generated for selective induction of Nox4D overexpression in differentiated cardiomyocytes (as discussed in *2.2.1*). Male and female Ind-csNox4D and WT (αMHC-MCM-*negative*;Nox4D) littermate controls were treated in parallel with tamoxifen (20 mg/kg body weight per day for 5 days) at 8 weeks of age, after which hearts were harvested 3 weeks later.

To evaluate the efficiency of the tamoxifen protocol to induce αMHC-MCM-mediated recombination, the expression of Nox4D at protein level was measured by Western blotting. Overexpression of Nox4D was detected by a 10-fold increase in protein level compared to WT controls (Figure 3.2). This was accompanied by no change in the mRNA level of full-length Nox4, confirming the induction of Nox4D is splice variant-specific (Figure 3.3).

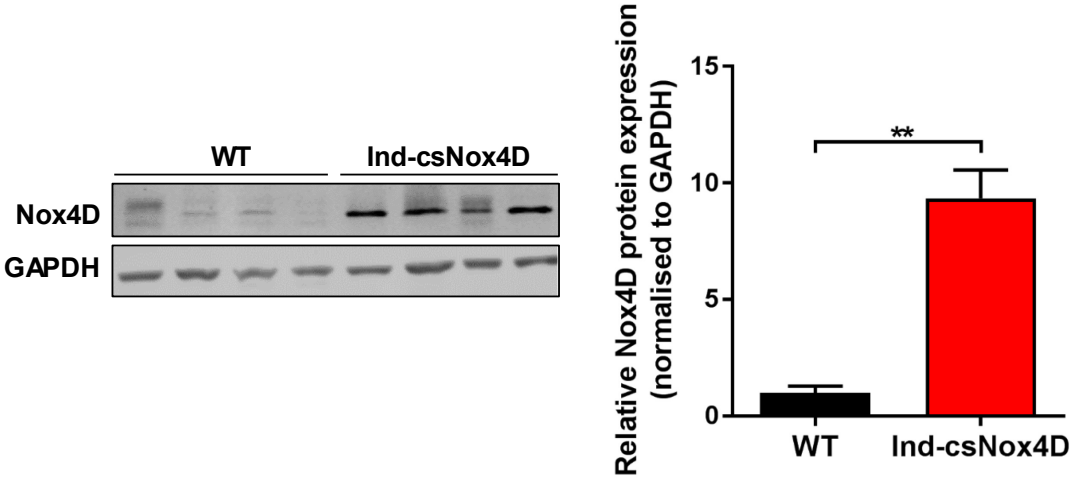

Figure 3.2. Induction of Nox4D overexpression in the adult heart. Representative immunoblot (left) and relative quantification (right) of Nox4D protein expression in hearts of adult WT and Ind-csNox4D transgenic (Tg) mice 3 weeks after tamoxifen administration. Tg mice show a 10-fold increase in cardiac Nox4D protein level compared to control mice. n = 4 per group. Data represent mean ± SEM. ***P*<0.01 by unpaired two-tailed t-test.

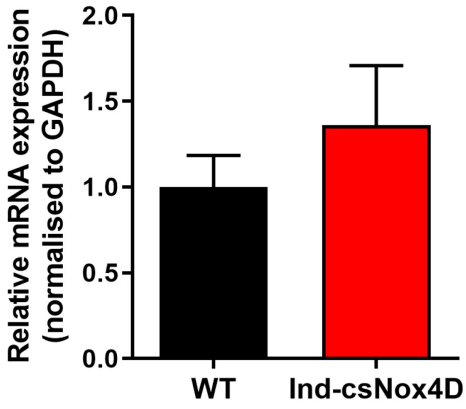

Figure 3.3. Induction of Nox4D overexpression in the adult heart is splice variant-specific. qPCR analysis of relative Nox4 mRNA expression in hearts of WT and Ind-csNox4D mice 3 weeks after tamoxifen administration. Full-length Nox4 mRNA is unchanged in Ind-csNox4D compared to control mice. n = 4 per group. Data represent mean ± SEM. Statistical analysis by unpaired two-tailed t-test.

Initial attempts were made to establish the subcellular localisation of overexpressed Nox4D compared to the endogenous protein in vivo by immunoreactivity, using a well-validated, in-house prepared polyclonal antibody directed against the carboxy-terminal region of Nox4, which is preserved in Nox4D.[154,185] However, it is recognised in our laboratory that this antibody performs less well for immunohistochemical applications, as demonstrated by the lack of specificity in signal in both WT and Ind-csNox4D hearts (Figure 3.4). Additional attempts to optimise immunofluorescence staining in vivo by prolongation of permeabilisation time and primary antibody incubation also proved unsuccessful.

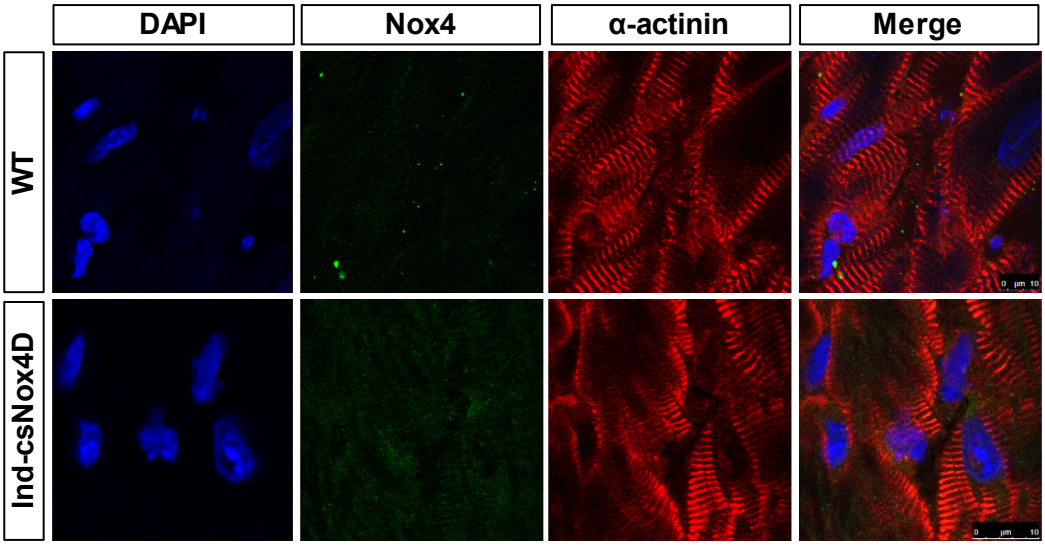

Figure 3.4. Localisation of Nox4D after induction of overexpression in the adult heart. Representative images of initial attempt at immunofluorescence staining for Nox4 (green) with the cardiomyocyte marker α-actinin (red) and nuclear marker DAPI (blue) on cardiac cryosections of Ind-csNox4D and WT control hearts harvested 3 weeks after tamoxifen induction, for characterisation of cellular localisation of Nox4D within cardiomyocytes in vivo. Under standard immunohistochemical staining conditions, the Nox4 antibody performs suboptimally. Scale bars: 10 μm. n = 4.

Given that previous data in NRVMs showed positive Nox4D staining when used in vitro (Figure 3.1), further optimisation of immunostaining with the Nox4 antibody was carried out in isolated adult cardiomyocytes from Ind-csNox4D and WT mice 2 weeks after tamoxifen induction. However, under standard staining conditions, there was little improvement in signal from the Nox4 antibody and, as such, the determination of Nox4D localisation and difference in expression between WT and Ind-csNox4D myocytes remained unclear (Figure 3.5).

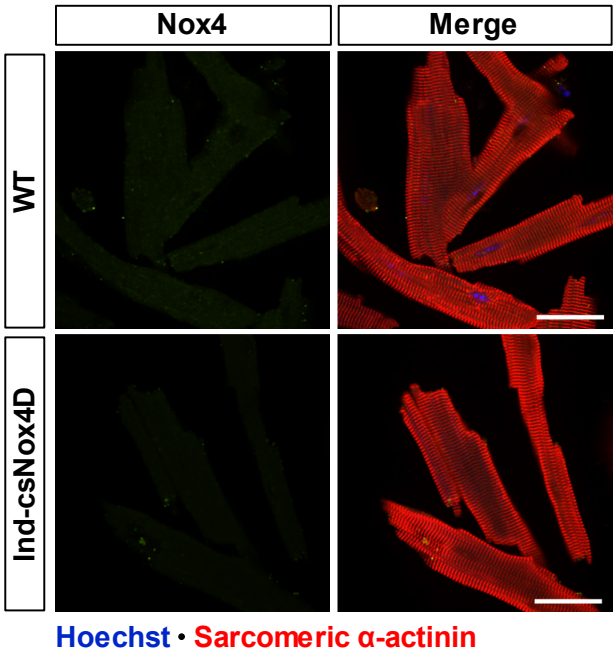

Figure 3.5. Optimisation of immunostaining of Nox4D localisation in isolated adult cardiomyocytes. Representative images of further optimisation of immunofluorescence staining of Nox4 (green) with α-actinin (red) and Hoechst as a nuclear stain (blue) in adult cardiomyocytes isolated from WT and Ind-csNox4D mice 2 weeks after tamoxifen induction. Striated cardiomyocytes are revealed by positive sarcomeric actinin staining whilst Nox4 staining remains suboptimal. Scale bars: 50 μm.

Using the same model of isolated adult cardiomyocytes, the conditions for immunofluorescence staining of Nox4D were further optimised to enhance antibody penetration and binding (Figure 3.6). This equated to an improvement in the specificity of the green signal and indicated that Nox4D is localised to the nuclear and cytosolic cellular compartments, as such staining was absent in the primary antibody negative control. This staining pattern was observed at a low level of expression in cardiomyocytes isolated from WT tissue. In Ind-csNox4D Tg cardiomyocytes, increased Nox4D expression was observed with predominant subcellular localisation within the nuclei.

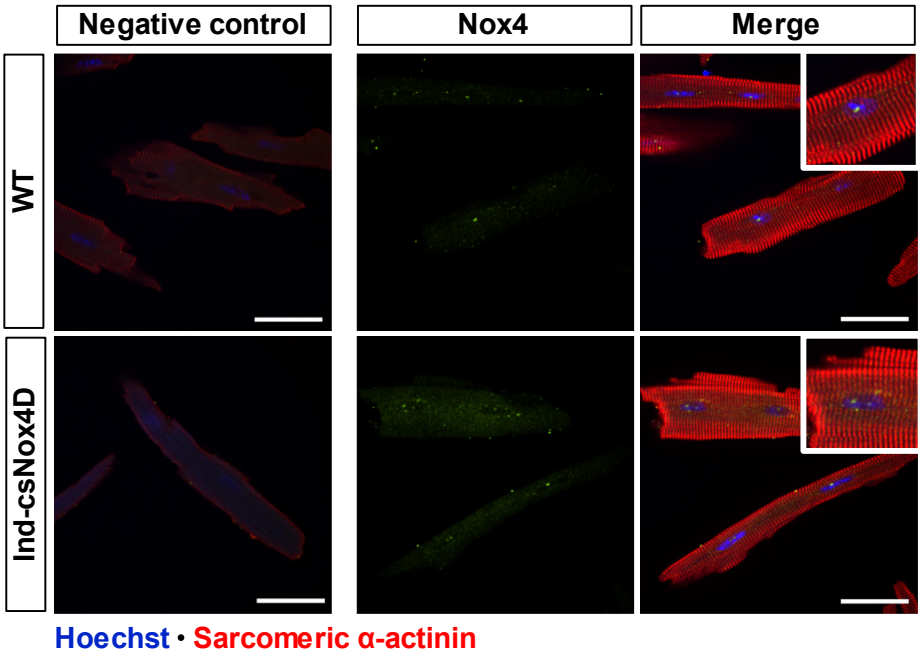

Figure 3.6. Final optimisation of immunostaining of Nox4D localisation in isolated adult cardiomyocytes. Representative images of finalised optimisation of immunofluorescence staining conditions for Nox4 (green) with α-actinin (red) and Hoechst as a nuclear stain (blue) in adult cardiomyocytes isolated from WT and Ind-csNox4D mice 2 weeks after tamoxifen induction. Negative control incubated with secondary antibodies and Hoechst only. The magnified portion of the merged images indicate nuclear and cytoplasmic localisation of Nox4D. Scale bars: 50 µm.

3.4.2 Induction of cardiomyocyte-specific Nox4D overexpression in vivo does not affect basal cardiac function, structure or morphology

To investigate the basal phenotype of the mice secondary to induction of cardiomyocyte-specific Nox4D overexpression, echocardiography was repeatedly performed in WT and Ind-csNox4D transgenic mice before and after induction. A series of time points were selected to permit functional monitoring and analysis during the first 2 weeks after tamoxifen induction as a relevant time frame for subsequent experiments.

Echocardiographic image analysis demonstrated no abnormalities in systolic function, as indicated by no change in ejection fraction compared to WT mice. Similarly, cardiac structure was unaffected as shown by no change in left ventricular end-diastolic volume (LVEDV, as a marker of LV dilatation), or interventricular diastolic septum thickness (IVS, d) (Figure 3.7). These results collectively highlighted that cardiomyocyte-specific Nox4D overexpression did not affect cardiac functional or structural parameters over the time frame observed.

In conjunction, the ratios of heart weight to body weight post-tamoxifen induction in Ind-csNox4D transgenic mice were also unchanged in comparison to WT mice, suggesting no effect of Nox4D overexpression on cardiac gross morphology (Figure 3.8).

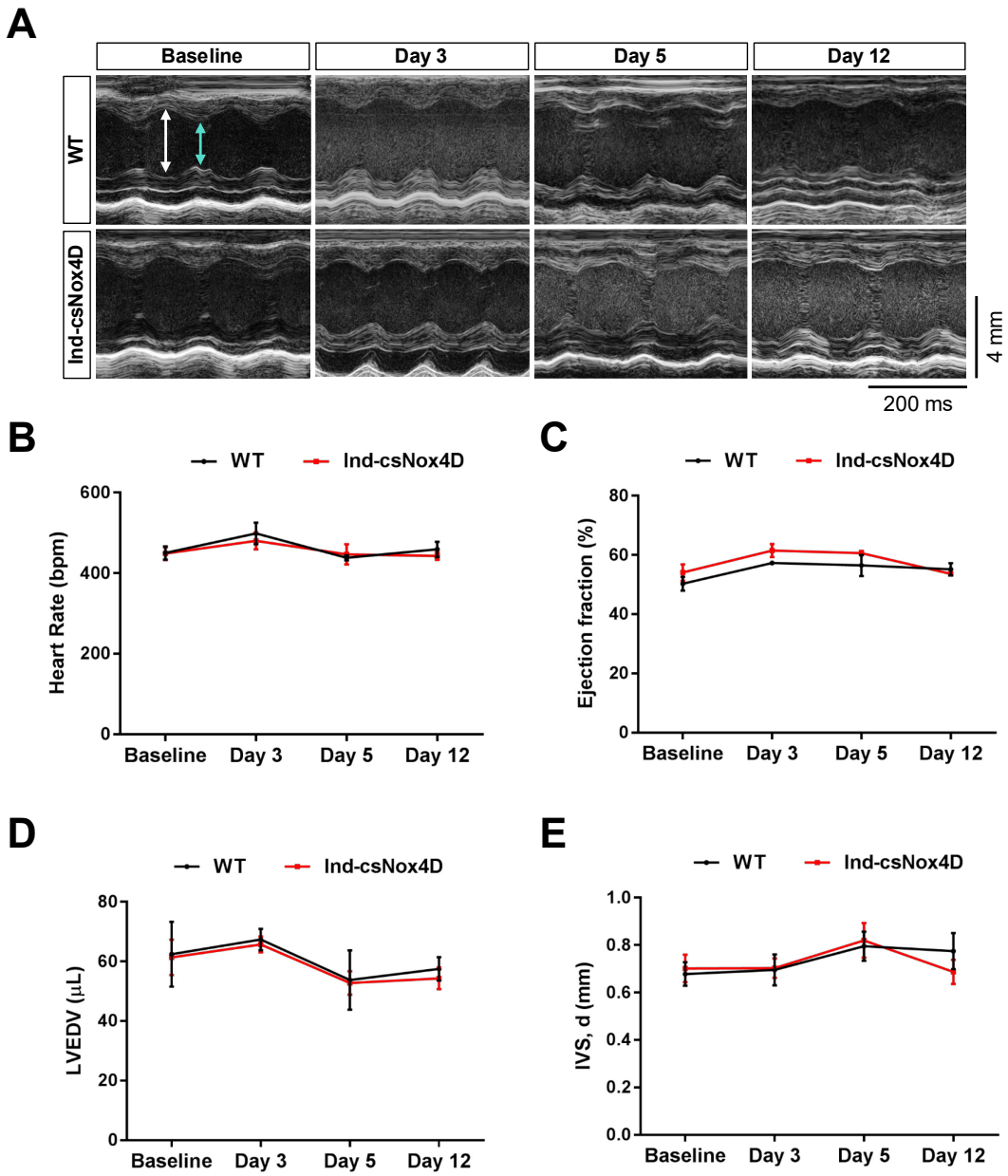

Figure 3.7. Cardiac structure and function are unchanged in inducible cardiomyocyte-specific Nox4D (Ind-csNox4D) transgenic mice. (A) Representative M-mode echocardiographic images of WT and Ind-csNox4D transgenic hearts at baseline and days 3, 5 and 12 after tamoxifen induction. White and cyan arrows indicate left ventricular end-diastolic diameter (LVEDD) and left-ventricular end-systolic diameter (LVESD), respectively. Scale bars: 200 ms, 4 mm. Echocardiographic images analysed within same range of heart rate (B) for measurement of ejection fraction (C), left ventricular end-diastolic volume (LVEDV) (D), and interventricular septum thickness at diastole (IVS, d) (E). n = 4 per group. Data represent mean ± SEM. Statistical analysis by two-way ANOVA with Bonferroni's post hoc correction.

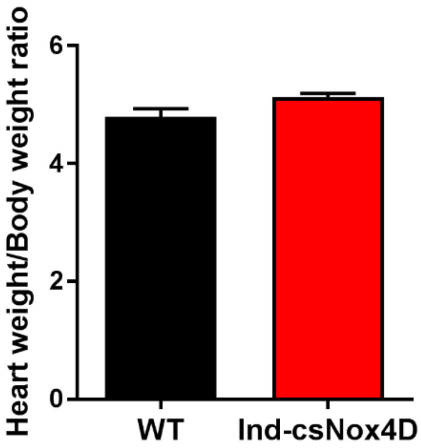

Figure 3.8. Inducible cardiomyocyte-specific Nox4D overexpression does not affect cardiac morphology. Heart weight to body weight ratio in WT and Ind-csNox4D transgenic mice indicates cardiac morphology is unchanged after tamoxifen induction. n = 8 per group. Data represent mean ± SEM. Statistical analysis by unpaired two-tailed t-test.

3.4.3 Cardiac-specific Nox4D overexpression does not affect basal cell proliferation in adult mice

The capacity for cardiac-specific Nox4D overexpression to induce proliferation of adult cardiomyocytes in the absence of injury was investigated immunohistochemically 3 weeks after tamoxifen induction by confocal microscopy. The proliferation markers Ki67 and phospho-histone H3 (pHH3) were utilised for the evaluation of cardiomyocyte cell cycling in adult hearts of Ind-csNox4D Tg mice compared to WT littermate controls. Cardiomyocytes indicative of proliferation were identified by nuclear expression of Ki67, highlighting G1, S, G2 and M-phase of the cell cycle, and histone H3 phosphorylation at serine 10, a marker of late G2/M-phase, in conjunction with positive cell immunostaining for sarcomeric α-actinin.

Quantification of the number of α-actinin-positive cardiomyocytes with Ki67-positive nuclei per microscopic field revealed that despite a small trend showing greater number in Ind-csNox4D myocardium, overall there was no difference compared to WT controls (Figure 3.9A and B). Similarly, although the same trend was observed for the number of α-actinin-positive cardiomyocytes with pHH3-positive nuclei in Ind-csNox4D hearts, this was not statistically different from that in WT hearts (Figure 3.9C and D).

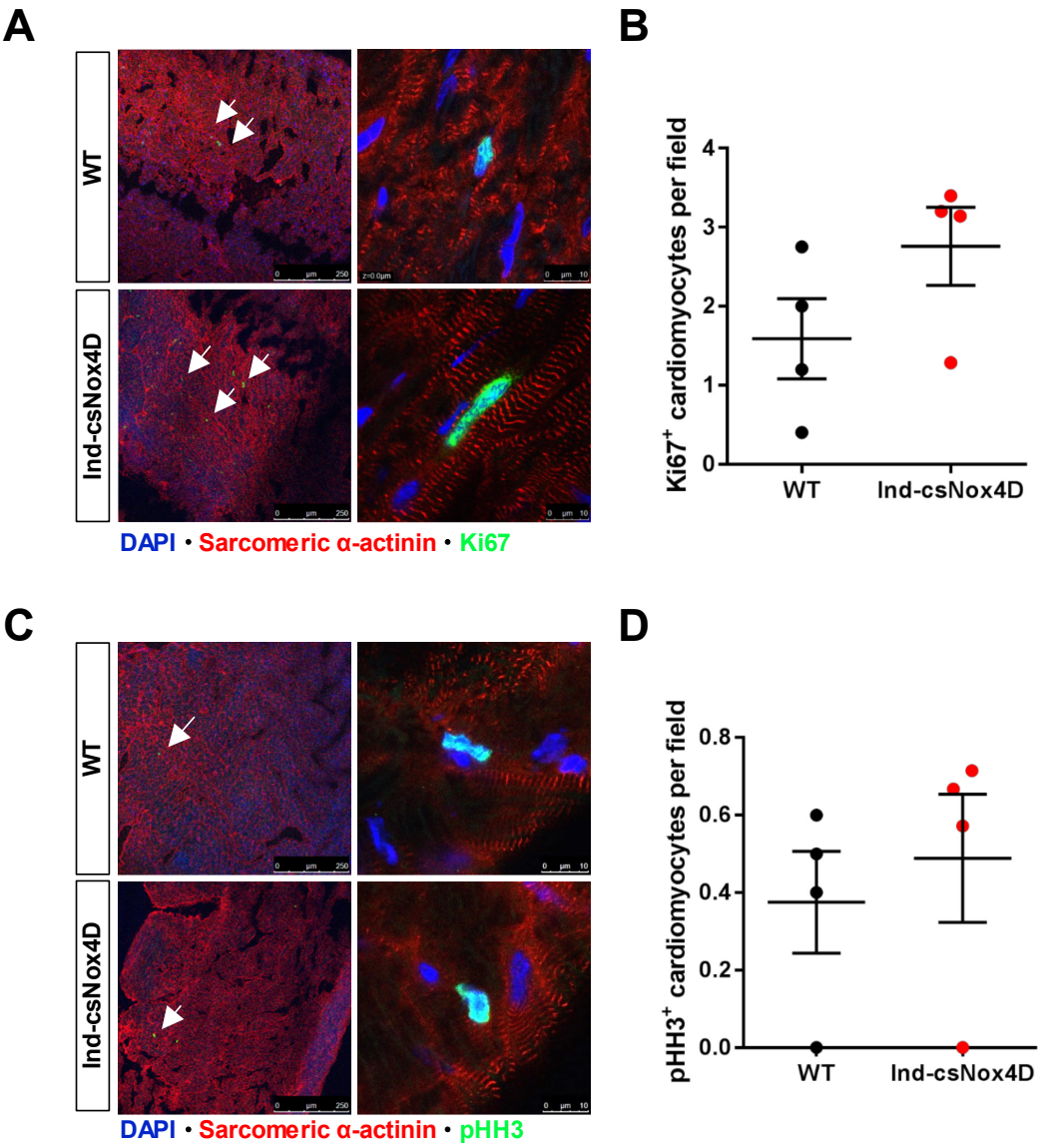

Figure 3.9. Cardiomyocyte-specific Nox4D overexpression induced in adult mice does not promote cardiomyocyte proliferation in the absence of injury. Representative images of immunofluorescence staining for cell proliferation markers Ki67 (A) and phospho-histone H3 (pHH3) (C) (both green) with α-actinin (red) as a cardiomyocyte marker and DAPI (blue) as a nuclear marker on cardiac cryosections of Ind-csNox4D and WT control hearts harvested 3 weeks after tamoxifen induction. Scale bars: 250 µm (left), 10 µm (right). White arrows and higher magnification images indicate positive cardiomyocyte nuclei, defined by co-localisation of green and blue signal in α-actinin-positive cells. (B) and (D) Quantification of the number of positive cardiomyocytes per field. Five fields of view, each of consistent cardiomyocyte count, were imaged per heart. n = 4 per group. Individual data points are shown with mean ± SEM. Statistical analysis by unpaired two-tailed t-test.

3.4.4 Cardiac-specific Nox4D overexpression does not affect redox signalling pathways or transcriptional profiles associated with cell cycle modulation

Following the initial in vitro data in which Akt phosphorylation was shown to be enhanced in response to Nox4D overexpression (Figure 3.1G), this was further investigated to establish if the same response could be elicited in the adult heart. The capacity for basal cardiomyocyte-specific Nox4D overexpression to promote Akt phosphorylation in vivo was assessed by Western blotting of myocardial lysates of Ind-csNox4D and WT adult hearts, 3 weeks after tamoxifen induction.

However, the level of phosphorylated Akt as a marker of activation of the PI3K-Akt pathway was shown to be unchanged in Ind-csNox4D hearts compared to WT controls, indicating no baseline activation of Akt secondary to induced cardiac-specific Nox4D overexpression (Figure 3.10A). Likewise, as the cell cycle inhibitor p27Kip1 is a direct target of Akt,[119] this was also measured as a downstream readout of Akt activation. Consistent with the level of phosphorylated Akt, no changes were seen in the level of p27Kip1 in the Tg compared to WT hearts, suggesting no Akt-mediated effect on downstream targets (Figure 3.10B).

Under normal physiological conditions, the mRNA expression of cell cycle activators and foetal contractile proteins or dedifferentiation markers in the heart would be expected to decrease after birth whilst the expression of cell cycle inhibitors would be predicted to rise, in line with the usual postnatal exit of cardiomyocytes from the cell cycle.[186] Therefore, in order to investigate the propensity of Nox4D-overexpressing adult cardiomyocytes to re-enter the cell cycle, a selection of these markers, as informed by recent reports in the literature,[162,187] was screened by qPCR analysis of myocardial lysate collected from Ind-csNox4D and WT hearts at the same time point as above after tamoxifen induction.

Overall, this screen revealed no changes in the mRNA expression levels of cell cycle activators (cyclins E1, A2 and D1), foetal contractile proteins (myosin heavy chain 7 [Myh7] and slow skeletal troponin I [ssTNI]) or other dedifferentiation markers (Runx1, Dab2, GATA4 and ckit) in hearts of Ind-csNox4D transgenic compared to WT control mice (Figure 3.11). As such, this demonstrated no changes in either the differentiation status or proliferative capacity of adult cardiomyocytes overexpressing Nox4D under baseline conditions.

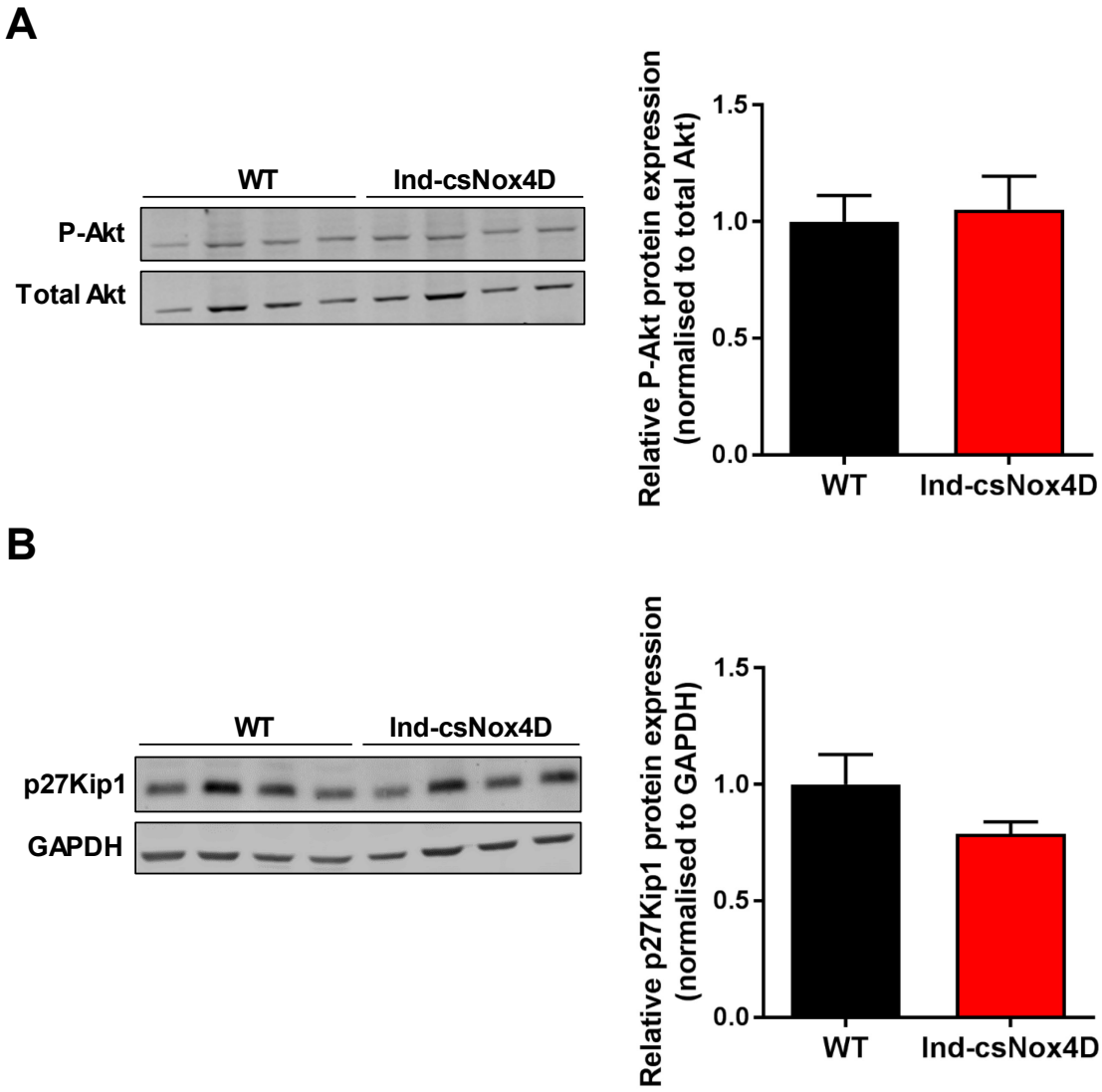

Figure 3.10. Cardiac-specific Nox4D overexpression does not enhance signalling of proliferative redox-sensitive pathway Akt. (A) and (B) Representative immunoblots (left) and relative quantification (right) of phosphorylated Akt (P-Akt, serine 473) (A) and downstream target p27Kip1 (B) protein expression in hearts of WT and Ind-csNox4D transgenic mice 3 weeks after tamoxifen induction. n = 4 per group. Data represent mean ± SEM. Statistical analysis by unpaired two-tailed t-test.

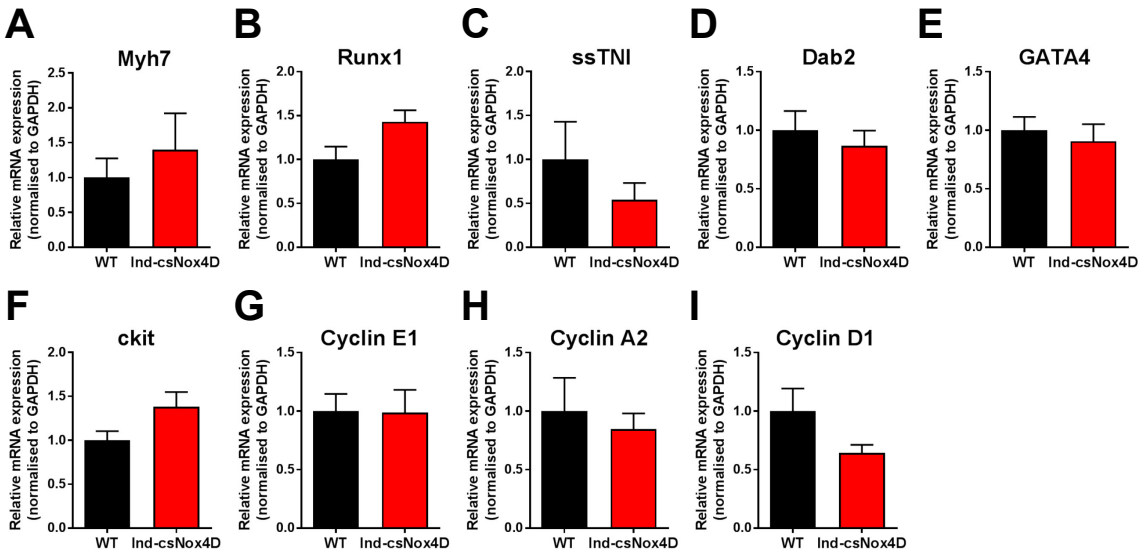

Figure 3.11. Nox4D overexpression in the adult heart does not affect gene expression profiles associated with dedifferentiation or cell cycle modulation. qPCR analysis of relative mRNA expression of markers of dedifferentiation in (A) myosin heavy chain 7 (Myh7), (B) Runx1, (C) slow skeletal troponin I (ssTNI), (D) Dab2, (E) GATA4, (F) ckit and markers of proliferation in (G) cyclin E1, (H) cyclin A2, and (I) cyclin D1, in hearts of WT and Ind-csNox4D mice 3 weeks after tamoxifen induction. n = 4 per group. Data represent mean ± SEM. Statistical analysis by unpaired two-tailed t-test.

3.4.5 Under baseline conditions, induction of cardiac-specific Nox4D overexpression does not provide an immediate proliferative window

Given the lack of phenotype when Ind-csNox4D transgenic hearts were assessed at 3 weeks post-tamoxifen induction, an alternative protocol was devised to determine whether the induction of cardiomyocyte-specific Nox4D overexpression would be associated with an immediate window of cardiomyocyte proliferation. To achieve this, Ind-csNox4D and WT mice were treated with tamoxifen again at 8 weeks of age, as described in *3.3.1*. Following completion of tamoxifen induction on day 5, mice were further injected with the nucleoside thymidine analogue EdU at 50 mg/kg body weight on days 5 and 8 for pulse-chase analysis on day 10. The use of EdU was preferable here due to improved tissue sample preservation and reproducibility as compared to BrdU-based assays that require a harsh DNA denaturation step prior to detection.[188,189]

Cardiomyocyte proliferation was measured by fluorescent labelling of incorporated EdU in conjunction with sarcomeric α-actinin immunostaining to mark cardiomyocytes that have newly synthesised DNA and therefore proceeded through S-phase. The number of α-actinin-positive cardiomyocytes with EdU-positive nuclei were counted per microscopic field, as described in *3.3.3*. Compared to WT hearts, although associated with a slight upward trend, the number of EdU-positive cardiomyocytes was shown to be unchanged in the hearts of Ind-csNox4D animals (Figure 3.12). This suggested no impact of Nox4D overexpression on cardiomyocyte proliferation even immediately after induction.

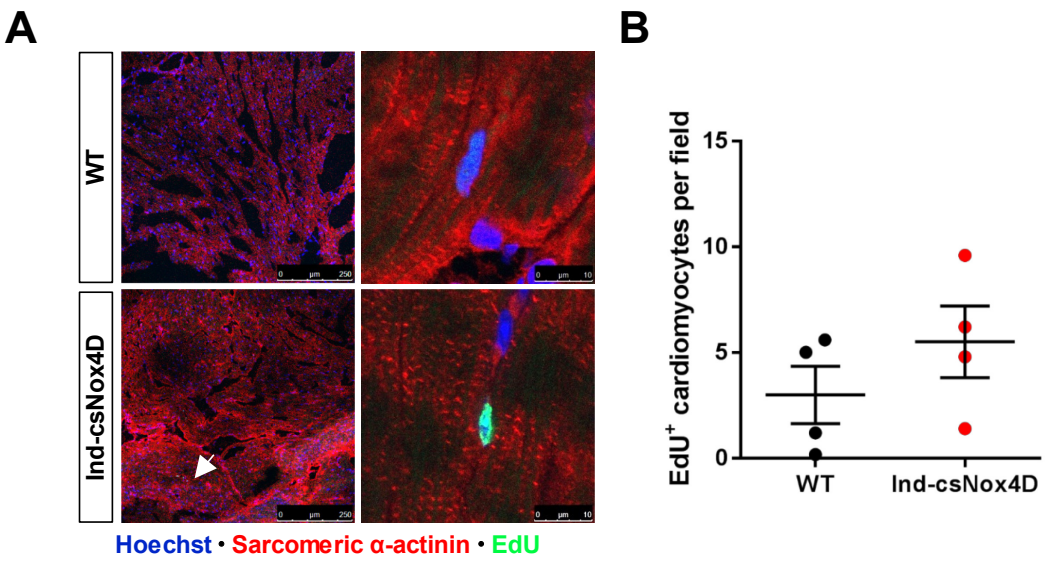

Figure 3.12. Induction of Nox4D in the adult heart is not associated with an immediate window for cardiomyocyte proliferation. To capture proliferation events, Ind-csNox4D and WT control animals were injected twice with 5-ethynyl-2'-deoxyuridine (EdU) during the 5-day period following tamoxifen induction and then harvested. (A) Representative images of immunofluorescence staining of EdU (green) incorporation, labelling cells that have synthesised DNA, with α-actinin (red) as a cardiomyocyte marker and Hoechst (blue) as a nuclear marker on cardiac cryosections of Ind-csNox4D and WT control hearts. Scale bars: 250 μm (left), 10 μm (right). White arrows and higher magnification images indicate positive cardiomyocyte nuclei, defined by co-localisation of green and blue signal in α-actinin-positive cells. (B) Quantification of the number of positive cardiomyocytes per field. Five fields of view, each of consistent cardiomyocyte count, were imaged per heart. n = 4 per group. Individual data points are shown with mean ± SEM. Statistical analysis by unpaired two-tailed t-test.

To establish whether the induction of cardiomyocyte-specific Nox4D overexpression would have an early impact on transcriptional profiles associated with cell cycle modulation, the same qPCR screen was conducted (as described in *3.3.4*) on WT and Ind-csNox4D hearts collected 5 days after tamoxifen induction.

As was observed in Ind-csNox4D hearts 3 weeks after tamoxifen induction, no changes were found in the mRNA expression levels of cell cycle activators (cyclins E1, A2 and D1), foetal contractile proteins (Myh7 and ssTNI) or other dedifferentiation markers (Runx1, Dab2, GATA4 and ckit) in Ind-csNox4D compared with WT hearts 5 days after tamoxifen induction. This was consistent with the quantification of EdU incorporation above, collectively demonstrating no difference in phenotype even at an earlier time point following induction of Nox4D overexpression.

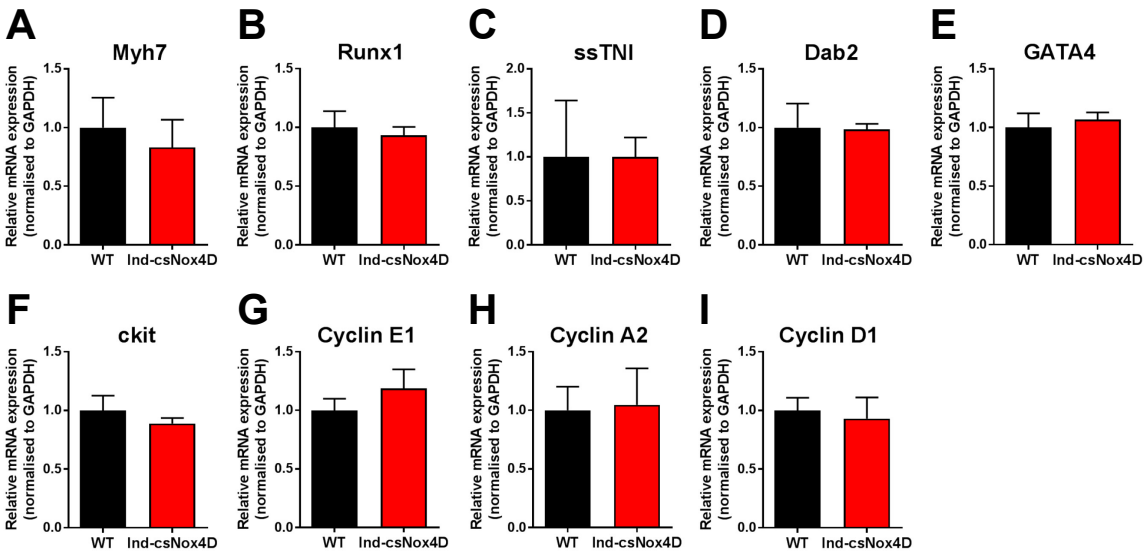

Figure 3.13. Nox4D overexpression in the adult heart does not affect transcript expression of markers of dedifferentiation or cell cycle modulation immediately after induction. qPCR analysis of relative mRNA expression of markers of dedifferentiation in (A) myosin heavy chain 7 (Myh7), (B) Runx1, (C) slow skeletal troponin I (ssTNI), (D) Dab2, (E) GATA4, (F) ckit and markers of proliferation in (G) cyclin E1, (H) cyclin A2, and (I) cyclin D1, in hearts of WT and Ind-csNox4D mice harvested 5 days after tamoxifen induction. n = 4 per group. Data represent mean ± SEM. Statistical analysis by unpaired two-tailed t-test.

3.5 Discussion

3.5.1 Generation of an inducible cardiomyocyte-specific transgenic mouse model with Nox4D overexpression

Transgenesis has repeatedly been proven as an invaluable tool in defining the function of a particular gene and its protein in vivo.[158] Therefore, to explore the functional role of Nox4D in the adult heart, we employed a gain-of-function, tissue-specific Cre/LoxP-mediated gene targeting strategy to generate an inducible transgenic mouse model of conditional cardiomyocyte-specific overexpression of Nox4D.

The first step in the baseline characterisation of this novel model was to validate the induction of Nox4D overexpression in response to tamoxifen. Adult Ind-csNox4D mice demonstrate a 10-fold upregulation in Nox4D protein level in the heart, thereby reproducibly validating the efficiency of this tamoxifen protocol to induce the translocation of Cre recombinase to the nucleus.[158,150] The overexpression of Nox4D in Ind-csNox4D hearts did not change the mRNA expression level of full-length Nox4, meaning that interpretation of its effects was not confounded by such changes.

Due to the impact of compartmentalised ROS generation and redox signalling,[154] a characteristic that we hypothesised to be important to the functional role of Nox4D in vitro is its nuclear localisation. This was previously predicted in the original identification of Nox4 splice variants, is consistent with its lack of transmembrane domain,[153] and was further characterised in our laboratory.[154] It was therefore of great interest to establish whether the subcellular localisation of endogenous and overexpressed Nox4D splice variant in cardiomyocytes would be the same in vivo, as this could be an important determinant for functional effect.

Although the immunostaining of Nox4D in vivo gave rise to some technical difficulty and required optimisation, final staining ex vivo in isolated WT and Ind-csNox4D cardiomyocytes provided a strong indication that Nox4D is localised to the nuclear and cytosolic compartments, with predominant handling within the nucleus, which is similar to that seen in vitro. To substantiate this finding, additional methods would be needed to overcome the limitations encountered with immunostaining such as cell fractionation and nuclear isolation (discussed in 6.4).

On a more global level, Ind-csNox4D hearts importantly show similar basal cardiac contractility, structure and gross morphology to WT littermates. Thus, the induction of cardiomyocyte-specific Nox4D overexpression in the adult mouse heart is well tolerated and does not appear to be associated with an obvious detrimental phenotype.

3.5.2 Impact of cardiomyocyte-targeted overexpression of Nox4D on cell cycle modulation in the adult heart

The adult mammalian heart retains a very limited regenerative potential as the majority of cardiomyocytes demonstrate permanent cell cycle exit after birth.[68,83,88] There now exist several reports of evidence to support a small capacity for pre-existing cardiomyocytes to re-enter the cell cycle in the adult heart, especially after injury such as MI.[9,86] However, any intrinsic regenerative pathways mounted by the adult heart are insufficient to achieve meaningful restoration of contractile function following pathological cardiomyocyte loss.[26,78]

In light of this, the ability to induce effective adult cardiomyocyte proliferation would represent both a novel and promising therapeutic strategy in the setting of cardiac injury.[23,26,184] The use of genetically-modified mice has formed the basis for several studies assessing the potential of specific genes and pathways to promote cardiomyocyte proliferation in normal and diseased hearts.[190] This has enabled recent findings showing that many developmental and signalling pathways are able to stimulate cell cycle re-entry in mature adult cardiomyocytes.[23]

As discussed in *1.3.4*, it is becoming increasingly recognised that cardiomyocyte cell cycle regulation may be sensitive to ROS-mediated redox signalling pathways.[191] However, this is likely a complex mechanism due to arguments that cardiomyocyte cell cycle arrest may be triggered by mitochondrial ROS-mediated oxidative stress,[79] and conversely, that cardiomyocytes residing in microenvironments of hypoxia may be responsible for cellular turnover in the adult heart (discussed in more detail in *1.2.5*).[87] As such, these studies suggest that ROS likely exert diverse functions in cell cycle modulation,[191] the effects of which are critically dependent on the cellular source, spatial regulation, and amount released.[131]

In pursuit of the above therapeutic strategy, the work described in this chapter demonstrates the impact of a novel transgenic model overexpressing a redox-active Nox4 splice variant to induce cardiomyocyte proliferation under baseline conditions.

In the absence of injury, the Ind-csNox4D transgenic heart does not appear to be associated with the promotion of cardiomyocyte proliferation 3 weeks after the induction of Nox4D overexpression. This is primarily evidenced by no change in microscopic visualisation of markers of the cell cycle – Ki67 and pHH3. Ki67 is a nuclear protein and is commonly used in studies as a marker of cell cycle progression, highlighting all active phases of the cell cycle.[192] As such, Ki67 is usually considered less specific and should not be used definitively.[43,81] Histone H3 phosphorylation at serine 10 is also a commonly used marker for cell cycle activity, more specifically detected in late G2/early mitosis.[193]

Although commonly used markers, what is highly important to note are the investigative challenges associated with assessment of cardiomyocyte proliferation by microscopy. These include the obscurity of identification of cardiomyocyte nuclei due to the heterogeneity and dense spatial packaging of cardiomyocytes with neighbouring non-myocytes in the myocardium.[25,40] Furthermore, cardiomyocytes can exhibit non-proliferative cell cycles by increasing their DNA content via polyploidisation and polynucleation without actually dividing.[194–196] Therefore, the utilisation of such methodology reinforces the need for very careful analysis with the awareness that the detection of some markers alone does not provide conclusive proof of bona fide cardiomyocyte proliferation but rather an indication of proliferative potential.

The baseline phenotype of the Ind-csNox4D heart was therefore investigated by additional methods for determination of activation of redox signalling and transcriptional regulators of cardiomyocyte cell cycling. Akt is involved in the regulation of cell cycle progression amongst other processes including cell death and migration.[197] The phosphorylation state of Akt is susceptible to redox modulation and may be differentially regulated by specific thiol oxidations of cysteine residues within the activation loop or the N-terminal pleckstrin homology (PH) domain,[132,183] or indirectly by oxidation of phosphatases.[151,198]

Such post-translational modifications are able to modulate the nuclear translocation of activated Akt,[183] the importance of such localisation was previously highlighted by a study in which cardiac-specific nuclear-targeted Akt was associated with increased cardiomyocyte cycling.[124] Given that the nucleus is known to contain several phosphatases,[199,200] we hypothesised that nuclear-localised Nox4D was associated with enhanced Akt kinase activation in vitro via redox-mediated inhibition of specific nuclear-localised phosphatases. In contrast, this effect did not appear to transfer from the in vitro to in vivo setting in the adult heart, as evidenced by no change in the level of phosphorylated Akt after induction of cardiac-specific Nox4D overexpression. Furthermore, as p27Kip1 is a direct downstream target of Akt, in which Akt-mediated phosphorylation of p27Kip1 impairs nuclear import of p27Kip1 and leads to its degradation,[119,121,201] we also saw no change in the levels of p27Kip1 in the Ind-csNox4D hearts, thus confirming no Akt-mediated proliferative signalling upregulation. However, it is worth remembering that the proportion of cycling cardiomyocytes would likely be small, and so there may have been Akt activation in small percentage of cardiomyocytes, but was difficult to detect in whole multicellular myocardial samples.

Another element that is becoming increasingly recognised for its role in cardiomyocyte regeneration is the process of dedifferentiation. This argues that mature adult cardiomyocytes can re-enter the cell cycle and divide through a 3-step process of

dedifferentiation, proliferation, and redifferentiation,[202] and was demonstrated by a coculture system with neonatal cardiomyocytes in which cytokinesis of adult cardiomyocytes was preceded by dedifferentiation.[202] It is thought that the cellular morphological rearrangement and gain in plasticity associated with cardiomyocyte dedifferentiation is what allows cardiomyocytes to become permissive to cell cycle re-entry.[187] This is accompanied by an upregulation in genes typically expressed in embryonic and foetal hearts. Transcript markers re-expressed in dedifferentiated cardiomyocytes therefore include early transcription factors such as GATA4, foetal contractile proteins such as Myh7 and ssTnI, and also genes usually restricted to stem cells, including ckit, Runx1 and Dab2.[162,187]

In light of this, we conducted a baseline screen for transcript markers of dedifferentiation and proliferation (cyclins E1, A2 and D1), but in agreement with our other findings, these proved to be unchanged. Alternatively, as stated above, it is also possible there were transcriptional changes in a minor subset of cardiomyocytes, but detection using whole myocardium was insufficiently sensitive.

Given the lack of baseline phenotype when assessed 3 weeks after tamoxifen induction, we reassessed Ind-csNox4D hearts for an immediate window of cardiomyocyte proliferation by EdU pulse-chase analysis. The labelled thymidine analogue EdU is also commonly used to detect proliferating cells as it is stably incorporated into newly synthesised DNA during DNA replication.[81] However, as with the above described problems associated with the use of antibodies raised against markers of the cell cycle, EdU incorporation does not exclusively identify cardiomyocytes that will divide due to non-proliferative cell cycles and incorporation during other cellular processes such as DNA repair.[43,195]

We identified that induction of Nox4D overexpression is not associated with an immediate window of cardiomyocyte proliferation due to only small changes in EdU incorporation, suggesting that Ind-csNox4D confers little or no enhancement in proliferative potential. Likewise, Nox4D overexpression in the adult heart neither seems to affect gene expression patterns associated with cell cycle modulation during this period.

Attempts to directly induce cardiomyocyte proliferation in the adult heart by temporal and spatial regulation of specific genetic pathways have been demonstrated by several studies, including cardiomyocyte-specific modification of Hippo/YAP,[114,119] microRNAs,[100,203] developmental transcription factors,[162] and ERBB2 receptor signalling.[204] Such inducible expression systems activating, for example, YAP[114] and the co-receptor ERBB2,[204] in the adult mammalian heart have been able to stimulate

cardiomyocyte proliferation in the absence of myocardial injury. However, in the case of ERBB2, this was observed in conjunction with pathological changes characterised by cardiac hypertrophy.[204] Collectively, these studies demonstrate the ability to enhance basal cardiomyocyte proliferation, but also the need for tight regulatory control.

Here we show that induction of cardiomyocyte-targeted overexpression of Nox4D in adult mice does not translate to enhanced proliferative potential in the absence of injury. This was unexpected given the contrasting effects we previously observed in vitro using neonatal cardiomyocytes, despite being able to reproduce the nuclear localisation in vivo. Thus, the lack of translation of effect from in vitro to in vivo is likely multifactorial. The cardiomyocyte cell type studied represents a major difference as neonatal myocytes are already more proliferative in nature due to their developmental immaturity,[40,205] whereas the adult myocyte may not be permissive to this redox-mediated pathway. The level of transgene expression can be difficult to control in vivo and as such could also influence the therapeutic effect. Lastly, it could be postulated that the impact of cardiac-specific Nox4D overexpression could become apparent in the setting of pathological stress, as this could provide the stimulus necessary for cardiomyocyte dedifferentiation and proliferation.[187] This will be addressed in the next chapter.

Chapter 4 The impact of inducible cardiomyocyte-specific Nox4D overexpression on recovery after myocardial infarction

4.1 Introduction

Myocardial infarction is a prevalent major cardiovascular event and leading cause of mortality and morbidity.[206] Owing to the insufficiency of cardiomyocyte self-renewal, the adult mammalian heart cannot compensate for the massive loss of functional cardiomyocytes caused by MI, resulting instead in compromised myocardial function and heart failure.[10,11,18]

Small animal models of myocardial ischaemia and infarction are important tools in cardiovascular research. Despite obvious differences in organ size and heart rate, with some dissimilarities in cardiac haemodynamics and electrophysiology, overall the mouse heart is considered to resemble the human heart sufficiently well in terms of anatomy and physiology.[207] Moreover, it has been demonstrated that adult mice show many of the clinical and haemodynamic features of heart failure seen in humans.[208] Combined with the wide applicability of gene targeting to the mouse, these experimental models have enabled extensive study on the consequences of genetic manipulation on molecular pathways underlying the ischaemic tolerance of the myocardium.[207,209] This aims to provide better mechanistic insight into the processes involved in cardiac repair and regeneration, with eventual translatability to the clinical setting for the prevention or treatment of heart failure.[18,210]

4.1.1 The pathophysiology of permanent coronary artery ligation

The mouse model of permanent ligation of the LAD coronary artery reliably induces infarctions involving the anterolateral, posterior, and apical regions of the heart, and is utilised to investigate cardiac function and long-term left ventricular (LV) remodelling post-myocardial infarction. This model fundamentally differs from models of transient ligation, in which the initial extent of the infarct is susceptible to modulation by factors that affect myocardial salvage upon reperfusion.[211,212] In contrast, at 24 hours post-MI by permanent ligation, the infarct area becomes fixed due to the absence of reperfusion, such that the entire area-at-risk (AAR) is infarcted. This scenario translates to patients with acute ST segment elevation MI who are unable to receive timely or successful reperfusion therapy due to contraindications or delay.[213,214] Cardiac function in this model is therefore subject to infarct expansion and healing, and the concomitant development of remodelling processes including LV hypertrophy and chamber dilatation.[210,211]

Myocardial ischaemia occurs when the coronary blood flow to the myocardium is reduced, and leads to infarction when the duration is prolonged, causing profound electric, metabolic, functional, and structural consequences within the myocardium.[215] Coronary occlusion causes immediate cessation of mitochondrial oxidative phosphorylation, forcing cardiomyocytes to switch to alternative ATP-generating

pathways including mobilisation from creatine phosphate[17] and anaerobic glycolysis.[216] The latter pathway results in a rapid increase in the levels of lactate in the ischaemic myocardium, leading to the onset of intracellular acidosis.[17] Cumulatively, these mechanisms impact on the activity of contractile proteins as their function is depressed by inorganic phosphate derived from the metabolism of creatine phosphate,[217] and decreased calcium binding secondary to acidosis.[218] Thus, the rapid exhaustion of ATP stores and accumulation of metabolites caused by these energetic shifts manifest functionally as a severe deterioration in systolic contractility. Compared to humans, this may occur at a much faster rate in experimental small animal models, as contractile force is quickly suppressed within the first minute of the onset of ischaemia.[17]

The metabolic effects described above cause further detriment to the ischaemic cardiomyocyte with marked perturbations in cellular ionic balance. Potassium efflux is increased whereas intracellular sodium and calcium are increased due to inhibition of ion channels by acidosis, collectively leading to excitation contraction uncoupling and increased susceptibility to ventricular arrhythmia.[219,220] The resultant increased osmotic load eventually leads to irreversible changes in ultrastructural cardiomyocyte features including striking distortion of mitochondrial architecture and sarcolemmal blebbing.[17,221,222] Deranged metabolism, sustained intracellular calcium overload, and oxidative stress collectively lead to advanced cardiomyocyte injury associated with progressive membrane damage, culminating in physical disruption of the sarcolemma and cardiomyocyte necrosis in the infarct environment.[220,222]

Prolonged ischaemia causes irreversible death in an increasing number of cardiomyocytes. This paradigm describes a wavefront of cardiomyocyte death due to the heterogeneity of the myocardial response to ischaemia, extending in order of susceptibility from the subendocardium to the subepicardium as the duration of the ischaemic insult increases.[17] Cardiomyocyte necrosis triggers an intense inflammatory reaction via the release of damage-associated molecular patterns (DAMPs), mediating leukocyte infiltration of the myocardial infarct that serves to clear dead cells and matrix debris, and initiate a reparative response.[223,224]

4.1.2 Assessment of myocardial infarct size

Despite standardisation of the permanent ligation protocol by maintenance of the consistency of the anatomical site at which the ligature is positioned, the model remains prone to variability in infarct size.[210,225] This is considered one of the model's principal limitations, and is reflective of the variability in the coronary circulation.[226] The differences in the branching pattern of the murine LAD together with its supplied myocardial vascular territories prevent complete reproducibility of the AAR and thus the consistency of cardiac damage.[207,227] Therefore, measurement of LV infarct size post-permanent

ligation is crucially important as it provides confirmation of the success of the surgical MI, and enables comparability of initial infarct injury across experimental groups for assessment of remodelling differences at later stages. If AAR is standardised, any differences observed in LV geometry and function are therefore independent of acute cardiomyocyte injury and are reflective of differences in recovery.[210]

Several techniques are available for the determination of myocardial infarct size, including late gadolinium-enhanced magnetic resonance imaging, histological staining, and plasma sampling.[226] In animal studies, triphenyltetrazolium chloride (TTC) staining is considered the gold standard technique for demarcation of the fractions of viable and non-viable tissue zones, and is used by many laboratories.[207,228–230] However, the major limiting factor associated with this technique is that it is an end-point evaluation, precluding long-term analysis of LV function and remodelling.[207]

The measurement of biomarkers by plasma sampling represents another index of cardiac injury. Due to their high specificity and sensitivity, cardiac troponins, particularly the I and T isoforms, are well-evaluated clinical biomarkers for the diagnosis and prognosis of myocardial injury.[231,232] Most troponin is localised within the 3-unit complex of the myofibrillar contractile apparatus, consisting of troponin I, T, and C. There is only one isoform of cardiac troponin I (cTnI) expressed in the myocardium, which is also-tissue-specific. This has allowed the generation of highly specific monoclonal antibodies that do not exhibit cross-reactivity with other non-cardiac isoforms.[233] Using these antibody-based assays, cardiac troponin I release from the injured myocardium is detectable early post-MI, the magnitude of elevation of which serves as a predictor of the extent of myocardial necrosis.[226] Furthermore, the prognostic value of cTnI release has also been demonstrated in small mouse models of permanent LAD ligation, showing a rapid rise in plasma levels following ligation and a peak between 24 and 48 hours, with significant correlation to histological infarct size and cardiac function. Thus, cTnI is also a valuable biomarker for the confirmation of MI and prediction of infarct size in small animal models.[226,234]

4.1.3 Postinfarction left ventricular adverse remodelling

The adult mammalian heart responds to the acute loss of myocardium induced by severe ischaemic damage through formation of a scar.[17] This refers to the unique pattern of remodelling events, involving the infarct zone, the encircling border zone of viable myocytes, and the remote non-infarcted zone, that are triggered in response to the abrupt increase in loading conditions caused by MI.[235] The interplay between all 3 integrated components of the myocardium, namely the cardiomyocytes, ECM, and capillary microvasculature, has important multifactorial roles in the postinfarction remodelling process.[236,237] This describes specific changes in the structure, size and

shape of the left ventricle, culminating in significant alteration of chamber architecture, which profoundly impacts on cardiac function and the development of heart failure.[238]

The loss of myocardial tissue post-MI causes an immediate decrease in ejection fraction.[210] During the early phase of remodelling, infarct expansion results from the degradation of the interstitial matrix and cardiomyocyte slippage through activation of matrix metalloproteinases (MMPs) released from neutrophils.[239] This promotes disproportionate LV wall thinning and chamber dilatation, which effectuates an increase in LVEDV. This alters the Frank-Starling relation in the infarct border zone and remote myocardium, and may preserve stroke volume by augmenting shortening in non-infarcted LV segments and therefore the pressure developed during systole.[240] Neurohormonal mechanisms are also invoked in response to disturbances in vascular haemodynamics, which yield transient functional compensation in the immediate phase post-MI. This is mediated by increased sympathetic nerve activation and catecholamine synthesis, leading to enhanced activation of the renin-angiotensin-aldosterone system and increased systemic vascular resistance.[235] In conjunction with myocardial stretch, these pathways also trigger the transcription and release of atrial and brain natriuretic peptides (ANP and BNP), which modulate activation of the renin-angiotensin-aldosterone system, normalise ventricular filling and improve pump function.[235,241] Elevations in the synthesis of ANP and BNP consequently function as molecular markers of remodelling or failure.[242]

However, the increased LVEDV induced by infarct expansion also concomitantly leads to an elevation of diastolic and systolic wall stress, which acts as a powerful stimulus for regional hypertrophy of the non-infarcted segment.[235] Increased wall stress triggers a complex network of intracellular signalling cascades, which initiate increased synthesis of contractile units through neurohormonal agonist-mediated activation of cell membrane receptors by angiotensin II, catecholamines, and endothelin,[243,244] as well as activation of mechanoreceptors. Cardiomyocyte hypertrophy, demonstrated by a significant increase in cell volume, develops to establish a more even distribution of the increased wall stresses. This represents another adaptive remodelling response that initially stabilises contractile function by offsetting increased load and attenuating further dilatation.[238]

As the remodelling phenotype progresses, the postinfarction heart becomes characterised by hallmark changes in global LV geometry.[241] Cardiomyocytes in viable remodelling segments may undergo apoptosis second to inflammatory signalling and biomechanical stress.[245] Due to chamber dilatation, remodelling post-MI is primarily a state of volume-overload and thus leads to myocyte lengthening and eccentric hypertrophy. Major targets of hypertrophic intracellular signalling pathways are

transcriptional regulators that drive the reinduction of a gene expression programme comparable to that seen during foetal development.[246] Myocyte enhancer factor 2 (MEF2),[247] nuclear factor of activated T cells (NFAT),[247] GATA4,[248] and myocardin[249] are transcription factors that have all been shown to be centrally involved both in early cardiac development and in the hypertrophic response to cardiac stress. Importantly, this complex response is subject to careful control through integration of other pathways that limit pro-hypertrophic signalling, such as those mediated by nitric oxide and natriuretic peptides.[242]

During infarct healing, the initial inflammatory phase is superseded by the proliferative phase, associated with suppression of pro-inflammatory pathways and infiltration and proliferation of interstitial fibroblasts.[17] Growth factor release and neurohormonal signalling stimulate the phenotypic transformation of fibroblasts into myofibroblasts, characterised by upregulated expression of contractile stress fibres and α-smooth muscle actin.[17,250] Activated myofibroblasts critically serve to enrich the ECM by deposition of matricellular proteins and initiate tissue repair by collagen synthesis.[235,251] Collagens type I and III are predominantly deposited in the infarct zone, and also in the remote zone if potentiated by extensive myocyte death.[235] Formation of a structural network of matrix proteins in the infarct region transitions into the maturation phase of infarct healing, signified by strengthening of fibrillar collagen by cross-linking and reduction of cellular content.[17,252] Stabilisation of the wound is aided by important maturation of the infarct vasculature.[253] The resultant fibrous tissue forms a scar that has been shown to replace the loss of myocytes by 4 weeks after MI.[254]

Postinfarction remodelling therefore does not only involve the cellular and molecular events associated with infarct healing, but is also intertwined with alterations including hypertrophy and fibrosis in the non-infarcted myocardial segments. Experimental models of MI have shown that the severity of these alterations is largely dependent on the size of the infarct.[17] Although initially adaptive, the events of ventricular remodelling collectively lead to progressive contractile dysfunction, increased incidence of arrhythmia, and increased mortality.[242] Compared to less severe models of myocardial infarction, permanent ligation typically yields accentuated dilated remodelling and exacerbated contractile dysfunction.[210] Cardiomyocyte replacement with a noncontractile scar may maintain the structural integrity of the ventricle and prevent rupture,[17] but also increases myocardial stiffness, resulting in a loss of elasticity and impairment in diastolic filling.[255] Failure to normalise increased wall stresses due to chronic volume-overload results in progressive chamber dilatation and a further increase in cardiac workload.[238] Thus, it is may be more appropriate to consider the sequence of processes involved in

postinfarction healing and repair as maladaptive remodelling that fails to compensate for the loss of essential cardiomyocytes.[242]

In light of this, it is extremely clear that the adult mammalian heart is unable to mount a substantial renewal response to counteract the increased demand imposed by infarctive injury.[18] Although current therapies have significantly improved prognosis, the burden of heart failure post-MI remains high.[256] Therapeutic harnessing of the mechanisms that influence regeneration is a visionary goal in the cardiovascular research field and is under extensive investigation through the use of preclinical animal models of myocardial infarction.[21] The proliferative potential of inducible Nox4D in the adult heart remains to be established in this setting.

4.2 Aims

The primary aim of this chapter is to investigate the impact of inducible cardiomyocyte-specific Nox4D overexpression on functional recovery post permanent ligation of the left anterior descending coronary artery. The effects on long-term ventricular remodelling will also be examined, with a specific focus on the ability of Nox4D to enhance the proliferative capacity of the myocardium after ischaemic injury. Regional effects will be determined by differentiation of the infarct, border, and remote non-infarcted zones.

4.3 Summary of methods

The impact of the Ind-csNox4D Tg model in the setting of pathological stress was investigated by induction of MI by permanent LAD coronary artery ligation. Female adult WT and Ind-csNox4D mice were administered tamoxifen at 8 weeks of age (section 2.3), then randomised to undergo MI or sham ligation at 10 – 12 weeks of age, followed by plasma sampling at 24 hours post-surgery for measurement of cTnI for quantification of myocardial injury (section 2.4 & 2.12). Echocardiography was performed at baseline, within 1 week of surgery, then at 1, 2, and 4 weeks post-surgery for assessment of global and regional cardiac contractile function by strain analysis (section 2.5). Cardiac tissues were harvested after 4 weeks (section 2.7) for regional infarct zone analysis of cell cycle markers and postinfarction remodelling processes at the cellular and transcript levels by several staining methods (section 2.11) and qPCR (section 2.9), respectively (Figure 2.5).

A separate cohort of animals was also used for assessment of EdU incorporation post-MI. As above, tamoxifen-treated adult WT and Ind-csNox4D Tg mice were subjected to MI or sham surgery, and harvested after 2 weeks during which a total of 4 doses of EdU were administered (Figure 2.7). EdU labelling was detected by fluorescence staining in conjunction with immunohistochemistry (sections *2.11.2* & *2.11.3*).

For investigation of the potential negative effects of nuclear-localised ROS generation, a tamoxifen dose response experiment was performed. Male and female adult Ind-csNox4D were injected with tamoxifen, but randomised to receive one of the following doses: 5 mg/kg, 10 mg/kg, 15 mg/kg, or 20 mg/kg, and harvested after 2 weeks (as described in section 2.3). Cardiac tissues were analysed by HPLC for quantification of ROS generation (section 2.13), and immunohistochemistry for assessment of DDR signalling.

4.4 Results

4.4.1 Induction of cardiomyocyte-targeted Nox4D overexpression elicits a differential temporal functional response post-myocardial infarction

To investigate the impact of inducible Nox4D overexpression in the adult heart on the functional response to myocardial ischaemic injury, female Ind-csNox4D transgenic mice and WT littermate controls were treated with tamoxifen at 8 weeks of age, then subjected to either MI by permanent LAD coronary artery ligation or sham ligation at 10 – 12 weeks of age. To assess functional recovery post-MI, animals were serially monitored by advanced ultrasound cardiac imaging and analysed by myocardial using strain once at baseline, within 1 week prior to surgery, and then at 1, 2, and 4 weeks after injury, at which point animals were sacrificed.

Baseline echocardiography in tamoxifen-treated animals prior to MI further confirmed the absence of abnormality in systolic function or structure secondary to the induction of cardiac-specific Nox4D overexpression, as demonstrated by no change compared to WT hearts in ejection fraction, LVEDV, LVESV, global longitudinal strain (GLS, as a more advanced index of systolic function), or end-diastolic left ventricular mass (LVM) (Figure 4.1) .

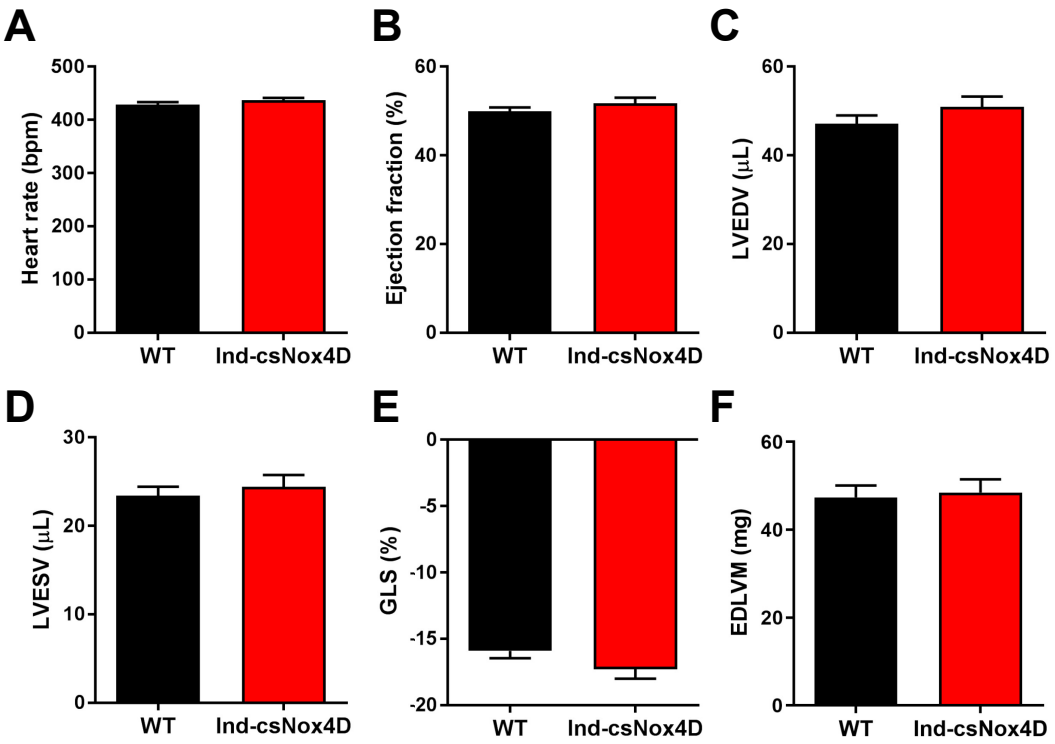

Figure 4.1. Systolic function is unchanged in Inducible cardiomyocyte-specific Nox4D animals prior to myocardial infarction. Baseline strain analysis, within 1 week prior to myocardial infarction or sham surgery, of B-mode parasternal long axis echocardiographic images of WT and Ind-csNox4D hearts within same range of heart rate (A) for measurement of ejection fraction (B), left ventricular end-diastolic volume (LVEDV) (C), left ventricular end-systolic volume (LVESV) (D), global longitudinal strain (GLS) (E), and left ventricular mass (LVM) (F). n = 20 (WT), 21 (Ind-csNox4D). Data represent mean ± SEM. Statistical analysis by unpaired two-tailed t-test.

To reliably assess the functional response of the Ind-csNox4D model compared to WT after MI, it was crucially important to employ a readout that permitted quantification of the initial injury. This was achieved by measurement of plasma cTnI at 24 hours post-MI as a biomarker for myocardial injury. There was no difference in the 24-hour release of cTnI in Ind-csNox4D mice compared to WT controls, suggesting no difference in the acute response to myocardial ischaemia (Figure 4.2). All sham ligation mice yielded cTnI measurements lower than or equal to the lowest sensitivity of the assay standard curve.

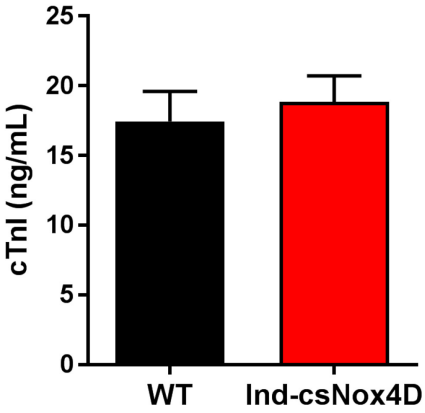

Figure 4.2. Cardiac troponin I release 24 hours post-myocardial infarction estimates similar myocardial injury in Inducible cardiomyocyte-specific Nox4D mice. ELISA-based detection of plasma cardiac troponin I (cTnI) 24 hours post-myocardial infarction as a biomarker for cardiac injury. The concentration of cTnI is unchanged in Ind-csNox4D relative to WT mice. n = 15 (WT), 16 (Ind-csNox4D). Data represent mean ± SEM. Statistical analysis by unpaired two-tailed t-test.

As mentioned above, 2D echocardiographic imaging was analysed by myocardial strain before and after MI for advanced assessment of traditional left ventricle (LV) functional parameters as well as global longitudinal strain (GLS). Representative analysis of an infarcted LV is shown in Figure 4.3, the accuracy of which relies on careful tracing of the endocardial and epicardial borders.

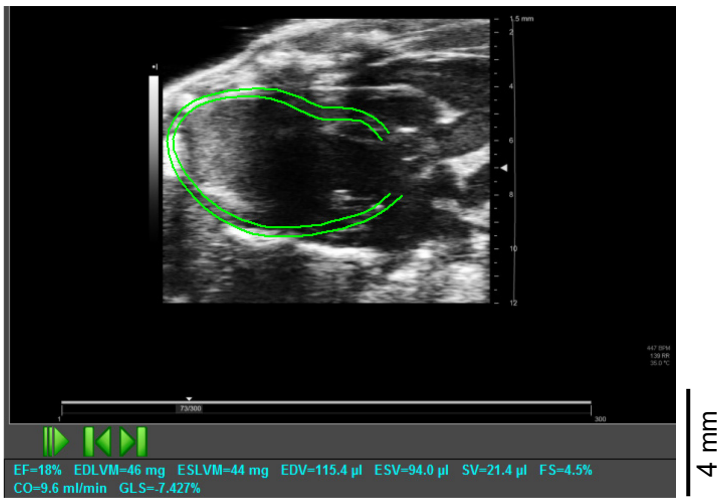

Figure 4.3. Analysis of cardiac contractility by Vevo Strain Software. Representative strain analysis of an infarcted heart in B-mode parasternal long axis view by Vevo® Strain technology. Left ventricular tracing (green) outlines endocardial border (inner) and epicardial border (outer) over two cardiac cycles for advanced assessment of traditional LV functional parameters and global deformation by strain (cyan).

To overcome the experimental variability associated with the permanent LAD ligation MI model and subsequent difficulty in interpretation of functional response, all functional readouts post-MI were individually plotted relative to the initial ischaemic injury as quantified by 24-hour cTnI.

At 2 weeks post-MI, LV function was initially assessed using volume-dependent parameters. Generally, ejection fraction and LVESV tended to deteriorate with increasing 24-hour cTnI as a consequence of the severity of the MI, whilst LVEDV and LVM remained more stable. Interestingly, for any given cTnI, Ind-csNox4D animals demonstrated a better functional response compared to WT animals in terms of ejection fraction, as shown by a statistical difference between the intercept of the regression lines. No significant difference between genotypes was observed for similar analyses of LVEDV and LVESV. Additionally, there was no difference in LVM, which, together with the lack of trend against increasing cTnI, suggests minimal development of LV hypertrophy at this time point (Figure 4.4).

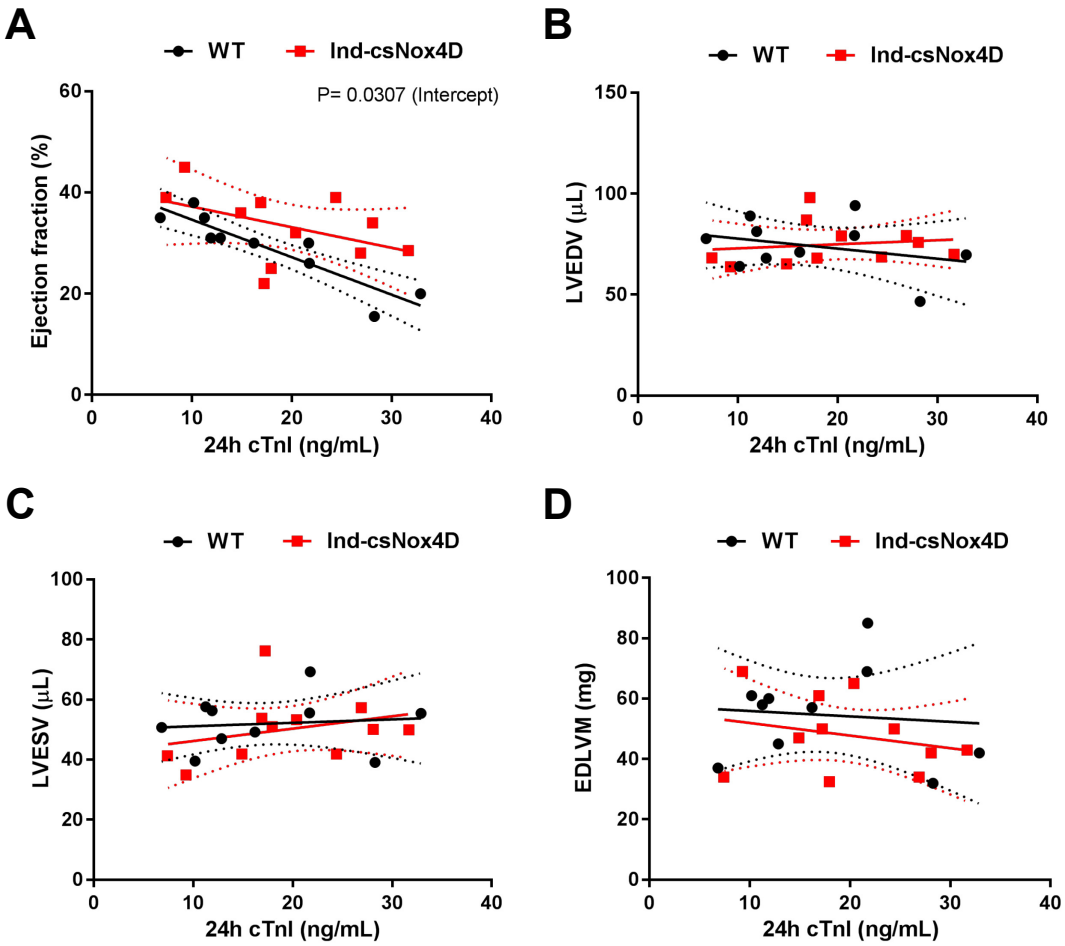

Figure 4.4. Cardiomyocyte-specific Nox4D overexpression in adult mice demonstrates functional improvement 2 weeks after myocardial infarction. Strain analysis of echocardiographic images of WT and Ind-csNox4D hearts 2 weeks after myocardial infarction by permanent left anterior descending coronary artery ligation for measurement of volume-based parameters relative to 24h cardiac troponin I (cTnI) - ejection fraction (A), left ventricular end-diastolic volume (LVEDV) (B), left ventricular end-systolic volume (LVESV) (C), and left ventricular mass (LVM) (D). n = 10 (WT), 11 (Ind-csNox4D). Individual data points are shown. Statistical analysis by linear regression, represented by regression lines (solid lines) with 95% confidence intervals (dotted lines), with comparison of the lines by slope and y-intercept.

We next assessed the response of the mice at 2 weeks post-MI in terms of GLS as a well-evaluated, volume-independent indicator of LV contractility. Strain is a measurement of deformation that refers to the change in length of the myocardium within a certain direction relative to its baseline length, and is calculated by speckle tracking algorithms that follow the motion of specific myocardial patterns. GLS reflects the shortening of the LV wall in a longitudinal direction, and is therefore negative in value. Compared to traditional parameters such as ejection fraction, GLS is considered a more sensitive measure of intrinsic cardiac systolic function.[257,258]

Whereas WT animals showed an increase in GLS in conjunction with increasing cTnI, denoting worsening LV function as the GLS becomes more positive, this was improved in Ind-csNox4D animals as the data points lay in a separate population at higher cTnI, resulting in a significant difference between the slopes of the regression lines (Figure 4.5). This suggested that cardiac-specific Nox4D overexpression was associated with better preservation of systolic function with worsening MI.

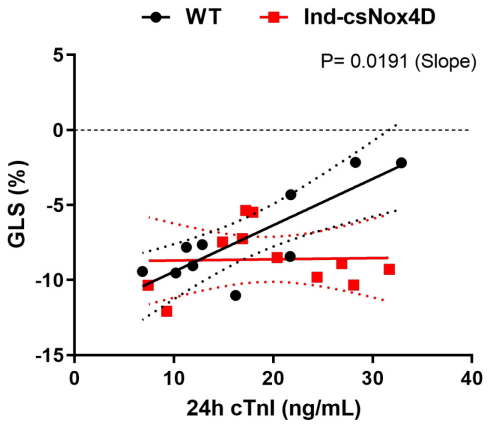

Figure 4.5. Induction of cardiomyocyte-specific Nox4D overexpression limits deterioration in global longitudinal strain 2 weeks after myocardial infarction. Strain analysis of echocardiographic images of WT and Ind-csNox4D hearts 2 weeks after myocardial infarction for assessment of global longitudinal strain (GLS) relative to 24h cardiac troponin I (cTnI), as an advanced measure of systolic function. n = 10 (WT), 11 (Ind-csNox4D). Individual data points are shown. Statistical analysis by linear regression, represented by regression lines (solid lines) with 95% confidence intervals (dotted lines), with comparison of the lines by slope and y-intercept.

Whereas GLS is a global indicator of function, derived from the average across all LV segments, speckle tracking echocardiography is also an ideal tool to measure regional contractile function.[258] Therefore, to investigate the effects of induced cardiac-specific Nox4D overexpression on the pattern of GLS observed at 2 weeks post-MI in further detail, myocardial strain was analysed regionally to permit understanding of LV function relative to zone. This was done using the segmental analysis component of the Vevo® Strain software, which calculates the relative strain in 6 regions of the LV, including the base, mid and apex of both the anterior and posterior surfaces of the chamber (Figure 4.6A). This is particularly pertinent as MI is a regional form of cardiac injury, and so these strain segments translate to the infarct zones created by MI, notably remote (base), border/remote (mid), and infarct (apex) (Figure 4.6B). Thus, regional strain analysis permits in depth measurement of zone-specific LV function relative to the MI.

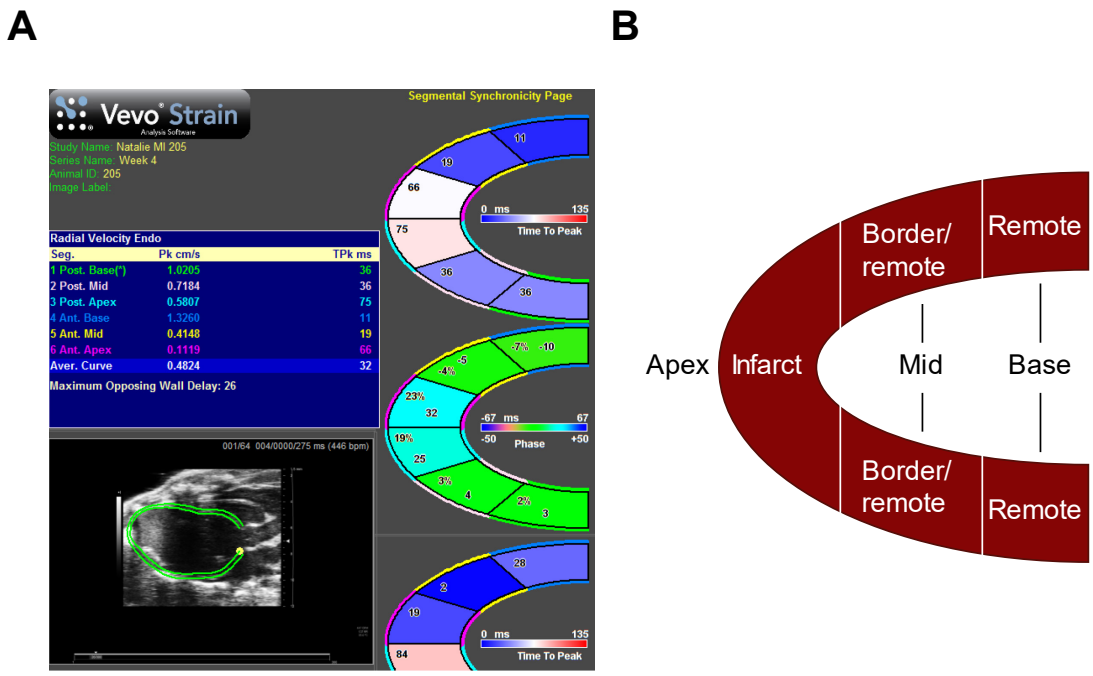

Figure 4.6. Segmental strain analysis of regional cardiac contractility by Vevo Strain Software. (A) Representative Segmental Synchronicity analysis of an infarcted heart in B-mode parasternal long axis view by Vevo® Strain technology. Parameters including strain and strain rate are measured in each left ventricular zone: posterior base, posterior mid, posterior apex, anterior base, anterior mid, and anterior apex. (B) Schematic representation of the left ventricle in long axis view after myocardial infarction. Regional zones are depicted: remote zone (anterior base and posterior base), border zone and remote zone (anterior mid and posterior mid), and infarct zone (anterior apex and posterior apex).

As well as longitudinal, segmental strain analysis also examines the regional radial strain, which describes the thickening of myocardial tissue in a transverse direction, and, as such, is positive in value. It is important to note that whilst strain describes the absolute deformation, strain rate is an additional readout that describes the rate at which the deformation occurs.[257,258] We therefore assessed the longitudinal and radial strain rate within each defined LV segment of Ind-csNox4D compared to WT hearts to establish potential differences in the contractile properties of the myocardial tissue.

The mean data describing the longitudinal strain rate and the radial strain rate in each Ind-csNox4D and WT LV region is shown in Figure 4.7A and B, respectively. As expected, this confirmed the decline in LV function on a zone-dependent level as shown by a relative deterioration in both directions of strain rate from the base to the apex, equating to the remote zone versus the infarct zone. This was particularly demonstrated by the longitudinal strain rate, which remained significantly greater in the anterior base compared to the anterior apex in WT as well as Ind-csNox4D hearts. Interestingly, both the longitudinal and radial strain rate demonstrated an overall trend for enhanced

contractility in each LV segment of Ind-csNox4D compared to WT control hearts, which was in agreement with the enhanced GLS in Ind-csNox4D hearts at this time point (Figure 4.5).

The regional functional effects of MI were next analysed relative to 24-hour cTnI. The anterior mid segment of the LV was first chosen, as any proliferative mechanisms involved in functional recovery might be expected to be preferentially localised to the border zone.[162] However, this showed little difference in longitudinal and radial strain rate between Ind-csNox4D and WT animals relative to 24-hour cTnI (Figure 4.7C and D). Equally, there was little difference between the same comparison within the anterior base region (Figure 4.7E and F).

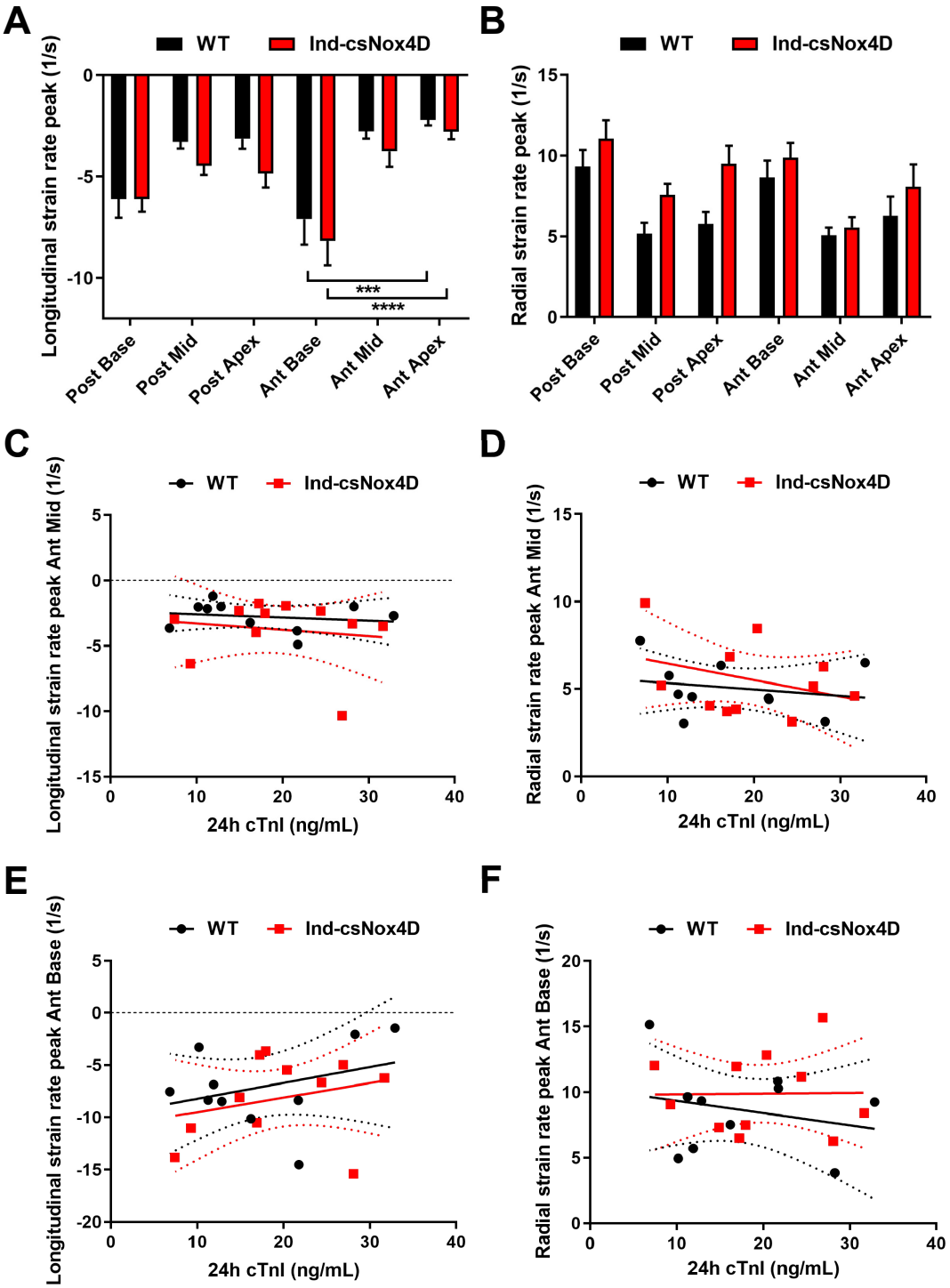

Figure 4.7. Inducible cardiomyocyte-specific Nox4D mice show similar strain rates in specific left ventricular segments 2 weeks after myocardial infarction. Segmental strain analysis of echocardiographic images of WT and Ind-csNox4D hearts 2 weeks after myocardial infarction for assessment of longitudinal strain rate (A) and radial strain rate (B) in 6 regional zones of the left ventricle: posterior base (post base), posterior mid (post mid), posterior apex (post apex), anterior base (ant base), anterior mid (ant mid), and anterior apex (ant apex). n = 10 (WT), 11 (Ind-csNox4D). Data represent mean ± SEM. ***P<0.001, ****P<0.0001 by two-way ANOVA with Bonferroni's post hoc correction. Further assessment of strain rate relative to 24h cardiac troponin I (cTnI) in anterior mid zone in (C) longitudinal and (D) radial, and in anterior

base zone in (E) longitudinal and (F) radial. n = 10 (WT), 11 (Ind-csNox4D). Individual data points are shown. Statistical analysis by linear regression, represented by regression lines (solid lines) with 95% confidence intervals (dotted lines), with comparison of the lines by slope and y-intercept.

At 4 weeks post-MI, 2D echocardiographic image assessment of LV function demonstrated the classical physical features of decline secondary to MI, characterised by LV dilatation and apical dyskinesis due to extensive scarring and wall thinning (Figure 4.8A). Compared to 2 weeks post-MI, all volume-dependent parameters as well as LVM showed more progressive decline with a greater relationship to increasing 24-hour cTnI and therefore MI severity. The structure and function observed in the echocardiographic images were mirrored in the analyses, showing that by 4 weeks, cardiac-specific Nox4D overexpression was insufficient to maintain the functional improvement seen at 2 weeks, suggesting a transient response. Despite a slight trend for some of the Ind-csNox4D animals to demonstrate better ejection fraction, for a given cTnI this was largely unchanged. Accordingly, the same pattern was also observed for LVEDV (suggesting minor or no attenuation of LV chamber dilatation), LVESV, and LVM (suggesting minimal attenuation of LV hypertrophy) (Figure 4.8B – E). Animal survival was also monitored over the 28-day experimental period, in which the only case of death post-MI occurred in the Ind-csNox4D group (1 case in total 17), and no death occurred in either sham group.

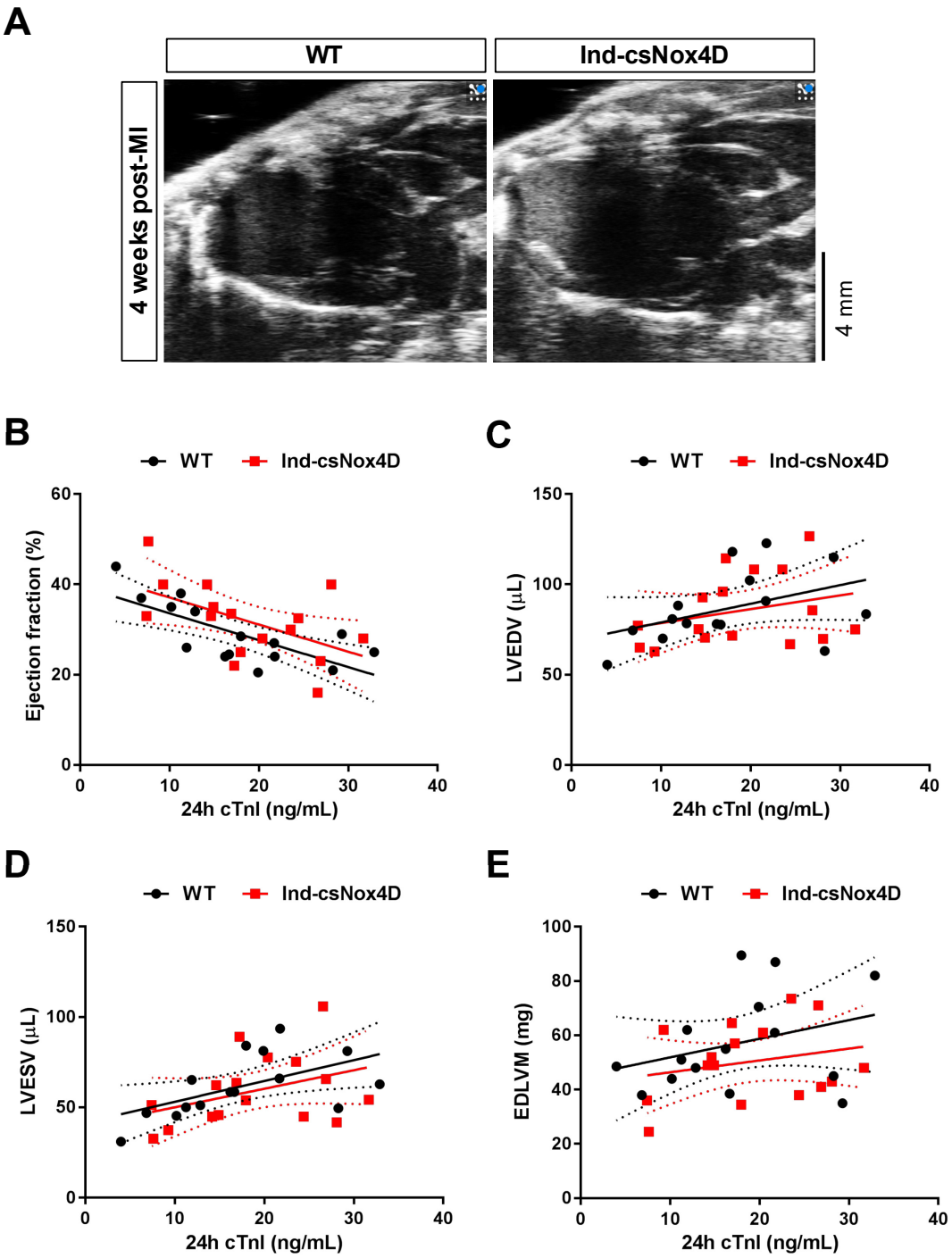

Figure 4.8. Cardiac-specific Nox4D overexpression does not sustain improvement in volume-dependent functional parameters 4 weeks after myocardial infarction. (A) Representative B-mode parasternal long axis echocardiographic images of WT and Ind-csNox4D hearts 4 weeks after myocardial infarction. Scale bar: 4 mm. Quantification of function by strain analysis of volume-based parameters relative to 24h cardiac troponin I (cTnI) – ejection fraction (B) left ventricular end-diastolic volume (LVEDV) (C), left ventricular end-systolic volume (LVESV) (D), and left ventricular mass (LVM) (E). n = 15 (WT), 16 (Ind-csNox4D). Individual data points are shown. Statistical analysis by linear regression, represented by regression lines (solid lines) with 95% confidence intervals (dotted lines), with comparison of the lines by slope and y-intercept.

The potential temporal functional effects elicited by induction of cardiomyocyte-specific Nox4D overexpression in the adult heart were further demonstrated globally by longitudinal strain. Unlike the distinct improvement in GLS seen in Ind-csNox4D compared to WT mice at 2 weeks, at 4 weeks the trend for improved GLS in Ind-csNox4D animals was much smaller. Although a small subset of Ind-csNox4D animals were able to retain better GLS, several were comparable to the WT animals relative to the same initial injury, which was therefore insufficient to achieve significant functional recovery (Figure 4.9A). Furthermore, the functional response of the Ind-csNox4D model to MI in terms of mean GLS, without normalisation to 24-hour cTnI, was also analysed by time-course in comparison to WT control, for assessment of overall significance. This showed that by 4 weeks post-MI, both WT and IndcsNox4D animals demonstrated significant decline in GLS relative to respective baseline control. No differences were found in GLS between WT and IndcsNox4D animals at any of the time points examined. Taken together, this suggests that whilst Ind-csNox4D animals may confer a functional benefit at 2 weeks post-MI when analysed relative to initial myocardial injury, this benefit is not maintained at 4 weeks, and, in light of the mean data, indicates that any functional benefit detected would be unlikely to lead to a clinically meaningful result (Figure 4.9B).

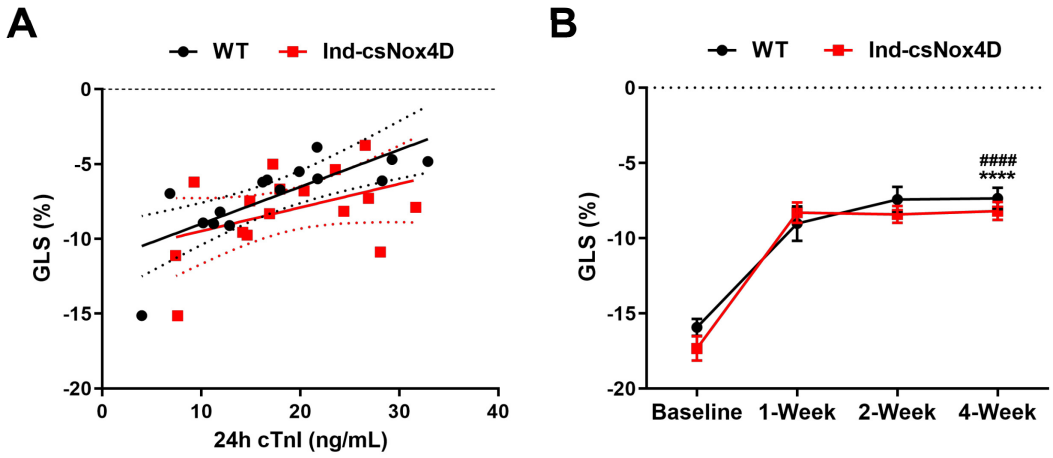

Figure 4.9. Induction of cardiomyocyte-specific Nox4D overexpression does not prevent deterioration in global longitudinal strain 4 weeks after myocardial infarction. (A) Strain analysis of echocardiographic images of WT and Ind-csNox4D hearts 4 weeks after myocardial infarction for assessment of global longitudinal strain (GLS) relative to 24h cardiac troponin I (cTnI). n = 15 (WT), 16 (Ind-csNox4D). Individual data points are shown. Statistical analysis by linear regression, represented by regression lines (solid lines) with 95% confidence intervals (dotted lines), with comparison of the lines by slope and y-intercept. (B) Strain analysis of echocardiographic images of WT and Ind-csNox4D hearts for assessment of mean GLS, without normalisation to 24h cTnI, at baseline, and 1 week, 2 weeks, and 4 weeks after myocardial infarction. n = 12 – 17 (WT), 13 – 19 (Ind-csNox4D). Data represent mean ± SEM. ****P<0.0001:

WT Baseline versus 4-Week; ####*P*<0.0001: Ind-csNox4D Baseline versus 4-Week by two-way ANOVA with Bonferroni's post hoc correction.

The strain rate at 4 weeks post-MI was also evaluated on a regional level by segmental analysis. Interestingly, in Ind-csNox4D hearts this again identified clear zone-specific differences between the anterior base and the anterior apex in both directions of strain rate, as well as in WT hearts between the posterior base and the posterior apex by longitudinal strain rate. However, the longitudinal strain rate of the anterior base of WT hearts had also declined to a comparable level to that of the anterior apex, meaning that the longitudinal strain rate of the anterior base of Ind-csNox4D hearts remained significantly better than the anterior base of WT hearts (Figure 4.10A and B).

Analysis of the regional functional differences relative to 24-hour cTnI showed little difference in both the longitudinal and radial strain rate of the anterior mid segment between WT and Ind-csNox4D hearts (Figure 4.10C and D). However, in agreement with the mean data, the longitudinal strain rate of the anterior base was improved in several Ind-csNox4D animals, resulting in a statistical difference between the intercept of the regression lines. Additionally, this region-specific result was further evidenced by a significant difference between groups in the radial strain rate, thus overall suggesting enhanced regional contractile properties in hearts overexpressing cardiac-targeted Nox4D (Figure 4.10E and F).

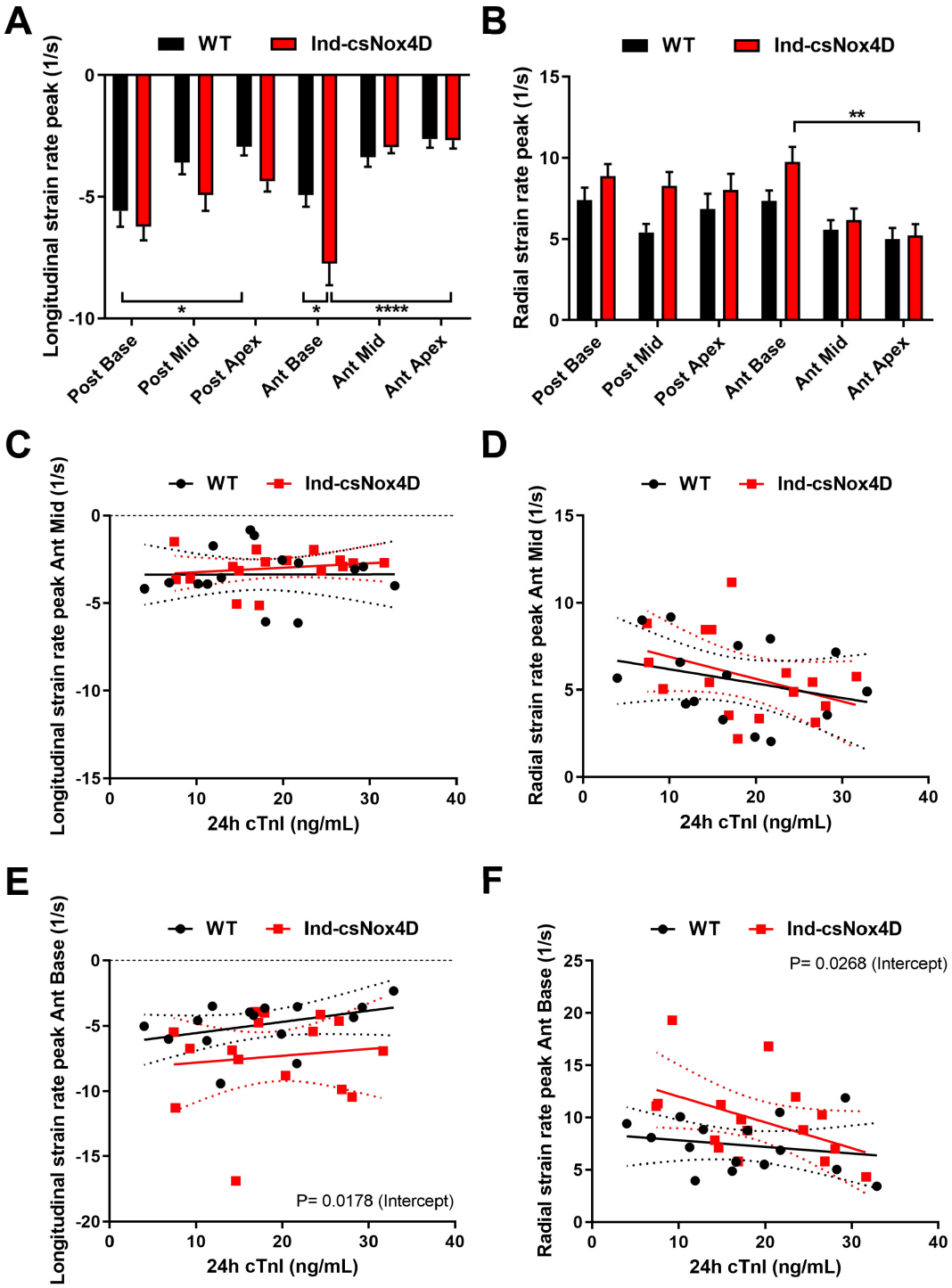

Figure 4.10. Inducible cardiomyocyte-specific Nox4D mice show regional improvement in strain rate 4 weeks after myocardial infarction. Segmental strain analysis of echocardiographic images of WT and Ind-csNox4D hearts 4 weeks after myocardial infarction for assessment of longitudinal strain rate (A) and radial strain rate (B) in 6 regional zones of the left ventricle: posterior base (post base), posterior mid (post mid), posterior apex (post apex), anterior base (ant base), anterior mid (ant mid), and anterior apex (ant apex). n = 15 (WT), 16 (Ind-csNox4D). Data represent mean ± SEM. **P*<0.05, ***P*<0.01, *****P*<0.0001 by two-way ANOVA with Bonferroni's post hoc correction. Further assessment of strain rate relative to 24h cardiac troponin I (cTnI) in anterior mid zone in (C) longitudinal and (D) radial, and in anterior base zone

in (E) longitudinal and (F) radial. n = 15 (WT), 16 (Ind-csNox4D). Individual data points are shown. Statistical analysis by linear regression, represented by regression lines (solid lines) with 95% confidence intervals (dotted lines), with comparison of the lines by slope and y-intercept.

To control for the induction of MI by permanent LAD ligation, a smaller group of WT and Ind-csNox4D animals were subjected to sham ligation and monitored functionally over the same 28-day period. At 4-weeks post-sham, echocardiographic imaging showed no LV structural abnormalities (Figure 4.11A). Images were analysed by the same technique as described for animals subjected to MI, demonstrating no decline in cardiac function in Ind-csNox4D compared to WT animals from baseline to 4 weeks post-sham, shown by no change in ejection fraction, LVEDV, LVESV, or LVM (Figure 4.11B – E).

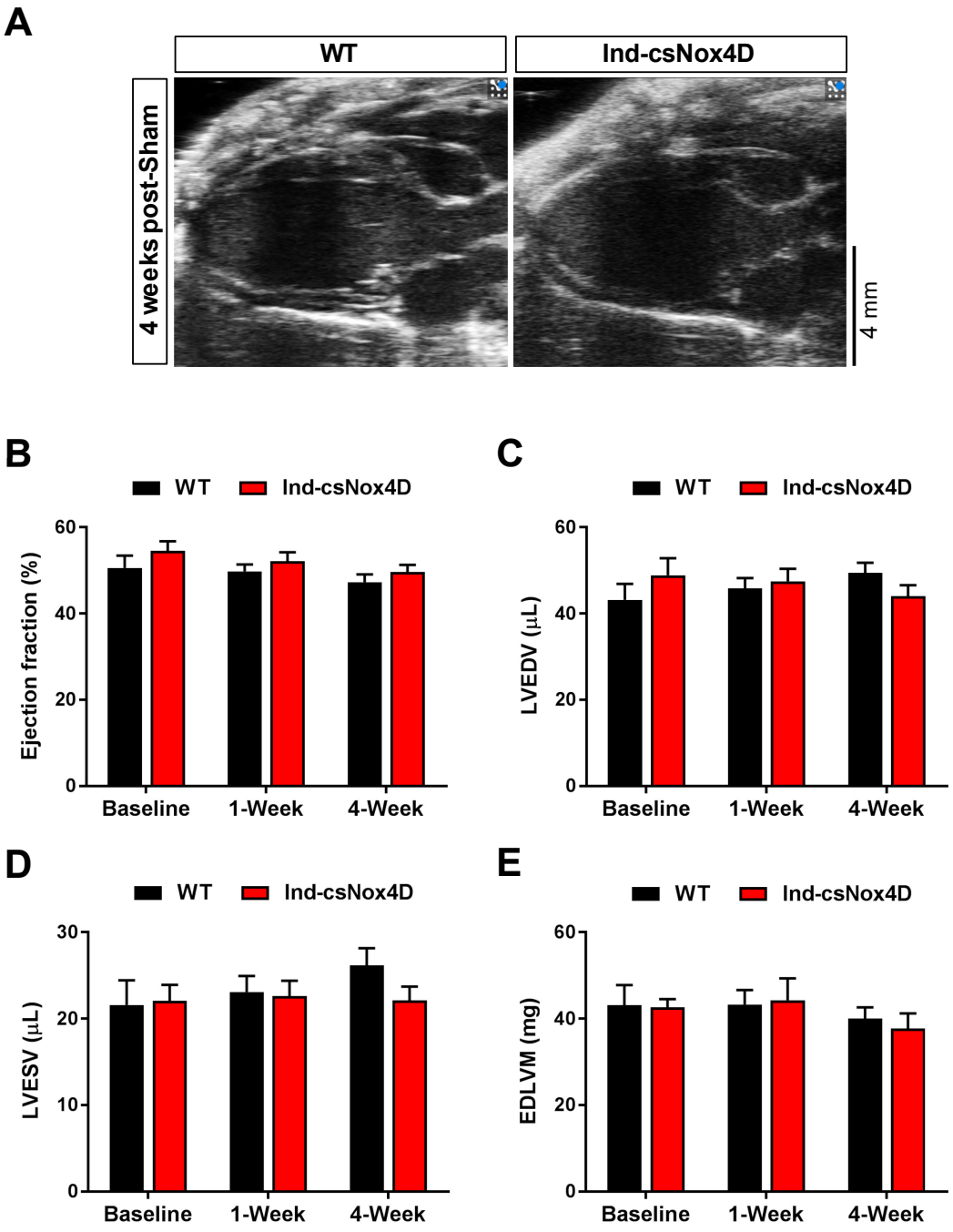

Figure 4.11. Inducible cardiomyocyte-specific Nox4D mice subjected to sham myocardial infarction show no change in cardiac structure and function 4 weeks after surgery. (A) Representative B-mode parasternal long axis echocardiographic images of WT and Ind-csNox4D hearts 4 weeks after sham myocardial infarction control surgery. Scale bar: 4 mm. Echocardiographic images analysed by strain for measurement of volume-based parameters – ejection fraction (B) left ventricular end-diastolic volume (LVEDV) (C), left ventricular end-systolic volume (LVESV) (D), and left ventricular mass (LVM) (E). n = 7 per group. Data represent mean ± SEM. Statistical analysis by two-way ANOVA with Bonferroni's post hoc correction.

4.4.2 *The localised protective effects of cardiac-specific Nox4D overexpression are insufficient to fully limit postinfarction remodelling processes*

WT and Ind-csNox4D hearts were harvested 4 weeks post-MI or sham ligation for analysis of cellular and molecular processes involved in adverse cardiac remodelling. As expected, post-mortem morphometric analysis showed that MI induced a significant increase in heart weight to body weight ratio in both WT and Ind-csNox4D mice compared with sham. However, this was not rescued by Nox4D overexpression as there was no change between genotypes after MI (Figure 4.12).

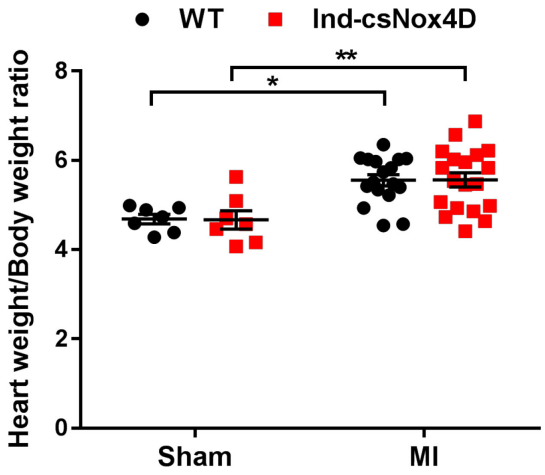

Figure 4.12. Cardiomyocyte-targeted Nox4D overexpression induced in adult mice does not protect against myocardial infarction-induced changes in cardiac morphology. Heart weight to body weight ratio measured 4 weeks after sham or myocardial infarction (MI) is significantly increased in both WT and Ind-csNox4D transgenic mice but not rescued in Ind-csNox4D mice. Sham; n = 7 per group, MI; n = 17 (WT), 19 (Ind-csNox4D). Individual data points are shown with mean ± SEM. *P<0.05, **P<0.01 by two-way ANOVA with Bonferroni's post hoc correction.

Similarly, this was further evidenced at transcript level where molecular markers of heart failure – ANP, BNP, and Myh7 – were raised in the infarct border zone and, to a lesser degree, the infarct remote zone of WT hearts relative to sham. Despite a trend for the expression of these markers to be reduced in Ind-csNox4D hearts after MI, this did not prove to be significant. The expression of myosin heavy chain 6 (Myh6) can be expected to decrease in the context of failure due to a shift in expression of the Myh7 isoform; this was largely unchanged in the WT hearts relative to sham, but may have demonstrated a decrease in Ind-csNox4D hearts (Figure 4.13).

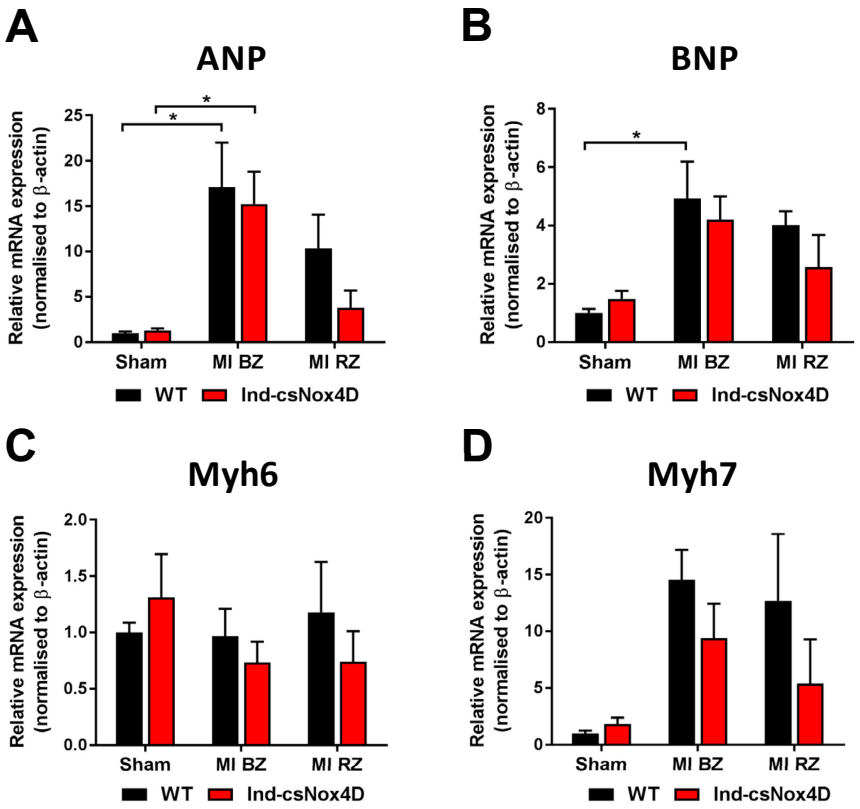

Figure 4.13. Cardiac-specific Nox4D overexpression does not prevent increased transcript expression of markers of hypertrophy 4 weeks after myocardial infarction. Regional zone qPCR analysis of relative mRNA expression of markers of hypertrophy 4 weeks after myocardial infarction (MI), in the infarct border zone (BZ), infarct remote zone (RZ), and sham control in (A) atrial natriuretic peptide (ANP), (B) brain natriuretic peptide (BNP), (C) myosin heavy chain 6 (Myh6), and (D) myosin heavy chain 7 (Myh7), in hearts of WT and Ind-csNox4D mice. n = 6 per group. Data represent mean ± SEM. *P<0.05 by two-way ANOVA with Bonferroni's post hoc correction.

The capacity for induced Nox4D overexpression to mediate protective effects in the adult heart after ischaemic injury was further measured histochemically by the development of fibrosis as another hallmark pathological feature of adverse remodelling. The total content of collagen, predominantly the fibrillar types I and III, deposited in cardiac tissues was visualised by picrosirius red and quantified as an indicator of fibrosis coverage.[259] This confirmed a significant increase in fibrosis after MI, the greatest proportion of which was localised to the site of the scar. Interestingly, the development of fibrosis was unchanged between WT and Ind-csNox4D hearts after sham, but was significantly reduced in Ind-csNox4D hearts after MI (Figure 4.14A and B). Furthermore, picrosirius red staining can also function as an indicator of the structure of the collagen network due to the birefringent properties of mature collagen, the cross-linked fibres of which can be detected using polarised light.[259] In agreement with total fibrosis coverage, Ind-csNox4D hearts also revealed a reduction in the fraction of cross-linked deposited collagen, although non-significant (Figure 4.14A and C).

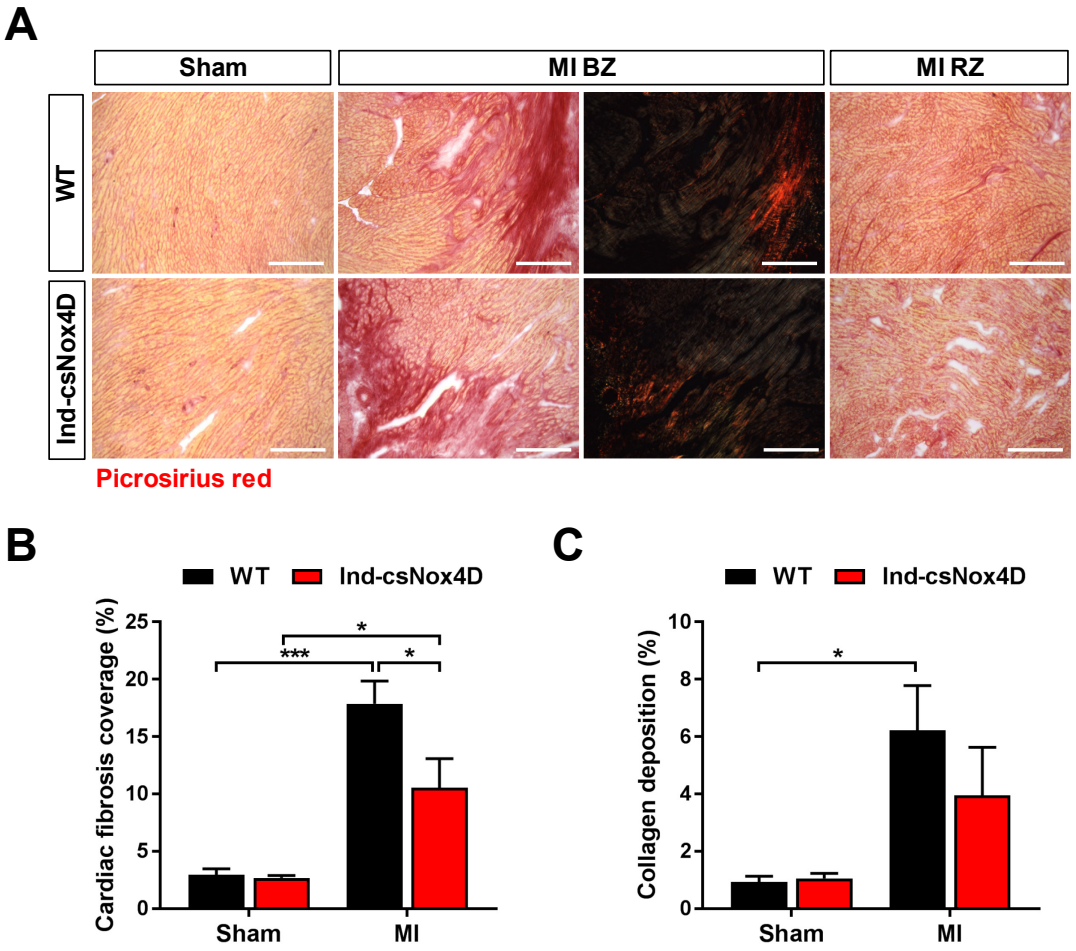

Figure 4.14. Cardiomyocyte-specific Nox4D overexpression induced in adult mice results in reduced fibrosis coverage 4 weeks after ischaemic injury. (A) Representative images of picrosirius red staining by standard light microscopy for analysis of fibrosis (dark red) on equivalent cardiac apical cryosections of WT and Ind-csNox4D hearts harvested 4 weeks after myocardial infarction (MI) or sham surgery. Muscle fibres and cytoplasm stain yellow. Staining is shown in the sham left ventricle, MI border zone (BZ) – same field also under polarised light, and MI remote zone (RZ). Scale bars: 250 μm. Quantification as a % of the whole cross-section of (A) total cardiac fibrosis coverage and (B) total collagen deposition as assessed by yellow/orange birefringence under polarised light. n = 4 per group. Data represent mean ± SEM. **P*<0.05, ****P*<0.001 by two-way ANOVA with Bonferroni's post hoc correction.

The hypertrophic response of Ind-csNox4D compared to WT cardiomyocytes was further analysed at the cellular level by WGA staining, which binds to the glycoproteins of cell membranes. MI induced a significant increase in cardiomyocyte cross-sectional area in both the infarct border zone and remote zone of WT hearts compared to WT sham controls. This was increased to a lesser degree in Ind-csNox4D hearts, although there was no statistical difference compared to WT hearts after MI (Figure 4.15). Moreover, staining of endothelial cells by isolectin B4 revealed a significant reduction in capillary density in the border zone of infarcted WT hearts compared to WT sham hearts. Similar to the trend observed in cardiomyocyte hypertrophy, infarcted Ind-csNox4D hearts demonstrated a smaller decrease in capillary density relative to Ind-csNox4D sham controls, however this was insufficient to fully rescue the response observed after MI in WT animals (Figure 4.16).

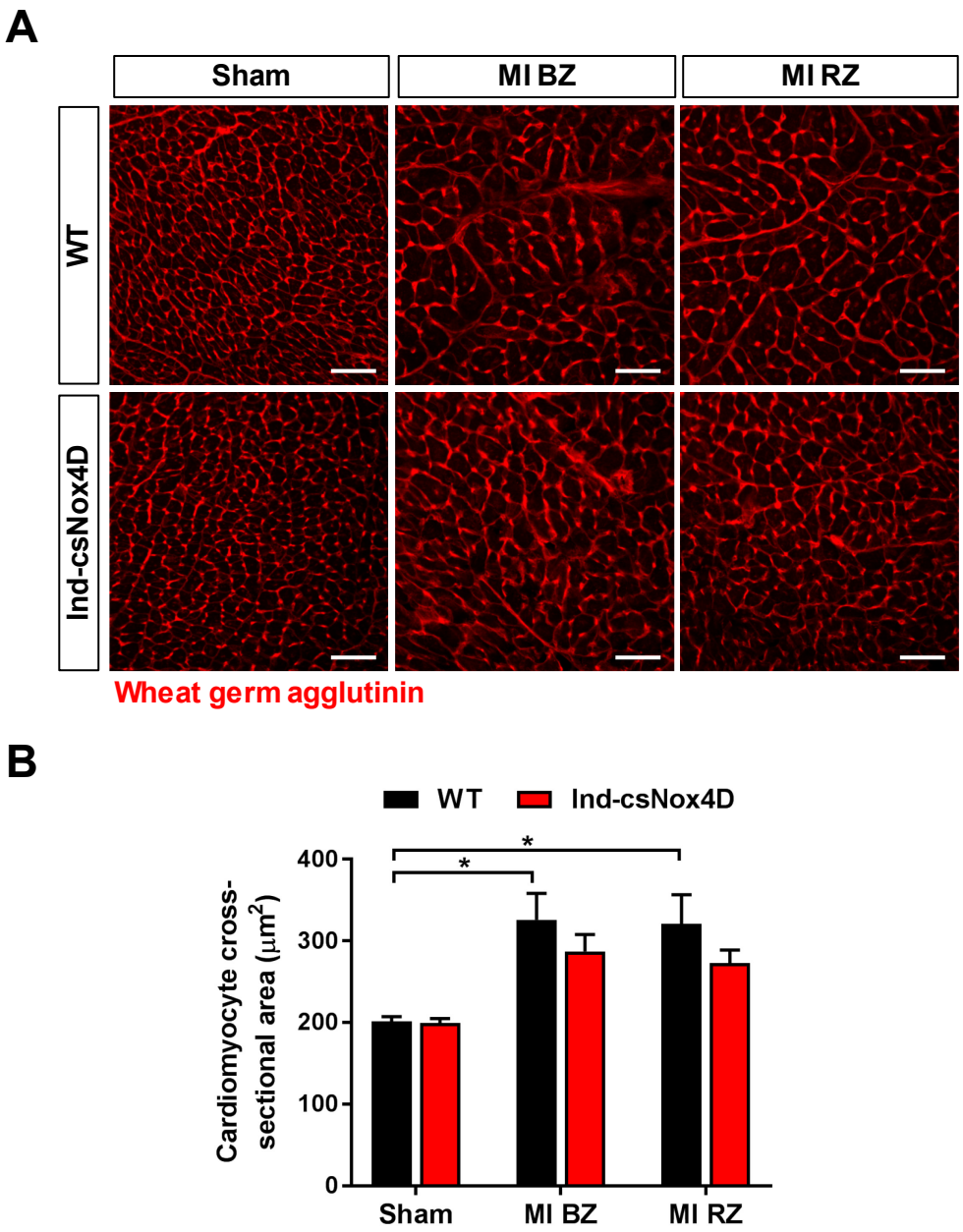

Figure 4.15. Inducible cardiomyocyte-specific Nox4D mice show equivalent cardiac hypertrophy 4 weeks after myocardial infarction. (A) Representative images of fluorescence staining of wheat germ agglutinin (WGA) (red) for visualisation of cell membranes on cardiac cryosections of WT and Ind-csNox4D hearts harvested 4 weeks after myocardial infarction (MI) or sham surgery. Staining is shown in the sham left ventricle, MI border zone (BZ), and MI remote zone (RZ). Scale bars: 50 μm. (B) Quantification of cardiomyocyte cross-sectional area. n = 4 per group. Data represent mean ± SEM. **P*<0.05 by two-way ANOVA with Bonferroni's post hoc correction.

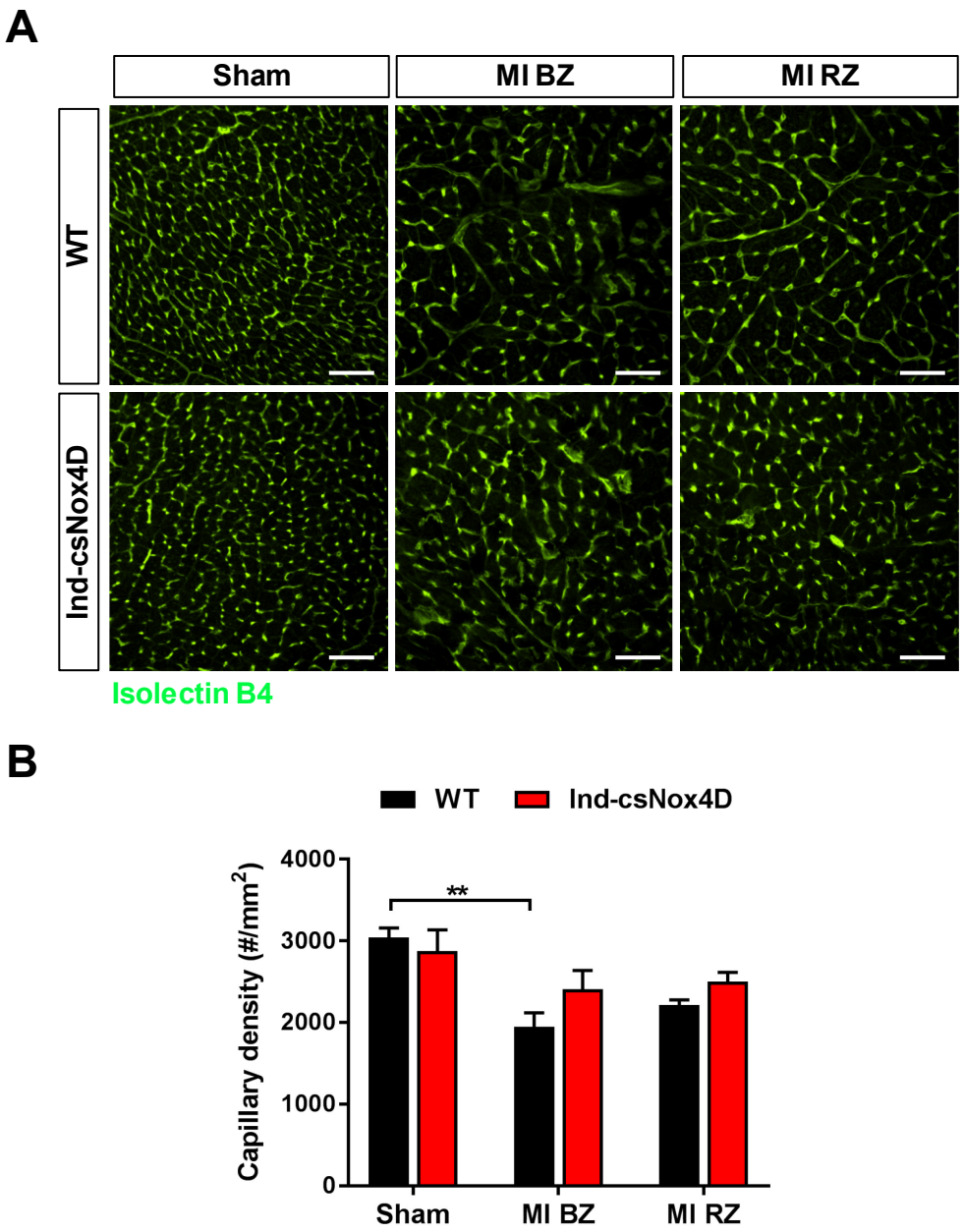

Figure 4.16. Inducible cardiomyocyte-specific Nox4D mice show equivalent cardiac capillary density 4 weeks after myocardial infarction. (A) Representative images of fluorescence staining of Isolectin B4 (green), marking endothelial cells, on cardiac cryosections of WT and Ind-csNox4D hearts harvested 4 weeks after myocardial infarction (MI) or sham surgery. Staining is shown in the sham left ventricle, MI border zone (BZ), and MI remote zone (RZ). Scale bars: 50 μm. (B) Quantification of capillary density. n = 4 per group. Data represent mean ± SEM. ***P*<0.01 by two-way ANOVA with Bonferroni's post hoc correction.

Apoptotic cardiomyocyte cell death was measured 4 weeks post-MI and sham by TUNEL assay. This technique utilises enzymatic in situ detection of DNA fragmentation, which represents a hallmark characteristic of apoptosis.[166] MI demonstrated the presence of positive TUNEL staining in both cardiomyocytes and non-cardiomyocytes. MI was associated with a trend showing an increase in the number of TUNEL-positive, α-actinin-positive cardiomyocytes observed after sham in WT control hearts. This was more elevated in the border zone of WT infarcted hearts compared to the remote zone. The number of apoptotic cardiomyocytes in Ind-csNox4D hearts also tended to increase in the border zone of infarcted hearts relative to sham. Although this remained lower compared to WT hearts after MI, this was not supported by a statistical difference (Figure 4.17).

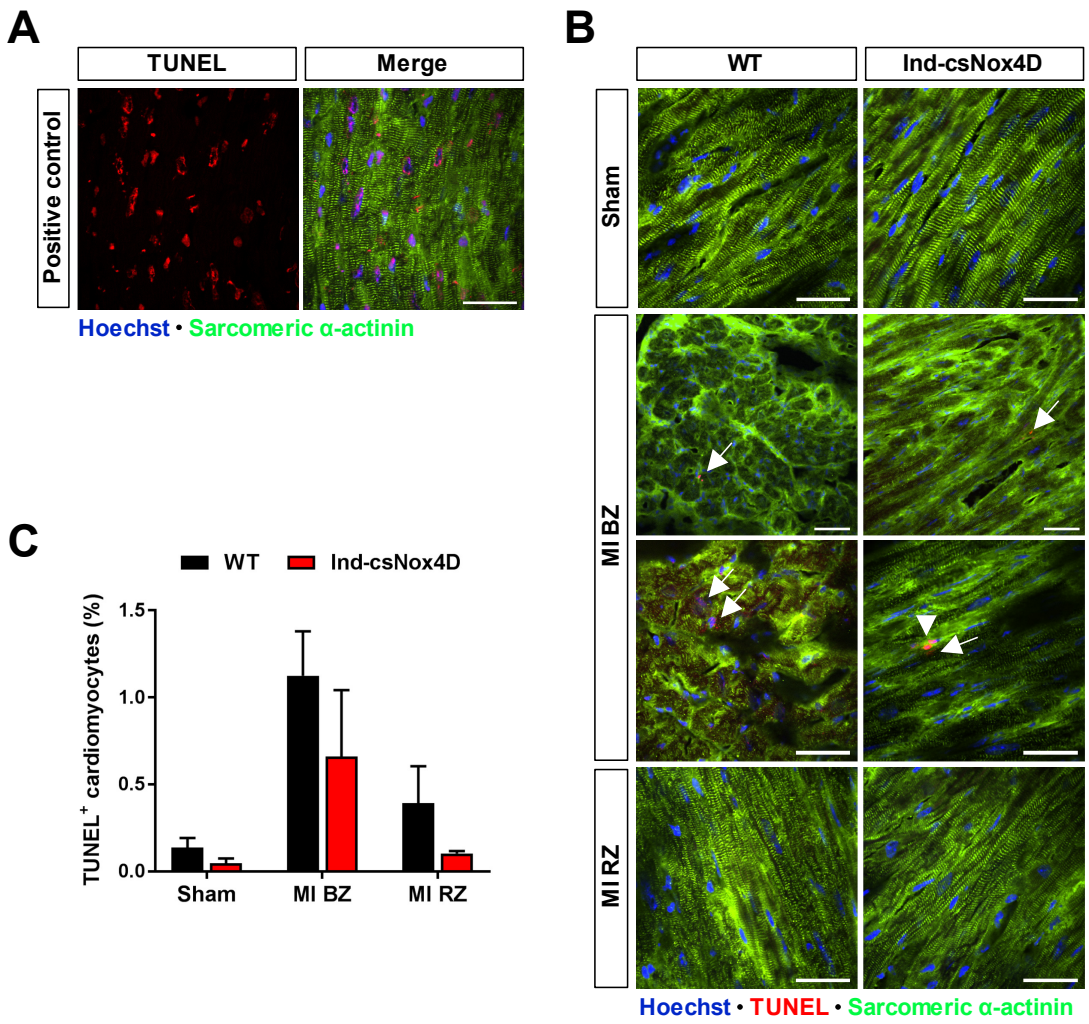

Figure 4.17. Inducible cardiomyocyte-specific Nox4D mice show trend for reduced cardiomyocyte apoptosis 4 weeks after myocardial infarction. Representative images of immunofluorescence staining for TUNEL (red), marking cells that are undergoing apoptosis, with α-actinin (green) as a cardiomyocyte marker and Hoechst (blue) as a nuclear marker on cardiac cryosections of WT and Ind-csNox4D hearts in (A) positive control with DNase treatment, and (B) 4 weeks after myocardial infarction (MI) or sham surgery. Staining is shown in the sham left ventricle, MI border zone (BZ) with lower magnification images of TUNEL-positive cells (upper) to demonstrate low frequency (arrows indicate positive cardiomyocyte nuclei, arrowheads indicate non-myocytes), and MI remote zone (RZ). Scale bars: 50 μm. (C) Quantification of the number of positive cardiomyocytes as a percentage of total number of cardiomyocytes counted in each zone. n = 4 per group. Data represent mean ± SEM. Statistical analysis by two-way ANOVA with Bonferroni's post hoc correction.

4.4.3 Cardiac-specific Nox4D overexpression does not enhance proliferative capacity in the infarct border or remote zones

To determine the impact of cardiomyocyte-specific Nox4D overexpression on cardiomyocyte proliferation in the setting of ischaemic stress, the expression of proliferation markers Ki67 and pHH3 was evaluated immunohistochemically in the border and remote zones of infarcted WT and Ind-csNox4D hearts. The cardiomyocyte identity of cells with positive nuclear expression of Ki67 or pHH3 in conjunction with positive sarcomeric α-actinin immunostaining was further verified by Z-stack confocal imaging, and quantified as a percentage of total cardiomyocytes counted in each relative zone.

Compared to sham controls, a small increase in the percent of cardiomyocytes with Ki67-positive nuclei was found in the border zones of both WT and Ind-csNox4D hearts after MI. However, this was not enhanced in Ind-csNox4D hearts as there was no difference in the border zone compared to WT hearts. Furthermore, there was little difference between the number of Ki67-positive cardiomyocytes in the remote zones of WT and Ind-csNox4D hearts, suggesting no change in the proliferative response of non-infarcted myocardium (Figure 4.18). Likewise, a similar trend was observed in the percent of cardiomyocytes positive for nuclear expression of pHH3, indicative of late G2/M-phase, showing that MI was associated with just a marginal increase in WT hearts. However, this was associated with was no difference versus Ind-csNox4D hearts in either the border or remote zones (Figure 4.19).

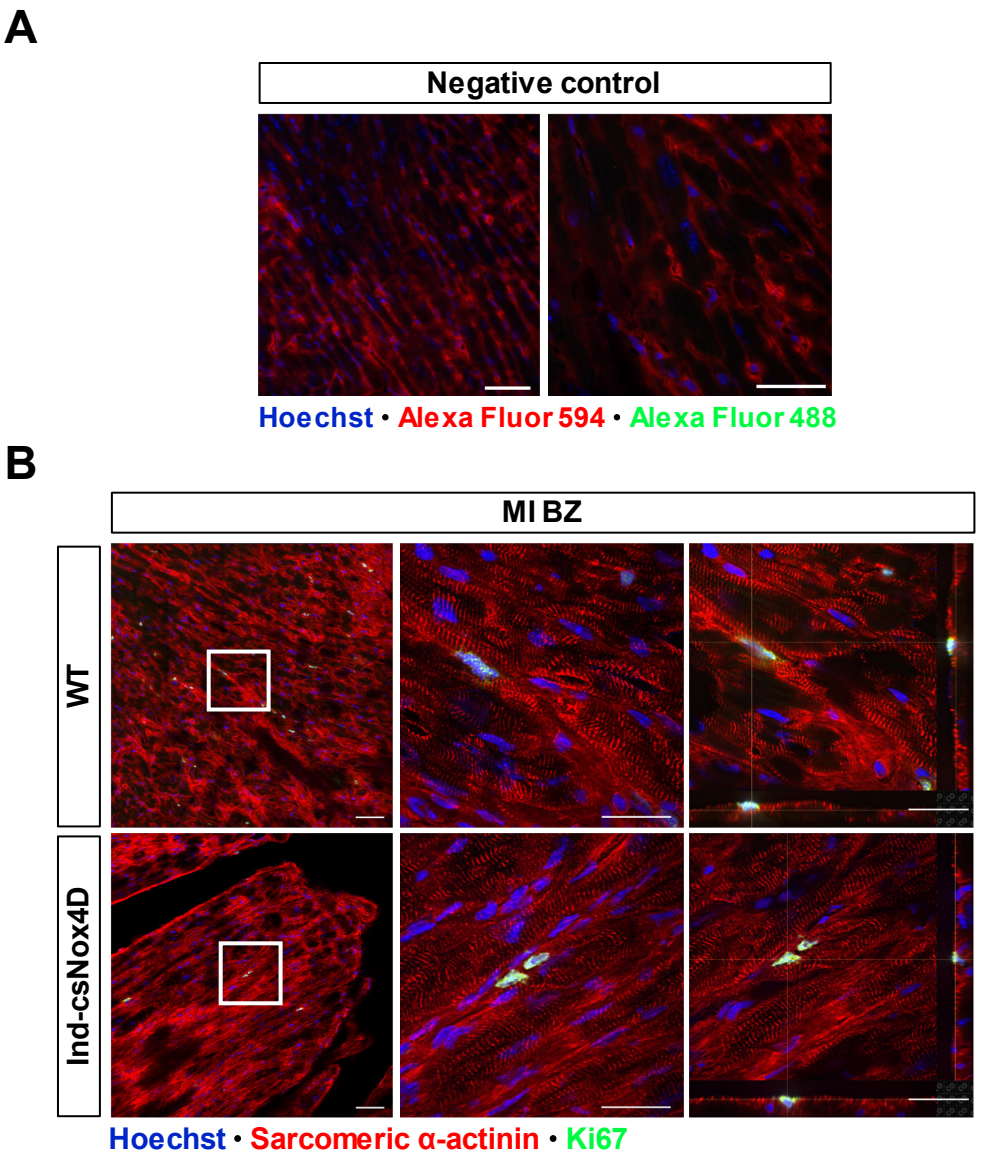

Figure 4.18. Cardiomyocyte-specific Nox4D overexpression induced in adult mice does not promote cardiomyocyte cell cycle activity in the infarct border or remote zone. (A) Representative images of immunofluorescence staining as negative control, incubated with secondary antibodies and Hoechst (blue) only for validation of primary antibody signal. Scale

bars: 50 µm. (B) Representative images of immunofluorescence staining for cell cycle progression marker Ki67 (green) with α-actinin (red) as a cardiomyocyte marker and Hoechst as a nuclear marker in the infarct border zone (BZ) of cardiac cryosections of WT and Ind-csNox4D hearts harvested 4 weeks after myocardial infarction (MI). Boxes (left) indicate images of higher magnification containing positive cardiomyocyte nuclei, shown by Z-stack maximum fluorescence intensity projection (middle) and orthogonal view (right) to confirm co-localisation of green and blue signal in α-actinin-positive cells. Scale bars: 50 µm (left), 25 µm (middle and right). (C) Quantification of the number of positive cardiomyocytes as a percentage of total number of cardiomyocytes counted in each zone. n = 4 per group. Data represent mean ± SEM. Statistical analysis by two-way ANOVA with Bonferroni's post hoc correction.

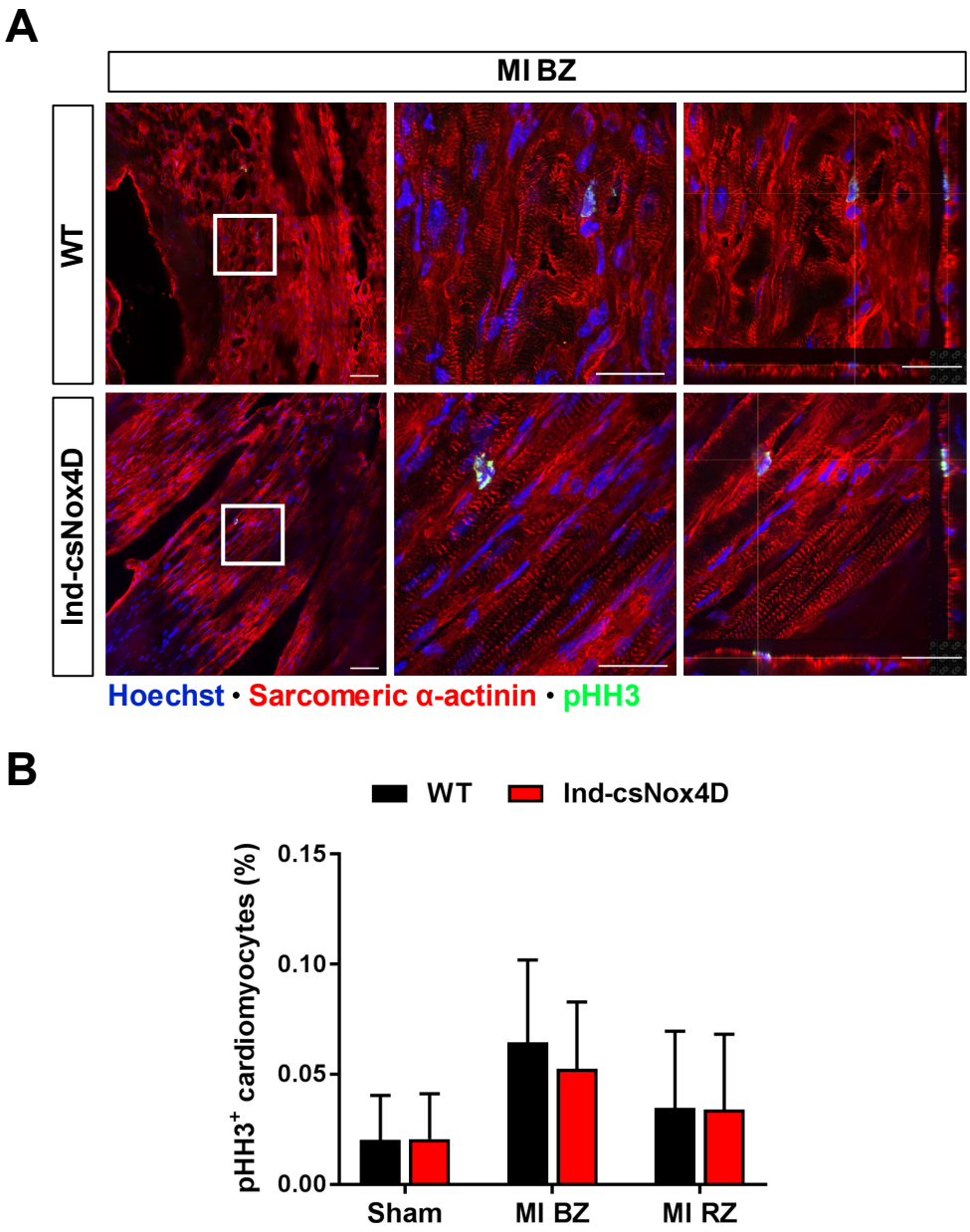

Figure 4.19. Cardiomyocyte-specific Nox4D overexpression induced in adult mice does not promote cardiomyocyte proliferation in the infarct border or remote zone. (A) Representative images of immunofluorescence staining for cell proliferation marker phospho-histone H3 (pHH3) (green) with α-actinin (red) as a cardiomyocyte marker and Hoechst as a nuclear marker in the infarct border zone (BZ) of cardiac cryosections of WT and Ind-csNox4D hearts harvested 4 weeks after myocardial infarction (MI). Boxes (left) indicate images of higher magnification containing positive cardiomyocyte nuclei, shown by Z-stack maximum fluorescence intensity projection (middle) and orthogonal view (right) to confirm co-localisation of green and blue signal in α-actinin-positive cells. Scale bars: 50 μm (left), 25 μm (middle and right). (C) Quantification of the number of positive cardiomyocytes as a percentage of total number of cardiomyocytes counted in each zone. n = 4 per group. Data represent mean ± SEM. Statistical analysis by two-way ANOVA with Bonferroni's post hoc correction.

In an attempt to provide some mechanistic basis for the effects of cardiac-specific Nox4D overexpression in the adult heart in response to MI, this was further investigated at transcript level by regional zone qPCR analysis. This screen targeted functional groups of genes that are likely important regulators of the regenerative potential of the heart. Overall, this revealed no changes in the mRNA expression levels of cell cycle activators, including cyclins (E1, A2 and D1), Cdks (Cdk2, Cdk4), and the mitosis marker aurora kinase B (Aurkb), or cell cycle inhibitors (p27Kip1, p21Cip1) in the infarct border zone or remote zones of WT and Ind-csNox4D hearts relative to respective sham controls. Equally, no differences were found in either the border zone or remote zone between Ind-csNox4D and WT hearts after MI (Figure 4.20).

The mRNA expression levels of markers re-expressed in dedifferentiated cardiomyocytes, which might contribute to the enhanced propensity for cell cycle re-entry in dedifferentiated cardiomyocytes,[187] were also analysed (as originally investigated in Chapter 3). Some zone-dependent changes in the transcript expression of markers of dedifferentiation were detected in WT hearts after MI. Runx1 showed an upward trend in only the border zone, whereas Dab2 was slightly increased in the border zone but significantly increased in the remote zone. GATA4 tended to be upregulated in both infarct zones whilst ssTNI and ckit were unchanged compared to WT sham controls. This response was not seen in Ind-csNox4D hearts, which demonstrated little change in the expression of these markers after MI compared to sham baseline. However, no significant differences were found between WT and Ind-csNox4D hearts in either infarct zone after MI (Figure 4.21).

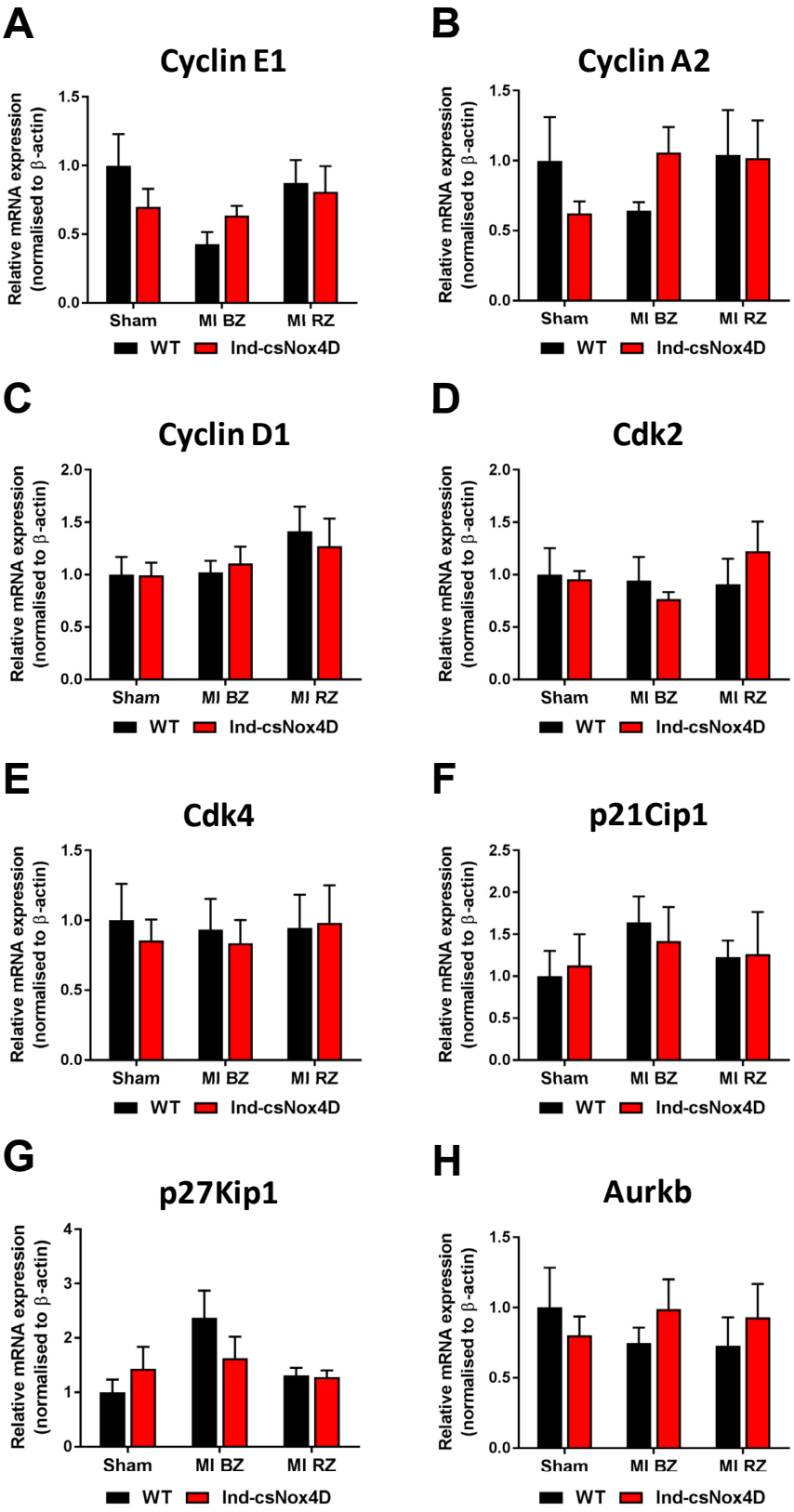

Figure 4.20. Nox4D overexpression in the adult heart does not affect transcript expression of markers of proliferation 4 weeks after myocardial infarction. Regional zone qPCR analysis of relative mRNA expression of markers of proliferation 4 weeks after myocardial infarction (MI), in the infarct border zone (BZ), infarct remote zone (RZ), and sham control in (A) cyclin E1, (B) cyclin A2, (C) cyclin D1, (D) cyclin-dependent kinase 2 (Cdk2), (E) Cdk4 (F) p21Cip1, (G)

p27Kip1, and (H) aurora kinase B (Aurkb) in hearts of WT and Ind-csNox4D mice. n = 6 per group. Data represent mean ± SEM. Statistical analysis by two-way ANOVA with Bonferroni's post hoc correction.

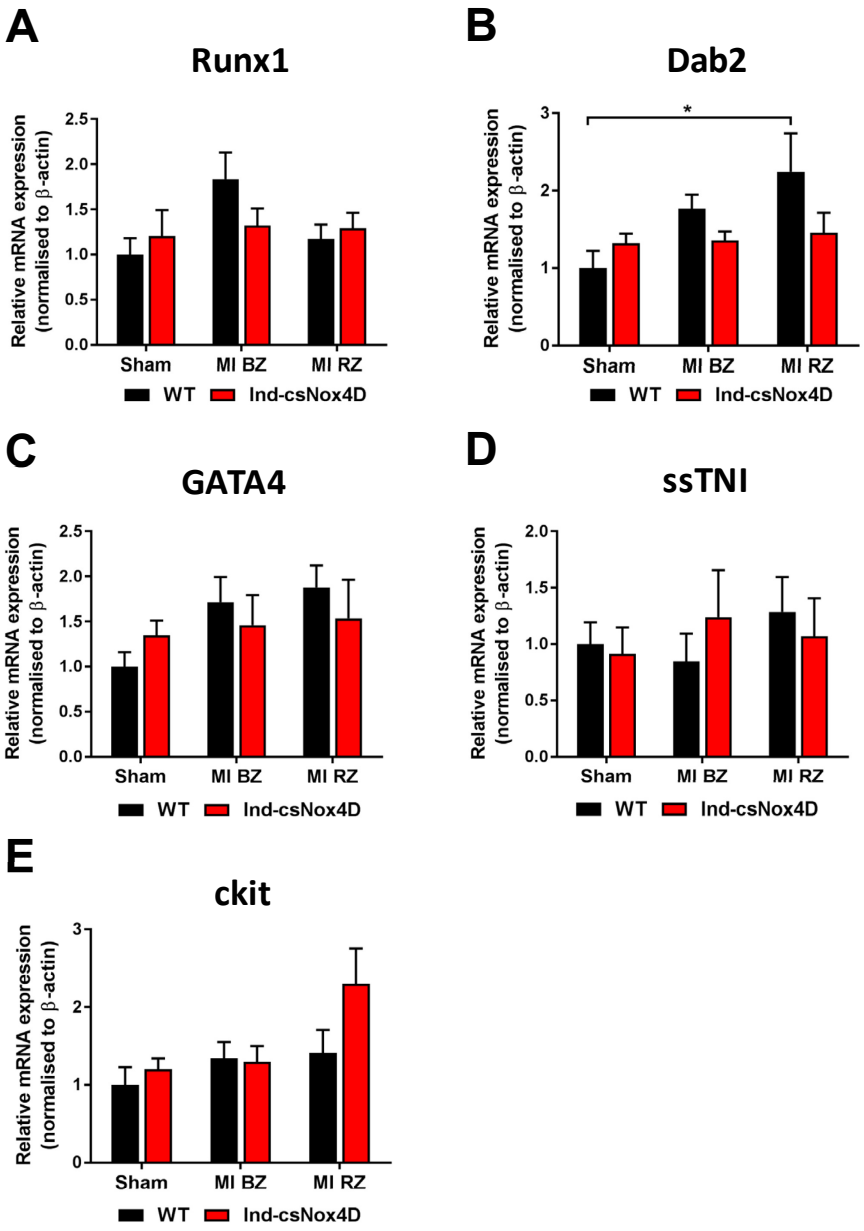

Figure 4.21. Nox4D overexpression in the adult heart does not affect transcript expression of markers of dedifferentiation 4 weeks after myocardial infarction. Regional zone qPCR analysis of relative mRNA expression of markers of proliferation 4 weeks after myocardial infarction (MI), in the infarct border zone (BZ), infarct remote zone (RZ), and sham control in (A) Runx1, (B) Dab2, (C) GATA4, (D) slow skeletal troponin I (ssTnI), and (E) ckit in hearts of WT and Ind-csNox4D mice. n = 6 per group. Data represent mean ± SEM. *P<0.05 by two-way ANOVA with Bonferroni's post hoc correction.

Angiogenesis represents another important mechanistic process that has been shown to enhance the regenerative response and functional recovery post-MI.[260] As infarcted Ind-csNox4D hearts showed a trend for increased maintenance of capillary density and vascular abundance, the expression of proangiogenesis factors (vascular endothelial growth factor A [Vegfa][261,262] and angiopoietin 2 [Angpt2][263]) was also screened by qPCR. After MI, this revealed an upward trend in Ind-csNox4D compared to WT hearts, particularly in the expression of Angpt2 (Figure 4.22).

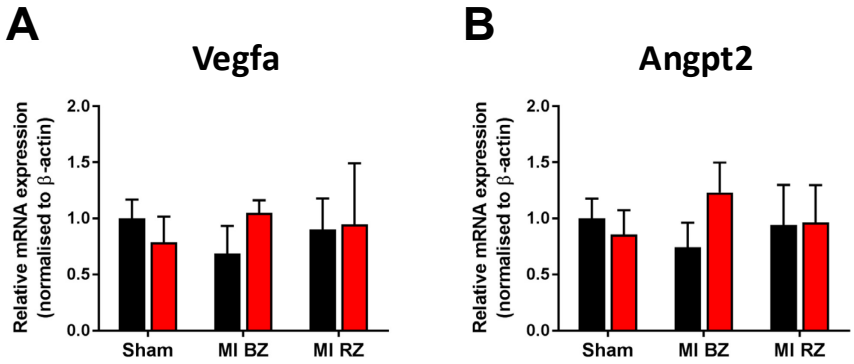

Figure 4.22. Cardiac-specific Nox4D overexpression does not significantly affect transcript expression of markers of angiogenesis 4 weeks after myocardial infarction. Regional zone qPCR analysis of relative mRNA expression of markers of angiogenesis 4 weeks after myocardial infarction (MI), in the infarct border zone (BZ), infarct remote zone (RZ), and sham control in (A) vascular endothelial growth factor A (Vegfa), (B) angiopoietin 2 (Angpt2) in hearts of WT and Ind-csNox4D mice. n = 6 per group. Data represent mean ± SEM. Statistical analysis by two-way ANOVA with Bonferroni's post hoc correction.

Lastly, as Nox4D is a ROS-generating isoform, to evaluate the possibility of deleterious effects as a result of nuclear-localised ROS release we screened for a potential upregulation in genes that form part of the Nrf2 antioxidant response element transcriptional pathway. However, at 4 weeks post-MI, we saw no changes in the expression of Nrf2 target genes[264,265] - glutamate-cysteine ligase catalytic subunit (Gclc) or glutathione S-transferase, alpha 2 (Gsta2) - between WT and Ind-csNox4D hearts. This was neither changed compared to sham-operated controls, suggesting no Nrf2-dependent upregulation in antioxidant genes in response to induced cardiomyocyte-specific Nox4D overexpression at this time point (Figure 4.23).

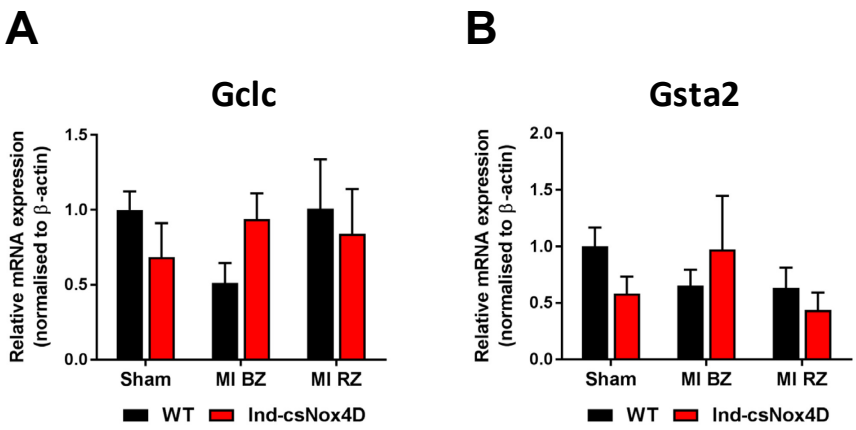

Figure 4.23. Cardiac-specific Nox4D overexpression does not affect transcript expression of Nrf2 target genes 4 weeks after myocardial infarction. Regional zone qPCR analysis of relative mRNA expression of target genes of the Nrf2 antioxidant pathway 4 weeks after myocardial infarction (MI), in the infarct border zone (BZ), infarct remote zone (RZ), and sham control in (A) glutamate-cysteine ligase, catalytic subunit (Gclc), (B) glutathione S-transferase, alpha 2 (Gsta2) in hearts of WT and Ind-csNox4D mice. n = 6 per group. Data represent mean ± SEM. Statistical analysis by two-way ANOVA with Bonferroni's post hoc correction.

To capture DNA replication events as a marker of proliferation at an earlier phase after MI, WT and Ind-csNox4D mice were injected with EdU (50 mg/kg body weight) every 4 days for 2 weeks, commencing 24 hours post-ligation. Cardiomyocyte proliferation was quantified as the percentage of α-actinin-positive cells with positive nuclear fluorescent labelling of incorporated EdU, the identity of which was again confirmed by Z-stack confocal imaging.

Interestingly, this technique was able to demonstrate that the percent of EdU-positive cardiomyocytes was significantly increased in the MI border zone of both WT and Ind-csNox4D hearts compared to WT and Ind-csNox4D sham-operated controls, respectively. In WT hearts, this was also significantly higher than the MI remote zone. These data provided additional evidence to suggest that the induction of cardiomyocyte-specific Nox4D overexpression plays no detectable role in enhancing the proliferative reserve of cardiomyocytes in response to MI, as there was no difference in the number of EdU-positive myocytes compared to WT hearts in either MI regional zone (Figure 4.24).

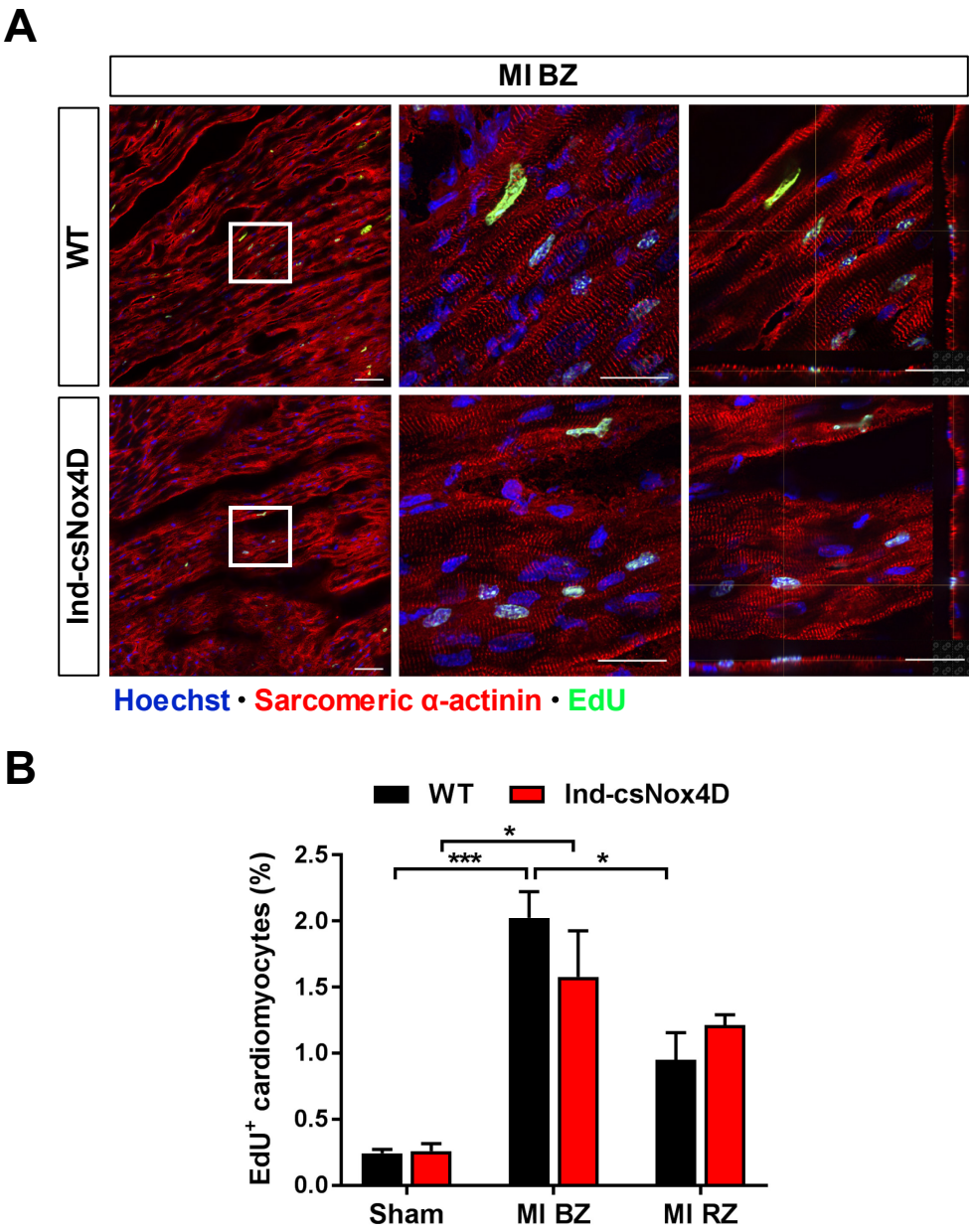

Figure 4.24. Cardiomyocyte-specific Nox4D overexpression induced in adult mice does not promote cardiomyocyte proliferation in the infarct border or remote zone 2 weeks after myocardial infarction. (A) Representative images of immunofluorescence staining of 5-ethynyl-2'-deoxyuridine (EdU) (green) incorporation, labelling cells that have synthesised DNA, with α-actinin (red) as a cardiomyocyte marker and Hoechst as a nuclear marker in the infarct border zone (BZ) of cardiac cryosections of WT and Ind-csNox4D hearts harvested 2 weeks after myocardial infarction (MI). Boxes (left) indicate images of higher magnification containing positive cardiomyocyte nuclei, shown by Z-stack maximum fluorescence intensity projection (middle) and orthogonal view (right) to confirm co-localisation of green and blue signal in α-actinin-positive cells. Scale bars: 50 μm (left), 25 μm (middle and right). (C) Quantification of the number of positive cardiomyocytes as a percentage of total number of cardiomyocytes counted in each zone. n = 4 per group (MI) and 3 per group (sham). Data represent mean ± SEM. **P*<0.05, ****P*<0.001 by two-way ANOVA with Bonferroni's post hoc correction.

4.5 Discussion

To date, there are no published studies regarding the role of cardiomyocyte Nox4D in MI, and so the results described in this chapter represent the first report investigating the effects of inducible overexpression of a nuclear-localised, redox-active Nox4 splice variant on functional recovery and myocardial regenerative capacity post-ischaemic injury in the adult mammalian heart.

4.5.1 Verification of the permanent LAD ligation model

Our use of the permanent LAD coronary artery ligation model reproducibly induced myocardial infarction in WT and Ind-csNox4D transgenic animals, characterised by the classical physical and geometric signs of LV apical wall thinning, elevations in LV dimensions and volumes, and progressive functional decline.[210,211,266] Furthermore, this study also demonstrates the translatable importance of plasma cTnI as a major biomarker for ischaemic cardiac injury in mice. The 24-hour plasma cTnI levels were shown to be closely related to functional parameters in order of increasing severity at 2 and 4 weeks post-ligation. No elevations in cTnI were observed after sham ligation, suggesting that generalised muscle injury sustained from surgery does not contribute to detectable release.[226]

Despite occlusion at the same anatomical level, a widely recognised limitation of the LAD ligation model is the intrinsic variability of MI infarct size.[225,227] Many preclinical studies assess the efficacy of their interventions by measurement of infarct size as an end-point outcome. Without early evaluation of infarct size, the resulting comparisons between experimental groups may be impaired by inter-animal variability.[210,226] In agreement with this limitation, variability in initial myocardial injury was encountered in the present study as evidenced by the acquired range of cTnI levels. However, this was circumvented in part by overall comparability of the mean 24-hour cTnI between WT and Ind-csNox4D groups, and analysis of functional parameters relative to 24-hour cTnI, which would not be permissible with other traditional staining methodologies.[228] For analysis of histological and transcriptional readouts of remodelling and proliferation, mice were selected within a similar range of 24-hour cTnI and therefore a comparable degree of injury.

4.5.2 Cardiac-specific Nox4D transgenic mice show a transient improvement in functional response after myocardial infarction

At 2 weeks post-MI, we found that Ind-csNox4D mice are able to demonstrate enhanced preservation of ejection fraction and GLS. However, by 4 weeks after MI, Ind-csNox4D mice show only little evidence of sustained improvement as indicated by minor or no changes in ejection fraction, LV volumes, LV mass or GLS, thereby suggesting a

transient improvement in functional response, insufficient to fully rescue recovery. As myocardial strain and strain rate are particularly suited for the measurement of regional myocardial contractile function, they represent the ideal parameters for quantification of the segmental LV dysfunction that is induced by postinfarction scarring.[161,257,258] Therefore, we next evaluated the regional longitudinal and radial strain rate as higher sensitivity indices of contractility in an aim to gain greater understanding of the temporal functional response elicited by Ind-csNox4D mice in response to MI. At 2 weeks post-MI, it would appear that the beneficial contractile effects seen in Ind-csNox4D hearts are more globally distributed across the LV, as both the longitudinal and radial strain rates demonstrate general improvement in all segments, thus contributing to the overall enhancement in GLS without major differences compared to WT hearts relative to cTnI in the anterior border (mid) or remote (base) zones. However, at 4 weeks post-MI, although Ind-csNox4D mice do not maintain the significant improvement in GLS, regional strain analysis enabled the identification of localised enhanced longitudinal and radial strain rate specifically within the anterior base of the LV. In light of this, it would appear that this difference in contractility confers some localised compensatory enhancement of function, but is insufficient to offset the global deterioration as demonstrated by ejection fraction and LV chamber dilatation, and therefore unlikely to achieve a clinically significant recovery .

However, the patterns of this functional response strongly suggest regional differences in Ind-csNox4D versus WT hearts in response to MI. An enhanced rate of myocardial deformation within the anterior base of Ind-csNox4D hearts suggests enhanced compensatory contractile function within the anterior border or remote non-infarcted regions. Interestingly, this is supported by studies in small animal models that have reported specific compensatory improvements in regional LV contractility 4 weeks post-permanent ligation secondary to distinct differences in postinfarction remodelling (discussed in more detail in section *4.5.3*).[261,267] Therefore, the potential mechanisms underlying the response seen in the present study could be reflective of differences in the repair process of the remaining viable myocardium.[17]

4.5.3 Inducible cardiomyocyte-specific Nox4D overexpression confers a partial reparative response during postinfarction remodelling

This was investigated further by regional zone pathological analysis of the infarcted tissues. Delineation of the MI regions is crucial for the study of the response to MI as the infarct zone is demonstrative of processes relating to scar formation and maturation, whilst the border and remote zones importantly reveal cellular events in still-viable myocytes as well as remote remodelling changes.[210]

As demonstrated previously in mice,[254] echocardiographic assessment of LV chamber dimensions and volumes revealed the progressive development of dilated ventricular remodelling by 4 weeks post-MI, as evidenced by a greater trend of LVM and LVEDV relative to 24-hour cTnI compared to that seen at 2 weeks post-MI. As expected, the WT response to infarctive injury is characterised by multiple features of remodelling. At 4 weeks post-MI, WT mice develop LV cardiomyocyte hypertrophy, as collectively evidenced by elevations in LV mass, heart weight to body weight ratio, cardiomyocyte cross-sectional area in conjunction with raised molecular markers indicative of pro-hypertrophic signalling. This is coupled with extensive fibrous scar formation and maturation, and cardiomyocyte apoptosis in the infarct border zone and remote non-infarcted myocardium.

In contrast, Ind-csNox4D transgenic mice appear to demonstrate a partially reduced remodelling response following MI, which could be in keeping with the observed effects on regional contractile function. Whilst there is no overall morphometric change in heart weight to body weight, Ind-csNox4D mice show some trends for reduction in LV mass relative to initial injury, smaller cardiomyocyte area, and downregulation of expression of markers of failure in both the border and remote zones. This is particularly interesting in light of previous research that established preserved cardiac function in an adult rat model of permanent ligation following AAV-mediated overexpression of Vegfb.[261] This aforementioned study reported improved regional function within the border zone of the anterior wall attributable to the induction of compensatory hypertrophy. This physiological-like hypertrophic response was characterised by the activation of contractile genes such as Myh6 in conjunction with repression of foetal genes of pathological hypertrophy, including Myh7, skeletal α-actin, and the cardiac natriuretic peptides. Furthermore, it was also found that the mechanism for enhanced contractile function was in part elicited by preservation of viable myocardial tissue through protection of cardiomyocytes from apoptosis, as opposed to promotion of proliferation.[261]

Regional qPCR analysis showed that Ind-csNox4D hearts are associated with comparatively less activation of Myh7, ANP and BNP particularly in the remote non-infarcted LV. However, this was not coupled with an upregulation in Myh6. As discussed in *4.2.3*, GATA4 has been shown to function as one of the target transcription factors that represent key points of convergence for many stress-induced hypertrophic signalling cascades.[242,248] Therefore, it is pertinent to note that in WT mice, we found an incremental transcript expression of GATA4 in the border and remote zone of infarcted hearts compared to sham-operated hearts, whereas in Ind-csNox4D hearts we observed reduced expression in both the infarct border and remote zones.

Moreover, experimental models have shown that occasional cardiomyocytes may undergo programmed cell death by apoptosis in the remodelling viable segments of the myocardium weeks or even months after infarction.[245] As such, cell viability is also considered a feature of the remodelling phenotype, as further loss of myocardium contributes to progressive functional decline.[235,242] This may be driven by molecular signals as part of intrinsic pathways, involving mitochondrial signalling, or extrinsic pathways via ligand binding to cell surface death receptors.[17] It is evident that Ind-csNox4D hearts may demonstrate increased propensity for anti-apoptotic or survival signalling, as shown by an initial trend for reduced apoptotic cardiomyocytes in both the infarct border and remote zones.

Therefore, given the collective potential trends on hypertrophic gene programmes in conjunction with cardiomyocyte area, LV mass, and apoptotic signalling, it is possible to speculate that the induction of Nox4D overexpression may exert a degree of redox-mediated attenuation of pathological hypertrophy and enhancement of postinfarction cardiomyocyte survival, with a potential shift towards a more compensatory or adaptive hypertrophy in localised segments of the infarcted LV. Thus, the *regionalised* pattern of effects is emphasised here as this could account for the observed lack of detectable effect on the global parameter heart to body weight ratio.

In addition, the potential for Ind-csNox4D mice to demonstrate enhanced reparative recovery is further evidenced by a significant reduction in total cardiac fibrosis at 4 weeks post-ligation, and a trend for reduction in the maturation of deposited cross-linked fibrillar collagen. However, these changes still proved insufficient to achieve significant rescue of overall global function. The described study on AAV-mediated delivery of Vegfb also reported enhanced repair through a reduction in fibrotic scar area. However, it is important to note that this study also reported that the regional contractile effects were able to equate to a significant improvement in global LV function, which, compared to the present study, in the absence of meaningful cardiomyocyte regeneration, is therefore likely reflective of a greater magnitude of effect on hypertrophic gene expression profiles and anti-apoptotic signalling pathways.

4.5.4 Cardiomyocyte-targeted Nox4D overexpression does not elicit regenerative recovery in response to myocardial infarction

A major endpoint of this study was to establish the proliferative potential of induced cardiac-specific Nox4D overexpression in the adult heart in the setting of myocardial infarctive injury. Unfortunately, within this study design, we found that following ischaemic stress, adult Ind-csNox4D transgenic mice do not mount a substantial

proliferative response to achieve meaningful restoration of cardiac structure and, ultimately, function.

Previous research in the adult mouse heart has demonstrated that 8 weeks after permanent LAD ligation, approximately 3% of cardiomyocytes adjacent to the infarct area show evidence of cell division, with minimal contribution from progenitor cells, whereas most DNA synthesis occurs in polyploid, multinucleate cells without cytokinesis, consistent with a hypertrophic response.[86] We were able to identify a very small increase in cardiomyocyte cell cycle activity in WT hearts after MI, as evidenced by microscopic visualisation of Ki67 and pHH3 expression at 4 weeks, and EdU incorporation at 2 weeks, indicative of G1 – M phase, late G2/early mitosis, and DNA replication, respectively. It is known that not only cardiomyocytes in the infarct border zone demonstrate cell cycle activity, but also cardiomyocytes in the remote non-infarcted region, which implies some activation of intercellular signalling pathways throughout the myocardium.[268] Consistent with this, although greatest in the infarct border zone, WT infarcted hearts also revealed an upward trend in the proportion of cardiomyocytes positive for these markers in the remote region, suggesting a level of zone dependency. Interestingly, the percentage of WT border zone cardiomyocytes indicative of active DNA synthesis by incorporation of EdU is in keeping with that found by a recent study which examined proliferation events over a similar duration.[98] Assuming a comparable rate and linearity of incorporation, the final quantity of EdU-positive cardiomyocytes demonstrates the same order of proportionality to the dose used as that found in the present study.

The minimal regenerative contribution of the adult heart to postinfarction recovery is further demonstrated here by transcript analysis of cell cycle markers. At 4 weeks post-MI, we found that WT hearts show no changes in mRNAs encoding genes critical for cell cycle progression (cyclins and Cdks), cytokinesis (aurora kinase B), or cell cycle inhibition.[43] This is in agreement with recent research that extensively profiled the transcriptional networks in multiple cardiac cell populations during cardiac development, repair and regeneration.[269] This work importantly identified that adult P56 cardiomyocytes failed to reactivate a proliferative gene programme characteristic of neonatal P1 myocytes following infarction but rather deployed a distinct injury-responsive gene profile, consistent with adverse remodelling, and further identified a crucial realisation that, in whole-heart transcriptomic studies, reversion to an early developmental proliferative phenotype under pathological conditions could in fact be attributable to contaminating non-myocyte populations.[269]

Extensive assessment of the above microscopic and transcript markers of cell cycle modulation in the Ind-csNox4D transgenic heart demonstrated that cardiac-specific Nox4D overexpression does not lead to an increase in the intrinsic regenerative capacity

of the adult heart after MI. This is in contrast to other studies of regeneration post-permanent ligation in response to genetic manipulation of, for example, transcription factors,[162] microRNAs,[98] cell cycle components,[93] and Hippo signalling,[113] which have reported rescue of function through activation of renewal mechanisms leading to enhanced cardiomyocyte proliferation in addition to reduced remodelling, suggesting that cell cycle activation was able to counteract the postinfarction adverse ventricular remodelling.

Because the stimulation of cardiomyocyte proliferation is likely to involve a partial dedifferentiation step, the expression levels of markers of dedifferentiation were also investigated. Cardiomyocyte dedifferentiation is characterised at the cellular level by rearrangement of the contractile apparatus and cytoskeleton alongside changes in energy metabolism. Closely connected with remodelling, dedifferentiation is induced in response to pathological stimuli in the heart, and driven by reciprocal changes in the expression pattern of mature and immature cardiomyocyte-specific genes. It is proposed that sarcomeric disassembly and reduced energy demand might provide cardiomyocytes with the additional plasticity necessary to re-enter the cell cycle and survive in conditions of hypoxia.[187,270] Given the parallel with remodelling, it may not be surprising that several of the gene expression changes associated with each process overlap, such as GATA4 and Myh7.

Interestingly, at 4 weeks post-MI, whilst WT hearts demonstrated evidence of zone-dependent elevations in Runx1, Dab2, and GATA4 (as highlighted above), this was not mirrored in Ind-csNox4D hearts. In contrast, infarcted Ind-csNox4D hearts demonstrate little change in the expression of these markers as compared to their sham counterparts, the interpretations of which could either relate to reduced induction of dedifferentiation, or that due to the time point at which markers were assessed, may in fact reflect enhanced completion of the dedifferentiation cycle with a greater proportion of redifferentiated functional myocytes.[202] The latter mechanism is vital for functional recovery as the extended presence of dedifferentiation signals leads to a compromise in contractility and thus promotes adverse remodelling.[187] However, given the absence of effect of Nox4D overexpression on proliferation, this remains somewhat inconclusive, and so may better relate to the proposed regionalised preservations in function via restriction of adverse remodelling.

An additional possibility that may contribute to the partial recovery seen in the Ind-csNox4D heart is increased vascular abundance. The process of postinfarction repair is normally accompanied by an early increase in angiogenesis.[271] qPCR analysis revealed a potential trend for increased expression of the proangiogenesis factors Vegfa and Angpt2, which, in combination with the trend for increased maintenance of capillary

density in the infarct border and remote zones, may be suggestive of increased myocardial vascularity.

In an aim to investigate the possible reasons underlying the observed lack of effect of inducible Nox4D overexpression on cardiomyocyte proliferation after MI, we conducted a dose response experiment to determine whether the induction of Nox4D transgene expression is susceptible to modulation by incremental tamoxifen administration, and whether the subsequent effects on ROS generation negatively impact on the resulting phenotype.

HPLC analysis of DHE-derived oxidation products 2 weeks after tamoxifen induction revealed a generalised upward trend in the release of superoxide (Figure 4.25A) and hydrogen peroxide and other reactive species (Figure 4.25B) in Ind-csNox4D tissues in order of increasing tamoxifen dosage, although this was not significant.[168] This suggested that the levels of localised ROS release, as an indirect marker of the level of Nox4D expression induced, may demonstrate a dose response relationship with tamoxifen, although this is not fully definitive given the relative decrease seen with the greatest dose.

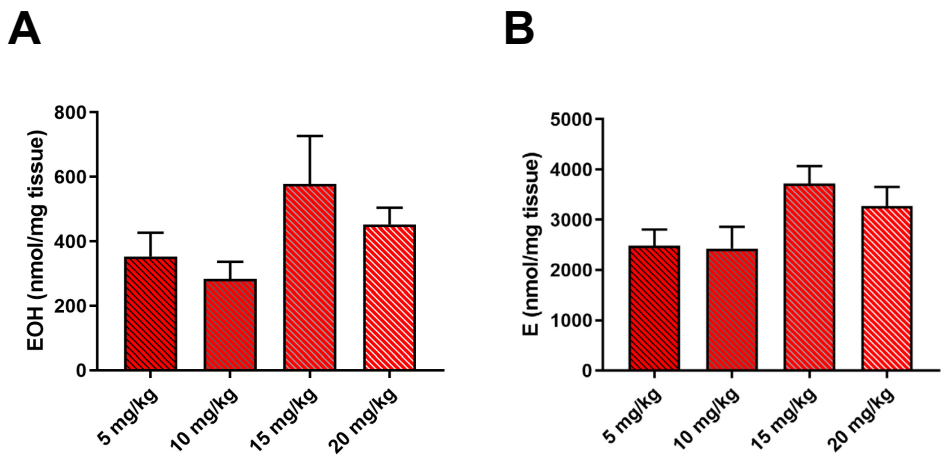

Figure 4.25. Incremental dosage of tamoxifen appears to be associated with a trend for greater reactive oxygen species generation. High-performance liquid chromatography (HPLC) analysis of dihydroethidium (DHE)-derived oxidation products for measurement of ROS generation in hearts of Ind-csNox4D mice harvested 2 weeks after administration of tamoxifen at doses of 5, 10, 15 and 20 mg/kg body weight in (A) 2-hydroxyethidium (EOH) for superoxide, and (B) ethidium (E) for hydrogen peroxide and other ROS. n = 3 per group. Data represent mean ± SEM. Statistical analysis by one-way ANOVA with Bonferroni's post hoc correction. HPLC by Dr Celio XC Santos.

Given the potential for excessive ROS production to be associated with oxidative damage,[131] it was important to establish the propensity of Nox4D overexpression to elicit detrimental cellular effects in vivo. This was assessed immunohistochemically by utilisation of the DNA damage response marker γ-H2AX (serine-139-phosphorylated H2AX). If the DNA damage is too extensive for repair, cells usually undergo permanent cell cycle exit or apoptosis.[272] This is regulated by multiple effector proteins, of which persistent phosphorylation of H2AX Y142 (tyrosine 142) has been shown to be a component of the pathways that leads to increased apoptotic cell death.[273] This is particularly pertinent in light of previous research demonstrating that postnatal cardiomyocyte cell cycle withdrawal is driven by increasing oxygen tension post-birth, leading to increased ROS generation and oxidative DNA damage.[79]

The proportion of cardiomyocytes positive for γ-H2AX showed a steady increase in response to increasing dosage of tamoxifen, which could therefore be suggestive of increasing Nox4D-derived ROS generation *or* enhanced nuclear translocation of Cre recombinase (Figure 4.26). Tamoxifen-induced αMHC-MCM activity has previously been linked to myocardial toxicity via activation of a DNA damage response, leading to cardiomyocyte death and dysfunction. However, these effects were observed at tamoxifen doses much greater than those employed here.[274] Even so, the level of γ-H2AX observed in the Ind-csNox4D heart after administration of the greatest dose of tamoxifen is comparable to that in the WT control. Therefore, it would seem less likely that this effect is solely dependent on the induction of Nox4D expression or Cre activity, and, as such, would need to be fully elucidated with further experiments using untreated controls.

Importantly, despite the possibility for increased ROS production in Ind-csNox4D hearts subjected to a greater tamoxifen dosage, together with increased DDR signalling, cardiomyocyte-specific Nox4D overexpression does not appear to be associated with increased Nrf2-mediated antioxidant signalling or cardiomyocyte apoptosis, as observed in sham-operated hearts.

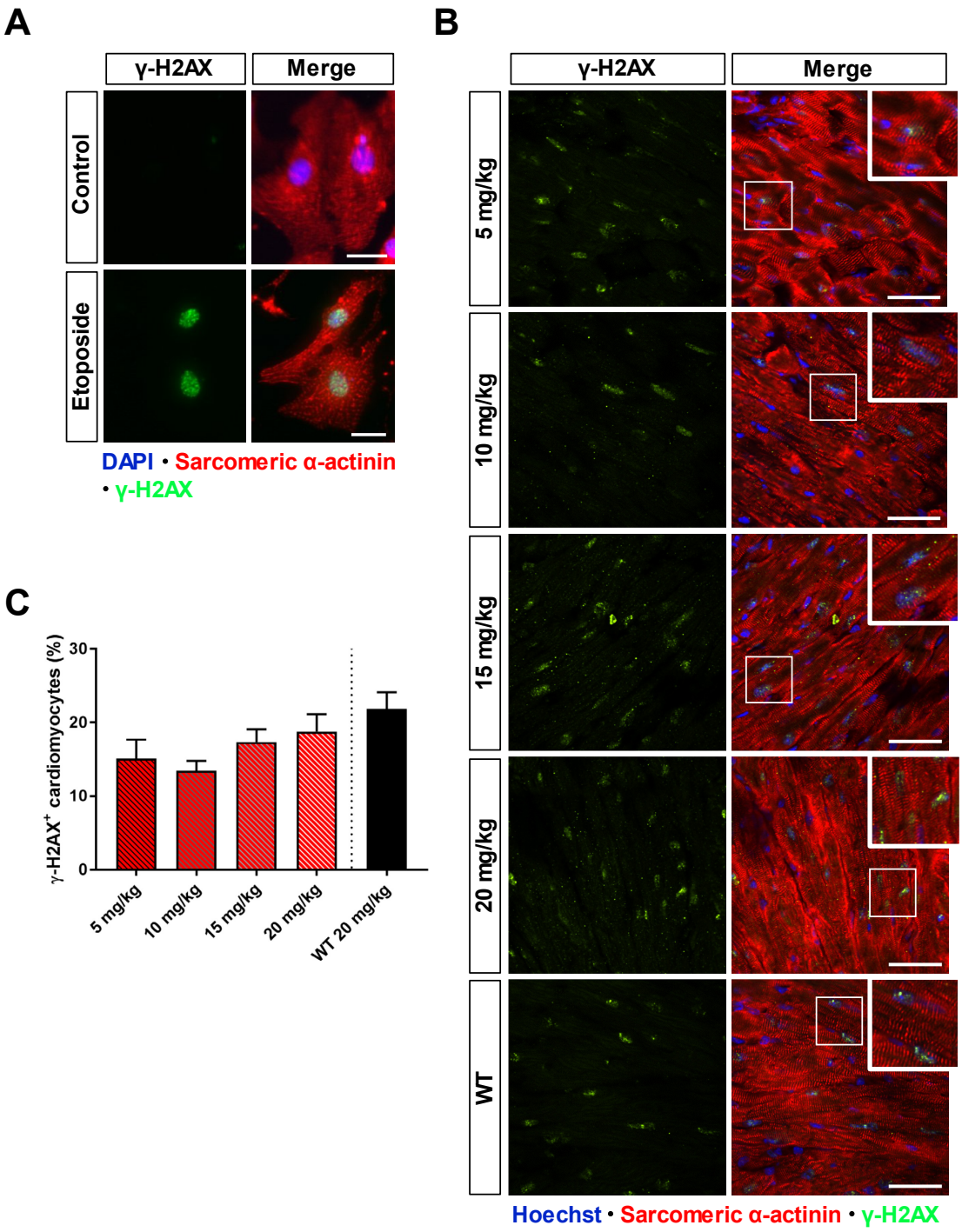

Figure 4.26. Incremental dosage of tamoxifen appears to be associated with a trend for greater cardiomyocyte DNA damage. Representative images of immunofluorescence staining for γ-H2AX (green) as a marker for DNA damage in (A) positive control in neonatal rat cardiomyocytes after 3-hour incubation with cytotoxic drug etoposide 10 μM or dimethyl sulfoxide (DMSO) with α-actinin (red) and DAPI (blue). Scale bars: 25 μm. (B) With α-actinin (red) and Hoechst (blue) on cardiac cryosections of Ind-csNox4D hearts harvested 2 weeks after administration of tamoxifen at doses of 5, 10, 15 and 20 mg/kg body weight, compared to WT mice also administered tamoxifen 20 mg/kg body weight. Boxes indicate areas of higher magnification containing positive cardiomyocyte nuclei. Scale bars: 50 μm. (C) Quantification of the number of positive cardiomyocytes as a % of total number of cardiomyocytes counted in each

zone. n = 3 per group. Data represent mean ± SEM. Statistical analysis by one-way ANOVA with Bonferroni's post hoc correction.

In conclusion, Ind-csNox4D transgenic mice demonstrate region-specific preservation of contractile function, which correlates with a partial reparative rescue of the remodelling response primarily, within the remote non-infarcted zone of the myocardium. Although we were not able to attribute this response to an increased cardiomyocyte proliferative capacity, the Ind-csNox4D heart does not appear to be associated with detrimental effects of excessive ROS exposure, however this warrants further investigation.

In agreement with the effects of inducible cardiomyocyte-specific Nox4D overexpression elicited in response to MI, it is known that various signalling networks that impact on several key features of the cardiac remodelling process are redox-sensitive, including contractile dysfunction, hypertrophy, interstitial fibrosis, capillary density, and cell survival. Such pathways can contribute in a protective or detrimental manner, the effects of which are likely highly dependent on the source and compartmentalisation of the signalling ROS.[131,275] Thus, it is possible to speculate that nuclear-localised, Nox4D-derived ROS may target compartment-specific signalling or transcriptional pathways involved in the modulation of the remodelling response to MI.

Overall, the findings of this study show that cardiomyocyte-targeted Nox4D overexpression induced in the adult heart has the potential to enhance recovery after MI, although the underlying mechanism remains to be discerned. There exist several possibilities to account for the insufficiency of this model to achieve significant rescue of functional recovery, and these relate to the optimal level of overexpression required for therapeutic effect, the susceptibility of the adult heart to this pathway, and the potential inability of Nox4D to promote proliferation of differentiated cardiomyocytes. Alternatively, redox signalling pathways mediated by Nox4D in this setting may be reflective of survival as opposed to proliferation. Thus, in order to gain a deeper insight into the pathophysiological response of inducible Nox4D overexpression to MI, it would be important to understand whether the proliferative effects seen previously in the neonatal myocyte can in principal be recapitulated in the adult myocyte. This will be investigated in the next chapter by use of an ex vivo model of isolated adult cardiomyocytes.

Chapter 5 The manipulation of Nox4D in an in vitro model of adult cardiomyocyte dedifferentiation

5.1 Introduction

Given the results of the previous chapter on the study of Nox4D overexpression in response to MI, it is important to note here that the work of the present chapter was undertaken in parallel, as driven by the original aims of the project in relation to the greater understanding of the potential role of Nox4D in cardiomyocyte proliferation.

It has become increasingly recognised that cardiac remodelling in response to both acute and chronic disease processes is intimately connected with partial dedifferentiation of cardiomyocytes. This describes the reversion to a less mature phenotype characterised by greater plasticity with important implications for cell cycle progression. Although remodelling describes a complex process of multicellular interplay, in vitro experiments with isolated adult cardiomyocytes are invaluable for delineation of the underlying molecular mechanisms.[187]

5.1.1 Dedifferentiation of cardiomyocytes in vivo and in vitro

Cardiomyocytes need to be able to adjust their metabolic and contractile activities in order to adapt under pathophysiological conditions.[187] The concept of cardiomyocyte dedifferentiation following myocardial injury has been reported in lower vertebrate species such as the zebrafish,[276,277] defined by key features including electric uncoupling, disassembly of sarcomeric structures, and reciprocal changes in the expression of mature versus immature cardiomyocyte-specific markers, resulting in the re-expression of genes typically expressed during embryonic or foetal developmental stages.[270,276–278] Dedifferentiation has also been observed in adult mammalian cardiomyocytes by structural rearrangement and sarcomeric disassembly.[75,109,279] Thus, it follows that dedifferentiation might serve as a pre-programmed survival mechanism for cardiomyocytes subjected to stress such as hypoxia, by providing resistance to altered metabolic states through inactivation of energy-intensive functions.[280,281]

Whilst neonatal cardiomyocytes have been widely used to study processes of remodelling due to their accessibility and ease of culturing, they remain limited by substantial differences to terminally differentiated adult cardiomyocytes in terms of morphology and response to stimuli.[279,281] Indeed, freshly isolated adult cardiomyocytes are classically characterised by their highly ordered three-dimensional sarcomeric structure. As such, the resulting susceptibility of these cells to the mechanical stress imposed by the isolation procedure is demonstrative of their typical fragility post-isolation, thus reflecting the need for the ability to adapt to changes in architecture to maintain viability.[187] The progressive active remodelling, or dedifferentiation, of isolated adult cardiomyocytes in long-term culture is well recognised.[282–284] Enhanced in the presence

of FBS, cardiomyocytes show rounding up of cell edges and outward spreading to re-establish cell-to-cell contacts, consistent with a loss of cross-striated appearance.[187]

This is in agreement with more recent observations of loss of angular morphology and sarcomeric structures within 7 days of culture, culminating in cells with distinctive formation of pseudopodia and partial redifferentiation associated with synchronous contraction in regions of higher density by 21 days. Thus the traditional parameter of rod-shaped morphology does not necessarily remain equatable with cell viability after extended periods of culture.[163] These observations collectively imply that reorganisation of the contractile and cytoskeletal apparatus are reversible features of dedifferentiation, and function to enable cardiac remodelling in the settings of myocardial injury or disease.[285]

5.1.2 Regulation of cardiomyocyte dedifferentiation by oncostatin M

Several factors have shown involvement in the modulation of cardiac remodelling in vivo.[187] A previous study aimed to characterise the signals that transduce cardiomyocyte dedifferentiation and remodelling in the adult heart, and discovered a consistent upregulation of the inflammatory cytokine oncostatin M (OSM) and positive correlation with dedifferentiation of cardiomyocytes in the hearts of human patients with cardiovascular disease in both the acute (MI border zone) and chronic (end-stage heart failure) setting. Interestingly, recapitulation of these findings in functional studies on adult mouse models showed that OSM exerts protective effects after acute myocardial injury but paradoxically promotes functional deterioration and lethality when chronically activated in heart failure, suggesting that dedifferentiation of cardiomyocytes is most beneficially important for survival under conditions of stress when transiently induced.[286]

OSM belongs to the interleukin-6 (IL-6) subfamily of cytokines, and has been termed a multifunctional cytokine with evidence of biological activity in various inflammatory, haematopoietic, and developmental processes.[287] Due to activation of the common coreceptor gp130, the cardiac functions of members of this class of cytokines have been mostly implicated in cardiomyocyte survival and hypertrophy.[288,289] However, important differences exist in the signalling properties between individual members due to utilisation of other receptors. OSM induces heterodimerisation of the gp130 coreceptor with either the leukaemia inhibitory factor (LIF) receptor (LIFR) or OSM receptor (Oβ), and therefore elicits its effects via the type I or type II receptor complexes, respectively.[290]

The role of OSM in cardiomyocyte dedifferentiation was substantiated by further experiments with isolated adult myocytes in vitro. Stimulation of cardiomyocyte cell cultures with OSM resulted in striking morphological changes characterised by elongation, reformation of contact with neighbouring cells, and massive loss of

sarcomeric structures consistent with activation of foetal gene markers.[286] Biochemical analysis revealed that the mechanism by which these effects are mediated is transduction of the Ras/Raf/MEK/ERK signalling cascade through activation of the type II OSM receptor. This involves recruitment of the serine-threonine protein kinase Raf by Ras, which promotes MEK1/2 (MAPK/ERK kinase) dual-specificity kinase, which in turn phosphorylates the effector kinase ERK1/2.[291]

Importantly, the dedifferentiation of cardiomyocytes induced by OSM is considered partially reversible, since the stimulation of OSM-treated adult cardiomyocytes with insulin-like growth factor 1 (IGF1) as a hypertrophic signal results in sarcomerogenesis in vitro.[187,281,292] Together with greater plasticity, the reversibility of cardiomyocyte dedifferentiation has significant implications for myocardial regeneration.[286]

5.1.3 Partial dedifferentiation of cardiomyocytes may promote proliferative potential

The premise that cardiomyocyte dedifferentiation may facilitate proliferation is supported by recent important findings that OSM-treated cardiomyocytes in vitro have demonstrated greater cell cycle progression as signified by elevated DNA synthesis as a marker of S-phase entry.[286] This is corroborated by additional evidence gained from experiments based on a coculture system of isolated adult and neonatal cardiomyocytes demonstrating cytokinesis of adult myocytes following an initial dedifferentiation step. The important finding of this study is the observation that redifferentiation of adult myocyte-derived daughter cells was essential for the restoration of contractile function. The stimulus for redifferentiation was delivered by intercellular propagation of calcium transients from neighbouring neonatal myocytes, which was proven inhibitable by hypoxia-mediated impairment of gap junction function. This 3-step process of dedifferentiation, proliferation, and redifferentiation describing cell cycle re-entry of mature adult cardiomyocytes was also shown in an in vivo model of acute MI, primarily at the site of the border zone. Redifferentiation of pre-existing adult-derived, newly formed myocytes was enhanced in an ischaemia-resistant gap junction mutant via promotion of cell-to-cell electric recoupling between cardiomyocytes of the infarct border zone and surviving myocardium.[202]

These findings further support the concept that partial dedifferentiation of cardiomyocytes represents an adaptive mechanism in contexts of stress such as hypoxia, whilst the heart remodels in an effort to reconstitute functionality. However, whilst dedifferentiation may provide the plasticity needed for cardiomyocyte proliferation, it is evident that the extended presence of dedifferentiation signals may compromise contractility as a result of irregularly arranged and reduced expression of myofilament

proteins, and thus, in the absence of redifferentiation, may compound the development of adverse ventricular remodelling.[281,286]

In spite of this, given the apparent priming effect of dedifferentiation on cardiomyocyte proliferation, it remains an interesting approach to utilise in the study of the proliferative potential of Nox4D. This is especially pertinent in light of the disparity of results encountered so far on the effects of Nox4D overexpression on proliferation of neonatal myocytes in vitro versus adult myocytes in vivo. As such, the potential functional role of Nox4D in the proliferation of cardiomyocytes remains to be fully consolidated.

5.2 Aims

The aims of this chapter are to investigate the effects of Nox4D overexpression on the proliferation of cardiomyocytes in the setting of oncostatin M-induced dedifferentiation using an ex vivo model of cultured isolated adult cardiomyocytes. To establish a complementary loss-of-function approach, an siRNA-mediated technique will also be developed in the aim of translation to a viral vector-based delivery tool.

5.3 Summary of methods

To develop a complementary loss-of-function approach, siRNA designed to target Nox4D splice variant was optimised in vitro using the H9c2 cell line. This required several optimisation steps due to the difficulties associated with splice variant-specific targeting (as discussed in sections 2.15 & *5.4.1*). Nox4D knockdown was verified at mRNA and protein levels by qPCR (section 2.9) and Western blotting (section 2.10), respectively.

The proliferative potential of Nox4D was further investigated ex vivo using a protocol for the isolation and culture of adult mouse cardiomyocytes (section 2.8). Cell viability was assessed at 72 hours post-isolation by dye exclusion methods (section *2.8.4*). The effects of Nox4D overexpression on cardiomyocyte proliferation in the setting of dedifferentiation were assessed using OSM as a potent mediator of cardiomyocyte dedifferentiation and FGF2 as a stimulus for S-phase entry (section *2.8.5*). For these culture experiments, adult cardiomyocytes were isolated from WT and csNox4D Tg mice. This was considered preferable compared to the Ind-csNox4D Tg model as the constitutive csNox4D model may demonstrate more uniformly distributed overexpression of Nox4D and also circumvents the requirement for tamoxifen administration. In brief, adult male and female WT and csNox4D cardiomyocytes were isolated in parallel and plated on the same day, then allowed to recover for 2 days (Figure 2.10). Cells were then treated with OSM and FGF2, and cell cycle progression events were quantified by positive incorporation of EdU or expression of proliferation markers (sections *2.11.2* & *2.11.3).* Quantification of stitched, fixed field confocal images was performed manually as described in section *2.11.7*.

5.4 Results

5.4.1 Development of splice variant-targeted Nox4D knockdown

To gain greater understanding of the physiological role of endogenous Nox4D, it was necessary to establish a loss-of-function approach by generation of a knockdown tool. However, due to the technical difficulties associated with splice variant-specific targeting without affecting the expression of the parent sequence, this required careful optimisation. Therefore, a series of steps were taken to sequentially achieve reliable Nox4D knockdown in vitro using the H9c2 cell line.

The transfection protocol was first designed according to a transfection reagent optimised for siRNA delivery, and validated against commercially available siRNA targeted against Nox4 as a positive control. Compared to untargeted siRNA control, this was associated with approximately 80% knockdown in Nox4 mRNA expression. This effect was abrogated when cells were treated with transfection reagent alone or untreated as additional controls (Figure 5.1A).

As previously mentioned, the only difference in sequence between Nox4D and full-length Nox4 is situated within the exon 2/12 junction.[153] As such, siRNA and primers were designed to target this site to enable specificity for Nox4D. An siRNA sequence with preliminary Nox4D knockdown efficacy was transfected and trialled against a series of 5 primer sets, the most optimal of which were primers 1 and 3, as determined by assessment of qPCR products for specific amplification of Nox4D only, confirmed by nucleotide sequencing (Figure 5.1B). These primer sets were then further optimised in conjunction with the qPCR reaction conditions, by reduction of primer concentration and an increase in template volume, for enhancement of Nox4D detection (Figure 5.1C & D). Finally, titration of the concentration of Nox4D siRNA to be transfected revealed that 10 nM was the optimal concentration associated with maximal knockdown efficacy and minimal cytotoxicity (Figure 5.1E), and was used for further experiments.

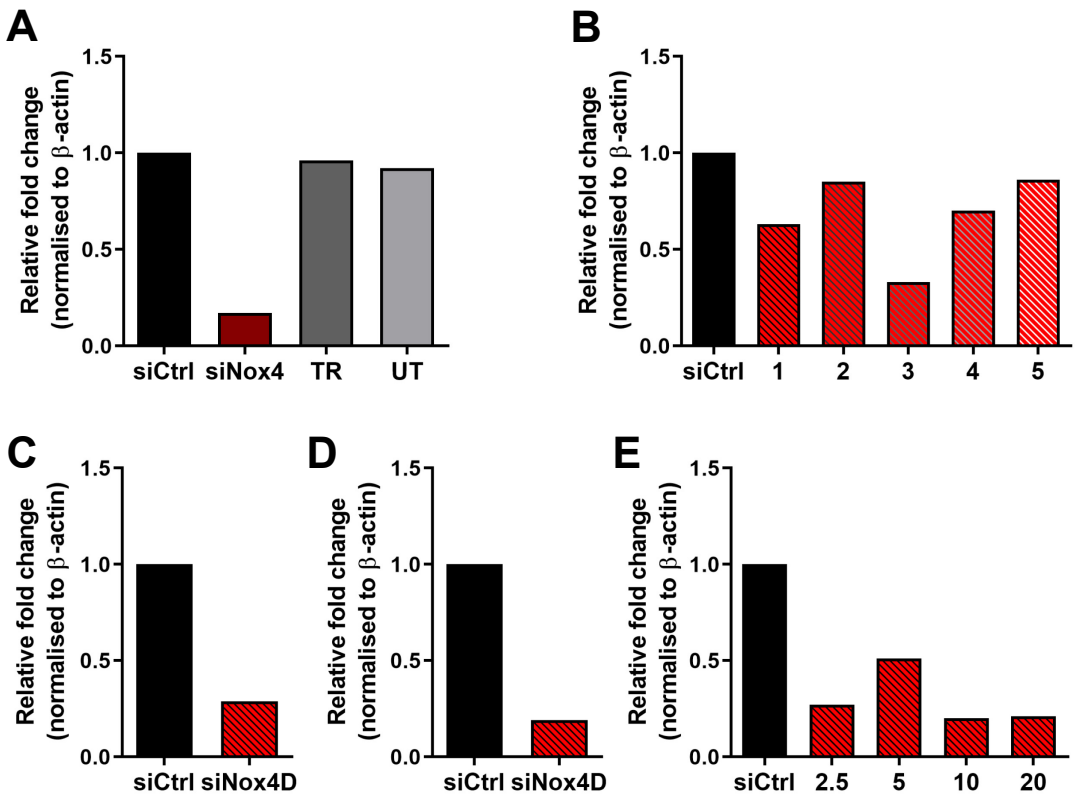

Figure 5.1. Optimisation of siRNA-mediated Nox4D knockdown in vitro. siRNA-mediated Nox4D knockdown and detection was progressively optimised in H9c2 cells and analysed by qPCR 72 hours post-transfection. (A) Relative Nox4 mRNA expression after transfection of pre-validated siRNA targeted to exon 3 of Nox4 (siNox4), untargeted siRNA control (siCtrl), and transfection reagent (TR) and untreated (UT) controls, as positive control of transfection protocol. (B) Relative Nox4D expression analysed against a series of 5 primer sets designed to target rat Nox4D after transfection of Nox4D siRNA sequence (siNox4D), normalised to respective siCtrl. Relative Nox4D expression after transfection of siNox4D against (C) primer set 1, and (D) primer set 3 in conjunction with optimisation of qPCR reaction conditions. (E) Relative Nox4D expression analysed against selected primer set 1 after transfection of siNox4D concentration gradient, normalised to respective siCtrl. n = 1 per group. Data represent mean of technical replicates.

Following optimisation of the technique, siRNA-mediated silencing of Nox4D finally resulted in nearly 80% knockdown of Nox4D mRNA expression levels compared to siRNA control (Figure 5.2A). Importantly, this was accompanied by no significant change in the mRNA expression level of Nox4, suggesting greater selectivity of the designed siRNA sequence for its splice variant target (Figure 5.2B). Knockdown of Nox4D was also verified at protein level by approximately 50% depletion of the 28-kDa band compared to siRNA control (Figure 5.3).

To further develop the utility of this knockdown tool and test the functional significance of Nox4D in different settings, the corresponding short hairpin RNA (shRNA) sequences were produced and cloned to generate both an adenovirus (AV) and an adeno-associated virus serotype 9 (AAV9) as vectors for shRNA expression and Nox4D knockdown in vitro and in vivo, respectively. However, due to the initial challenges associated with the establishment of Nox4D knockdown, we were unable to undertake further experiments with these viral delivery tools in addition to the time taken for their generation.

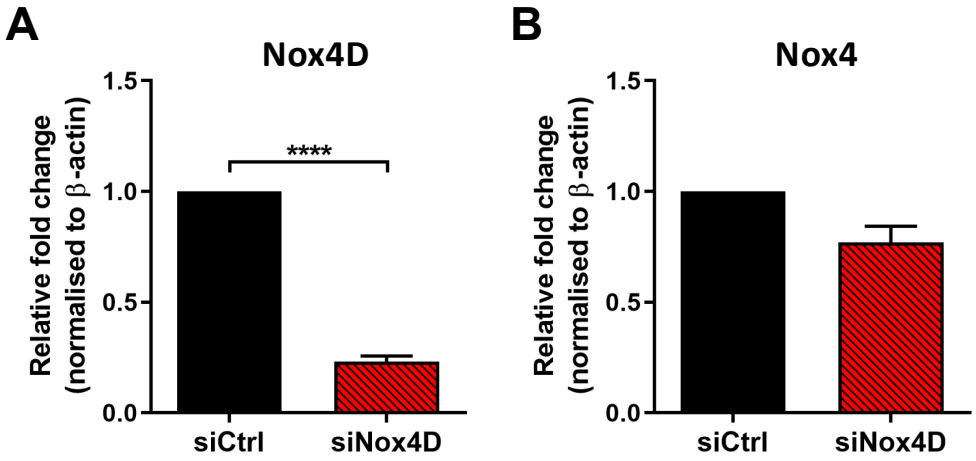

Figure 5.2. Targeted siRNA mediates Nox4D knockdown. qPCR analysis of relative mRNA expression of Nox4D (A) and Nox4 (B) in H9c2 cells 72 hours post-transfection of siRNA designed to specifically target Nox4D (siNox4D) or untargeted siRNA control sequence (siCtrl). Nox4D is preferentially silenced over full-length Nox4. n = 4 per group. Data represent mean ± SEM. ****P<0.0001 by unpaired two-tailed t-test.

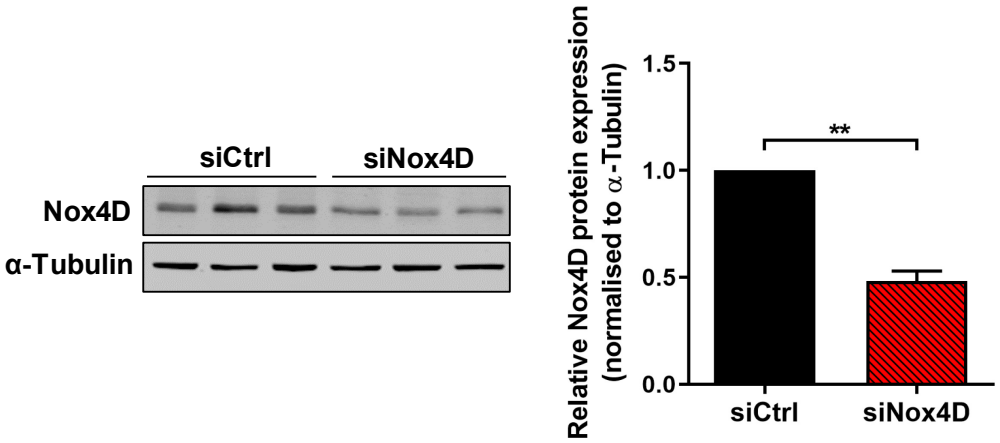

Figure 5.3. Targeted siRNA mediates Nox4D knockdown at protein level. Representative immunoblot (left) and relative quantification (right) of Nox4D protein expression in H9c2 cells 72 hours post-transfection of siRNA designed to specifically target Nox4D (siNox4D) or untargeted siRNA control sequence (siCtrl). n = 3 per group. Data represent mean ± SEM. ***P*<0.01 by unpaired two-tailed t-test.

5.4.2 Establishment of model of cultured isolated adult mouse cardiomyocytes

In parallel, extensive work was undertaken to adopt and establish in-house a recently published protocol for the isolation and culture of adult mouse cardiomyocytes for the study of the proliferative potential of Nox4D ex vivo.[163] Several attempts were made to develop the technique required to achieve satisfactory yield of viable cardiac myocytes. This led to an average yield of 70% rod-shaped myocytes that adhered to laminin-coated culture surfaces after calcium reintroduction and displayed characteristic angular morphology and organised sarcomeric architecture (Figure 5.4). This highly ordered sarcomeric striation pattern was further demonstrated in fixed myocytes on the same day as isolation by immunostaining for the actin-binding protein α-actinin, which localises to the sarcomeric Z-disk.[293] Staining of the nuclei also indicated that several myocytes displayed bi/multinucleation (Figure 5.5).

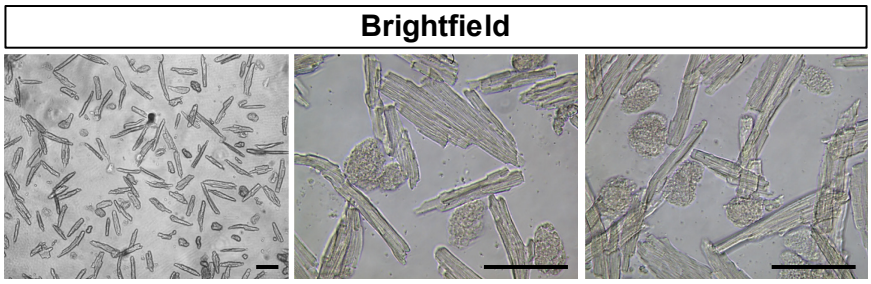

Figure 5.4. Isolation of rod-shaped cardiomyocytes from the adult mouse heart. Representative brightfield images of adult mouse whole heart digestion products on laminin-coated culture surfaces 1 hour after plating, demonstrating approximate yields of 70% rod-shaped, viable cardiomyocytes. Scale bars: 100 μm. n = 9.

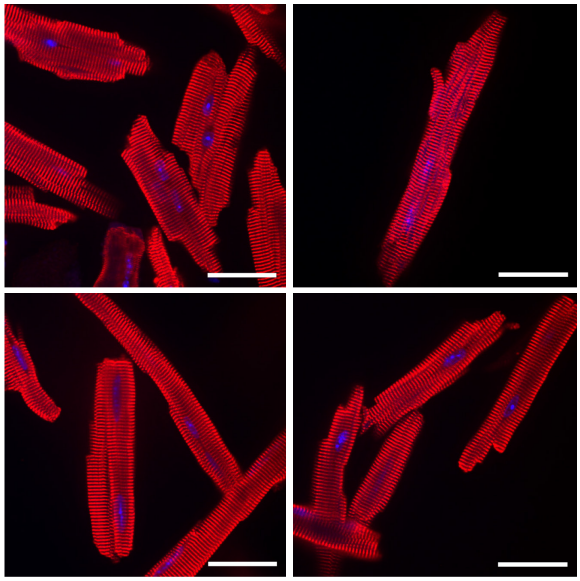

Figure 5.5. Isolated adult mouse cardiomyocytes have organised sarcomeric structures. Representative images of immunofluorescence staining of fixed WT adult mouse cardiomyocytes on day of isolation with α-actinin (red) as a sarcomeric marker and Hoechst (blue) as a nuclear marker. Scale bars: 50 μm. n = 2.

Isolated cardiac myocytes were maintained in the same culture medium supplemented with a defined lipid mixture and insulin-transferrin-selenium, as established previously. To validate the viability of cultured isolated cardiac myocytes in our hands before conducting experiments over a prolonged culture period, cells were stained by 2 methods at 72 hours post-isolation. Application of the dyes trypan blue and 7-AAD were excluded by rod-shaped cardiomyocytes, confirming viability by the presence of intact cell membranes, whereas cells that stained positive for each respective dye were considered non-viable (Figure 5.6). Non-viable cells were generally rounded in morphology and/or displayed irregular membranes. As such, although decreased in number, cardiomyocytes with rod-shaped, square-edged morphology represented a good indicator of viability at this time point.

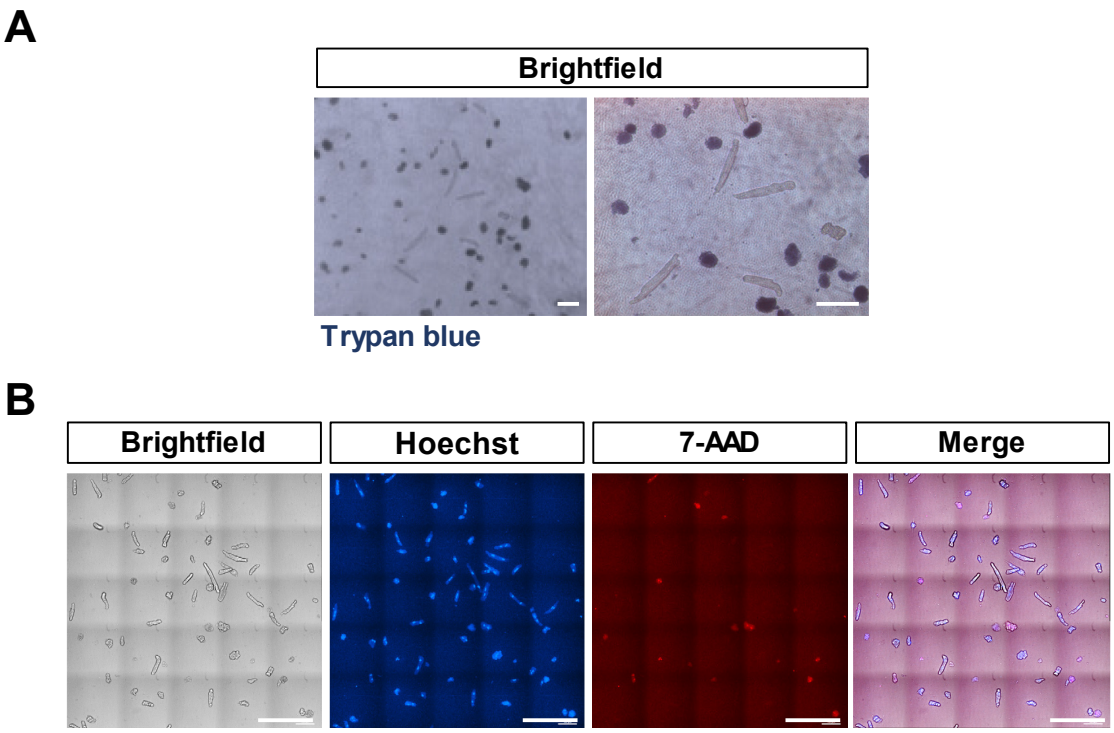

Figure 5.6. Isolated adult cardiomyocytes remain viable after three days in culture. Survival of isolated adult mouse cardiomyocytes was assessed after 72 hours in culture. (A) Representative brightfield images of myocytes stained with trypan blue, in which cells permeable to the dye are stained blue and considered dead. Scale bars: 100 µm. (B) Representative brightfield and fluorescence stitched images of myocytes stained with Hoechst (blue), labelling nuclei and 7-aminoactinomycin D (7-AAD; red), labelling DNA in cells with disrupted membranes only. Co-localisation of blue and red signal is indicative of non-viable cells. Scale bars: 250 µm. n = 1.

5.4.3 Nox4D overexpression is associated with modulation of cell cycle progression of dedifferentiated adult mouse cardiomyocytes

In keeping with the hypothesis that dedifferentiated cardiomyocytes show enhanced propensity to re-enter the cell cycle, we utilised a known mediator of cardiomyocyte dedifferentiation – OSM – to explore whether adult cardiac myocytes can in principle be induced to proliferate by Nox4D overexpression.

Multiple attempts were required to establish a robust model of dedifferentiated adult myocytes in vitro. The key factor that enabled the realisation of dedifferentiation was the removal of the myosin II ATPase inhibitor BDM[294] from the medium after 48 hours in culture. Thus, isolated cardiomyocytes were cultured in BDM-containing medium for the initial recovery period only as it was observed that this was associated with increased viability.

Isolated WT adult mouse cardiomyocytes were initially treated with an incremental concentration of OSM 48 hours post-isolation for determination of the optimal conditions for the proposed dedifferentiation protocol. Compared to untreated control cells, incubation with OSM was associated with striking morphological changes characterised by a substantial increase in cell size and expansion by formation of multiple extensions from the cell body. Visualisation by brightfield microscopy revealed the first changes of rounding and extension in individual myocytes within 2 days of exposure to OSM. By 6 days, nearly all cardiomyocytes showed transformation to a dedifferentiated phenotype. This was accompanied by a concentration-dependent downregulation in sarcomeric structures and re-expression of dedifferentiation markers, as observed by immunofluorescence staining for α-actinin and α-smooth muscle actin after 8 days of treatment with OSM, respectively. The lowest effective concentration of OSM (50 ng/mL) was selected as the optimum concentration for further experiments. Untreated cardiomyocytes also progressively demonstrated cellular expansion and some structural rearrangement during the defined culture period, although considerably less pronounced in conjunction with greater retention of expression of α-actinin in comparison to OSM-stimulated myocytes (Figure 5.7).

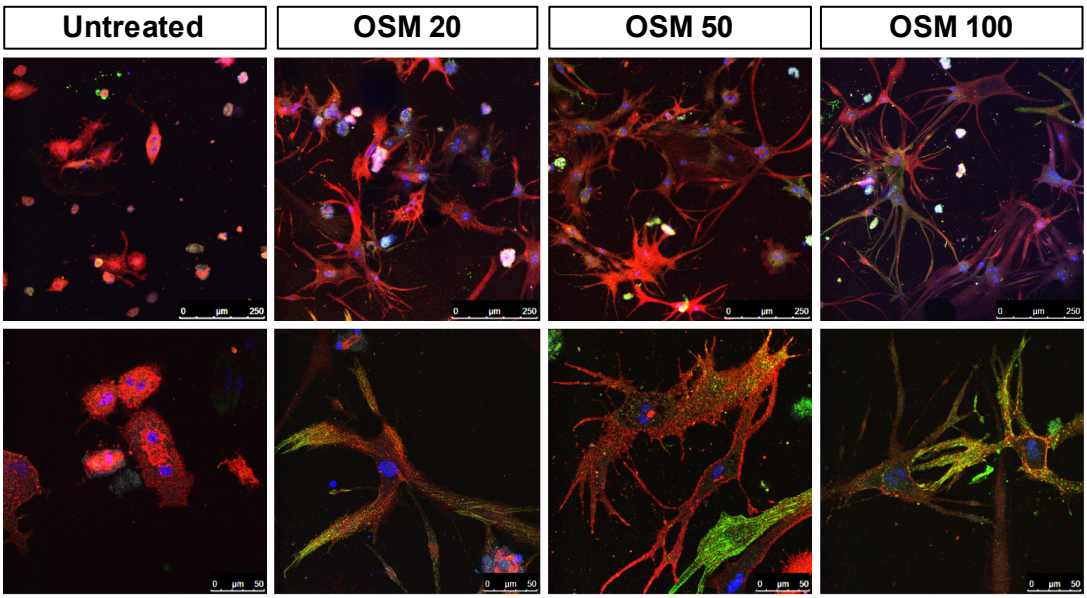

Figure 5.7. Oncostatin M induces dedifferentiation of adult mouse cardiomyocytes. Representative images of immunofluorescence staining for dedifferentiation marker α-smooth muscle actin (green) with α-actinin (red) as a cardiomyocyte marker and DAPI (blue) as a nuclear marker in isolated WT adult mouse cardiomyocytes after 8 days in culture, during which cells were treated with an oncostatin M (OSM) dose response (at 20, 50, and 100 ng/mL) for 6 days after an initial 48-hour recovery period. Scale bars: 250 µm (upper), 50 µm (lower). n = 1.

To explore the effects of Nox4D overexpression on the cell cycle progression of dedifferentiated adult myocytes, we employed and adapted a protocol previously shown to promote proliferation of dedifferentiated *neonatal* myocytes. Cardiomyocytes were isolated from adult male and female WT and constitutive csNox4D Tg mice, plated and allowed to recover for 2 days, then treated with OSM for 6 days before final exposure to FGF2 as a stimulus for S-phase entry. The culture medium was supplemented with EdU for the final 2 days to capture S-phase events.

Cell size was measured as an initial readout to assess the potential effects of Nox4D overexpression on the morphological properties of dedifferentiated cardiomyocytes. Compared to untreated controls, treatment with OSM alone and OSM plus FGF2 induced a significant increase in the cell size of cardiomyocytes isolated from WT mice. The same response was also elicited in cardiomyocytes isolated from csNox4D Tg mice. Treatment with FGF2 alone was also associated with a trend for increased cell size in both WT and csNox4D cardiomyocytes compared to respective control, although not significant. No differences were observed between cultured WT and csNox4D cardiomyocytes in any of the experimental conditions (Figure 5.8).

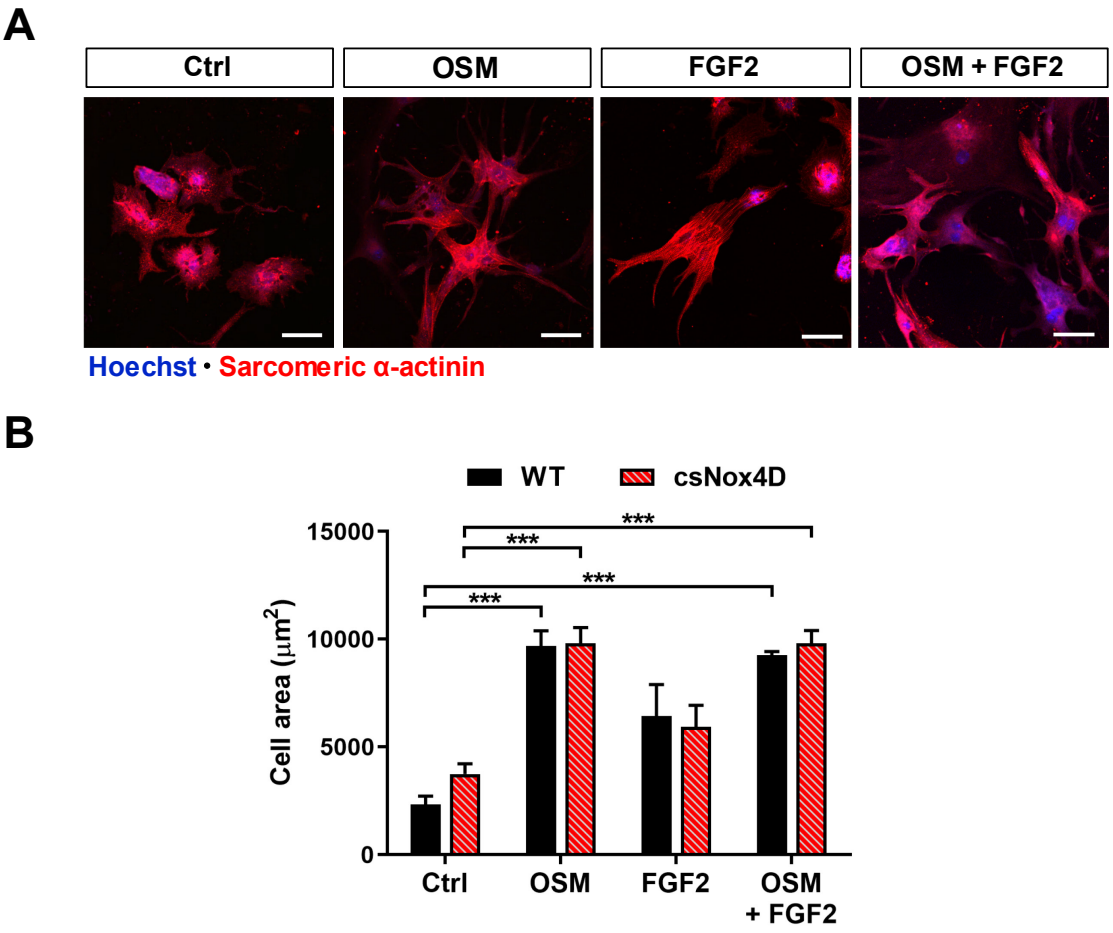

Figure 5.8. Cell size is unchanged in dedifferentiated Nox4D-overexpressing cardiomyocytes. (A) Representative images of immunofluorescence staining for cardiomyocyte marker α-actinin (red) with Hoechst (blue) as a nuclear marker in isolated WT adult mouse cardiomyocytes cultured in the presence of oncostatin M (OSM) 50 ng/mL for 6 days after an initial 48-hour recovery period, followed by further treatment with fibroblast growth factor 2 (FGF2) 100 ng/mL for an additional 2 days. Cardiomyocytes treated with only FGF2 for the final 2 days served as controls. Scale bars: 50 μm. (B) Quantification of cell area of adult cardiomyocytes isolated from WT and csNox4D transgenic mice cultured as in (A). Cell area is unchanged in Nox4D-overexpressing cardiomyocytes. n = 3 (WT), 4 (csNox4D). Data represent mean ± SEM. ***P<0.001 by two-way ANOVA with Bonferroni's post hoc correction.

The capacity for Nox4D overexpression to promote proliferation of adult cardiomyocytes in the setting of dedifferentiation was primarily quantified by EdU incorporation as a marker of cells that have demonstrated cycling through S-phase of the cell cycle. Cells were also immunostained with sarcomeric α-actinin to verify cardiomyocyte identity.

Interestingly, in the absence of treatment, the number of EdU-positive csNox4D cardiomyocytes showed an upward trend compared to that in WT cardiomyocytes, suggesting the possibility of a Nox4D-related effect even without OSM-induced dedifferentiation. Surprisingly, compared to control cells, pretreatment with OSM alone was not associated with an increase in EdU incorporation in either WT or csNox4D myocytes, and additional treatment with FGF2 neither conferred an additive effect. However, it was generally observed that prior incubation with OSM seemed to be associated with a greater preservation of viable cardiomyocytes for the duration of the culture protocol, as observed by a reduced increase in the number of rounded dead cells compared to that in untreated cells by microscopy. A somewhat unexpected result was observed in csNox4D cardiomyocytes after incubation with FGF2 alone for the final 2 days. In this condition, the number of csNox4D cardiomyocytes with EdU positivity showed a strong upward trend in comparison to WT cardiomyocytes, although this individual comparison was not significant (overall two-way ANOVA source of variation: genotype; $P < 0.05$). The number of FGF2-treated, EdU-positive csNox4D cardiomyocytes was also significantly greater than when pretreated with OSM (Figure 5.9).

Overall, it is also important to note certain morphological observations that in some cases, EdU-positive nuclei demonstrated an appearance possibly indicative of mitotic division, such as that in the micrograph shown for OSM-treated csNox4D myocytes. Furthermore, EdU-positivity was often seen in myocytes with reduced α-actinin expression, potentially suggesting greater sarcomeric disassembly as an important factor for myocyte proliferation (Figure 5.9A).

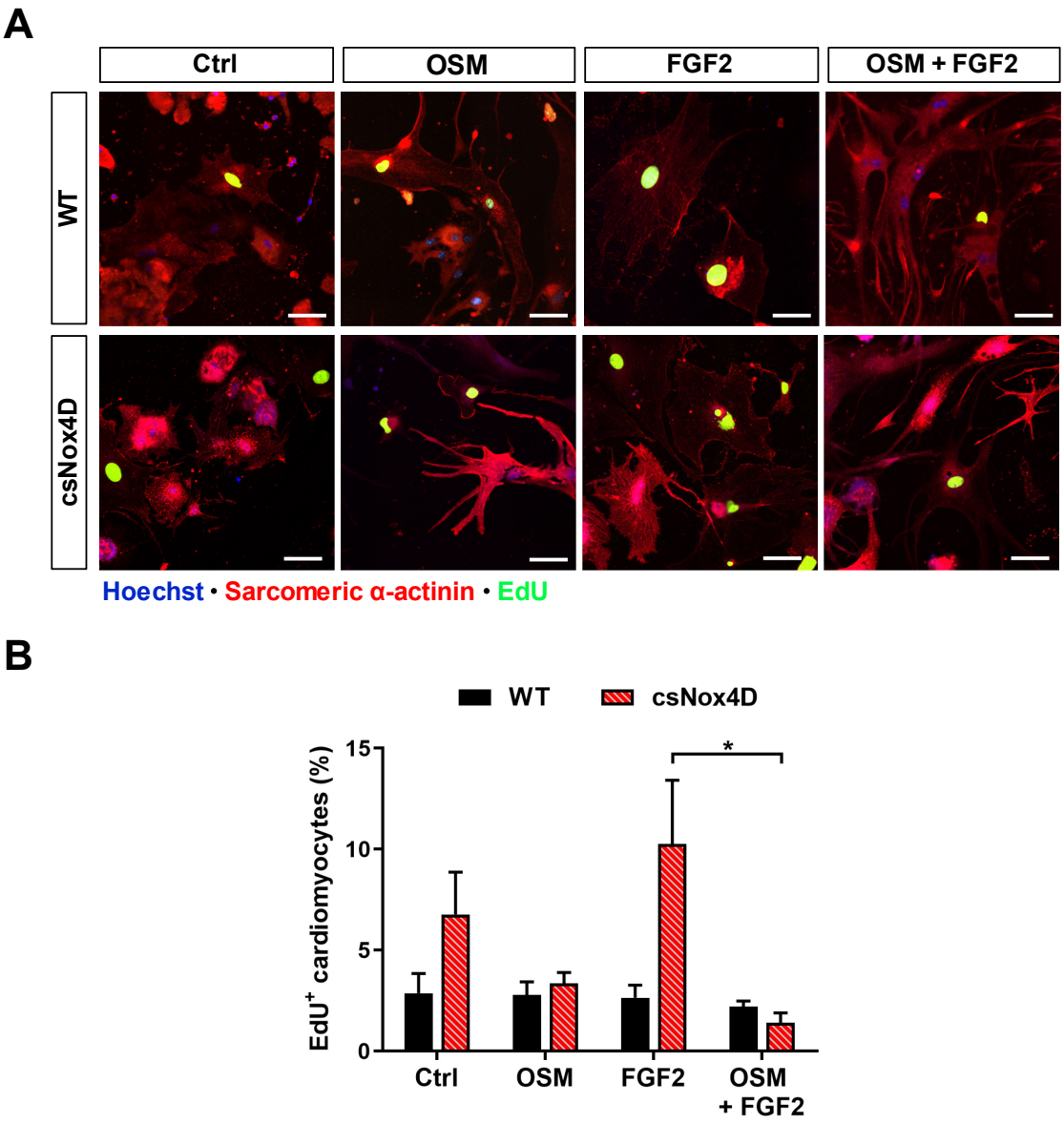

Figure 5.9. Nox4D overexpression increases DNA synthesis in dedifferentiated cardiomyocytes. (A) Representative images of immunofluorescence staining of 5-ethynyl-2'-deoxyuridine (EdU) (green) incorporation, labelling cells that have synthesised DNA, with α-actinin (red) as a cardiomyocyte marker and Hoechst (blue) as a nuclear marker in isolated WT control and csNox4D adult mouse cardiomyocytes cultured in the presence of oncostatin M (OSM) 50 ng/mL for 6 days after an initial 48-hour recovery period, followed by further treatment with fibroblast growth factor 2 (FGF2) 100 ng/mL and supplementation of all conditions with EdU 10 μM for an additional 2 days. Cardiomyocytes treated with only FGF2 for the final 2 days served as controls. Scale bars: 50 μm. (B) Quantification of the number of EdU-positive cardiomyocytes as a percentage of the total number of cardiomyocytes counted per defined area. n = 3 (WT), 4 (csNox4D). Data represent mean ± SEM. **P*<0.05 by two-way ANOVA with Bonferroni's post hoc correction.

To gain further evidence to support the proliferative potential of isolated cardiomyocytes with Nox4D overexpression, myocytes treated with the same protocol were immunostained with additional proliferation markers Ki67 and pHH3 to evaluate the proportion of cells with general cell cycling activity and the propensity to undergo division, respectively. Whilst data could not be analysed in all experimental conditions due to technical limitations, this provided a preliminary insight.

There was little difference in the number of untreated Ki67-positive WT and csNox4D cardiomyocytes. Similar to the pattern of observed EdU incorporation, neither pretreatment with OSM alone or plus FGF2 was associated with increased expression of Ki67 in WT or csNox4D dedifferentiated cardiomyocytes compared to respective control. Interestingly, a large increase in the percentage of FGF2-treated csNox4D myocytes positive for expression of Ki67 was observed in comparison to FGF2-treated WT myocytes. However, this comparison was not proven significant, likely due to the requirement for additional replicates (overall two-way ANOVA source of variation: treatment stimulus; $P = 0.0771$) (Figure 5.10). Likewise, although partially a limited analysis, the pattern of data for expression of pHH3 was in agreement with that for Ki67 and EdU incorporation. Compared to WT control myocytes, active stimulation of dedifferentiation with OSM or OSM plus further treatment with FGF2 was associated with no change in the percentage of pHH3-positive cells. The same rise was seen in csNox4D myocytes treated with FGF2, demonstrating that these cells were also positive for pHH3, suggestive of active G2/M-phase transition (Figure 5.11).

Again, similar morphological patterns were observed in that dedifferentiated cardiomyocytes demonstrating nuclear positivity for Ki67 or pHH3 often in conjunction showed reduced expression of sarcomeric α-actinin. Notably, some clustered formations of positive cells often of smaller size were observed, such as those in the micrograph shown for FGF2-treated, Ki67-expressing csNox4D myocytes (Figure 5.10A), and FGF2-treated, pHH3-expressing csNox4D myocytes (Figure 5.11A).

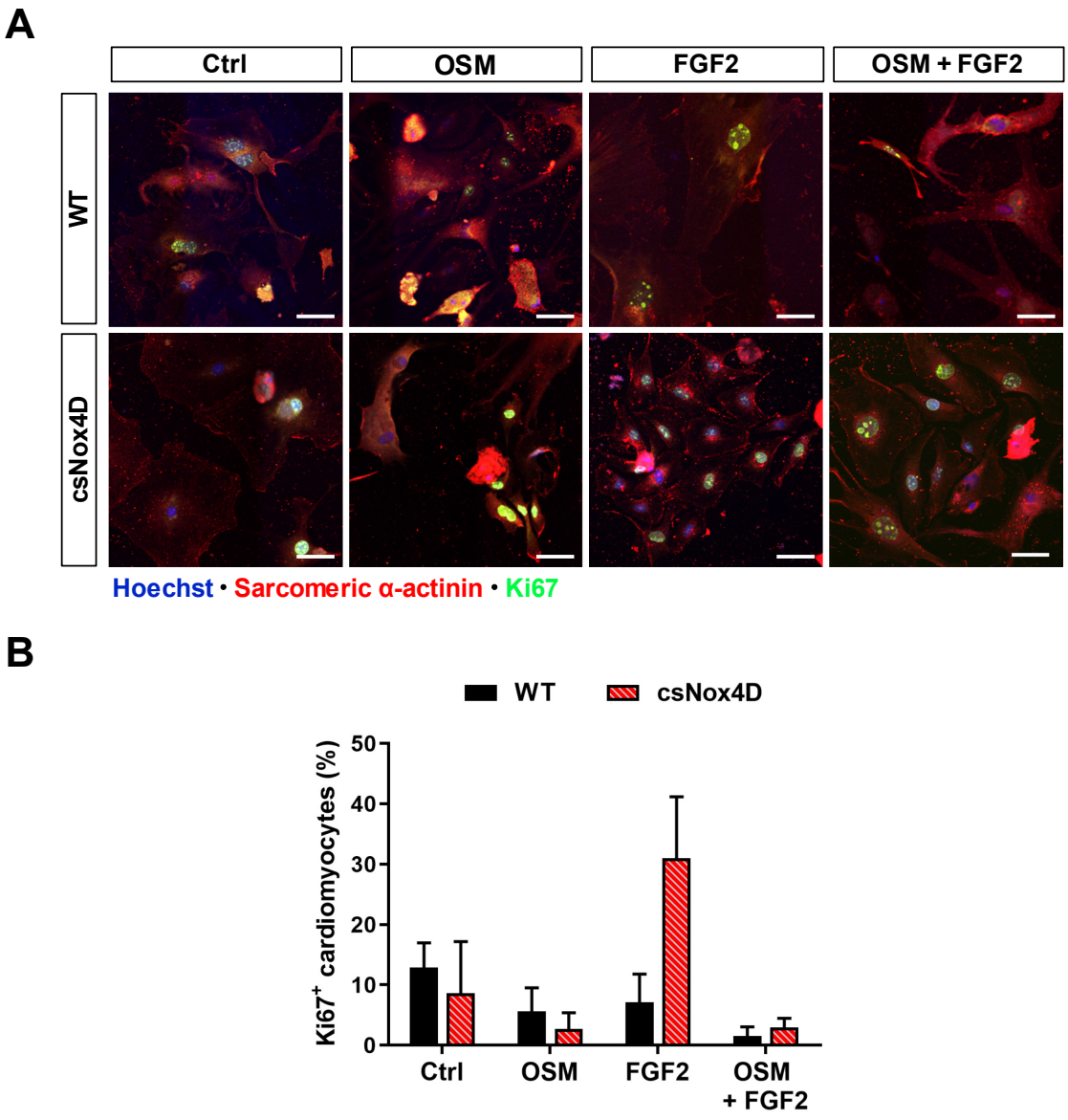

Figure 5.10. Nox4D overexpression promotes cell cycling in dedifferentiated cardiomyocytes. (A) Representative images of immunofluorescence staining of cell proliferation marker Ki67 (green) with α-actinin (red) as a cardiomyocyte marker and Hoechst (blue) as a nuclear marker in isolated csNox4D and WT control adult mouse cardiomyocytes cultured in the presence of oncostatin M (OSM) 50 ng/mL for 6 days after an initial 48-hour recovery period, followed by further treatment with fibroblast growth factor 2 (FGF2) 100 ng/mL for an additional 2 days. Cardiomyocytes treated with only FGF2 for the final 2 days served as controls. Scale bars: 50 µm. (B) Quantification of the number of Ki67-positive cardiomyocytes as a percentage of the total number of cardiomyocytes counted per defined area. n = 2 (WT), 3 (csNox4D). Data represent mean ± SEM. Statistical analysis by two-way ANOVA with Bonferroni's post hoc correction.

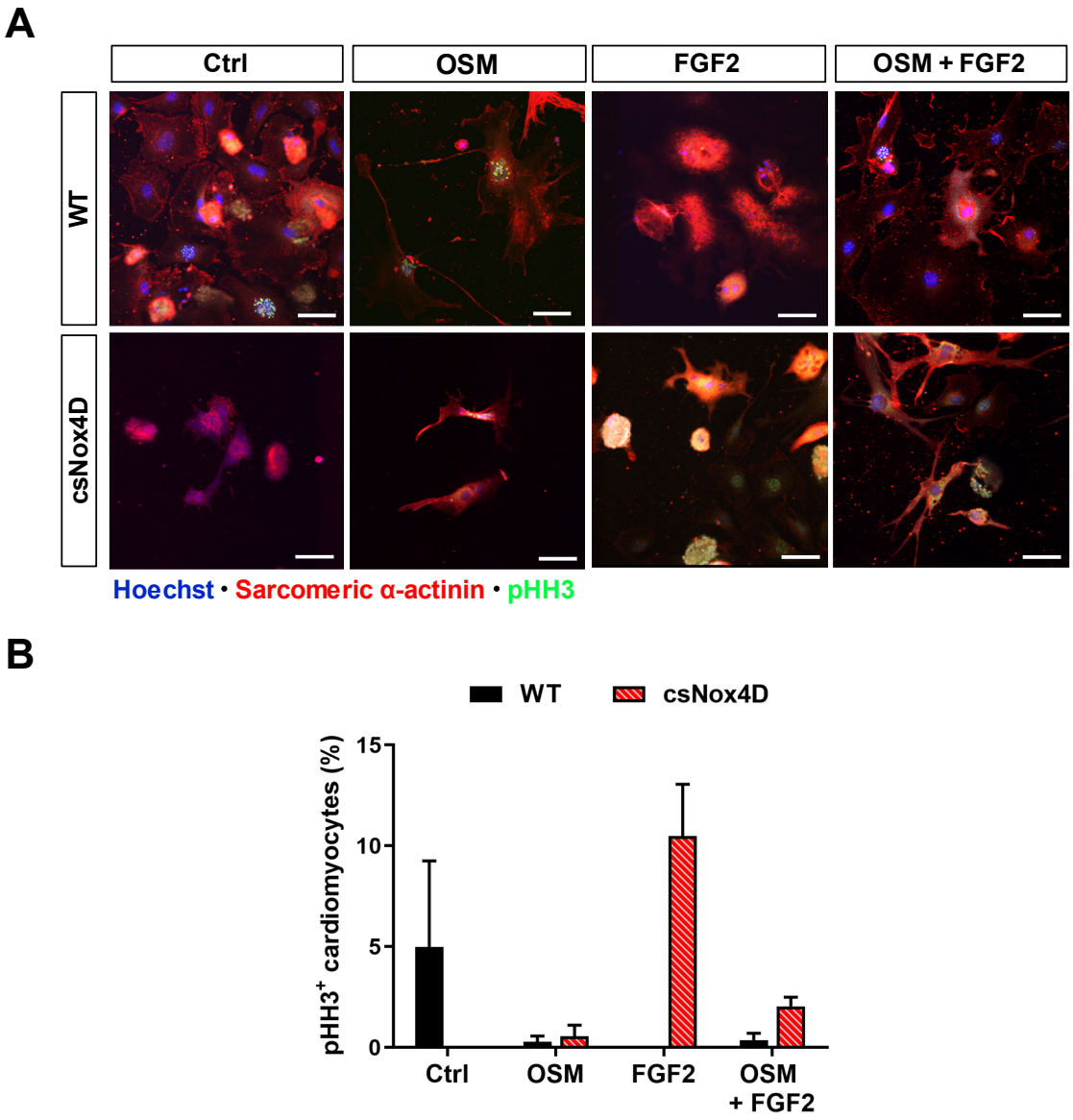

Figure 5.11. Nox4D overexpression is associated with enhanced proliferation in dedifferentiated cardiomyocytes. (A) Representative images of immunofluorescence staining of cell proliferation marker phospho-histone H3 (pHH3) (green) with α-actinin (red) as a cardiomyocyte marker and Hoechst (blue) as a nuclear marker in isolated csNox4D and WT control adult mouse cardiomyocytes cultured in the presence of oncostatin M (OSM) 50 ng/mL for 6 days after an initial 48-hour recovery period, followed by further treatment with fibroblast growth factor 2 (FGF2) 100 ng/mL for an additional 2 days. Cardiomyocytes treated with only FGF2 for the final 2 days served as controls. Scale bars: 50 μm. (B) Quantification of the number of pHH3-positive cardiomyocytes as a percentage of the total number of cardiomyocytes counted per defined area. n = 2 (WT), 3 (csNox4D). Data represent mean ± SEM. Statistical analysis by two-way ANOVA with Bonferroni's post hoc correction.

5.5 Discussion

The work of this chapter collectively details the techniques developed for the manipulation of Nox4D in vitro. Here, we provide further data based on a gain-of-function approach outlining a role for Nox4D in the modulation of cell cycle progression of adult cardiomyocytes when subjected to dedifferentiation. We also demonstrate the susceptibility of Nox4D expression to silencing in the long-term development of converse studies on the effects of loss-of-function.

5.5.1 Targeted siRNA mediates Nox4D knockdown

RNA interference has become a widely applied approach for target-specific knockdown of gene expression.[295] In this study, the establishment of siRNA-mediated Nox4D knockdown presented several technical challenges that required extensive optimisation. Given that the proper selection of a target sequence for a chosen gene of interest represents one of the most critical components of successful gene silencing,[296] the specific targeting of Nox4D splice variant is fundamentally limited by its lack of uniqueness in base sequence in comparison to full-length Nox4.[153] This is compounded by the relatively low levels of abundance of endogenous Nox4D, impeding its detection. Nevertheless, careful optimisation of these limiting factors enabled the successful targeting and assessment of Nox4D expression, demonstrating reliable evidence of Nox4D knockdown at both mRNA and protein level.

Direct translation of the designed siRNA sequence to the corresponding shRNA expression construct was undertaken for incorporation into AV and AAV9 delivery vectors as a means of obtaining enhanced transduction efficiency and prolonged gene transfer[297] in cardiomyocytes and other cell types for further study on the functional effects of endogenous Nox4D. This is especially pertinent for adult cardiomyocytes since these cells are generally considered poorly permissive to non-viral transfection techniques, especially in their terminally differentiated phenotype.[284] As such, adenoviral[298–300] and AAV9-based techniques[301] are associated with much more efficient transduction of adult myocytes, mainly in vitro and in vivo, respectively. Attempts were initially made to validate the resulting shRNA sequence, since conversion from siRNA to shRNA does not guarantee the retention of silencing efficacy,[295] however this was limited by poor tolerability of the AAV2-shRNA plasmid in vitro, and so will directly be readdressed as a primary readout in the future assessment of viral transduction and knockdown capability.

5.5.2 Isolated adult cardiomyocytes adapt to maintain viability in culture

We employed a recently published, Langendorff-free method for the isolation of viable cardiac myocytes from the adult mouse heart for their study ex vivo.[163] After an initial period of in-house optimisation and development of the required technique, this was able to reproducibly achieve average yields of 70% rod-shaped cells, leading to highly pure myocyte fractions of calcium-tolerant, healthy cells with organised sarcomeric striations. This is conducive to attainment of the key goal of primary adult cardiomyocyte culture, defined as the production of a homogeneous cell population that is amenable to maintenance over an extended time frame in exceedance of the acute isolation.[284] This also importantly enables a period of recovery from the stresses of the isolation procedure induced by enzymatic digestion and physical disruption.[302] Thus, for our adult myocyte cultures to be sufficiently successful to allow the measurement of parameters after a prolonged duration, it was paramount for the initial quality and myocyte yield of the isolation procedure to be as high as possible in order to overcome the significant loss in total myocyte number seen during the first week of culture.[299,303] The viability of isolated cardiomyocytes in culture over the duration of the protocol was validated after recovery in the presence of BDM, as evidenced by exclusion of the dyes trypan blue and 7-AAD at 72 hours post-isolation, as well as 8 days after removal of BDM from the medium as shown by morphological adaptation.

It is known that after successful isolation, plating and culture, isolated adult cardiac myocytes undergo extensive morphological rearrangement in adaptation to culture conditions.[282–284] We reproducibly demonstrated the induction of dedifferentiation in cultured adult cardiomyocytes, both untreated and actively stimulated by OSM; an important observation that was only realised after removal of BDM from the culture medium. Such a finding has also been observed by other groups,[163,299] and implies some information regarding the mechanism by which cardiomyocytes begin to dedifferentiate. Inhibition of myosin II ATPase by BDM prevents strong cross-bridge formation and damage due to terminal contracture and energy expenditure.[284,294] Although addition of BDM to the culture medium has been shown to improve the number and morphology of isolated cells,[304,305] it is essential that it is removed from the medium before measurement of parameters such as those relating to contractility or calcium transients. The disadvantage of its removal is that several myocytes are lost due to hypercontraction,[163] but given that rearrangement of the contractile apparatus is a hallmark feature of cardiomyocyte dedifferentiation, it follows that this would seem dependent on the mobilisation of contractile proteins enabled by relief of myosin II ATPase inhibition.

We observed that dedifferentiation of adult cardiomyocytes ex vivo is associated with enhanced viability, as cells adapt to the culture environment through outward spreading

and expansion in order to re-establish contact with adjacent cells.[187] This is agreeable with the published observation that the viability marker of angular rod-shaped morphology is only useful during the immediate phase of culture, as dedifferentiation commences by rounding of cellular edges during the first few days of culture (although subject to culture medium constituents and conditions).[163,306] This pattern of cardiomyocyte biology is therefore consistent with the theory that dedifferentiation represents a pre-programmed survival mechanism that enables protection under stress.[202] The cytokine OSM was recently identified as a major signal for the induction of cardiomyocyte dedifferentiation.[286] Consistent with the effects reported by this study,[286] we found that incubation of adult cardiomyocyte cultures with OSM was associated with significantly greater and accelerated dedifferentiation, characterised by the massive loss of sarcomeric structures and increased expression of α-smooth muscle actin coupled with enhanced formation of pseudopodia-like extensions. Compared to untreated myocytes, it was observed that OSM-treated cells were associated with a greater preservation in viability, as shown visually by a reduced loss of cells relative to the original plating number, suggesting that accelerated stimulation of dedifferentiation increases the rate of adaptation in culture.

5.5.3 The role of Nox4D in the proliferation of dedifferentiated adult cardiomyocytes in vitro

Isolated adult cardiomyocytes subjected to dedifferentiation in culture demonstrate the ability to enter the cell cycle, as primarily evidenced by EdU incorporation as a marker of S-phase activity. The clear cardiomyocyte identity of these cells is supported by 2 observations; that the isolation procedure produces a highly pure myocyte fraction which is clearly identifiable in culture,[163] and that they stain positive for expression of sarcomeric α-actinin.[307] This is in contrast to the obscurities encountered in vivo due to the cellular heterogeneity and close spatial packing within the myocardium.[81]

Whilst we were able to reproduce the characteristic OSM-induced marked elevations in cell size and changes in morphology, we surprisingly found that treatment of both WT and Nox4D-overexpressing adult cardiomyocytes with OSM alone or with FGF2 is not associated with an enhanced ability to enter the cell cycle. This was confirmed by visualisation of Ki67 and pHH3 expression in addition to EdU incorporation, and is in contrast to recent findings despite similarities in the treatment protocol and FBS inclusion.[286] However, an important difference that could account for the disparity between results is that the previously demonstrated OSM-induced increase in EdU incorporation, further increased with the addition of FGF2, was seen in neonatal cardiomyocytes.[286] The authors of this study attributed this finding to the partial induction of a cardiac-progenitor-like state, since they also found an increase in the expression of

typical progenitor cell markers, including Runx1,[308] Dab2,[309] and ckit[310] in OSM-treated cardiomyocytes.[286] Previous reports have shown that basic FGF (FGF2) signalling promotes DNA synthesis and proliferation of embryonic[311] and neonatal[312] myocytes, however in adult cardiomyocytes may be more associated with the induction of hypertrophy.[187] It is also known that the progression of neonatal to adult cardiomyocytes is characterised by a transition from proliferative to hypertrophic growth, usually termed terminal differentiation.[101] As such, one could argue that the differences in proliferation rate seen here in OSM-treated adult myocytes versus that in neonatal myocytes could be reflective of the intrinsic proliferative potential of the developmental stage of the myocyte in conjunction with the differential response to stimulation by FGF2.[27] This means that, despite OSM-mediated reversion to a more immature phenotype, dedifferentiated adult myocytes may not be able to sufficiently harness the same response to proliferative signals as elicited by neonatal myocytes, and so may be limited in response to an overall maintenance in survival, as observed here by a reduction in cell loss, as opposed to significant generation of new myocytes. Alternatively, this could also imply that dedifferentiated adult myocytes do show enhanced proliferation but at a slower rate, and so the final 2-day EdU incubation period may have been of insufficient duration for detection of maximum events.

It is important to remember that we detected that a small subpopulation of OSM-treated myocytes show evidence of potential for mitosis by expression of pHH3, also supported by microscopic observations of cellular morphology suggestive of mitosis. This illustrates that some OSM-treated myocytes show evidence of progression through the cell cycle, as opposed to events of only non-proliferative cell cycles characterised by DNA synthesis with or without karyokinesis in the absence of cell division.[81] However, this would need to be substantiated by evidence of cytokinesis.

In the study of the effects of Nox4D overexpression on the proliferation of dedifferentiated adult myocytes, the only difference detected was the consistent pattern of enhanced expression of all proliferation markers in csNox4D myocytes treated with FGF2. Although this would need to be corroborated by further work, it is intriguing that this effect was greater than when co-stimulated with OSM. FGF2 exerts many of its effects in cardiomyocytes through interaction with the high affinity type 1 FGF receptor (FGFR1). As described above, it is known that in adult myocytes, FGF2 is a potent stimulus of growth and cytoskeletal remodelling, mediating re-expression of α-smooth muscle actin whilst maintaining contractile capacity, whereas its stimulation of proliferation has been shown to occur by activation of the Ras/MAPK signalling pathway.[313–316]

Furthermore, specific morphological patterns were noted not exclusively, but more frequently in cardiomyocytes treated with FGF2. We observed 2 distinct morphological

states defined by the level and arrangement of sarcomeric α-actinin expression. The morphological state that often coincided with positive incorporation of EdU or expression of Ki67 or pHH3 is described by very diffuse and reduced expression of α-actinin (this contrast is demonstrated in the micrograph shown for FGF2-treated, EdU-positive csNox4D myocytes, Figure 5.9A). This was particularly noted in csNox4D myocytes, and is suggestive of an increase in sarcomeric disassembly, providing additional plasticity in order to overcome steric hindrance and progress through M-phase and cytokinesis.[317,318] FGF2-treated csNox4D myocytes with positivity for a proliferation marker were also often observed in clustered formations, possibly indicative of a greater rate of expansion.

As such, the finding that endogenously dedifferentiated csNox4D myocytes stimulated with FGF2 in vitro show enhanced cell cycle progression with evidence of M-phase transition is demonstrative of a Nox4D-mediated effect. This could be reflective of a greater sensitivity to FGF2-mediated signalling via nuclear-localised, ROS-mediated potentiation of kinase activation.[154,198] It would also seem that the extent of dedifferentiation is important as the effect is much greater than with dual treatment with OSM and FGF2. For greater translatability to the in vivo setting, it would be necessary to study whether the proliferation of dedifferentiated csNox4D cardiomyocytes equates to redifferentiation to a functional phenotype with restoration of contractility. Based on previous reports, it is likely that this would require a longer culture period or a trigger such as a hypertrophic signal[187] or intercellular gap junction communication.[202] For a deeper understanding of the mechanisms underlying these findings, it would be essential to employ the developed adenoviral vector for establishment of Nox4D knockdown in isolated WT cardiomyocytes as a loss-of-function approach.

In conclusion, the findings of this chapter are supportive to existing evidence that dedifferentiation of adult cardiomyocytes provides the stability to survive under situations of stress. Logically, it would seem to play an important role in cardiomyocyte cell cycle progression since the process of sarcomeric breakdown must be necessary for proliferation. However, it remains to be understood how the effects and extent of dedifferentiation may be modulated to provide the optimal balance for proliferation of adult cardiomyocytes, and how this may be influenced by other signalling pathways.

Chapter 6 General discussion

6.1 Summary of findings

The pathophysiology of heart failure is underscored by the inability of the adult mammalian heart to regenerate lost or damaged myocardium.[78] The classical paradigm that the adult heart is a terminally differentiated organ has been convincingly overturned by an increasing body of evidence suggesting that postnatal and mature cardiomyocytes are capable of renewal, albeit at a low level.[42] However, heart failure remains a global public health problem as this level of intrinsic cardiomyocyte turnover is insufficient for the restoration of contractile function.[21,78] Whilst current interventions, including angiotensin-converting enzyme inhibitors, beta blockers, and cardiac resynchronisation therapy, reduce mortality, they fail to address the underlying damage such as that caused by a major cardiac event, and are therefore non-curative.[21] At present, the only established method to replace lost cardiomyocytes is cardiac transplantation, which is usually reserved for severe heart failure. Given the insufficient availability of donor organs and significant complications associated with organ rejection, the development of novel therapeutic strategies that restore functional and structural integrity by repopulation of the damaged heart with replacement cardiomyocytes has been a long-standing goal of the cardiovascular field.[26,81]

The stimulation of endogenous mechanisms of proliferation within the resident cardiomyocyte pool as a means of sourcing viable cardiomyocytes has emerged as an attractive strategy for cardiac regeneration.[41] Therefore, in order to therapeutically target pathways that control cardiac regeneration, it is crucial to understand the endogenous mechanisms which underlie the regulation of the cardiomyocyte cell cycle.[21] In pursuit of this, we sought to investigate the effects of a novel, nuclear-localised regulator of redox signalling on cardiomyocyte cell cycle progression in the adult heart.

The work presented here describes the impact of a transgenic model of inducible cardiomyocyte-specific Nox4D overexpression at baseline and after myocardial injury. The basal characterisation of this model validated the splice variant-specific induction of Nox4D overexpression in response to tamoxifen, as confirmed by a significant increase in Nox4D protein levels in the heart. Consistent with previously published work on the characterisation of Nox4D in vitro[154] and further work in neonatal cardiomyocytes, we found that overexpressed Nox4D in vivo is localised to the nuclear and cytosolic compartments, with predominant handling within the nucleus. Ind-csNox4D mice demonstrate a similar cardiac phenotype to their WT counterparts in terms of contractility, structure, and gross morphology, suggesting that this level of Nox4D expression is well-tolerated in the adult heart. However, in the absence of injury, the Ind-csNox4D model is not overtly associated with an enhanced propensity for cardiomyocyte dedifferentiation or proliferation.

Next, to investigate whether the role of cardiomyocyte-targeted Nox4D would become apparent in the context of injury, Ind-csNox4D mice were subjected to permanent LAD coronary artery ligation to induce MI. We selected this model of injury as MI is a prevalent major cardiovascular event associated with significant cardiomyocyte loss and robust long-term remodelling, and is therefore a clinically relevant model for the development of heart failure.[210,319] The LV functional responses of the mice to MI were analysed in detail by speckle-tracking echocardiography, starting with simple volume-dependent indices and global measurement of longitudinal strain, then progressing to more sensitive indices at the regional level by segmental analysis of longitudinal and radial strain rate.[258] Interestingly, Ind-csNox4D mice show an improved functional response after MI, as signified by enhanced ejection fraction and GLS at 2 weeks, but this effect is transient and no longer present at 4 weeks. However, although a global improvement in function is not maintained, Ind-csNox4D mice do show evidence of region-specific differences in longitudinal and radial strain rate 4 weeks post-MI compared to WT controls within the anterior base of the LV, demonstrative of localised enhanced contractility.

This mode of functional recovery seen in Ind-csNox4D mice correlated with a partial reparative response during postinfarction remodelling, consisting of trends for reduction in LV mass, decreased cardiomyocyte area, and downregulated transcript expression of markers of failure in the infarct border and remote zones in the absence of morphometric changes. Furthermore, Ind-csNox4D hearts demonstrate a trend for enhanced propensity for anti-apoptotic signalling and increased myocardial capillarisation in conjunction with a significant reduction in cardiac fibrosis. However, this collective pattern of seemingly regionalised effects is not coupled with, or mediated by, an augmentation in cardiomyocyte proliferation. We were not able to detect a role for Nox4D to promote cardiomyocyte dedifferentiation and cell cycle re-entry in the adult mammalian heart even when primed with an injurious stimulus.

Given the lack of effect on cardiomyocyte renewal in vivo, we conducted further study to address the possibility that too high a level of overexpression of a ROS-generating enzyme within the nucleus may be linked to deleterious consequences.[131,154] However, despite the potential dose dependency association between tamoxifen with ROS production and DDR signalling, this does not appear attributable to the levels of MCM activation or Nox4D induction, and neither do these effects seem to be associated with enhanced antioxidant signalling or cell death. As such, this would imply that the partial nature of the response afforded by cardiomyocyte-specific Nox4D overexpression after MI is not due to inhibitory effects of excessive ROS exposure, and may involve contribution from other factors.

In an attempt to assess in a more controlled model whether Nox4D is able to stimulate proliferation of cardiomyocytes in the adult versus the neonatal setting, this was tested further in vitro. We utilised an ex vivo model of isolated adult cardiomyocytes for the induction of dedifferentiation in culture as a means to assess the capacity of Nox4D to enhance their proliferative potential, and provide an experimental platform that would facilitate elucidation of the underlying ROS-dependent molecular mechanisms involved at the cellular level.

Consistent with previous studies,[163,284] the induction of dedifferentiation of adult cardiomyocytes in vitro, both without treatment and actively stimulated by OSM, is associated with prolonged viability, enabling protection from the stress of isolation as cells undergo morphological adaptation to the culture environment in order to avoid unfavourable mechanical distortion.[187] Adult cardiomyocyte dedifferentiation is accelerated in culture by incubation with OSM, which regulates reversion to a more immature state characterised by loss of pre-existing sarcomeric structures in conjunction with re-expression of foetal genes and elongation towards neighbouring cells for re-establishment of cell-to-cell contacts.[286] We found that dedifferentiated adult myocytes demonstrate the capacity to re-enter the cell cycle, as primarily evidenced by DNA synthesis.[81] Whilst we observed that treatment of both WT and Nox4D-overexpressing adult cardiomyocytes with OSM alone or with FGF2 is not associated with enhanced proliferative capacity in comparison to control untreated myocytes, we found a consistent pattern of enhanced expression of proliferation markers in Nox4D myocytes treated with FGF2. This effect is therefore likely suggestive of a redox interaction between FGF2-mediated proliferative signalling pathways and compartmentalised ROS release by Nox4D.

6.2 Physiological impact of inducible Nox4D overexpression in the adult mammalian heart

6.2.1 Nox4D is linked to cardiomyocyte proliferation in a context-dependent manner

Our preliminary findings indicate that Nox4D increases the proliferation of neonatal cardiac myocytes. By overexpressing Nox4D in vitro, neonatal myocytes show enhanced proliferative capacity by characteristic changes in cell size and cell number, increased expression of markers of cell cycle progression, and increased activation of the PI3K/Akt signalling pathway and downstream targets.

The NADPH oxidase enzyme complex uses NADPH as an electron donor to produce $O_2^{\bullet -}$ and H_2O_2 from molecular oxygen. Compared to other redox enzymes that produce

ROS as by-products, Noxs are the only known mammalian enzyme system dedicated to the generation of ROS.[131,145] It is now recognised that ROS generated by Nox enzymes are involved in intracellular signalling processes that regulate cellular differentiation and proliferation.[145] Nox4D has been demonstrated to be localised to the nucleus in neonatal myocytes and other cardiovascular cell types, although the mechanisms underlying its intracellular trafficking remain unclear,[154] but could reflect differences in the subcellular targeting of Nox isoforms as a function of site-specific requirements for ROS.[153] As discussed in *3.4.2*, it is of interest that many protein phosphatases are highly enriched in, or even exclusive to, the nuclear subcellular compartment, where they regulate various processes by dephosphorylation of key substrates. A number of roles of nuclear protein phosphatases have been outlined, such as modulation of stress response pathways, RNA processing, and gene transcription. Also, many nuclear protein phosphatases, including protein phosphatase 1 (PP1), PP2A, Cdc25, and Cdc14, have pivotal roles in the regulation of cell cycle progression, as this is highly controlled by reversible protein phosphorylation.[320] The susceptibility of phosphatases as protein sensors to Nox-derived signalling ROS is well recognised,[151,198] and so the redox modulation of nuclear protein phosphatases would seem a likely target for nuclear-localised Nox4D.

Akt is a key player in signal transduction pathways that are activated in response to various stimuli, including growth factors and cytokines, and is therefore considered to be centrally involved in numerous cellular functions including proliferation and survival. The activation of downstream effectors that mediate such pathways is dependent on the translocation of phosphorylated Akt to the nucleus, where it may be inactivated by dephosphorylation of threonine residues by PP2A.[321] Indeed, the impact of nuclear Akt has been demonstrated in the myocardium, in which cardiac-specific expression of nuclear-targeted Akt was associated with increased cardiomyocyte cycling.[124] In light of these findings, it is plausible to reason that the Nox4D-dependent activation of Akt seen in neonatal cardiomyocytes may represent a potentiation mechanism for downstream proliferative signalling within the nucleus via redox-inhibition of Akt dephosphorylation.

However, given that overexpressed Nox4D is also localised in part within the cytosol, the effects on proliferation may also be mediated by cytosolic redox pathways.[154] Nox-mediated signal transduction mechanisms involved in proliferation may also function through amplification of receptor tyrosine kinase (RTK)-mediated processes by inhibition of another class of phosphatases, the PTPs. This would therefore seem complementary to the proposed mode of Nox4D-mediated nuclear Akt activation, since Akt may be phosphorylated downstream of RTK stimulation.[145,321] H_2O_2 is a mild oxidant and has been shown to target PTPs as they contain sensitive cysteine residues that are

vulnerable to oxidation. All PTPs contain an essential cysteine residue within the signature active site motif that is essential for their catalytic function, oxidation of which leads to enzymatic inactivation and potentiation of proliferative signalling cascades mediated by RTKs.[322]

PTEN is an important redox-regulated PTP that plays a negative regulatory role in signalling pathways involved in cell growth,[323] inhibition of which has been shown to mediate cardiomyocyte proliferation in embryonic, postnatal, and adult hearts.[100] PTEN cleaves the phosphoinositide second messenger – phosphatidylinositol 3,4,5-triphosphate (PIP_3) – as its substrate to reverse the action of PI3K.[323] Interestingly, the potentiation of Akt activation secondary to PTEN inhibition by Nox-derived ROS has been directly shown in a cellular model of Nox1 overexpression.[324] Thus, it could be postulated that oxidative inhibition of PTEN represents a complementary mechanism underlying enhanced proliferation in Nox4D-overexpressing neonatal myocytes by increasing the proportion of activated Akt that can translocate to the nucleus.

Moreover, it is intriguing that RTK activation in response to growth factor stimulation can induce the rapid and transient production of ROS, as ROS are required for growth factor-induced tyrosine phosphorylation.[323,325] Furthermore, ROS have been found to activate RTKs in a ligand-independent manner through transactivation,[322] such that addition of H_2O_2 has been shown to augment intracellular tyrosine phosphorylation levels and induce cell proliferation in the absence of growth factor.[326] Therefore, it may follow that increased intracellular generation of H_2O_2 by overexpression of Nox4D may amplify Akt activation by negative regulation of PTEN independently of receptor-ligand binding. Taken together, overexpressed Nox4D may serve to potentiate signal transduction pathways downstream of Akt at multiple cellular levels.

However, when we investigated cardiomyocyte-targeted overexpression of Nox4D in the setting of the adult mouse heart, we were not able to reproduce the same effects on proliferation either at baseline or after ischaemic injury. We reasoned that this loss of phenotype could be caused by a number of factors: (i) the potential mislocalisation of Nox4D protein when overexpressed in adult cardiomyocytes; (ii) the level of Nox4D induced in this model in relation to the presumed therapeutic window of expression; (iii) the potential association between an overexpressed Nox enzyme and the deleterious effects of excessive ROS exposure; and (iv) the age at which Nox4D overexpression is induced and the susceptibility of the adult heart to redox regulation of proliferation.

Immunostaining of adult cardiomyocytes isolated from Ind-csNox4D mice revealed that the induction of Nox4D overexpression in vivo results in similar intracellular location to that in neonatal myocytes in vitro, although the precise localisation within the nucleus

and cytosol remains to be determined. To address the physiological relevance of the relative level of Nox4D protein induced in the Ind-csNox4D model by αMHC-MCM, we conducted a tamoxifen dose response experiment to investigate the potential association between Nox4D expression and harmful effects due to excessive ROS production. Mitochondrial ROS are known for their ability to cause cellular toxicity by promoting damage of macromolecules such as DNA base oxidation and single- or double-strand breaks,[327,328] and so we reasoned that an overexpressed nuclear source of ROS could be associated with the same effects if expressed too highly. Indeed, activation of the DNA damage response secondary to Nox4D overexpression was shown previously in cultured VSMCs by increased phosphorylation of H2AX at serine 139 in an oxidative-dependent manner.[154]

However, we found that this effect was not replicated in vivo in response to increasing Nox4D expression, suggesting that elevation of nuclear ROS release does not negatively regulate cardiomyocyte proliferation as a result of oxidative DNA damage, which is in contrast to what might be predicted by current theory regarding the effects of increased ROS on postnatal cardiomyocyte cell cycle withdrawal.[79,87] DDR signalling usually results in cell cycle arrest or apoptosis if the damage is too extensive to be repaired.[327] Therefore, in view of the low rates of cardiomyocyte apoptosis in sham-operated WT or Ind-csNox4D hearts, it is possible that the incidence of γ-H2AX positivity could be causally associated with cell cycle arrest if DNA damage accumulation occurs without recruitment of repair mechanisms. It would be interesting to investigate whether the association between Nox4D expression and DDR signalling changes after MI, as cardiac stress would be expected to be associated with further increased ROS production, which has previously been linked to single-strand breaks in the setting of pressure overload-induced heart failure.[272]

Lastly, to address the possibility that the lack of efficacy of Nox4D to stimulate cardiomyocyte proliferation in the adult heart is due to key differences in the developmental stage of the heart, or the age at which Nox4D overexpression is induced, we evaluated the ex vivo culture model of adult cardiomyocytes for the study of proliferation in the setting of dedifferentiation. This is especially relevant since cardiomyocyte renewal in the adult mammalian heart may not necessarily recapitulate the events of development, meaning that the capacity of certain factors that stimulate myocardial proliferation during embryonic and early neonatal life may be lost in the adult heart.[89]

Cardiomyocyte dedifferentiation is considered to enable a reduction in energy consumption due to changes in metabolism and inactivation of energy-intensive processes, thus providing protection from situations of stress such as ischaemia.[281]

Therefore, the dedifferentiation of adult cardiomyocytes in culture may permit simulation of the in vivo ischaemic environment of the infarct border zone in which surviving myocytes have uncoupled from the myocardium and are at high risk of cell death.[202] In this setting, our findings on cultured cardiomyocytes provide evidence to support a role for Nox4D in the potentiation of FGF2-induced adult cardiomyocyte proliferation.

Based on this observation, it could be speculated that Nox4D may either promote the dedifferentiation process itself, or enhance proliferation through FGF2-mediated signalling. In agreement with the proposed mechanism of action in neonatal cardiomyocytes, the latter pathway would seem more likely. The capacity of diffusible factors such as FGF2 to exert a mitogenic effect on cardiomyocytes has been mostly obtained in neonatal cardiomyocytes, as these cells maintain a transient proliferative capacity after isolation.[27] In contrast, the proliferative activity of FGF2 in the adult heart is largely opposed by FGF16, a member of the FGF family that is preferentially expressed postnatally with a possible role in cardiomyocyte cell cycle withdrawal after birth.[329] In support of this, we found that FGF2 is able to stimulate cell cycle activity in dedifferentiated adult cardiomyocytes, likely as a result of their reversion to a more immature state.[187] Interestingly, FGF2 is known to exert its biological effects in cardiomyocytes through interaction with the tyrosine kinase receptor FGFR1.[330] An important signal transduction pathway downstream of RTKs that mediates cell proliferation in response to growth factor stimulation is the MAPK pathway, in particular ERK1/2.[331] This pathway is activated in response to FGF2 stimulation and is therefore implicated in its mitogenic activity.[315,332] Furthermore, the activation of ERK1/2 by Nox-derived ROS has been widely reported in numerous cell types,[145] and was the first redox-sensitive signalling pathway demonstrated to be modulated within the nuclei of VSMCs by Nox4D.[154] It has also been shown that Nox4D is capable of H_2O_2 production,[154] which is the major oxidant species implicated in redox regulation of cell proliferation.[145] Therefore, as postulated in neonatal myocytes, it follows that Nox4D may act as an intracellular signal amplifier in adult cardiomyocytes subjected to gradual dedifferentiation in culture that potentiates proliferative signalling through FGF2 via redox inhibition of PTPs. Further work is required to understand whether this effect is mediated through ERK1/2 signalling or whether additional growth factor-stimulated pathways such as PI3K/Akt are involved, which will also enable elucidation of the differential response seen in dedifferentiated myocytes actively induced by OSM.

Although this model may recapitulate dedifferentiating cardiomyocytes in the ischaemic environment in vivo, we were only able to detect some evidence for a role for Nox4D in the proliferation of dedifferentiated adult myocytes ex vivo. One reason for this could be the severity of the permanent LAD ligation model used to induce MI.[210] Another reason

for this could be an important difference in the strategies used to generate Nox4D overexpression. For our adult cardiomyocyte isolation studies, we utilised a constitutive model of cardiomyocyte-specific Nox4D overexpression in which Nox4D is overexpressed under the regulation of the Mlc2v promoter, which directs Cre recombinase expression starting at approximately E8.[160] This was preferable as we reasoned that the constitutive model may have more uniform overexpression of Nox4D whereas the inducible model may be subject to greater variation depending on the myocardial absorption and distribution of tamoxifen. However, it was later realised that in comparison to the Ind-csNox4D model, the expression level of Nox4D protein is 5-fold lower in the csNox4D model (Figure 2.8). This could have important implications for the difference in effect due to the developmental stage and relative level at which Nox4D is overexpressed. Therefore, it could be concluded overall that the capacity of Nox4D to enhance proliferative signalling pathways and cell cycle re-entry in cardiomyocytes is likely dependent on the level of expression and resulting impact on local redox balance, and possibly the maturity level of the cardiomyocyte.

6.2.2 Induction of Nox4D in the adult heart may regulate redox-dependent prosurvival signalling pathways after ischaemic injury

Our findings on the study of the response of Ind-csNox4D mice to MI suggest that Nox4D exerts partial beneficial actions in the heart characterised by locally enhanced contractile function and modulation of hypertrophy, apoptosis, fibrosis, and capillarisation. Although associated with incomplete preservation of cardiac function and recovery, these data are not coupled with a regenerative response and may instead reflect a potential prosurvival role for Nox4D in the amelioration of postinfarction remodelling.

At present, descriptions of the effects of Nox4D, or other Nox4 splice variants, in the healthy or diseased heart in the literature are very limited. A recent study aimed to characterise Nox4 expression in human explant samples from healthy and failing hearts of ischaemic or dilated origin.[333] RNA sequencing of the cardiac transcriptome revealed that the Nox4 gene is extensively spliced in heart failure with the suggestion that Nox4D may be downregulated in the ischaemic failing heart. However, this study is based on a limited sample set with significant differences in the age of the patients from which the tissues were sampled. The quantitative assessment of the detected protein isoforms may have been affected by the lack of direct sequencing evidence for their identification and discrimination from other isoforms, and the functional characterisation of these variants was neither investigated. As such, the interpretations of this study may be limited to the implication that Nox4D is expressed in the human heart.[333]

The development of cardiac remodelling in response to disease or injury involves a complex rearrangement of cardiomyocyte structure and function as well as the restructuring of the non-myocyte compartment through hallmark changes in the ECM and vasculature.[275] Maladaptive remodelling is characterised by pathological hypertrophy accompanied by disproportionate interstitial fibrosis, cardiomyocyte death, vascular dysfunction, energy deficit, and chamber dilatation.[334] Several different molecular targets of redox signalling in cardiac remodelling processes have been identified.[138] Such redox-dependent modifications can affect the structural conformation, stability, and function of signalling proteins, and have been shown to include protein kinases (e.g. MAPKs, calcium-calmodulin kinase II [CaMKII], protein kinase A [PKA], protein kinase G [PKG]), class II histone deacetylases (HDACs), and transcription factors (Figure 6.1).[275]

Cardiac hypertrophy is driven by a reprogramming of the normal pattern of cardiomyocyte gene expression, in which a number of transcription factors are involved, which are in turn regulated by a multitude of interacting signalling pathways.[242,244] Increasing evidence suggests that spatially confined ROS release may specifically target these signalling pathways, such as ERK1/2 and Akt, or may influence transcription factor binding directly, such as the dis-inhibition of Mef2-dependent prohypertrophic gene transcription via oxidation of HDACs.[131,335,336] The impact of redox pathways on fibrosis has also been demonstrated in multiple cell types, in which activation of TGF-β by ROS has been shown to promote myofibroblast transformation as well as the transcription of profibrotic factors.[131,337] Furthermore, cardiomyocyte apoptosis may in part be subject to modulation by the local redox environment.[335] ROS-dependent activation of c-Jun N-terminal kinase (JNK) in response to β-adrenoceptor stimulation in adult rat cardiomyocytes has been shown to activate the mitochondrial death pathway and cytochrome *c* release,[338] whilst apoptosis signal-regulating kinase 1 (ASK1) may be redox-activated upstream of p38MAPK and JNK to induce cardiomyocyte apoptosis (Figure 6.1).[339]

Likewise, redox pathways during cardiac remodelling are also activated to augment important protective effects. Notably, it has been shown that full-length Nox4 is capable of mediating numerous distinct prosurvival processes.[335] In response to chronic pressure overload, Nox4 was found to facilitate functional adaptation to stress by enhancement of cardiomyocyte Hif1α-Vegf signalling, which was associated with enhanced myocardial capillary density through elevated paracrine angiogenic activity.[149] This pathway is important for protection in this disease model as it is known to drive coordinated cardiac hypertrophy and angiogenesis, which are vital for the preservation of cardiac function.[340] Other targets of Nox4 in chronic cardiac stress may also involve the Nrf2-dependent

upregulation of cytoprotective genes,[152] and induction of activating transcription factor 4 (ATF4) via inhibition of PP1 to enhance cardiomyocyte survival.[151] Furthermore, studies in non-cardiomyocyte cells have shown an inhibitory role for Nox4-derived ROS in apoptosis, the mechanisms involved in which may include activation of survival kinases such as Akt (Figure 6.1).[341]

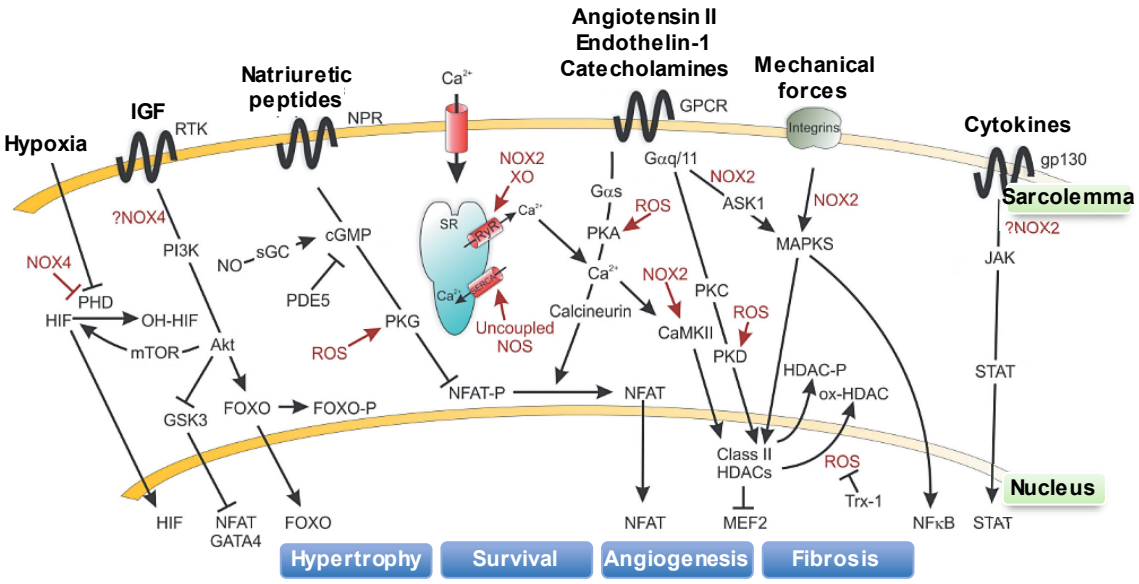

Figure 6.1. Redox regulation of stress response signalling cascades in the heart. The major stress stimuli that induce cardiac remodelling include neurohormonal agonists, mechanical forces, cytokines, growth factors, and hypoxia. Key pathways with evidence for redox regulation may affect protein translation and metabolism, but ultimately control gene expression, leading to important effects that determine whether the remodelling response is adaptive or maladaptive, including cardiomyocyte hypertrophy, survival, paracrine angiogenic signalling, and fibrosis. Redox modifications by reactive oxygen species (ROS), and source where known, of specific molecular targets are shown in red. OH, hydroxylation; Ox, oxidation; P, phosphorylation; ASK1, apoptosis signal-regulating kinase 1; CaMKII, calcium calmodulin-dependent kinase; GSK3, glycogen synthase-3; GPCR, G-protein coupled receptor; HDACs, histone deacetylases; HIF, hypoxia-inducible factor; IGF, insulin-like growth factor; MAPKs, mitogen-activated protein kinases; mTOR, mammalian target of rapamycin; NPR, natriuretic peptide receptors; NOS, nitric oxide synthases; PDE5, phosphodiesterase type 5; PI3K, phosphoinositide 3-kinase; PHD, HIF prolyl hydroxylase; PKA/C/D/G, protein kinase; RTK, receptor tyrosine kinases; SR, sarcoplasmic reticulum; Trx-1, thioredoxin-1; XO, xanthine oxidase. Adapted from Burgoyne et al, 2012.[131]

These findings reinforce the importance of source- and compartment-specific ROS signalling as functional determinants of the resulting remodelling phenotype.[342] The specificity of such signalling pathways is likely to be highly dependent on the confinement to which ROS are released, as this is lost upon excessive cellular exposure to ROS or mislocalisation of the ROS source, leading to aberrant biochemical function.[275] Interestingly, expression of a specific RTK protein in acute myeloid leukaemia (AML)

patient samples and cell lines were found to correlate with elevated ROS levels.[343] These cells showed upregulated expression of the Nox4D isoform at the nuclear membrane with increased production of H_2O_2 downstream of RTK-mediated activation of prosurvival pathways PI3K and STAT5, and possible redox potentiation of this mode of RTK signalling by inhibition of a transmembrane PTP.[343] Although in a cancer cell model, this study is particularly interesting as it implicates a pro-survival role for Nox4D-derived H_2O_2, and also suggests Nox4D as a source of ROS in response to constitutive RTK activation. Whether such ROS-dependent prosurvival signalling pathways are relevant in the partial reparative response of the Ind-csNox4D transgenic model to MI remains unclear, but poses an intriguing avenue to investigate.

Based on the current literature on the regulation of cardiac remodelling by redox signalling pathways, it would seem plausible to hypothesise that Nox4D-dependent nuclear ROS release may impact on various signalling or transcriptional processes associated with cardioprotection. In addition to proliferation, the PI3K-Akt pathway is a known regulator of cardiomyocyte survival.[119] PTEN is also known for its regulatory involvement in apoptosis in addition to cell growth.[323] Although not activated at baseline, it is possible that injurious stimulation of the Ind-csNox4D model may yield greater activation of Akt, which may preferentially favour transduction of downstream survival effectors as opposed to proliferation, but in light of incomplete restoration of function, this may more likely reflect an insufficient level of activation. Given its distinct localisation, it would be interesting to establish whether the pathways modulated by Nox4D are independent of, or complementary to those exerted by Nox4. Overall, it is clear that in depth mechanistic studies are needed to unravel the precise pathways that may be involved.

6.3 Translational implications

Although it is evident that further work is needed to fully realise whether Nox4D may hold therapeutic potential in the adult heart, considerations must be made with respect to the broader clinical picture in the advancement of regenerative interventions towards translation. The existence of intrinsic regenerative capacity in the adult mammalian heart has engendered significant interest, however the augmentation of endogenous pathways to replace the ~1 billion cardiomyocytes lost during MI is a big ambition.[18,41] The replacement of pathological cardiac tissue by induction of proliferation in surviving cardiomyocytes is a strategy that should therefore address multiple underlying repair pathways in addition to formation of new cardiomyocytes for enhancement of contractility and survival.[15] A holistic approach to reconstituting human heart function has recently been proposed, defined by a set of 5 hallmarks of cardiac regeneration that are consistently seen in organisms with innate regenerative capacity.[184] These hallmarks

include remuscularisation of the cardiac wall, electromechanical stabilisation, vascularisation by angiogenesis and arteriogenesis, resolution of fibrosis, and balanced immunological activation.[184]

Stimulation of innate programs to induce cardiomyocyte cell cycle re-entry is particularly advantageous as it enables the generation of autologous cardiomyocytes and thus facilitates their mechanical, electrical, and vascular integration within the myocardium. A significant challenge surrounds the ability of the proposed manipulation to induce genuine cardiomyocyte renewal at the required magnitude to enhance long-term myocardial outcomes and be considered therapeutically meaningful.[41] However, the large-scale dedifferentiation and electric uncoupling that would be necessary for cardiomyocyte proliferation would pose further compromise to myocardial function if prolonged.[11] A major concern that could limit pro-proliferative therapies is their oncogenic potential. Interventions should be developed to selectively target cardiomyocyte pathways, and should be intensely evaluated for assessment of their safety.[41] Genetic manipulations would require efficient gene therapy approaches, although pharmacological targeting with small molecules may be preferable, which may be locally delivered using viral vectors that are biologically targeted to the heart.[21,41]

Furthermore, in the development of therapies that may target redox pathways associated with proliferation, it is evident that a much more targeted approach than non-specific antioxidant therapy is required for the modulation of oxidant species in the heart. Given the diversity of the signalling effects of ROS, it is necessary to selectively modulate either specific ROS sources in a cell-specific or even cell compartment-specific manner, or downstream molecular pathways. The targeting of Nox enzymes would require careful development to ensure isoform selectivity and avoidance of suppression of beneficial effects that mediate protection. Likewise, an approach designed to enhance Nox function should not be associated with deleterious effects as a result of excessive ROS production. As such, it is vital that the optimum level within the therapeutic index is established to maintain the specificity and confinement of the desired redox modifications.[138,150]

6.4 Limitations and future work

It should first be mentioned that the use of the αMHC-MCM-*negative* genotype as WT control throughout this study may represent a confounding factor. This is in light of a previous study that found cardiac fibrosis and reduced LV function in αMHC-MCM-*positive* adult animals at 6 – 7 weeks following a tamoxifen injection protocol of 20 mg/kg per day for 5 days, irrespective of the presence of the floxed target gene.[344] This phenotype was attributed to the nuclear levels of the MerCreMer protein or its duration

in the nucleus, or a combination of both.[344] This is in keeping with a previously described study that also reported cardiac fibrosis and dysfunction in tamoxifen-induced αMHC-MCM mice, but at doses in excess of 30 mg/kg per day for 3 days.[274] Although we did not detect any obvious signs of αMHC-MCM-mediated toxicity in our experiments, these studies highlight the importance of including tamoxifen-treated αMHC-MCM single-genotype animals as controls, which should be implemented in future relevant studies.

The physiological relevance of the level of Nox4D protein expression induced by the tamoxifen protocol employed in this study remains to be established. Further manipulation of cardiac-targeted Nox4D expression in the Ind-csNox4D model by modulation of the tamoxifen induction dose is likely undesirable due to poor translatability and likely poor ability to control even distribution of cellular expression levels. It is possible that reducing the dose of tamoxifen may only serve to achieve reduced Nox4D expression at whole heart level, but may actually reflect a 'mosaic' pattern of expression depending on the response of individual cardiomyocytes to tamoxifen exposure, and the distribution of tamoxifen across the cardiomyocyte population.

A more translatable method would be a viral-based delivery system using an AAV9 vector for the in vivo gene transfer of Nox4D. The use of AAV9 vectors as investigational tools for transduction of the heart has become increasingly popular in recent years due to their favourable safety profile, high efficiency, and cardiotropism.[301] The expression of the transferred gene may be further confined by the use of tissue-specific promoters, which provide an added layer of control over transgene expression.[301,345] The promoters recognised so far for their ability to achieve restricted transgene expression in cardiomyocytes include the αMHC, Mlc2v, and cardiac troponin genes.[301] In comparison to αMHC, it has been demonstrated that the Mlc2v and cardiac troponin promoters yield lower transgene expression levels,[345] and so it would be preferable to design a Nox4D expression construct under the control of either of these alternative promoters. This would permit the investigation of the Nox4D overexpression phenotype in the adult heart at comparatively reduced expression, but would need to include validation of the distribution of expression. Due to the limitations associated with use of the Nox4 antibody for immunohistochemical applications, it would be necessary to use additional methods for further confirmation of Nox4D expression. This could be performed by cell fractionation, as shown previously,[154] of whole cardiac tissues or isolated cardiomyocytes. Fluorescence in situ hybridisation (FISH) could also be used to establish the spatial-temporal pattern of Nox4D expression.[346]

In order to more optimally establish whether the proliferative and reparative potential of Nox4D may be enhanced in the adult heart in vivo, it would be necessary to subject WT C57BL/6J mice to MI in conjunction with AAV9-mediated gene transfer of Nox4D. This

would permit greater elucidation of the limited response to MI seen in the Ind-csNox4D model, as AAV9-mediated delivery would be able to address currently unanswered questions regarding the effects of Nox4D expression titration. Conversely, parallel experiments using the developed AAV9 vector for in vivo silencing of Nox4D would be important for the study of the relevance of endogenous Nox4D. As discussed in *4.5.1*, a widely recognised limitation of experimental MI models is the intrinsic variability of MI infarct size. An added complication is that a given infarct size measurement can translate to a range of plasma biomarker release.[226] Cardiac magnetic resonance imaging is a non-invasive technology that can reliably and serially measure infarct size,[210] and can be performed in addition to biomarker measurement for correlative measurements. Furthermore, permanent LAD ligation is a severe model of MI and so it may be more clinically relevant to measure the response to ischaemic injury using the ischaemia/reperfusion model.[210]

Investigation of the mechanistic pathways that may be regulated by cardiomyocyte Nox4D in normal and stressed hearts is a priority. This could be addressed by screening technologies such as multicellular transcriptional analysis by RNA sequencing gene expression profiling and proteomic analysis for the identification of potential transcriptional and protein targets, respectively. Initial probing for signal transduction pathways that may be activated should include Akt, ERK1/2 and downstream targets. The measurement of proliferation in adult cardiomyocytes in vivo is renowned for its challenges associated with cellular identification and overestimation of division due to non-proliferative cell cycling.[81] Therefore, further assessment of the proliferative capacity of Nox4D in the adult heart should include more direct methods such as advanced reporter models that permit lineage tracing and measurement of cytokinesis.[95] The investigation of ROS release and potential non-specific effects in Nox4D-overexpressing hearts, particularly after MI, should also be continued.

To complement the delineation of the mechanistic pathways involved in vivo, and to fully understand the proliferative potential of Nox4D in adult cardiomyocytes, further experiments to expand sample sizes should be carried out on the dedifferentiation of cardiomyocytes ex vivo. It would be interesting to repeat the same experiment with isolated WT cardiomyocytes and overexpress Nox4D in vitro. Equally, this should also be done with our developed AV for Nox4D knockdown. As performed previously,[286] high-throughout western blotting could be used as a screening technique against a large panel of phospho-specific antibodies to establish the signalling pathways that may be upregulated in Nox4D-overexpressing myocytes in response to FGF2 stimulation. The differential cellular morphologies detected in cultured myocytes may be associated with events of mitosis, but without conclusive evidence of cytokinesis, may be representative

of polyploidisation or karyokinesis. Therefore, future analyses should include direct measurement of cytokinesis with immunofluorescent markers and time-lapse microscopy, and assessment of the ploidy and nucleation states of cardiomyocytes. For greater translatability, the ability of dedifferentiated cardiomyocytes to redifferentiate back to a functional phenotype should also be assessed. Furthermore, cardiomyocyte identity could be further verified by isolation from a cardiomyocyte-specific, fate-mapping reporter model such as GFP.[202]

Lastly, a key limitation inherent to animal studies is the use of young, otherwise healthy, homogeneous populations that lack the comorbidities and confounding drug therapies typically representative of the patient population. Increasing age is known to correlate with worsening capacity for myocardial repair, and so studies in relatively young animals can lead to false-positive results in large-animal or human studies, but can be minimised by using highly non-regenerative, aged animals.[21,347]

6.5 Conclusions

The current work presents a novel transgenic model of inducible, cardiomyocyte-specific Nox4D overexpression. Induction of Nox4D overexpression in the adult mouse heart is well tolerated, but in contrast to overexpression in cultured neonatal cardiomyocytes, is not associated with increased activity of pathways that promote proliferation under normal physiological conditions. In the setting of pathological stress induced by myocardial ischaemic injury, inducible Nox4D is again not associated with regenerative recovery, but may confer a partial reparative response characterised by regionally enhanced contractile function and increased cardiomyocyte survival. This response remains insufficient to globally restore LV function, but poses an interesting avenue to pursue in future study. Additional work in isolated cardiomyocytes importantly provides evidence that Nox4D may enhance proliferation in adult myocytes when dedifferentiated, and so the realisation of this in vivo may depend on certain priming stimuli in combination with optimal levels of Nox4D expression. However, it remains a possibility that the maturity level at which Nox4D is overexpressed may represent an ultimate limiting factor due to the underlying cell cycle regulatory networks that are differentially expressed.

The studies presented here add to accumulating evidence that NADPH oxidases play complex roles in cellular proliferation, the understanding of which requires cell-specific analysis of the temporal and spatial characteristics of their expression and function. Therefore, the further development of Nox4D as a protective Nox isoform is highly dependent on the capacity for modulation of Nox4D expression to optimise cardiomyocyte redox balance and more effectively enhance pathways that govern proliferation and survival for the promotion of regeneration and repair in the adult mammalian heart.

References

1. Kikuchi K, Poss KD. Cardiac Regenerative Capacity and Mechanisms. *Annual Review of Cell and Developmental Biology*. 2012;28(1):719–741.

2. Christoffels VM, Pu WT. Developing insights into cardiac regeneration. *Development*. 2013;140(19):3933–7.

3. Jensen B, Wang T, Christoffels VM, Moorman AFM. Evolution and development of the building plan of the vertebrate heart. *Biochimica et Biophysica Acta (BBA) - Molecular Cell Research*. 2013;1833(4):783–794.

4. Vivien CJ, Hudson JE, Porrello ER. Evolution, comparative biology and ontogeny of vertebrate heart regeneration. *npj Regenerative Medicine*. 2016;1:16012.

5. Bettex DA, Prêtre R, Chassot PG. Is our heart a well-designed pump? the heart along animal evolution. *European Heart Journal*. 2014;35(34):2322–2332.

6. Andrés-Delgado L, Mercader N. Interplay between cardiac function and heart development. *Biochimica et Biophysica Acta (BBA) - Molecular Cell Research*. 2016;1863(7):1707–1716.

7. Maillet M, van Berlo JH, Molkentin JD. Molecular basis of physiological heart growth: fundamental concepts and new players. *Nature reviews. Molecular cell biology*. 2013;14(1):38–48.

8. Zhou P, Pu WT. Recounting Cardiac Cellular Composition. *Circulation research*. 2016;118(3):368–70.

9. Bergmann O, Zdunek S, Felker A, Salehpour M, Alkass K, Bernard S, Sjostrom SL, Szewczykowska M, Jackowska T, dos Remedios C, Malm T, Andrä M, Jashari R, Nyengaard JR, Possnert G, et al. Dynamics of Cell Generation and Turnover in the Human Heart. *Cell*. 2015;161(7):1566–1575.

10. Foglia MJ, Poss KD. Building and re-building the heart by cardiomyocyte proliferation. *Development*. 2016;143(5):729–40.

11. Li M, Izpisua Belmonte JC. Mending a Faltering Heart. *Circulation Research*. 2016;118(2):344–351.

12. Zacchigna S, Giacca M. Extra- and intracellular factors regulating cardiomyocyte proliferation in postnatal life. *Cardiovascular Research*. 2014;102(2):312–320.

13. Xin M, Olson EN, Bassel-Duby R. Mending broken hearts: cardiac development as a basis for adult heart regeneration and repair. *Nature Publishing Group*.

2013;14(8):529–541.

14. British Heart Foundation. UK Factsheet. 2018;(November).

15. Broughton KM, Sussman MA. Myocardial Regeneration for Humans — Modifying Biology and Manipulating Evolution —. *Circulation Journal*. 2016;81(2):142–148.

16. Nabel EG, Braunwald E. A tale of coronary artery disease and myocardial infarction. *The New England journal of medicine*. 2012;366(1):54–63.

17. Frangogiannis NG. Pathophysiology of Myocardial Infarction. In: *Comprehensive Physiology*.Vol 5. Hoboken, NJ, USA: John Wiley & Sons, Inc.; 2015:1841–1875.

18. Laflamme MA, Murry CE. Heart regeneration. *Nature*. 2011;473(7347):326–35.

19. Lázár E, Sadek HA, Bergmann O. Cardiomyocyte renewal in the human heart: insights from the fall-out. *European Heart Journal*. 2017;0:1–10.

20. Gibbons RJ, Holmes DR, Reeder GS, Bailey KR, Hopfenspirger MR, Gersh BJ. Immediate Angioplasty Compared with the Administration of a Thrombolytic Agent Followed by Conservative Treatment for Myocardial Infarction. *New England Journal of Medicine*. 1993;328(10):685–691.

21. Cahill TJ, Choudhury RP, Riley PR. Heart regeneration and repair after myocardial infarction: translational opportunities for novel therapeutics. *Nature Reviews Drug Discovery*. 2017;10:699–717.

22. Steg PG, James SK, Atar D, Badano LP, Lundqvist CB, Borger MA, Di Mario C, Dickstein K, Ducrocq G, Fernandez-Aviles F, Gershlick AH, Giannuzzi P, Halvorsen S, Huber K, Juni P, et al. ESC Guidelines for the management of acute myocardial infarction in patients presenting with ST-segment elevation. *European Heart Journal*. 2012;33(20):2569–2619.

23. Leach JP, Martin JF. Cardiomyocyte Proliferation for Therapeutic Regeneration. *Current Cardiology Reports*. 2018;20(8):63.

24. Velagaleti RS, Pencina MJ, Murabito JM, Wang TJ, Parikh NI, D'Agostino RB, Levy D, Kannel WB, Vasan RS. Long-Term Trends in the Incidence of Heart Failure After Myocardial Infarction. *Circulation*. 2008;118(20):2057–2062.

25. Ezekowitz JA, Kaul P, Bakal JA, Armstrong PW, Welsh RC, McAlister FA. Declining In-Hospital Mortality and Increasing Heart Failure Incidence in Elderly Patients With First Myocardial Infarction. *Journal of the American College of Cardiology*. 2009;53(1):13–20.

26. Lafontant PJE, Field LJ. The cardiomyocyte cell cycle. *Novartis Foundation*

symposium. 2006;274:196–207; discussion 208-213, 272–276.

27. Pasumarthi KBS. Cardiomyocyte Cell Cycle Regulation. *Circulation Research*. 2002;90(10):1044–1054.

28. Urbanek K, Rota M, Cascapera S, Bearzi C, Nascimbene A, De Angelis A, Hosoda T, Chimenti S, Baker M, Limana F, Nurzynska D, Torella D, Rotatori F, Rastaldo R, Musso E, et al. Cardiac Stem Cells Possess Growth Factor-Receptor Systems That After Activation Regenerate the Infarcted Myocardium, Improving Ventricular Function and Long-Term Survival. *Circulation Research*. 2005;97(7):663–673.

29. Sanganalmath SK, Bolli R. Cell Therapy for Heart Failure. *Circulation Research*. 2013;113(6):810–834.

30. Madden LR, Mortisen DJ, Sussman EM, Dupras SK, Fugate JA, Cuy JL, Hauch KD, Laflamme MA, Murry CE, Ratner BD. Proangiogenic scaffolds as functional templates for cardiac tissue engineering. *Proceedings of the National Academy of Sciences*. 2010;107(34):15211–15216.

31. Srivastava D, DeWitt N. In Vivo Cellular Reprogramming: The Next Generation. *Cell*. 2016;166(6):1386–1396.

32. van Berlo JH, Molkentin JD. An emerging consensus on cardiac regeneration. *Nature Medicine*. 2014;20(12):1386–1393.

33. van Berlo JH, Kanisicak O, Maillet M, Vagnozzi RJ, Karch J, Lin S-CJ, Middleton RC, Marbán E, Molkentin JD. C-Kit+ Cells Minimally Contribute Cardiomyocytes To the Heart. *Nature*. 2014;509:337–341.

34. Nigro P, Bassetti B, Cavallotti L, Catto V, Carbucicchio C, Pompilio G. Cell therapy for heart disease after 15 years: Unmet expectations. *Pharmacological Research*. 2018;127:77–91.

35. Ptaszek LM, Mansour M, Ruskin JN, Chien KR. Towards regenerative therapy for cardiac disease. *The Lancet*. 2012;379(9819):933–942.

36. Gyöngyösi M, Haller PM, Blake DJ, Martin Rendon E. Meta-Analysis of Cell Therapy Studies in Heart Failure and Acute Myocardial Infarction. *Circulation Research*. 2018;123(2):301–308.

37. Gnecchi M, Zhang Z, Ni A, Dzau VJ. Paracrine Mechanisms in Adult Stem Cell Signaling and Therapy. *Circulation Research*. 2008;103(11):1204–1219.

38. Chen JX, Krane M, Deutsch M-A, Wang L, Rav-Acha M, Gregoire S, Engels MC, Rajarajan K, Karra R, Abel ED, Wu JC, Milan D, Wu SM. Inefficient

Reprogramming of Fibroblasts into Cardiomyocytes Using Gata4, Mef2c, and Tbx5. *Circulation Research*. 2012;111(1):50–55.

39. Jopling C, Sleep E, Raya M, Martí M, Raya A, Belmonte JCI. Zebrafish heart regeneration occurs by cardiomyocyte dedifferentiation and proliferation. *Nature*. 2010;464(7288):606–609.

40. Porrello ER, Mahmoud AI, Simpson E, Hill JA, Richardson JA, Olson EN, Sadek HA. Transient regenerative potential of the neonatal mouse heart. *Science*. 2011;331(6020):1078–1080.

41. Lin Z, Pu WT. Strategies for cardiac regeneration and repair. *Science Translational Medicine*. 2014;6(239):239rv1.

42. Doppler SA, Deutsch M-A, Serpooshan V, Li G, Dzilic E, Lange R, Krane M, Wu SM. Mammalian Heart Regeneration: The Race to the Finish Line. *Circulation Research*. 2017;120(4):630–632.

43. Bicknell KA, Coxon CH, Brooks G. Can the cardiomyocyte cell cycle be reprogrammed? *Journal of molecular and cellular cardiology*. 2007;42(4):706–21.

44. Humphrey T, Brooks G, Harper J V., Brooks G. The Mammalian Cell Cycle: An Overview. In: *Cell Cycle Control*. New Jersey: Humana Press; 2004:113–154.

45. Lodish H, Berk A, Zipursky S, Al E. Overview of the Cell Cycle and Its Control. In: *Molecular Cell Biology*. New York: W. H. Freeman; 2000:Section 13.1.

46. Barnum KJ, O'Connell MJ. Cell cycle regulation by checkpoints. *Methods in molecular biology (Clifton, N.J.)*. 2014;1170:29–40.

47. Ivanchuk SM, Rutka JT. The Cell Cycle: Accelerators, Brakes, and Checkpoints. *Neurosurgery*. 2004;54(3):692–700.

48. Lavoie JN, L'Allemain G, Brunet A, Müller R, Pouysségur J. Cyclin D1 expression is regulated positively by the p42/p44MAPK and negatively by the p38/HOGMAPK pathway. *The Journal of biological chemistry*. 1996;271(34):20608–16.

49. Pavletich NP. Mechanisms of cyclin-dependent kinase regulation: Structures of Cdks, their cyclin activators, and Cip and INK4 inhibitors. *Journal of Molecular Biology*. 1999;287(5):821–828.

50. Polyak K, Kato JY, Solomon MJ, Sherr CJ, Massague J, Roberts JM, Koff A. p27Kip1, a cyclin-Cdk inhibitor, links transforming growth factor-beta and contact inhibition to cell cycle arrest. *Genes & development*. 1994;8(1):9–22.

51. Alcorta DA, Xiong Y, Phelps D, Hannon G, Beach D, Barrett JC. Involvement of

the cyclin-dependent kinase inhibitor p16 (INK4a) in replicative senescence of normal human fibroblasts. *Proceedings of the National Academy of Sciences of the United States of America*. 1996;93(24):13742–7.

52. Reynisdóttir I, Polyak K, Iavarone A, Massagué J. Kip/Cip and Ink4 Cdk inhibitors cooperate to induce cell cycle arrest in response to TGF-beta. *Genes & development*. 1995;9(15):1831–45.

53. Poss KD, Wilson LG, Keating MT. Heart regeneration in zebrafish. *Science*. 2002;298(5601):2188–90.

54. Gonzalez-Rosa JM, Martin V, Peralta M, Torres M, Mercader N. Extensive scar formation and regression during heart regeneration after cryoinjury in zebrafish. *Development*. 2011;138(9):1663–1674.

55. Wang J, Panáková D, Kikuchi K, Holdway JE, Gemberling M, Burris JS, Singh SP, Dickson AL, Lin Y-F, Sabeh MK, Werdich AA, Yelon D, MacRae CA, Poss KD. The regenerative capacity of zebrafish reverses cardiac failure caused by genetic cardiomyocyte depletion. *Development*. 2011;138(16):3421–3430.

56. Parente V, Balasso S, Pompilio G, Verduci L, Colombo GI, Milano G, Guerrini U, Squadroni L, Cotelli F, Pozzoli O, Capogrossi MC. Hypoxia/Reoxygenation Cardiac Injury and Regeneration in Zebrafish Adult Heart. Salloum FN, ed. *PLoS ONE*. 2013;8(1):e53748.

57. Kretzschmar K, Watt FM. Lineage tracing. *Cell*. 2012;148(1–2):33–45.

58. Kikuchi K, Holdway JE, Werdich AA, Anderson RM, Fang Y, Egnaczyk GF, Evans T, MacRae CA, Stainier DYR, Poss KD. Primary contribution to zebrafish heart regeneration by gata4 + cardiomyocytes. *Nature*. 2010;464(7288):601–605.

59. Gemberling M, Karra R, Dickson AL, Poss KD. Nrg1 is an injury-induced cardiomyocyte mitogen for the endogenous heart regeneration program in zebrafish. *eLife*. 2015;4:e05871.

60. Zhao L, Borikova AL, Ben-Yair R, Guner-Ataman B, MacRae CA, Lee RT, Burns CG, Burns CE. Notch signaling regulates cardiomyocyte proliferation during zebrafish heart regeneration. *Proceedings of the National Academy of Sciences*. 2014;111(4):1403–1408.

61. Gupta V, Gemberling M, Karra R, Rosenfeld GE, Evans T, Poss KD. An injury-responsive gata4 program shapes the zebrafish cardiac ventricle. *Current Biology*. 2013;23(13):1221–1227.

62. Molkentin JD, Lin Q, Duncan SA, Olson EN. Requirement of the transcription factor GATA4 for heart tube formation and ventral morphogenesis. *Genes and Development*. 1997;11(8):1061–1072.

63. Kikuchi K, Holdway JE, Major RJ, Blum N, Dahn RD, Begemann G, Poss KD. Retinoic Acid Production by Endocardium and Epicardium Is an Injury Response Essential for Zebrafish Heart Regeneration. *Developmental Cell*. 2011;20(3):397–404.

64. Porrello ER, Mahmoud AI, Simpson E, Johnson BA, Grinsfelder D, Canseco D, Mammen PP, Rothermel BA, Olson EN, Sadek HA. Regulation of neonatal and adult mammalian heart regeneration by the miR-15 family. *Proceedings of the National Academy of Sciences of the United States of America*. 2013;110(1):187–92.

65. Strungs EG, Ongstad EL, O'Quinn MP, Palatinus JA, Jourdan LJ, Gourdie RG. Cryoinjury models of the adult and neonatal mouse heart for studies of scarring and regeneration. *Methods in Molecular Biology*. 2013;1037:343–353.

66. Yu W, Huang X, Tian X, Zhang H, He L, Wang Y, Nie Y, Hu S, Lin Z, Zhou B, Pu W, Lui KO, Zhou B. GATA4 regulates Fgf16 to promote heart repair after injury. *Development*. 2016;143:936–949.

67. Itou J, Kawakami H, Burgoyne T, Kawakami Y. Life-long preservation of the regenerative capacity in the fin and heart in zebrafish. *Biology open*. 2012;1:739–46.

68. Soonpaa MH, Field LJ. Assessment of cardiomyocyte DNA synthesis in normal and injured adult mouse hearts. *The American journal of physiology*. 1997;272(1 Pt 2):H220-6.

69. Notari M, Ventura-Rubio A, Bedford-Guaus SJ, Jorba I, Mulero L, Navajas D, Martí M, Raya Á. The local microenvironment limits the regenerative potential of the mouse neonatal heart. *Science Advances*. 2018;4(5):eaao5553.

70. Walsh S, Pontén A, Fleischmann BK, Jovinge S. Cardiomyocyte cell cycle control and growth estimation in vivo-An analysis based on cardiomyocyte nuclei. *Cardiovascular Research*. 2010;86(3):365–373.

71. Poolman RA, Brooks G. Expressions and activities of cell cycle regulatory molecules during the transition from myocyte hyperplasia to hypertrophy. *Journal of Molecular and Cellular Cardiology*. 1998;30(10):2121–2135.

72. Poolman RA, Gilchrist R, Brooks G. Cell cycle profiles and expressions of

p21CIP1 and p27KIP1 during myocyte development. *International Journal of Cardiology*. 1998;67(2):133–142.

73. Mahmoud AI, Kocabas F, Muralidhar SA, Kimura W, Koura AS, Thet S, Porrello ER, Sadek HA. Meis1 regulates postnatal cardiomyocyte cell cycle arrest. *Nature*. 2013;497(7448):249–253.

74. Porrello ER, Johnson BA, Aurora AB, Simpson E, Nam Y-J, Matkovich SJ, Dorn GW, van Rooij E, Olson EN. miR-15 Family Regulates Postnatal Mitotic Arrest of Cardiomyocytes. *Circulation Research*. 2011;109(6):670–679.

75. Bersell K, Arab S, Haring B, Kühn B. Neuregulin1/ErbB4 signaling induces cardiomyocyte proliferation and repair of heart injury. *Cell*. 2009;138(2):257–70.

76. Kikuchi K. Advances in understanding the mechanism of zebrafish heart regeneration. *Stem Cell Research*. 2014;13(3):542–555.

77. González-Rosa JM, Sharpe M, Field D, Soonpaa MH, Field LJ, Burns CE, Burns CG. Myocardial Polyploidization Creates a Barrier to Heart Regeneration in Zebrafish. *Developmental Cell*. 2018;44(4):433-446.e7.

78. Elhelaly WM, Lam NT, Hamza M, Xia S, Sadek HA. Redox Regulation of Heart Regeneration: An Evolutionary Tradeoff. *Frontiers in Cell and Developmental Biology*. 2016;4:137.

79. Puente BN, Kimura W, Muralidhar SA, Moon J, Amatruda JF, Phelps KL, Grinsfelder D, Rothermel BA, Chen R, Garcia JA, Santos CX, Thet S, Mori E, Kinter MT, Rindler PM, et al. The oxygen-rich postnatal environment induces cardiomyocyte cell-cycle arrest through DNA damage response. *Cell*. 2014;157(3):565–579.

80. Rumyantsev PP. Interrelations of the Proliferation and Differentiation Processes during Cardiac Myogenesis and Regeneration. *International Review of Cytology*. 1977;51:187–273.

81. Senyo SE, Lee RT, Kuhn B. Cardiac regeneration based on mechanisms of cardiomyocyte proliferation and differentiation. *Stem Cell Research*. 2014;13(3):532–541.

82. Eschenhagen T, Bolli R, Braun T, Field LJ, Fleischmann BK, Frisén J, Giacca M, Hare JM, Houser SR, Lee RT, Marbán E, Martin JF, Molkentin JD, Murry CE, Riley PR, et al. Cardiomyocyte Regeneration: A Consensus Statement. *Circulation*. 2017;136:680–686.

83. Soonpaa MH, Kim KK, Pajak L, Franklin M, Field LJ. Cardiomyocyte DNA synthesis and binucleation during murine development. *The American journal of physiology*. 1996;271(5 Pt 2):H2183-9.

84. Soonpaa MH, Field LJ. Survey of Studies Examining Mammalian Cardiomyocyte DNA Synthesis. *Circulation Research*. 2010;83:15–26.

85. Karra R, Poss KD. Redirecting cardiac growth mechanisms for therapeutic regeneration. *Journal of Clinical Investigation*. 2017;127(2):427–436.

86. Senyo SE, Steinhauser ML, Pizzimenti CL, Yang VK, Cai L, Wang M, Wu T-D, Guerquin-Kern J-L, Lechene CP, Lee RT. Mammalian heart renewal by pre-existing cardiomyocytes. *Nature*. 2012;493(7432):433–436.

87. Kimura W, Xiao F, Canseco DC, Muralidhar S, Thet S, Zhang HM, Abdulrahman Y, Chen R, Garcia J a, Shelton JM, Richardson J a, Ashour AM, Asaithamby A, Liang H, Xing C, et al. Hypoxia fate mapping identifies cycling cardiomyocytes in the adult heart. *Nature*. 2015;523(7559):226–30.

88. Frisén J, Walsh S, Bhardwaj RD, Bergmann O, Jovinge S, Alkass K, Bernard S, Buchholz BA, Zdunek S, Barnabé-Heider F, Zupicich J, Druid H. Evidence for Cardiomyocyte Renewal in Humans. *Science*. 2009;324(5923):98–102.

89. Porrello ER, Olson EN. A neonatal blueprint for cardiac regeneration. *Stem Cell Research*. 2014;13(3):556–570.

90. Chaudhry HW, Dashoush NH, Tang H, Zhang L, Wang X, Wu EX, Wolgemuth DJ. Cyclin A2 Mediates Cardiomyocyte Mitosis in the Postmitotic Myocardium. *Journal of Biological Chemistry*. 2004;279(34):35858–35866.

91. Cheng RK, Asai T, Tang H, Dashoush NH, Kara RJ, Costa KD, Naka Y, Wu EX, Wolgemuth DJ, Chaudhry HW. Cyclin A2 Induces Cardiac Regeneration After Myocardial Infarction and Prevents Heart Failure. *Circulation Research*. 2007;100(12):1741–1748.

92. Shapiro SD, Ranjan AK, Kawase Y, Cheng RK, Kara RJ, Bhattacharya R, Guzman-Martinez G, Sanz J, Garcia MJ, Chaudhry HW. Cyclin A2 induces cardiac regeneration after myocardial infarction through cytokinesis of adult cardiomyocytes. *Science translational medicine*. 2014;6(224):224ra27.

93. Pasumarthi KBS, Nakajima H, Nakajima HO, Soonpaa MH, Field LJ. Targeted Expression of Cyclin D2 Results in Cardiomyocyte DNA Synthesis and Infarct Regression in Transgenic Mice. *Circulation Research*. 2005;96(1):110–118.

94. Hassink RJ, Pasumarthi KB, Nakajima H, Rubart M, Soonpaa MH, de la Riviere AB, Doevendans PA, Field LJ. Cardiomyocyte cell cycle activation improves cardiac function after myocardial infarction. *Cardiovascular Research*. 2008;78(1):18–25.

95. Mohamed TMA, Ang YS, Radzinsky E, Zhou P, Huang Y, Elfenbein A, Foley A, Magnitsky S, Srivastava D. Regulation of Cell Cycle to Stimulate Adult Cardiomyocyte Proliferation and Cardiac Regeneration. *Cell*. 2018;173(1):104-116.e12.

96. Porrello ER. microRNAs in cardiac development and regeneration. *Clinical science*. 2013;125(4):151–66.

97. Eulalio A, Mano M, Ferro MD, Zentilin L, Sinagra G, Zacchigna S, Giacca M. Functional screening identifies miRNAs inducing cardiac regeneration. *Nature*. 2012;492(7429):376–381.

98. Lesizza P, Prosdocimo G, Martinelli V, Sinagra G, Zacchigna S, Giacca M. Single-Dose Intracardiac Injection of Pro-Regenerative MicroRNAs Improves Cardiac Function After Myocardial Infarction. *Circulation research*. 2017;120(8):1298–1304.

99. Gabisonia K, Prosdocimo G, Aquaro GD, Carlucci L, Zentilin L, Secco I, Ali H, Braga L, Gorgodze N, Bernini F, Burchielli S, Collesi C, Zandonà L, Sinagra G, Piacenti M, et al. MicroRNA therapy stimulates uncontrolled cardiac repair after myocardial infarction in pigs. *Nature*. 2019;569(7756):418–422.

100. Chen J, Huang ZP, Seok HY, Ding J, Kataoka M, Zhang Z, Hu X, Wang G, Lin Z, Wang S, Pu WT, Liao R, Wang DZ. Mir-17-92 cluster is required for and sufficient to induce cardiomyocyte proliferation in postnatal and adult hearts. *Circulation Research*. 2013;112(12):1557–1566.

101. Yester JW, Kühn B. Mechanisms of Cardiomyocyte Proliferation and Differentiation in Development and Regeneration. *Current Cardiology Reports*. 2017;19(2):13.

102. Niessen K, Karsan A. Notch Signaling in Cardiac Development. *Circulation Research*. 2008;102(10):1169–1181.

103. Campa VM, Gutiérrez-Lanza R, Cerignoli F, Díaz-Trelles R, Nelson B, Tsuji T, Barcova M, Jiang W, Mercola M. Notch activates cell cycle reentry and progression in quiescent cardiomyocytes. *The Journal of cell biology*. 2008;183(1):129–41.

104. Collesi C, Zentilin L, Sinagra G, Giacca M. Notch1 signaling stimulates proliferation of immature cardiomyocytes. *The Journal of Cell Biology*. 2008;183(1):117–128.

105. Felician G, Collesi C, Lusic M, Martinelli V, Ferro MD, Zentilin L, Zacchigna S, Giacca M. Epigenetic Modification at Notch Responsive Promoters Blunts Efficacy of Inducing Notch Pathway Reactivation After Myocardial Infarction. *Circulation Research*. 2014;115(7):636–649.

106. Lee K-F, Simon H, Chen H, Bates B, Hung M-C, Hauser C. Requirement for neuregulin receptor erbB2 in neural and cardiac development. *Nature*. 1995;378(6555):394–398.

107. Gassmann M, Casagranda F, Orioli D, Simon H, Lai C, Klein R, Lemke G. Aberrant neural and cardiac development in mice lacking the ErbB4 neuregulin receptor. *Nature*. 1995;378(6555):390–394.

108. Reuter S, Soonpaa MH, Firulli AB, Chang AN, Field LJ. Recombinant neuregulin 1 does not activate cardiomyocyte DNA synthesis in normal or infarcted adult mice. Hsieh PCH, ed. *PLoS ONE*. 2014;9(12):e115871.

109. Engel FB, Schebesta M, Duong MT, Lu G, Ren S, Madwed JB, Jiang H, Wang Y, Keating MT. p38 MAP kinase inhibition enables proliferation of adult mammalian cardiomyocytes. *Genes & development*. 2005;19(10):1175–87.

110. Engel FB, Hsieh PCH, Lee RT, Keating MT. FGF1/p38 MAP kinase inhibitor therapy induces cardiomyocyte mitosis, reduces scarring, and rescues function after myocardial infarction. *Proceedings of the National Academy of Sciences*. 2006;103(42):15546–15551.

111. Zhou Q, Li L, Zhao B, Guan K. The hippo pathway in heart development, regeneration, and diseases. *Circulation research*. 2015;116(8):1431–47.

112. Heallen T, Morikawa Y, Leach J, Tao G, Willerson JT, Johnson RL, Martin JF. Hippo signaling impedes adult heart regeneration. *Development*. 2013;140(23):4683–90.

113. Leach JP, Heallen T, Zhang M, Rahmani M, Morikawa Y, Hill MC, Segura A, Willerson JT, Martin JF. Hippo pathway deficiency reverses systolic heart failure after infarction. *Nature*. 2017;550(7675):260–264.

114. Lin Z, Von Gise A, Zhou P, Gu F, Ma Q, Jiang J, Yau AL, Buck JN, Gouin KA, Van Gorp PRR, Zhou B, Chen J, Seidman JG, Wang DZ, Pu WT. Cardiac-specific YAP activation improves cardiac function and survival in an experimental murine MI

model. *Circulation Research*. 2014;115(3):354–363.

115. Xin M, Kim Y, Sutherland LB, Murakami M, Qi X, McAnally J, Porrello ER, Mahmoud AI, Tan W, Shelton JM, Richardson JA, Sadek HA, Bassel-Duby R, Olson EN. Hippo pathway effector Yap promotes cardiac regeneration. *Proceedings of the National Academy of Sciences*. 2013;110(34):13839–13844.

116. Yu F-X, Zhao B, Panupinthu N, Jewell JL, Lian I, Wang LH, Zhao J, Yuan H, Tumaneng K, Li H, Fu X-D, Mills GB, Guan K-L. Regulation of the Hippo-YAP Pathway by G-Protein-Coupled Receptor Signaling. *Cell*. 2012;150(4):780–791.

117. Heallen T, Zhang M, Wang J, Bonilla-Claudio M, Klysik E, Johnson RL, Martin JF. Hippo pathway inhibits Wnt signaling to restrain cardiomyocyte proliferation and heart size. *Science*. 2011;332(6028):458–61.

118. Xin M, Kim Y, Sutherland LB, Qi X, McAnally J, Schwartz RJ, Richardson JA, Bassel-Duby R, Olson EN. Regulation of insulin-like growth factor signaling by Yap governs cardiomyocyte proliferation and embryonic heart size. *Science signaling*. 2011;4(196):ra70.

119. Lin Z, Zhou P, von Gise A, Gu F, Ma Q, Chen J, Guo H, van Gorp PRR, Wang D-Z, Pu WT. Pi3kcb links Hippo-YAP and PI3K-AKT signaling pathways to promote cardiomyocyte proliferation and survival. *Circulation research*. 2015;116(1):35–45.

120. Molkentin JD, Dorn II GW. Cytoplasmic Signaling Pathways That Regulate Cardiac Hypertrophy. *Annual Review of Physiology*. 2001;63(1):391–426.

121. Liang J, Zubovitz J, Petrocelli T, Kotchetkov R, Connor MK, Han K, Lee J-H, Ciarallo S, Catzavelos C, Beniston R, Franssen E, Slingerland JM. PKB/Akt phosphorylates p27, impairs nuclear import of p27 and opposes p27-mediated G1 arrest. *Nature medicine*. 2002;8(10):1153–60.

122. Shiraishi I, Melendez J, Ahn Y, Skavdahl M, Murphy E, Welch S, Schaefer E, Walsh K, Rosenzweig A, Torella D, Nurzynska D, Kajstura J, Leri A, Anversa P, Sussman MA. Nuclear Targeting of Akt Enhances Kinase Activity and Survival of Cardiomyocytes. *Circulation Research*. 2004;94(7):884–891.

123. Rota M, Boni A, Urbanek K, Padin-Iruegas ME, Kajstura TJ, Fiore G, Kubo H, Sonnenblick EH, Musso E, Houser SR, Leri A, Sussman MA, Anversa P. Nuclear Targeting of Akt Enhances Ventricular Function and Myocyte Contractility. *Circulation Research*. 2005;97(12):1332–1341.

124. Gude N, Muraski J, Rubio M, Kajstura J, Schaefer E, Anversa P, Sussman MA.

Akt promotes increased cardiomyocyte cycling and expansion of the cardiac progenitor cell population. *Circulation research*. 2006;99(4):381–8.

125. Nakada Y, Canseco DC, Thet S, Abdisalaam S, Asaithamby A, Santos CX, Shah A, Zhang H, Faber JE, Kinter MT, Szweda LI, Xing C, Deberardinis R, Oz O, Lu Z, et al. Hypoxia induces heart regeneration in adult mice. *Nature*. 2016;20173(October):1–21.

126. Lehtinen MK, Yuan Z, Boag PR, Yang Y, Villén J, Becker EBE, DiBacco S, de la Iglesia N, Gygi S, Blackwell TK, Bonni A. A Conserved MST-FOXO Signaling Pathway Mediates Oxidative-Stress Responses and Extends Life Span. *Cell*. 2006;125(5):987–1001.

127. Tao G, Kahr PC, Morikawa Y, Zhang M, Rahmani M, Heallen TR, Li L, Sun Z, Olson EN, Amendt BA, Martin JF. Pitx2 promotes heart repair by activating the antioxidant response after cardiac injury. *Nature*. 2016;534(7605):119–123.

128. Han P, Zhou X-H, Chang N, Xiao C-L, Yan S, Ren H, Yang X-Z, Zhang M-L, Wu Q, Tang B, Diao J-P, Zhu X, Zhang C, Li C-Y, Cheng H, et al. Hydrogen peroxide primes heart regeneration with a derepression mechanism. *Cell Research*. 2014;24(9):1091–1107.

129. Buggisch M, Ateghang B, Ruhe C, Strobel C, Lange S, Wartenberg M, Sauer H. Stimulation of ES-cell-derived cardiomyogenesis and neonatal cardiac cell proliferation by reactive oxygen species and NADPH oxidase. *Journal of Cell Science*. 2007;120(5):885–894.

130. Murray TVA, Smyrnias I, Schnelle M, Mistry RK, Zhang M, Beretta M, Martin D, Anilkumar N, de Silva SM, Shah AM, Brewer AC. Redox regulation of cardiomyocyte cell cycling via an ERK1/2 and c-Myc-dependent activation of cyclin D2 transcription. *Journal of Molecular and Cellular Cardiology*. 2015;79:54–68.

131. Burgoyne JR, Mongue-Din H, Eaton P, Shah AM. Redox signaling in cardiac physiology and pathology. *Circulation research*. 2012;111(8):1091–106.

132. Chiu J, Dawes IW. Redox control of cell proliferation. *Trends in cell biology*. 2012;22(11):592–601.

133. Chiarugi P. ReviewPTPs versus PTKs: The redox side of the coin. *Free Radical Research*. 2005;39(4):353–364.

134. Tzahor E, Poss KD. Cardiac regeneration strategies: Staying young at heart. *Science*. 2017;356(June):1035–1039.

135. Sugamura K, Keaney, JF. Reactive oxygen species in cardiovascular disease. *Free Radical Biology and Medicine*. 2011;51(5):978–992.

136. Lambeth JD. NOX enzymes and the biology of reactive oxygen. *Nature reviews. Immunology*. 2004;4(3):181–189.

137. Burgoyne JR, Oka S, Ale-Agha N, Eaton P. Hydrogen peroxide sensing and signaling by protein kinases in the cardiovascular system. *Antioxidants & redox signaling*. 2013;18(9):1042–52.

138. Santos CXC, Raza S, Shah AM. Redox signaling in the cardiomyocyte: From physiology to failure. *International Journal of Biochemistry and Cell Biology*. 2016;74:145–151.

139. Cadenas S. ROS and redox signaling in myocardial ischemia-reperfusion injury and cardioprotection. *Free Radical Biology and Medicine*. 2018;117:76–89.

140. Minhas KM, Saraiva RM, Schuleri KH, Lehrke S, Zheng M, Saliaris AP, Berry CE, Vandegaer KM, Li D, Hare JM. Xanthine Oxidoreductase Inhibition Causes Reverse Remodeling in Rats With Dilated Cardiomyopathy. *Circulation Research*. 2006;98(2):271–279.

141. Kaludercic N, Carpi A, Nagayama T, Sivakumaran V, Zhu G, Lai EW, Bedja D, De Mario A, Chen K, Gabrielson KL, Lindsey ML, Pacak K, Takimoto E, Shih JC, Kass DA, et al. Monoamine Oxidase B Prompts Mitochondrial and Cardiac Dysfunction in Pressure Overloaded Hearts. *Antioxidants & Redox Signaling*. 2014;20(2):267–280.

142. Alkaitis MS, Crabtree MJ. Recoupling the cardiac nitric oxide synthases: Tetrahydrobiopterin synthesis and recycling. *Current Heart Failure Reports*. 2012;9(3):200–210.

143. Lassègue B, San Martín A, Griendling KK. Biochemistry, physiology, and pathophysiology of NADPH oxidases in the cardiovascular system. *Circulation Research*. 2012;110(10):1364–1390.

144. Barnes JL, Gorin Y. Myofibroblast differentiation during fibrosis: role of NAD(P)H oxidases. *Kidney international*. 2011;79(9):944–56.

145. Chan EC, Jiang F, Peshavariya HM, Dusting GJ. Regulation of cell proliferation by NADPH oxidase-mediated signaling: Potential roles in tissue repair, regenerative medicine and tissue engineering. *Pharmacology & Therapeutics*. 2009;122(2):97–108.

146. Pietrowski E, Bender B, Huppert J, White R, Luhmann HJ, Kuhlmann CRW. Pro-inflammatory effects of interleukin-17A on vascular smooth muscle cells involve NAD(P)H- oxidase derived reactive oxygen species. *Journal of Vascular Research*. 2010;48(1):52–58.

147. Hwang J, Saha A, Boo YC, Sorescu GP, McNally JS, Holland SM, Dikalov S, Giddens DP, Griendling KK, Harrison DG, Jo H. Oscillatory Shear Stress Stimulates Endothelial Production of O2- from p47phox-dependent NAD(P)H Oxidases, Leading to Monocyte Adhesion. *Journal of Biological Chemistry*. 2003;278(47):47291–47298.

148. Looi YH, Grieve DJ, Siva A, Walker SJ, Anilkumar N, Cave AC, Marber M, Monaghan MJ, Shah AM. Involvement of Nox2 NADPH Oxidase in Adverse Cardiac Remodeling After Myocardial Infarction. *Hypertension*. 2008;51(2):319–325.

149. Zhang M, Brewer AC, Schröder K, Santos CXC, Grieve DJ, Wang M, Anilkumar N, Yu B, Dong X, Walker SJ, Brandes RP, Shah AM. NADPH oxidase-4 mediates protection against chronic load-induced stress in mouse hearts by enhancing angiogenesis. *Proceedings of the National Academy of Sciences of the United States of America*. 2010;107(42):18121–6.

150. Zhang M, Mongue-Din H, Martin D, Catibog N, Smyrnias I, Zhang X, Yu B, Wang M, Brandes RP, Schröder K, Shah AM. Both cardiomyocyte and endothelial cell Nox4 mediate protection against hemodynamic overload-induced remodelling. *Cardiovascular research*. 2018;114(3):401–408.

151. Santos CX, Hafstad AD, Beretta M, Zhang M, Molenaar C, Kopec J, Fotinou D, Murray T V, Cobb AM, Martin D, Zeh Silva M, Anilkumar N, Schröder K, Shanahan CM, Brewer AC, et al. Targeted redox inhibition of protein phosphatase 1 by Nox4 regulates eIF2α-mediated stress signaling. *The EMBO journal*. 2016;35(3):319–34.

152. Smyrnias I, Zhang X, Zhang M, Murray TVA, Brandes RP, Schröder K, Brewer AC, Shah AM. Nicotinamide adenine dinucleotide phosphate oxidase-4-dependent upregulation of nuclear factor erythroid-derived 2-like 2 protects the heart during chronic pressure overload. *Hypertension*. 2015;65(3):547–53.

153. Goyal P, Weissmann N, Rose F, Grimminger F, Schäfers HJ, Seeger W, Hänze J. Identification of novel Nox4 splice variants with impact on ROS levels in A549 cells. *Biochemical and Biophysical Research Communications*. 2005;329(1):32–39.

154. Anilkumar N, Jose GS, Sawyer I, Santos CXC, Sand C, Brewer AC, Warren D, Shah AM. A 28-kDa splice variant of NADPH oxidase-4 is nuclear-localized and involved in redox signaling in vascular cells. *Arteriosclerosis, Thrombosis, and Vascular Biology*. 2013;33(4).

155. Nisimoto Y, Jackson HM, Ogawa H, Kawahara T, Lambeth JD. Constitutive NADPH-Dependent Electron Transferase Activity of the Nox4 Dehydrogenase Domain. *Biochemistry*. 2010;49(11):2433–2442.

156. Patterson M, Barske L, Van Handel B, Rau CD, Gan P, Sharma A, Parikh S, Denholtz M, Huang Y, Yamaguchi Y, Shen H, Allayee H, Crump JG, Force TI, Lien C-L, et al. Frequency of mononuclear diploid cardiomyocytes underlies natural variation in heart regeneration. *Nature genetics*. 2017;49(9):1346–1353.

157. Feil S, Valtcheva N, Feil R. *Inducible cre mice*.; 2009.

158. Kim T, Zhelyabovska O, Liu J, Yang Q. Generation of an inducible, cardiomyocyte-specific transgenic mouse model with PPAR β/δ overexpression. *Methods in molecular biology (Clifton, N.J.)*. 2013;952:57–65.

159. Sohal DS, Nghiem M, Crackower MA, Witt SA, Kimball TR, Tymitz KM, Penninger JM, Molkentin JD. Temporally regulated and tissue-specific gene manipulations in the adult and embryonic heart using a tamoxifen-inducible Cre protein. *Circulation Research*. 2001;89(1):20–25.

160. Davis J, Maillet M, Miano JM, Molkentin JD. Lost in transgenesis: a user's guide for genetically manipulating the mouse in cardiac research. *Circulation research*. 2012;111(6):761–77.

161. Dandel M, Lehmkuhl H, Knosalla C, Suramelashvili N, Hetzer R. Strain and strain rate imaging by echocardiography - basic concepts and clinical applicability. *Current cardiology reviews*. 2009;5(2):133–48.

162. Xiang FL, Guo M, Yutzey KE. Overexpression of Tbx20 in adult cardiomyocytes promotes proliferation and improves cardiac function after myocardial infarction. *Circulation*. 2016;133(11):1081–1092.

163. Ackers-Johnson M, Li PY, Holmes APP, O'Brien SM, Pavlovic D, Foo RS. A Simplified, Langendorff-Free Method for Concomitant Isolation of Viable Cardiac Myocytes and Non-Myocytes from the Adult Mouse Heart. *Circulation Research*. 2016;119(8):909–920.

164. Livak KJ, Schmittgen TD. Analysis of Relative Gene Expression Data Using Real-Time Quantitative PCR and the 2−ΔΔCT Method. *Methods*. 2001;25(4):402–408.

165. Chazotte B. Labeling Membrane Glycoproteins or Glycolipids with Fluorescent Wheat Germ Agglutinin. *Cold Spring Harbor Protocols*. 2011;2011(5):pdb.prot5623-pdb.prot5623.

166. Gavrieli Y, Sherman Y, Ben-Sasson SA. Identification of programmed cell death in situ via specific labeling of nuclear DNA fragmentation. *The Journal of Cell Biology*. 1992;119(3):493–501.

167. Lattouf R, Younes R, Lutomski D, Naaman N, Godeau G, Senni K, Changotade S. Picrosirius Red Staining: A Useful Tool to Appraise Collagen Networks in Normal and Pathological Tissues. *Journal of Histochemistry and Cytochemistry*. 2014;62(10):751–758.

168. Fernandes DC, Wosniak J, Pescatore LA, Bertoline MA, Liberman M, Laurindo FRM, Santos CXC. Analysis of DHE-derived oxidation products by HPLC in the assessment of superoxide production and NADPH oxidase activity in vascular systems. *American Journal of Physiology-Cell Physiology*. 2007;292(1):C413–C422.

169. Laurindo FRM, Fernandes DC, Santos CXC. Assessment of Superoxide Production and NADPH Oxidase Activity by HPLC Analysis of Dihydroethidium Oxidation Products. In: *Methods in enzymology*.Vol 441.; 2008:237–260.

170. Bedard K, Krause K-H. The NOX family of ROS-generating NADPH oxidases: physiology and pathophysiology. *Physiological reviews*. 2007;87(1):245–313.

171. Brandes RP, Weissmann N, Schroder K. NADPH oxidases in cardiovascular disease. *Free Radical Biology and Medicine*. 2010;49(5):687–706.

172. Pagliaro P, Penna C. Redox signalling and cardioprotection: Translatability and mechanism. *British Journal of Pharmacology*. 2015;172(8):1974–1995.

173. Nabeebaccus AA, Zoccarato A, Hafstad AD, Santos CX, Aasum E, Brewer AC, Zhang M, Beretta M, Yin X, West JA, Schröder K, Griffin JL, Eykyn TR, Abel ED, Mayr M, et al. Nox4 reprograms cardiac substrate metabolism via protein O-GlcNAcylation to enhance stress adaptation. *JCI insight*. 2017;2(24):e96184.

174. Mongue-Din H, Patel AS, Looi YH, Grieve DJ, Anilkumar N, Sirker A, Dong X, Brewer AC, Zhang M, Smith A, Shah AM. NADPH Oxidase-4 Driven Cardiac Macrophage Polarization Protects Against Myocardial Infarction–Induced Remodeling. *JACC: Basic to Translational Science*. 2017;2(6):688–698.

175. Nabeebaccus A, Hafstad A, Eykyn T, Yin X, Brewer A, Zhang M, Mayr M, Shah A. Cardiac-targeted NADPH oxidase 4 in the adaptive cardiac remodelling of the

murine heart. *The Lancet*. 2015;385:S73.

176. Matsushima S, Kuroda J, Ago T, Zhai P, Ikeda Y, Oka S, Fong G-H, Tian R, Sadoshima J. Broad Suppression of NADPH Oxidase Activity Exacerbates Ischemia/Reperfusion Injury Through Inadvertent Downregulation of Hypoxia-inducible Factor-1α and Upregulation of Peroxisome Proliferator–activated Receptor-α. *Circulation Research*. 2013;112(8):1135–1149.

177. Sciarretta S, Zhai P, Shao D, Zablocki D, Nagarajan N, Terada LS, Volpe M, Sadoshima J. Activation of NADPH Oxidase 4 in the Endoplasmic Reticulum Promotes Cardiomyocyte Autophagy and Survival During Energy Stress Through the Protein Kinase RNA-Activated-Like Endoplasmic Reticulum Kinase/Eukaryotic Initiation Factor 2α/Activating Transcription Factor 4 Pathway. *Circulation Research*. 2013;113(11):1253–1264.

178. Tao L, Bei Y, Li Y, Xiao J. Neonatal Rat Cardiomyocytes Isolation, Culture, and Determination of MicroRNAs' Effects in Proliferation. In: *Methods in molecular biology (Clifton, N.J.)*.Vol 1733.; 2018:203–213.

179. Polymenis M, Aramayo R. Translate to divide: control of the cell cycle by protein synthesis. *Microbial cell (Graz, Austria)*. 2015;2(4):94–104.

180. Kronja I, Orr-Weaver TL. Translational regulation of the cell cycle: when, where, how and why? *Philosophical Transactions of the Royal Society B: Biological Sciences*. 2011;366(1584):3638–3652.

181. Condorelli G, Drusco A, Stassi G, Bellacosa A, Roncarati R, Iaccarino G, Russo MA, Gu Y, Dalton N, Chung C, Latronico MVG, Napoli C, Sadoshima J, Croce CM, Ross J. Akt induces enhanced myocardial contractility and cell size in vivo in transgenic mice. *Proceedings of the National Academy of Sciences*. 2002;99(19):12333–12338.

182. Fujio Y, Nguyen T, Wencker D, Kitsis RN, Walsh K. Akt promotes survival of cardiomyocytes in vitro and protects against ischemia-reperfusion injury in mouse heart. *Circulation*. 2000;101(6):660–7.

183. Antico Arciuch VG, Galli S, Franco MC, Lam PY, Cadenas E, Carreras MC, Poderoso JJ. Akt1 intramitochondrial cycling is a crucial step in the redox modulation of cell cycle progression. *PloS one*. 2009;4(10):e7523.

184. Bertero A, Murry CE. Hallmarks of cardiac regeneration. *Nature Reviews Cardiology*. 2018;15(10):579–580.

185. Anilkumar N, Weber R, Zhang M, Brewer A, Shah AM. Nox4 and Nox2 NADPH

oxidases mediate distinct cellular redox signaling responses to agonist stimulation. *Arteriosclerosis, thrombosis, and vascular biology*. 2008;28(7):1347–54.

186. Takeuchi T. Regulation of cardiomyocyte proliferation during development and regeneration. *Development, growth & differentiation*. 2014;56(5):402–9.

187. Szibor M, Pöling J, Warnecke H, Kubin T, Braun T. Remodeling and dedifferentiation of adult cardiomyocytes during disease and regeneration. *Cellular and Molecular Life Sciences*. 2014;71(10):1907–1916.

188. Chehrehasa F, Meedeniya ACB, Dwyer P, Abrahamsen G, Mackay-Sim A. EdU, a new thymidine analogue for labelling proliferating cells in the nervous system. *Journal of Neuroscience Methods*. 2009;177(1):122–130.

189. Zeng B, Tong S, Ren X, Xia H. Cardiac cell proliferation assessed by EdU, a novel analysis of cardiac regeneration. *Cytotechnology*. 2016;68(4):763–770.

190. Field LJ. Modulation of the cardiomyocyte cell cycle in genetically altered animals. *Annals New York Academy of Sciences*. 2004;1015:160–170.

191. Kimura W, Muralidhar S, Canseco D, Puente B, Zhang C, Xiao F, Abderrahman Y, Sadek H. Redox Signaling in Cardiac Renewal. *Antioxidants & redox signaling*. 2014;21(11):1660–1673.

192. Gerdes J, Lemke H, Baisch H, Wacker HH, Schwab U, Stein H. Cell cycle analysis of a cell proliferation-associated human nuclear antigen defined by the monoclonal antibody Ki-67. *Journal of immunology (Baltimore, Md.: 1950)*. 1984;133(4):1710–5.

193. Goto H, Tomono Y, Ajiro K, Kosako H, Fujita M, Sakurai M, Okawa K, Iwamatsu A, Okigaki T, Takahashi T, Inagaki M. Identification of a novel phosphorylation site on histone H3 coupled with mitotic chromosome condensation. *The Journal of biological chemistry*. 1999;274(36):25543–9.

194. Soonpaa MH, Rubart M, Field LJ. Challenges measuring cardiomyocyte renewal. *Biochimica et Biophysica Acta - Molecular Cell Research*. 2013;1833(4):799–803.

195. Leone M, Magadum A, Engel FB, Adler C, Friedburg H, Herget G, Neuburger M, Schwalb H, Aguirre A, Montserrat N, Zacchigna S, Nivet E, Hishida T, Krause M, Kurian L, et al. Cardiomyocyte proliferation in cardiac development and regeneration: a guide to methodologies and interpretations. *American journal of physiology. Heart and circulatory physiology*. 2015;309(8):H1237-50.

196. van Amerongen MJ, Engel FB. Features of cardiomyocyte proliferation and its potential for cardiac regeneration. *Journal of cellular and molecular medicine*. 2008;12(6A):2233–44.

197. Brazil DP, Park J, Hemmings BA. PKB binding proteins. Getting in on the Akt. *Cell*. 2002;111(3):293–303.

198. Brandes RP, Weissmann N, Schroder K. Redox-mediated signal transduction by cardiovascular Nox NADPH oxidases. *Journal of Molecular and Cellular Cardiology*. 2014;73:70–79.

199. Kotani H, Ito M, Hamaguchi T, Ichikawa K, Nakano T, Shima H, Nagao M, Ohta N, Furuichi Y, Takahashi T, Umekawa H. The delta isoform of protein phosphatase type 1 is localized in nucleolus and dephosphorylates nucleolar phosphoproteins. *Biochemical and biophysical research communications*. 1998;249(1):292–6.

200. Liu R-M, Choi J, Wu J-H, Gaston Pravia KA, Lewis KM, Brand JD, Mochel NSR, Krzywanski DM, Lambeth JD, Hagood JS, Forman HJ, Thannickal VJ, Postlethwait EM. Oxidative Modification of Nuclear Mitogen-activated Protein Kinase Phosphatase 1 Is Involved in Transforming Growth Factor β1-induced Expression of Plasminogen Activator Inhibitor 1 in Fibroblasts. *Journal of Biological Chemistry*. 2010;285(21):16239–16247.

201. Nacusi LP, Sheaff RJ. Akt1 sequentially phosphorylates p27kip1 within a conserved but non-canonical region. *Cell division*. 2006;1:11.

202. Wang WE, Li L, Xia X, Fu W, Liao Q, Lan C, Yang D, Chen H, Yue R, Zeng CS, Zhou L, Zhou B, Duan DD, Chen X, Houser SR, et al. Dedifferentiation, Proliferation and Redifferentiation of Adult Mammalian Cardiomyocytes After Ischemic Injury. *Circulation*. 2017;136(9):834–848.

203. Tian Y, Liu Y, Wang T, Zhou N, Kong J, Chen L, Snitow M, Morley M, Li D, Petrenko N, Zhou S, Lu M, Gao E, Koch WJ, Stewart KM, et al. A microRNA-Hippo pathway that promotes cardiomyocyte proliferation and cardiac regeneration in mice. *Science translational medicine*. 2015;7(279):279ra38.

204. D'Uva G, Aharonov A, Lauriola M, Kain D, Yahalom-Ronen Y, Carvalho S, Weisinger K, Bassat E, Rajchman D, Yifa O, Lysenko M, Konfino T, Hegesh J, Brenner O, Neeman M, et al. ERBB2 triggers mammalian heart regeneration by promoting cardiomyocyte dedifferentiation and proliferation. *Nature Cell Biology*. 2015;17(5):627–638.

205. Porrello ER, Olson EN. A neonatal blueprint for cardiac regeneration. *Stem cell*

research. 2014;13(3 Pt B):556–70.

206. Pagidipati NJ, Gaziano TA. Estimating deaths from cardiovascular disease: a review of global methodologies of mortality measurement. *Circulation*. 2013;127(6):749–56.

207. Redfors B, Shao Y, Omerovic E. Myocardial infarct size and area at risk assessment in mice. *Experimental and clinical cardiology*. 2012;17(4):268–72.

208. Hasenfuss G. Animal models of human cardiovascular disease, heart failure and hypertrophy. *Cardiovascular Research*. 1998;39(1):60–76.

209. Doevendans P, J. Daemen M, de Muinck ED, Smits JF. Cardiovascular phenotyping in mice. *Cardiovascular Research*. 1998;39(1):34–49.

210. Lindsey ML, Bolli R, Canty JM, Du X-J, Frangogiannis NG, Frantz S, Gourdie RG, Holmes JW, Jones SP, Kloner RA, Lefer DJ, Liao R, Murphy E, Ping P, Przyklenk K, et al. Guidelines for experimental models of myocardial ischemia and infarction. *American Journal of Physiology-Heart and Circulatory Physiology*. 2018;314(4):H812–H838.

211. Muthuramu I, Lox M, Jacobs F, De Geest B. Permanent Ligation of the Left Anterior Descending Coronary Artery in Mice: A Model of Post-myocardial Infarction Remodelling and Heart Failure. *Journal of Visualized Experiments*. 2014;(December):1–7.

212. Hausenloy DJ, Yellon DM. Myocardial ischemia-reperfusion injury: a neglected therapeutic target. *The Journal of clinical investigation*. 2013;123(1):92–100.

213. Gharacholou SM, Alexander KP, Chen AY, Wang TY, Melloni C, Gibler WB, Pollack C V., Ohman EM, Peterson ED, Roe MT. Implications and reasons for the lack of use of reperfusion therapy in patients with ST-segment elevation myocardial infarction: Findings from the CRUSADE initiative. *American Heart Journal*. 2010;159(5):757–763.

214. Cohen M, Boiangiu C, Abidi M. Therapy for ST-Segment Elevation Myocardial Infarction Patients Who Present Late or Are Ineligible for Reperfusion Therapy. *Journal of the American College of Cardiology*. 2010;55(18):1895–1906.

215. Heusch G. Myocardial Ischemia: Lack of Coronary Blood Flow or Myocardial Oxygen Supply/Demand Imbalance? *Circulation Research*. 2016;119(2):194–196.

216. Kübler W, Spieckermann PG. Regulation of glycolysis in the ischemic and the

anoxic myocardium. *Journal of molecular and cellular cardiology*. 1970;1(4):351–77.

217. Kentish JC. The effects of inorganic phosphate and creatine phosphate on force production in skinned muscles from rat ventricle. *The Journal of physiology*. 1986;370:585–604.

218. Solaro RJ, Lee JA, Kentish JC, Allen DG. Effects of acidosis on ventricular muscle from adult and neonatal rats. *Circulation research*. 1988;63(4):779–87.

219. Thandroyen FT, Bellotto D, Katayama A, Hagler HK, Willerson JT, Buja LM. Subcellular electrolyte alterations during progressive hypoxia and following reoxygenation in isolated neonatal rat ventricular myocytes. *Circulation Research*. 1992;71(1):106–119.

220. Buja LM. Myocardial ischemia and reperfusion injury. *Cardiovascular Pathology*. 2005;14(4):170–175.

221. Buja LM, Hagler HK, Willerson JT. Altered calcium homeostasis in the pathogenesis of myocardial ischemic and hypoxic injury. *Cell calcium*. 1988;9(5–6):205–17.

222. Jennings RB, Reimer KA. Lethal myocardial ischemic injury. *The American journal of pathology*. 1981;102(2):241–55.

223. Frangogiannis NG. Inflammation in cardiac injury, repair and regeneration. *Current Opinion in Cardiology*. 2015;30(3):240–245.

224. Frangogiannis NG. The immune system and the remodeling infarcted heart: cell biological insights and therapeutic opportunities. *Journal of Cardiovascular Pharmacology*. 2014;63(3):185–195.

225. Degabriele NM, Griesenbach U, Sato K, Post MJ, Zhu J, Williams J, Jeffery PK, Geddes DM, Alton EWFW. Critical appraisal of the mouse model of myocardial infarction. *Experimental Physiology*. 2004;89(4):497–505.

226. Frobert A, Valentin J, Magnin J-L, Riedo E, Cook S, Giraud M-N. Prognostic Value of Troponin I for Infarct Size to Improve Preclinical Myocardial Infarction Small Animal Models. *Frontiers in physiology*. 2015;6:353.

227. Chen J, Ceholski DK, Liang L, Fish K, Hajjar RJ. Variability in coronary artery anatomy affects consistency of cardiac damage following myocardial infarction in mice 2 3. *Am J Physiol Heart Circ Physiol*. 2017.

228. Bohl S, Medway DJ, Schulz-Menger J, Schneider JE, Neubauer S, Lygate CA.

Refined approach for quantification of in vivo ischemia-reperfusion injury in the mouse heart. *American journal of physiology. Heart and circulatory physiology*. 2009;297(6):H2054-8.

229. Frey A, Saxon V-M, Popp S, Lehmann M, Mathes D, Pachel C, Hofmann U, Ertl G, Lesch K-P, Frantz S. Early citalopram treatment increases mortality due to left ventricular rupture in mice after myocardial infarction. *Journal of Molecular and Cellular Cardiology*. 2016;98:28–36.

230. Lindsey ML, Iyer RP, Zamilpa R, Yabluchanskiy A, DeLeon-Pennell KY, Hall ME, Kaplan A, Zouein FA, Bratton D, Flynn ER, Cannon PL, Tian Y, Jin Y-F, Lange RA, Tokmina-Roszyk D, et al. A Novel Collagen Matricryptin Reduces Left Ventricular Dilation Post-Myocardial Infarction by Promoting Scar Formation and Angiogenesis. *Journal of the American College of Cardiology*. 2015;66(12):1364–74.

231. Thygesen K, Mair J, Katus H, Plebani M, Venge P, Collinson P, Lindahl B, Giannitsis E, Hasin Y, Galvani M, Tubaro M, Alpert JS, Biasucci LM, Koenig W, Mueller C, et al. Recommendations for the use of cardiac troponin measurement in acute cardiac care. *European Heart Journal*. 2010;31(18):2197–2204.

232. Hall TS, Hallén J, Krucoff MW, Roe MT, Brennan DM, Agewall S, Atar D, Lincoff AM. Cardiac troponin I for prediction of clinical outcomes and cardiac function through 3-month follow-up after primary percutaneous coronary intervention for ST-segment elevation myocardial infarction. *American Heart Journal*. 2015;169(2):257-265.e1.

233. Babuin L, Jaffe AS. Troponin: the biomarker of choice for the detection of cardiac injury. *CMAJ : Canadian Medical Association journal = journal de l'Association medicale canadienne*. 2005;173(10):1191–202.

234. Santulli G, Xie W, Reiken SR, Marks AR. Mitochondrial calcium overload is a key determinant in heart failure. *Proceedings of the National Academy of Sciences of the United States of America*. 2015;112(36):11389–94.

235. St John Sutton MG, Sharpe N. *Left Ventricular Remodeling After Myocardial Infarction Pathophysiology and Therapy*.; 2000.

236. Erlebacher JA, Weiss JL, Weisfeldt ML, Bulkley BH. Early dilation of the infarcted segment in acute transmural myocardial infarction: role of infarct expansion in acute left ventricular enlargement. *Journal of the American College of Cardiology*. 1984;4(2):201–8.

237. Weber KT. Extracellular matrix remodeling in heart failure: a role for de novo angiotensin II generation. *Circulation*. 1997;96(11):4065–82.

238. Pfeffer MA, Braunwald E. Ventricular remodeling after myocardial infarction. Experimental observations and clinical implications. *Circulation*. 1990;81(4):1161–72.

239. Mukherjee R, Brinsa TA, Dowdy KB, Scott AA, Baskin JM, Deschamps AM, Lowry AS, Escobar GP, Lucas DG, Yarbrough WM, Zile MR, Spinale FG. Myocardial infarct expansion and matrix metalloproteinase inhibition. *Circulation*. 2003;107(4):618–25.

240. Lew WY, Chen ZY, Guth B, Covell JW. Mechanisms of augmented segment shortening in nonischemic areas during acute ischemia of the canine left ventricle. *Circulation research*. 1985;56(3):351–8.

241. Kerkela R, Ulvila J, Magga J. Natriuretic Peptides in the Regulation of Cardiovascular Physiology and Metabolic Events. *J Am Heart Assoc*. 2015;4:2423.

242. Shah AM, Mann DL. In search of new therapeutic targets and strategies for heart failure: Recent advances in basic science. *The Lancet*. 2011;378(9792):704–712.

243. Dorn GW, Force T. Protein kinase cascades in the regulation of cardiac hypertrophy. *The Journal of clinical investigation*. 2005;115(3):527–37.

244. Heineke J, Molkentin JD. Regulation of cardiac hypertrophy by intracellular signalling pathways. *Nature Reviews Molecular Cell Biology*. 2006;7(8):589–600.

245. Sam F, Sawyer DB, Chang DL-F, Eberli FR, Ngoy S, Jain M, Amin J, Apstein CS, Colucci WS. Progressive left ventricular remodeling and apoptosis late after myocardial infarction in mouse heart. *American Journal of Physiology-Heart and Circulatory Physiology*. 2000;279(1):H422–H428.

246. French BA, Kramer CM. Mechanisms of Post-Infarct Left Ventricular Remodeling. *Drug discovery today: Disease mechanisms*. 2007;4(3):185–196.

247. Molkentin JD. Calcineurin-NFAT signaling regulates the cardiac hypertrophic response in coordination with the MAPKs. *Cardiovascular Research*. 2004;63(3):467–475.

248. van Berlo JH, Elrod JW, Aronow BJ, Pu WT, Molkentin JD. Serine 105 phosphorylation of transcription factor GATA4 is necessary for stress-induced cardiac hypertrophy in vivo. *Proceedings of the National Academy of Sciences*.

2011;108(30):12331–12336.

249. Kuwahara K, Kinoshita H, Kuwabara Y, Nakagawa Y, Usami S, Minami T, Yamada Y, Fujiwara M, Nakao K. Myocardin-Related Transcription Factor A Is a Common Mediator of Mechanical Stress- and Neurohumoral Stimulation-Induced Cardiac Hypertrophic Signaling Leading to Activation of Brain Natriuretic Peptide Gene Expression. *Molecular and Cellular Biology*. 2010;30(17):4134–4148.

250. Willems IE, Havenith MG, De Mey JG, Daemen MJ. The alpha-smooth muscle actin-positive cells in healing human myocardial scars. *The American journal of pathology*. 1994;145(4):868–75.

251. Frangogiannis NG. Matricellular Proteins in Cardiac Adaptation and Disease. *Physiological Reviews*. 2012;92(2):635–688.

252. Zimmerman SD, Thomas DP, Velleman SG, Li X, Hansen TR, McCormick RJ. Time course of collagen and decorin changes in rat cardiac and skeletal muscle post-MI. *American Journal of Physiology-Heart and Circulatory Physiology*. 2001;281(4):H1816–H1822.

253. Ren G, Michael LH, Entman ML, Frangogiannis NG. Morphological Characteristics of the Microvasculature in Healing Myocardial Infarcts. *Journal of Histochemistry & Cytochemistry*. 2002;50(1):71–79.

254. Yang F, Liu Y-H, Yang X-P, Xu J, Kapke A, Carretero OA. Myocardial infarction and cardiac remodelling in mice. *Experimental physiology*. 2002;87(5):547–55.

255. Matsubara LS, Matsubara BB, Okoshi MP, Cicogna AC, Janicki JS. Alterations in myocardial collagen content affect rat papillary muscle function. *American Journal of Physiology-Heart and Circulatory Physiology*. 2000;279(4):H1534–H1539.

256. Braunwald E. The war against heart failure: the Lancet lecture. *Lancet*. 2015;385(9970):812–24.

257. Mirea O, Duchenne J, Voigt J-U. Recent advances in echocardiography: strain and strain rate imaging. *F1000Research*. 2016;5:787.

258. Smiseth OA, Torp H, Opdahl A, Haugaa KH, Urheim S. Myocardial strain imaging: how useful is it in clinical decision making? *European heart journal*. 2016;37(15):1196–207.

259. de Jong S, van Veen TAB, de Bakker JMT, van Rijen HVM. Monitoring cardiac fibrosis: a technical challenge. *Netherlands heart journal : monthly journal of the Netherlands Society of Cardiology and the Netherlands Heart Foundation*.

2012;20(1):44–8.

260. Kobayashi K, Maeda K, Takefuji M, Kikuchi R, Morishita Y, Hirashima M, Murohara T. Dynamics of angiogenesis in ischemic areas of the infarcted heart. *Scientific Reports*. 2017;7(1):7156.

261. Camporesi S, Zacchigna S, Recchia FA, Lionetti V, Giacca M, Pepe M, Collesi C, Pattarini L, Zentilin L, Puligadda U, Sinagra G, Ruozi G. Cardiomyocyte VEGFR-1 activation by VEGF-B induces compensatory hypertrophy and preserves cardiac function after myocardial infarction. *The FASEB Journal*. 2009;24(5):1467–1478.

262. Tao Z, Chen B, Tan X, Zhao Y, Wang L, Zhu T, Cao K, Yang Z, Kan YW, Su H. Coexpression of VEGF and angiopoietin-1 promotes angiogenesis and cardiomyocyte proliferation reduces apoptosis in porcine myocardial infarction (MI) heart. *Proceedings of the National Academy of Sciences*. 2011;108(5):2064–2069.

263. Sandhu R, Teichert-Kuliszewska K, Nag S, Proteau G, Robb MJ, Campbell AIM, Kuliszewski MA, Kutryk MJB, Stewart DJ. Reciprocal regulation of angiopoietin-1 and angiopoietin-2 following myocardial infarction in the rat. *Cardiovascular Research*. 2004;64(1):115–124.

264. Wang S-X, Wang J, Shao J-B, Tang W, Zhong J-Q. Plumbagin Mediates Cardioprotection Against Myocardial Ischemia/Reperfusion Injury Through Nrf-2 Signaling. *Medical Science Monitor*. 2016;22:1250–1257.

265. Shanmugam G, Narasimhan M, Tamowski S, Darley-Usmar V, Rajasekaran NS. Constitutive activation of Nrf2 induces a stable reductive state in the mouse myocardium. *Redox biology*. 2017;12:937–945.

266. Reichert K, Colantuono B, McCormack I, Rodrigues F, Pavlov V, Abid MR. Murine Left Anterior Descending (LAD) Coronary Artery Ligation: An Improved and Simplified Model for Myocardial Infarction. *Journal of Visualized Experiments*. 2017;(122):1–6.

267. Seeger T, Xu QF, Muhly-Reinholz M, Fischer A, Kremp EM, Zeiher AM, Dimmeler S. Inhibition of let-7 augments the recruitment of epicardial cells and improves cardiac function after myocardial infarction. *Journal of Molecular and Cellular Cardiology*. 2016;94:145–152.

268. Hesse M, Welz A, Fleischmann BK. Heart regeneration and the cardiomyocyte cell cycle. *Pflugers Archiv European Journal of Physiology*. 2018;470(2):241–248.

269. Quaife-Ryan GA, Sim CB, Ziemann M, Kaspi A, Rafehi H, Ramialison M, El-Osta

A, Hudson JE, Porrello ER. Multicellular Transcriptional Analysis of Mammalian Heart Regeneration. *Circulation*. 2017;136(12):1123–1139.

270. Taegtmeyer H, Sen S, Vela D. Return to the fetal gene program: a suggested metabolic link to gene expression in the heart. *Annals of the New York Academy of Sciences*. 2010;1188:191–8.

271. Virag JI, Murry CE. Myofibroblast and Endothelial Cell Proliferation during Murine Myocardial Infarct Repair. *The American Journal of Pathology*. 2003;163(6):2433–2440.

272. Kuramoto Y, Komuro I, Lee J-K, Sakai T, Yamaguchi T, Nakagawa A, Okada K, Hikoso S, Shibamoto M, McKinnon PJ, Hashimoto A, Ito M, Higo T, Sumida T, Shiojima I, et al. DNA single-strand break-induced DNA damage response causes heart failure. *Nature Communications*. 2017;8:15104.

273. Cook PJ, Ju BG, Telese F, Wang X, Glass CK, Rosenfeld MG. Tyrosine dephosphorylation of H2AX modulates apoptosis and survival decisions. *Nature*. 2009;458(7238):591–596.

274. Bersell K, Choudhury S, Mollova M, Polizzotti BD, Ganapathy B, Walsh S, Wadugu B, Arab S, Kühn B. Moderate and high amounts of tamoxifen in αMHC-MerCreMer mice induce a DNA damage response, leading to heart failure and death. *Disease models & mechanisms*. 2013;6(6):1459–69.

275. Sag CM, Santos CXC, Shah AM. Redox regulation of cardiac hypertrophy. *Journal of Molecular and Cellular Cardiology*. 2014;73:103–111.

276. Jopling C, Sleep E, Raya M, Martí M, Raya A, Carlos J, Belmonte I. Zebrafish heart regeneration occurs by cardiomyocyte dedifferentiation and proliferation. *Nature*. 2010;464(7288):606–609.

277. Zhang R, Han P, Yang H, Ouyang K, Lee D, Lin Y-F, Ocorr K, Kang G, Chen J, Stainier DYR, Yelon D, Chi NC. In Vivo Cardiac Reprogramming Contributes to Zebrafish Heart Regeneration. *Nature*. 2013;498(7455):497.

278. Jopling C, Boue S, Belmonte JCI. Dedifferentiation, transdifferentiation and reprogramming: three routes to regeneration. *Nature Reviews Molecular Cell Biology 2011 12:2*. 2011;12(2):79.

279. Zhang Y, Li T-S, Lee S-T, Wawrowsky KA, Cheng K, Galang G, Malliaras K, Abraham MR, Wang C, Marbán E. Dedifferentiation and Proliferation of Mammalian Cardiomyocytes. Kowaltowski AJ, ed. *PLoS ONE*. 2010;5(9):e12559.

280. Thijssen VL, Ausma J, Borgers M. Structural remodelling during chronic atrial fibrillation: act of programmed cell survival. *Cardiovascular research*. 2001;52(1):14–24.

281. Pöling J, Gajawada P, Lörchner H, Polyakowa V, Szibor M, Böttger T, Warnecke H, Kubin T, Braun T. The Janus face of OSM-mediated cardiomyocyte dedifferentiation during cardiac repair and disease. *Cell Cycle*. 2012;11(3):439–445.

282. Leach RN, Desai JC, Orchard CH. Effect of cytoskeleton disruptors on L-type Ca channel distribution in rat ventricular myocytes. *Cell Calcium*. 2005;38(5):515–526.

283. Hammer K, Ruppenthal S, Viero C, Scholz A, Edelmann L, Kaestner L, Lipp P. Remodelling of Ca2+ handling organelles in adult rat ventricular myocytes during long term culture. *Journal of Molecular and Cellular Cardiology*. 2010;49(3):427–437.

284. Louch WE, Sheehan KA, Wolska BM. Methods in Cardiomyocyte Isolation, Culture, and Gene Transfer. *J Mol Cell Cardiol.* 2011;51(3):288–298.

285. Fedak PWM, Verma S, Weisel RD, Li R-K. Cardiac remodeling and failure: From molecules to man (Part II). *Cardiovascular Pathology*. 2005;14(2):49–60.

286. Kubin T, Poling J, Kostin S, Gajawada P, Hein S, Rees W, Wietelmann A, Tanaka M, Lorchner H, Schimanski S, Szibor M, Warnecke H, Braun T. Oncostatin M is a major mediator of cardiomyocyte dedifferentiation and remodeling. *Cell Stem Cell*. 2011;9(5):420–432.

287. Tanaka M, Miyajima A. Oncostatin M, a multifunctional cytokine. In: *Reviews of Physiology, Biochemistry and Pharmacology*. Berlin, Heidelberg: Springer Berlin Heidelberg; 2003:39–52.

288. Hirota H, Chen J, Betz UA, Rajewsky K, Gu Y, Ross J, Müller W, Chien KR. Loss of a gp130 cardiac muscle cell survival pathway is a critical event in the onset of heart failure during biomechanical stress. *Cell*. 1999;97(2):189–98.

289. Yamauchi-Takihara K, Hirota H, Kunisada K, Matsui H, Fujio Y, Taga T, Kishimoto T. Roles of gp130 signaling pathways in cardiac myocytes: recent advances and implications for cardiovascular disease. *Journal of cardiac failure*. 1996;2(4 Suppl):S63-8.

290. Heinrich PC, Behrmann I, Haan S, Hermanns HM, Müller-Newen G, Schaper F. Principles of interleukin (IL)-6-type cytokine signalling and its regulation. *The*

Biochemical journal. 2003;374(Pt 1):1–20.

291. Fu Z-X, Li L, Zhou L-Y, Qi L-L, Shi Z, Zhao G-D. The Ras/Raf/MEK/ERK signaling pathway and its role in the occurrence and development of HCC. *Oncology Letters*. 2016;12(5):3045–3050.

292. Donath MY, Zapf J, Eppenberger-Eberhardt M, Froesch ER, Eppenberger HM. Insulin-like growth factor I stimulates myofibril development and decreases smooth muscle alpha-actin of adult cardiomyocytes. *Proceedings of the National Academy of Sciences of the United States of America*. 1994;91(5):1686–1690.

293. Young P, Ferguson C, Bañ S, Gautel M. *Molecular structure of the sarcomeric Z-disk: two types of titin interactions lead to an asymmetrical sorting of α-actinin*.; 1998.

294. Ostap EM. 2,3-Butanedione monoxime (BDM) as a myosin inhibitor. *Journal of Muscle Research and Cell Motility*. 2002;23(4):305–308.

295. Barøy T, Sørensen K, Lindeberg MM, Frengen E. shRNA Expression Constructs Designed Directly from siRNA Oligonucleotide Sequences. *Molecular Biotechnology*. 2010;45(2):116–120.

296. Moore CB, Guthrie EH, Huang MT-H, Taxman DJ. Short hairpin RNA (shRNA): design, delivery, and assessment of gene knockdown. *Methods in molecular biology (Clifton, N.J.)*. 2010;629:141–58.

297. Sliva K, Schnierle BS. Selective gene silencing by viral delivery of short hairpin RNA. *Virology Journal*. 2010;7(1):248.

298. Li Z, Sharma R V., Duan D, Davisson RL. Adenovirus-mediated gene transfer to adult mouse cardiomyocytes is selectively influenced by culture medium. *The Journal of Gene Medicine*. 2003;5(9):765–772.

299. Judd J, Lovas J, Huang GN. Isolation, Culture and Transduction of Adult Mouse Cardiomyocytes. *Journal of Visualized Experiments*. 2016;114:e54012–e54012.

300. Zhou Y-Y, Wang S-Q, Zhu W-Z, Chruscinski A, Kobilka BK, Ziman B, Wang S, Lakatta EG, Cheng H, Xiao R-P. Culture and adenoviral infection of adult mouse cardiac myocytes: methods for cellular genetic physiology. *American Journal of Physiology-Heart and Circulatory Physiology*. 2017;279(1):H429–H436.

301. Zacchigna S, Zentilin L, Giacca M. Adeno-associated virus vectors as therapeutic and investigational tools in the cardiovascular system. *Circulation Research*. 2014;114(11):1827–1846.

302. Mitcheson JS, Hancox JC, Levi AJ. Cultured adult cardiac myocytes: Future applications, culture methods, morphological and electrophysiological properties. *Cardiovascular Research*. 1998;39(2):280–300.

303. Dubus I, Samuel JL, Marotte F, Delcayre C, Rappaport L. β-adrenergic agonist stimulate the synthesis of noncontractile but not contractile proteins in cultured myocytes isolated from adult rat heart. *Circulation Research*. 1990;66(3):867–874.

304. Kivistö T, Mäkiranta M, Oikarinen EL, Karhu S, Weckström M, Sellin LC. 2,3-Butanedione monoxime (BDM) increases initial yields and improves long-term survival of isolated cardiac myocytes. *The Japanese journal of physiology*. 1995;45(1):203–10.

305. Thum T, Borlak J. Butanedione monoxime increases the viability and yield of adult cardiomyocytes in primary cultures. *Cardiovascular toxicology*. 2001;1(1):61–72.

306. Louch WE, Bito V, Heinzel FR, Macianskiene R, Vanhaecke J, Flameng W, Mubagwa K, Sipido KR. Reduced synchrony of Ca2+ release with loss of T-tubules - a comparison to Ca2+ release in human failing cardiomyocytes. *Cardiovascular Research*. 2004;62(1):63–73.

307. Bird S, Doevendans PA, van Rooijen MA, Brutel de la Riviere A, Hassink RJ, Passier R, Mummery CL. The human adult cardiomyocyte phenotype. *Cardiovascular Research*. 2003;58(2):423–434.

308. Dzierzak E, Speck NA. Of lineage and legacy: The development of mammalian hematopoietic stem cells. *Nature Immunology*. 2008;9(2):129–136.

309. Hofsteen P, Robitaille AM, Chapman DP, Moon RT, Murry CE. Quantitative proteomics identify DAB2 as a cardiac developmental regulator that inhibits WNT/β-catenin signaling. *Proceedings of the National Academy of Sciences*. 2016;113(4):1002–1007.

310. Tallini YN, Greene KS, Craven M, Spealman A, Breitbach M, Smith J, Fisher PJ, Steffey M, Hesse M, Doran RM, Woods A, Singh B, Yen A, Fleischmann BK, Kotlikoff MI. c-kit expression identifies cardiovascular precursors in the neonatal heart. *Proceedings of the National Academy of Sciences of the United States of America*. 2009;106(6):1808–13.

311. Pasumarthi KBS, Doble BW, Kardami E, Cattini PA. Over-expression of CUG- or AUG-initiated Forms of Basic Fibroblast Growth Factor in Cardiac Myocytes Results in Similar Effects on Mitosis and Protein Synthesis but Distinct Nuclear

Morphologies. *Journal of Molecular and Cellular Cardiology*. 1994;26(8):1045–1060.

312. Pasumarthi KB, Kardami E, Cattini PA. High and low molecular weight fibroblast growth factor-2 increase proliferation of neonatal rat cardiac myocytes but have differential effects on binucleation and nuclear morphology. Evidence for both paracrine and intracrine actions of fibroblast growth factor-2. *Circulation research*. 1996;78(1):126–36.

313. Gosteli-Peter MA, Harder BA, Eppenberger HM, Zapf J, Schaub MC. Triiodothyronine induces over-expression of α-smooth muscle actin, restricts myofibrillar expansion and is permissive for the action of basic fibroblast growth factor and insulin-like growth factor I in adult rat cardiomyocytes. *Journal of Clinical Investigation*. 1996;98(8):1737–1744.

314. Kardami E. Stimulation and inhibition of cardiac myocyte proliferation in vitro. *Molecular and cellular biochemistry*. 1990;92(2):129–35.

315. Kouhara H, Hadari YR, Spivak-Kroizman T, Schilling J, Bar-Sagi D, Lax I, Schlessinger J. A lipid-anchored Grb2-binding protein that links FGF-receptor activation to the Ras/MAPK signaling pathway. *Cell*. 1997;89(5):693–702.

316. Sheikh F, Fandrich RR, Kardami E, Cattini PA. Overexpression of long or short FGFR-1 results in FGF-2-mediated proliferation in neonatal cardiac myocyte cultures. *Cardiovascular Research*. 1999;42(3):696–705.

317. Hesse M, Raulf A, Pilz GA, Haberlandt C, Klein AM, Jabs R, Zaehres H, Fügemann CJ, Zimmermann K, Trebicka J, Welz A, Pfeifer A, Röll W, Kotlikoff MI, Steinhäuser C, et al. Direct visualization of cell division using high-resolution imaging of M-phase of the cell cycle. *Nature Communications*. 2012;3(1):1076.

318. Ahuja P, Perriard E, Perriard J-C, Ehler E. Sequential myofibrillar breakdown accompanies mitotic division of mammalian cardiomyocytes. *Journal of Cell Science*. 2004;117(15):3295–3306.

319. Klocke R, Tian W, Kuhlmann MT, Nikol S. Surgical animal models of heart failure related to coronary heart disease. *Cardiovascular Research*. 2007;74(1):29–38.

320. Moorhead GBG, Trinkle-Mulcahy L, Ulke-Lemée A. Emerging roles of nuclear protein phosphatases. *Nature Reviews Molecular Cell Biology*. 2007;8(3):234–244.

321. Martelli AM, Tabellini G, Bressanin D, Ognibene A, Goto K, Cocco L, Evangelisti C. The emerging multiple roles of nuclear Akt. *Biochimica et Biophysica Acta*

(BBA) - Molecular Cell Research. 2012;1823(12):2168–2178.

322. Chiarugi P, Cirri P. Redox regulation of protein tyrosine phosphatases during receptor tyrosine kinase signal transduction. *Trends in Biochemical Sciences*. 2003;28(9):509–514.

323. Cho SH, Lee CH, Ahn Y, Kim H, Kim H, Ahn CY, Yang KS, Lee SR. Redox regulation of PTEN and protein tyrosine phosphatases in H2O2-mediated cell signaling. *FEBS Letters*. 2004;560(1–3):7–13.

324. Kwon J, Lee S-R, Yang K-S, Ahn Y, Kim YJ, Stadtman ER, Rhee SG. Reversible oxidation and inactivation of the tumor suppressor PTEN in cells stimulated with peptide growth factors. *Proceedings of the National Academy of Sciences of the United States of America*. 2004;101(47):16419–24.

325. Xu D, Rovira II, Finkel T. Oxidants Painting the Cysteine Chapel: Redox Regulation of PTPs. *Developmental Cell*. 2002;2(3):251–252.

326. Gamou S, Shimizu N. Hydrogen peroxide preferentially enhances the tyrosine phosphorylation of epidermal growth factor receptor. *FEBS Letters*. 1995;357(2):161–164.

327. Hoeijmakers JHJ. DNA damage, aging, and cancer. *The New England journal of medicine*. 2009;361(15):1475–85.

328. Marnett LJ, Riggins JN, West JD. Endogenous generation of reactive oxidants and electrophiles and their reactions with DNA and protein. *Journal of Clinical Investigation*. 2003;111(5):583–593.

329. Lu SY, Sontag DP, Detillieux KA, Cattini PA. FGF-16 is released from neonatal cardiac myocytes and alters growth-related signaling: a possible role in postnatal development. *American Journal of Physiology-Cell Physiology*. 2008;294(5):C1242–C1249.

330. Detillieux KA, Sheikh F, Kardami E, Cattini PA. Biological activities of fibroblast growth factor-2 in the adult myocardium. *Cardiovascular Research*. 2003;57(1):8–19.

331. McCubrey JA, Steelman LS, Chappell WH, Abrams SL, Wong EWT, Chang F, Lehmann B, Terrian DM, Milella M, Tafuri A, Stivala F, Libra M, Basecke J, Evangelisti C, Martelli AM, et al. Roles of the Raf/MEK/ERK pathway in cell growth, malignant transformation and drug resistance. *Biochimica et Biophysica Acta (BBA) - Molecular Cell Research*. 2007;1773(8):1263–1284.

332. Sheikh F, Hirst CJA, Jin Y, Bock ME, Fandrich RR, Nickel BE, Doble BW, Kardami E, Cattini PA. Inhibition of TGFβ signaling potentiates the FGF-2-induced stimulation of cardiomyocyte DNA synthesis. *Cardiovascular Research*. 2004;64(3):516–525.

333. Varga Z V, Pipicz M, Baán JA, Baranyai T, Koncsos G, Leszek P, Kuśmierczyk M, Sánchez-Cabo F, García-Pavía P, Brenner GJ, Giricz Z, Csont T, Mendler L, Lara-Pezzi E, Pacher P, et al. Alternative Splicing of NOX4 in the Failing Human Heart. *Frontiers in physiology*. 2017;8:935.

334. Opie LH, Commerford PJ, Gersh BJ, Pfeffer MA. Controversies in ventricular remodelling. *The Lancet*. 2006;367(9507):356–367.

335. Santos CXC, Anilkumar N, Zhang M, Brewer AC, Shah AM. Redox signaling in cardiac myocytes. *Free Radical Biology and Medicine*. 2011;50(7):777–793.

336. Ago T, Liu T, Zhai P, Chen W, Li H, Molkentin JD, Vatner SF, Sadoshima J. A Redox-Dependent Pathway for Regulating Class II HDACs and Cardiac Hypertrophy. *Cell*. 2008;133(6):978–993.

337. Barcellos-Hoff MH, Dix TA. Redox-mediated activation of latent transforming growth factor-beta 1. *Molecular Endocrinology*. 1996;10(9):1077–1083.

338. Remondino A, Kwon SH, Communal C, Pimentel DR, Sawyer DB, Singh K, Colucci WS. Beta-adrenergic receptor-stimulated apoptosis in cardiac myocytes is mediated by reactive oxygen species/c-Jun NH2-terminal kinase-dependent activation of the mitochondrial pathway. *Circulation research*. 2003;92(2):136–8.

339. Nishida K, Otsu K. The Role of Apoptosis Signal-Regulating Kinase 1 in Cardiomyocyte Apoptosis. *Antioxidants & Redox Signaling*. 2006;8(9–10):1729–1736.

340. Sano M, Minamino T, Toko H, Miyauchi H, Orimo M, Qin Y, Akazawa H, Tateno K, Kayama Y, Harada M, Shimizu I, Asahara T, Hamada H, Tomita S, Molkentin JD, et al. p53-induced inhibition of Hif-1 causes cardiac dysfunction during pressure overload. *Nature*. 2007;446(7134):444–448.

341. Mochizuki T, Furuta S, Mitsushita J, Shang WH, Ito M, Yokoo Y, Yamaura M, Ishizone S, Nakayama J, Konagai A, Hirose K, Kiyosawa K, Kamata T. Inhibition of NADPH oxidase 4 activates apoptosis via the AKT/apoptosis signal-regulating kinase 1 pathway in pancreatic cancer PANC-1 cells. *Oncogene*. 2006;25(26):3699–3707.

342. Zhang M, Perino A, Ghigo A, Hirsch E, Shah AM. NADPH Oxidases in Heart

Failure: Poachers or Gamekeepers? *Antioxidants & Redox Signaling*. 2012;18(9):1024–1041.

343. Moloney JN, Jayavelu AK, Stanicka J, Roche SL, O'Brien RL, Scholl S, Böhmer F-D, Cotter TG. Nuclear membrane-localised NOX4D generates pro-survival ROS in FLT3-ITD-expressing AML. *Oncotarget*. 2017;8(62):105440–105457.

344. Lexow J, Poggioli T, Sarathchandra P, Santini MP, Rosenthal N. Cardiac fibrosis in mice expressing an inducible myocardial-specific Cre driver. *Disease models & mechanisms*. 2013;6(6):1470–6.

345. Pacak C a, Sakai Y, Thattaliyath BD, Mah CS, Byrne BJ. Tissue specific promoters improve specificity of AAV9 mediated transgene expression following intra-vascular gene delivery in neonatal mice. *Genetic vaccines and therapy*. 2008;6:13.

346. Levsky JM, Singer RH. Fluorescence in situ hybridization: past, present and future. *Journal of Cell Science*. 2003;116(14):2833–2838.

347. Ferdinandy P, Schulz R, Baxter GF. Interaction of cardiovascular risk factors with myocardial ischemia/reperfusion injury, preconditioning, and postconditioning. *Pharmacological Reviews*. 2007;59(4):418–458.